Prepared for the

NASA Lewis Research Center
Dr. Sanjay Garg, Technical Monitor
21,000 Brookpark Rd.
Cleveland, OH 44135

Cooperative Control Theory And Integrated Flight And Propulsion Control

Final Report for Grant NAG3-998

Covering the Period 1990 - 1993

by

David K. Schmidt, Principal Investigator
and
John D. Schierman
Department of Aerospace Engineering
University of Maryland at College Park
College Park, MD 20742

November 1994

Table of Contents

Cooperative Control Theory And Integrated Flight And Propulsion Control

David K. Schmidt
and
John D. Schierman

Department of Aerospace Engineering
University of Maryland at College Park

November 1994

Introduction and Summary

This constitutes a final technical report, documenting the activities and research results obtained under a grant (NAG3-998) from the NASA Lewis Research Center, awarded to Arizona State University. The principal investigator was Dr. David Schmidt, and the grant technical monitor was Dr. Sanjay Garg of NASA Lewis. The focus of the research was the investigation of dynamic interactions between airframe and engines for advanced ASTOVL aircraft configurations, and the analysis of the implications of these interactions on the stability and performance of the airframe and engine control systems. In addition, the need for integrated flight and propulsion control for such aircraft was addressed.

The major contributions of this research was the exposition of the fact that airframe and engine interactions could be present, and their effects could include loss of stability and performance of the control systems. Also, the significance of two-directional, as opposed to one-directional, coupling was identified and explained. A multivariable stability and performance analysis methodology was developed, and applied to several candidate aircraft configurations. In these example evaluations, the significance of these interactions was underscored. Also exposed was the fact that with interactions present along with some integrated control approaches, the engine command/limiting logic (which represents an important non-linear component of the engine control system) can impact closed-loop airframe/engine system stability. Finally, a brief investigation of control-law synthesis techniques appropriate for the class of systems was pursued, and it was determined that multivariable techniques, included model-following formulations of LQG and/or H_∞ methods showed promise. However, for practical reasons, decentralized control architectures are preferred, which is an architecture incompatible with these synthesis methods.

Review of Grant Technical Objectives

Historically, little dynamic interactions occurred between airframe and propulsion subsystems, in terms of the high-frequency attitude response. And this allows the airframe and engine control laws to be separately designed, built, and tested. However, the dynamic interactions between the airframe and engine may be substantial in advanced fighter aircraft, for example, which utilize the propulsion system for augmenting the lift and maneuvering capabilities of the vehicle. For such aircraft, separate airframe and engine control law designs may or may not be viable, and this question has generated the study of Integrated Flight and Propulsion Control (IFPC). Adding to the complexity of the control problem, it has been recognized that the interactions between these two subsystems are not currently well understood, and uncertainty in the dynamic models of these interactions may be significant.

Three major technical objectives of this research grant were identified from the outset, and they include the following:

(1) To identify and understand potential sources of dynamic interactions between the airframe and propulsion subsystems.

(2) To develop a theoretical framework to evaluate the significance of the potential interactions, from the perspective of integrated flight and propulsion control.

(3) To develop control synthesis methodologies yielding control laws that are robust against modeling uncertainty in the interactions between the airframe and engine.

All three of these topics have been addressed in the research, with particular emphasis on the first two. The main results in these areas are summarized below, and documented in greater detail in the papers that appear in the Appendix to this report.

Potential Sources of Airframe/Engine Interactions

Clearly, engines interact with all airframes, since their purpose is to provide propulsive thrust. But some advanced vehicle designs are considering the use of the engine for lift augmentation and/or for attitude control. Potential sources of unique and unusual airframe/engine interactions were explored for such aircraft, in the scope of integrated flight/propulsion control in [1], [2], [5], [6]. Two primary vehicular models were used in case studies. The first was representative of an F/A-18A fighter aircraft equipped with a 2-D Thrust-Vectoring/Thrust-Reversing (TVTR) aft nozzle and, later, with reaction control system (RCS) jets drawing bleed air from the engine's compressor. The second was representative of an E7-D ASTOVL aircraft equipped with RCS jets, a 2-

D TVTR nozzle, a ventral nozzle and ejectors which redirect engine core and bypass flow.

It was shown that for such aircraft designs the potential for two-directional interactions between the airframe and engine subsystems may be significant. Thrust vectoring, RCS jets and redirected engine flow are all systems designed to augment the lift and/or control attitude of the airframe. Therefore, engine thrust can influence the lift and attitude dynamics in the bandwidth of the attitude control loops. On the other hand, commands to control the airframe responses through the use of propulsive augmentation can influence the engine dynamics in the same frequency range. These and other potential airframe/engine interactions are elaborated in [5].

Although it was initially believed that only engine-to-airframe interactions would be significant (one-directional coupling), analysis of both the F/A-18A and E7-D vehicle models demonstrated substantial airframe-to-engine interactions as well (or two-directional coupling). Further analysis demonstrated that configurations that redirect engine flow (through the use of RCS jets, a ventral nozzle and ejectors) are more problematic in this regard than other configurations. The implications of one versus two-directional coupling was then explored. It was seen that if the system exhibits two-directional coupling, stability as well as performance may be compromised, whereas if the coupling is primarily one-directional, only performance can be seriously affected.

Several system representations and control law architectures were investigated. One significant result found was that if an "auto-throttle" is implemented to regulate the airframe's forward speed, then the engine control system's non-linear command logic and limit protection can affect the stability robustness of the integrated airframe/engine system.

Finally, nonlinear aspects of engine control, such as engine limit protection through control mode switching logic, was investigated in the context of IFPC. This topic was further discussed in [5].

Analysis Methodology

An analysis methodology was developed to further reveal how the interactions between the airframe and engine manifest themselves, and to assess their significance. This analysis method was presented in [1], [2], [5]-[7], and was later denoted as the Interacting Subsystem (IS) Analysis Method in [8]. The analysis allows for the investigation of both the airframe's effects on the engine control loops and the engine's effects on the flight control loops. The analysis has been demonstrated on both scalar and

multivariable airframe and engine subsystems, and can be utilized for either centralized or decentralized control systems.

This analysis method involves reflecting the airframe/engine interactions into what have been denoted as the "additive, multiplicative and disturbance interaction matrices." The "sizes" of these critical interaction matrices, measured by their singular values, quantifies effects of airframe/engine coupling on closed-loop stability and/or performance. The additive and multiplicative interaction matrices were shown to affect both stability and performance, whereas the disturbance interaction matrix affects only disturbance rejection performance. The maximum allowable "size" of the additive or multiplicative interaction matrix to assure stability was established for multivariable systems. The maximum allowable magnitude of the additive or multiplicative interaction term to assure acceptable performance was established for scalar loops. These interaction matrices were shown to be explicit functions of the dynamic cross-coupling between airframe and engine subsystems. Because of this, it was seen that the analysis technique could be easily extended to assess stability and performance *robustness* against modeling uncertainties in the airframe/engine coupling.

Although primarily a linear analysis technique, the IS methodology was conceptually expanded to embody quasi-linear approximations of nonlinear systems in [5]. Analogous to the critical interaction matrices, sinusoidal input describing function matrices were utilized to quantify the effects of airframe/engine coupling on the susceptibility of the system to possess limit cycles.

The IS analysis method was demonstrated using both the F/A-18A and E7-D airframe/engine systems, as noted previously, and proved useful in identifying critical frequency ranges where the interactions between the airframe and engine were especially problematic, [1], [2], [5]-[8]. The analysis indicated potentially poor stability robustness within these critical frequency ranges due to uncertainty in the interactions. Sensitivity studies proved that the analysis method accurately predicted the frequencies at which instability would first occur with increased airframe/engine coupling. Gain cross-over frequencies for classical single-loop analyses did not, however, correspond to these critical frequencies. It was also demonstrated that the analysis accurately assessed the effects of disturbances encountered in each loop due to the airframe/engine interactions. Finally, for the E7-D model, it was also shown that the magnitude of allowable uncertainty to assure acceptable engine performance was smaller than that which was allowed to assure acceptable stability robustness.

The IS analysis methodology was also compared and contrasted to the Singular Value (SV) and Structured Singular Value (SSV) analysis approaches in [8]. With regard

to the stability robustness analysis, the accuracy of the IS analysis method was, in general, comparable to the SSV analysis method. However, it was seen that the SV analysis method gave conservative measures of stability robustness and predicted critical frequencies that did not correspond to the frequencies of instability. Further, the IS analysis was able to indicate an accurate measure of performance robustness (although only for scalar loops), whereas the SV and SSV methods were found to give conservative measures of performance robustness. The major benefit seen in the IS analysis approach was that valuable information can be provided by this method without necessarily requiring uncertainty models, which may be difficult to model or estimate.

Finally, the analysis framework embodied by the IS method was compared and contrasted to a related synthesis approach developed by Northrop and Systems Control Technology, as presented in,

> Rock, S.M., Emami-Naeini, A., Anex, R.P., "Propulsion Control Specifications in Integrated Flight/Propulsion Control Systems," AIAA Paper No. 88-3236, AIAA/ASME/SAE/ASEE 24th Joint Propulsion Conference, Boston, Mass., 1988.

In this related framework, the engine subsystem was considered as a "generalized" actuator for flight control. Because of this, the airframe dynamics could not influence the engine dynamics and, consequently, only one-directional coupling was considered. It was shown by the IS analysis method, however, that by assuming the system to only have one-directional dynamic coupling could be very inappropriate, and lead to catastrophic results.

Control Synthesis Methodologies

Two *centralized* control synthesis methodologies were developed specifically for integrated flight/propulsion control. Control laws were synthesized for the F/A-18A aircraft/engine model, and the results were presented in [3] and [4]. The first methodology was designated the Extended-Implicit-Model-Following/Loop-Transfer-Recovery (EIMF/LTR) design approach, whereas the second method was designated the EIMF/H_∞ approach.

Model following was an integral part of the formulations considered - due to the desire that certain airframe responses closely approximate classical airframe dynamics which reflect excellent handling qualities. This design goal implies that the engine dynamics should not be observable in airframe responses in spite of potential open-loop airframe/engine dynamic coupling. Hence, another design goal was that the control system should decouple airframe and engine responses. However, engine temperature and pressure limits should not be exceeded, and stable combustion should be maintained.

Therefore, the control law must also regulate responses such as fan and compressor speeds, and temperatures and pressures throughout the engine. Further, it was assumed desirable to regulate aircraft velocity. This was therefore a hybrid control problem - one of dynamically shaping certain airframe responses while simultaneously regulating engine responses and aircraft velocity. The term "Extended" above was used to denote that this new model-following approach addressed this hybrid control problem. Finally, implicit rather than explicit model following was utilized to eliminate the dynamic pre-filter present in the latter control structure. This led to a closed-loop system of lower dynamic order that is easier to evaluate and simpler to implement.

The EIMF/LTR synthesis method was a two-step process in which a state feedback control law was designed via minimization of a Linear Quadratic (LQ) loss function. Compensators were then obtained to realize an output-feedback control law by using standard loop-transfer-recovery procedures - which give stability robustness similar to that of the state feedback control law. However, in the EIMF/H_∞ synthesis method, output-feedback compensation was directly realized in one step. This method involved a unique H_∞ formulation that reflected the EIMF design goals.

Both control synthesis approaches delivered excellent model following and regulation performance with modest gain crossover frequencies, thus keeping actuation bandwidth requirements to a minimum. The airframe responses closely approximated those desired, and good disturbance-rejection performance was seen in the engine loops. As defined by singular value tests, the EIMF/LTR control law delivered reasonable multivariable robustness. However, the multivariable robustness for the EIMF/H_∞ control law was poor, and further research is suggested here. For both methods, design parameters could be varied to improve the robustness, but this came at a cost of degraded model following performance.

Limitations of Decentralized Control Law Architectures

It would be very desirable to determine if and when centralized or integrated control systems are required - based solely on the open-loop airframe/engine plant and closed-loop feedback system requirements. Implementation of centralized integrated airframe/engine control laws could potentially be quite complex, and decentralized controllers that would meet the overall design objectives may be a more favorable alternative. However, design freedom is more limited in decentralized control due to the absence of cross-feeds between the airframe and engine subsystems.

It has been recognized that there is a need to develop necessary conditions for decentralized control laws to be able to potentially deliver the required feedback system

properties (stability, adequate stability robustness, acceptable performance and adequate performance robustness). Such necessary conditions should highlight limitations of achievable performance and robustness of decentralized controllers. If these necessary conditions are not met, *no* decentralized control law design can achieve all required feedback system properties - and the design must turn to centralized approaches. In order to be utilized prior to the control law synthesis, these necessary conditions cannot be explicit functions of the control laws.

We have begin the investigation into the limitations of decentralized control laws, and this effort is basically the topic of the follow-on phase of this project, funded under another grant. However, necessary and sufficient condition for the existence of a stabilizing decentralized control law have been identified.

List of Publications Generated Under this Grant

The following is a list of conference and journal publications that have resulted from this research grant. Copies of these papers are included in the Appendix to this report. This research grant has resulted in one archival journal publication and seven refereed conference proceeding publications. Additionally, the paper presented at the 1993 Guidance, Navigation and Control Conference [Ref. 8] is currently being edited and prepared for consideration to the *Journal of Guidance, Control, and Dynamics.*. Finally, it is expected that a Ph.D. dissertation will result from this research grant.

Archival Journal Publication

[1] Schierman, J., Schmidt, D., "Analysis Of Airframe And Engine Control Interactions and Integrated Flight/Propulsion Control," *Journal Of Guidance, Control, And Dynamics*, Vol. 15, No. 6, Nov.-Dec., 1992, pp. 1388-1396.

Conference Proceeding Publications

[2] Schmidt, D., Schierman, J., Garg, S., "Analysis of Airframe/Engine Interactions - An Integrated Control Perspective," AIAA # 90-1918, *Proceedings* of the 26th Joint Propulsion Conference, Orlando, Fl., July, 1990. ***This paper received the Air Breathing Propulsion Technical Committee's Best Paper Award for 1990.***

[3] Schmidt, D., Schierman, J., "Extended Implicit Model Following As Applied To Integrated Flight and Propulsion Control," AIAA Paper No. 90-3444, *Proceedings* of the AIAA Guidance, Navigation and Control Conference, Portland, Oregon, August, 1990.

[4] Schierman, J., Schmidt, D., "Robust Control Synthesis For Integrated Flight and Propulsion Control," *Proceedings* of the IEEE Conference on Decision and Control, Honolulu, Hawaii, December, 1990.

[5] Schmidt, D., Schierman, J., "A Framework for the Analysis of Airframe/Engine Interactions and Integrated Flight/Propulsion Control," *Proceedings* of the American Control Conference, Boston, Mass., June, 1991.

[6] Schierman, J., Schmidt, D., "Analysis Of Airframe/Engine Interactions In Integrated Flight And Propulsion Control," AIAA No. 91-2794, *Proceedings* of the AIAA Guidance, Navigation and Control Conference, New Orleans, August, 1991.

[7] Schierman, J., Schmidt, D., Lovell, T., "Analysis Of Airframe/Engine Interactions For A STOVL Aircraft With Integrated Flight/Propulsion Control," AIAA No. 92-4623, *Proceedings* of the AIAA Guidance, Navigation and Control Conference, Hilton Head, August, 1992.

[8] Schierman, J., Schmidt, D., Lovell, T., "A Comparative Study of Multivariable Robustness Analysis Methods as Applied to Integrated Flight and Propulsion Control," AIAA No. 93-3809, *Proceedings* of the AIAA Guidance, Navigation and Control Conference, Monterey, August, 1993. ***Winner of the AIAA "Best Presentation Award," Session GNC 19.***

Graduate Students Supported Under The Grant

Graduate students supported under this grant include the following.

Mr. Alan Lovell, MSAE, Arizona State Univ. August, 1994.

Mr. John Schierman, PhD Arizona State, December, 1994, (expected)

Appendix

Copies of Publications

JOURNAL OF GUIDANCE, CONTROL, AND DYNAMICS
Vol. 15, No. 6, November-December 1992

Analysis of Airframe and Engine Control Interactions and Integrated Flight/Propulsion Control

P/A
93A14596

John D. Schierman* and David K. Schmidt†
Arizona State University, Tempe, Arizona 85287

A framework is presented for the analysis of dynamic cross-coupling between airframe and engine control systems. This approach is developed for assessing the significance of airframe/engine interactions with regard to system stability, performance, and critical frequency ranges where interactions are especially problematic. The stability robustness against airframe/engine interactions are of particular interest, and a robustness analysis approach is developed and presented. The difference between systems exhibiting two-directional vs one-directional coupling is also discussed. Two control configurations of a vehicle previously considered in several integrated flight/propulsion control studies are then evaluated using the technique, and it is shown that the baseline configuration reflects little significant airframe/engine interactions. Consequently, classical decentralized airframe and engine control laws appear to be quite adequate. However, analysis of the other system configuration shows significant performance degradation in the engine loop because of airframe/engine coupling.

Introduction

ADVANCED concepts for highly maneuverable fighter aircraft and those capable of short takeoff and vertical landing utilize the propulsion system for augmenting the lift and maneuvering capabilities of the vehicle. The integrated flight and propulsion control (IFPC) problem addressed herein and elsewhere[1-5] focuses on the interactions between airframe and engine systems, especially in control law synthesis and analysis of such configurations.

The main purpose of this paper is not to discuss any particular IFPC control law synthesis procedure but first to present an analysis framework that will expose how the interactions manifest themselves and second to determine if cross-coupling dynamics between the airframe and engine are of sufficient "magnitude" to significantly affect stability and/or performance of the feedback systems. The analysis technique also addresses the issue of the system's robustness against uncertainties in these interactions. Airframe/engine interactions are often a significant source of uncertainty in the system's dynamics.

Another objective of the paper is to use the analysis approach to evaluate airframe/engine cross-coupling on a vehicle that has been the subject of several studies in IFPC. The analysis reveals that critical cross-coupling is not present for this vehicle, as modeled, for the operating condition and control configuration evaluated. As a result, the classical control laws considered in this example would appear to deliver adequate stability robustness and performance. A second control configuration is then considered, and the analysis shows increased cross-coupling due to an added reaction control system (RCS) causing a significant degradation in engine loop performance.

Presented as Paper 90-1918 at the AIAA/SAE/ASME/ASEE 26th Joint Propulsion Conference, Orlando, FL, July 16-18, 1990; received Oct. 3, 1991; revision received Feb. 28, 1992; accepted for publication March 6, 1992.

*Research Associate and Doctoral Candidate, Aerospace Research Center, College of Engineering and Applied Sciences. Student Member AIAA.

†Professor of Engineering and Center Director, Aerospace Research Center, College of Engineering and Applied Sciences. Associate Fellow AIAA.

Potential Sources of Airframe/Engine Interactions

The airframe/engine interactions highlighted in this section are elaborated on in Refs. 1-9. Consider for discussion purposes the vehicle system in Fig. 1. Thrust reversing nozzles may be considered for improving forward speed control of the aircraft. Vectoring of the engine's aft nozzle may be used to augment attitude control power, and ventral nozzle thrust may augment aerodynamic lift. Left and right ejectors, drawing primary thrust from the engine's mixed flow (core and bypass flow) and secondary thrust from intakes over the top of the fuselage may also augment lift and enhance pitch and roll control power. The lift and attitude responses of the airframe will be influenced by thrust disturbances in these sources, and effects of the ejector's secondary flow may significantly influence the airframe aerodynamics.

On the other hand, commands in thrust reversing, thrust vectoring, and ventral and ejector thrust may cause pressure disturbances in the augmentor or mixing plane. If the nozzle is operating in an unchoked condition, these pressure disturbances may propagate through the fan bypass duct and cause engine transients such as a reduction in fan surge margin.

Reaction control system jets, used for airframe attitude control, as well as upper wing surface blowing, used for lift augmentation, usually draw bleed air from the engine's compressor. Thus, core flow dynamics can also influence the lift and attitude responses of the airframe. Increased RCS thrust will cause reduced core pressure due to compressor bleed flow demand, creating engine flow disturbances. Also, flight dynamic pressure, angle of attack, sideslip angle, and inlet flow distortions can influence the effectiveness of the RCS control jets and cause reduced fan surge margin.

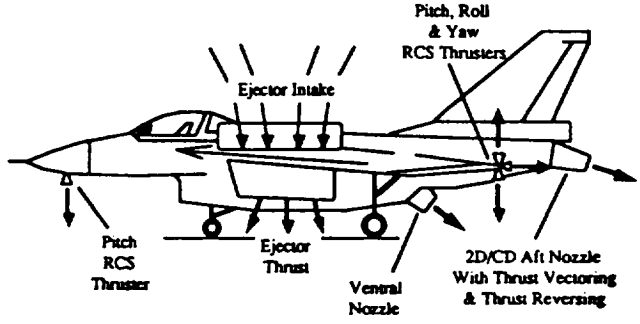

Fig. 1 Typical vehicle configuration.

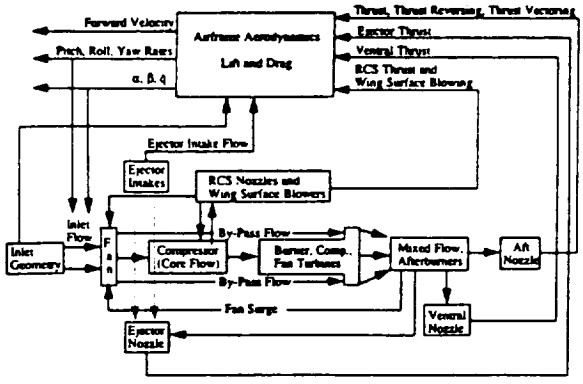

Fig. 2 Example interactions between airframe and engine subsystems.

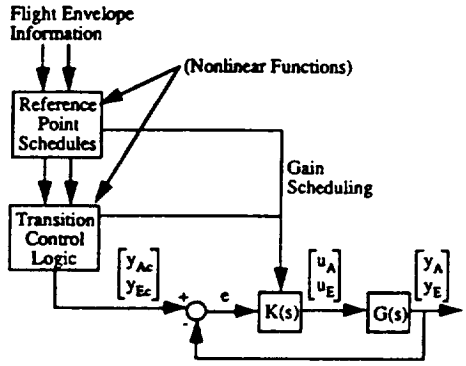

Fig. 3 Full nonlinear airframe/engine system representation.

It is important to note here that, for the type of vehicle being considered, the propulsion system not only affects the (slower responding) transitional velocity of the vehicle but also may be both a lift and moment "actuator," affecting the vehicle's (faster responding) attitude dynamics. All of these interactions just described between the airframe and engine are shown in Fig. 2.

Analysis Framework

The technique to be presented is a quasilinear approach for assessing airframe and engine interactions.[10] This procedure seeks to provide a better understanding of the effects of these interactions. It is recognized that many of the interactions discussed previously involve nonlinear phenomena, and detailed nonlinear simulations will ultimately be required. However, the justification for the quasilinear analysis and the treatment of engine limits is specifically noted herein.

Consider the airframe/engine nonlinear system similar to that discussed in Refs. 11–13 and shown in Fig. 3. y_{Ac} is the vector of commands to the flight control system, and y_{Ec} is the vector of commands to the engine control system. u_A is the vector of aircraft control inputs (flap deflection δ_F, thrust vector nozzle deflection δ_{TV}, etc.), and u_E is the vector of engine control inputs (fuel flow rate w_F, nozzle area A_7, etc.). Finally, y_A is the vector of aircraft responses (angle of attack α, pitch rate q, etc.), and y_E is the vector of engine responses (turbine temperature T_4, fan speed N_2, etc.).

Implicit in the feedback portion of this system is that the matrix $G(s)$, the quasilinear input/output mapping of the vehicular system, is a member of a set of such mappings, $\mathcal{G}(s)$, and strongly depends on the particular flight and engine operating condition. In fact, each such operating point manifests a particular quasilinear system model and control architecture, which define the matrices $G(s)$ and $K(s)$. Furthermore, these mappings may reflect a particular control mode, such as "riding an engine limit." In such a case, the controlled responses $y_E(s)$ depend on the operating limit. In the discussion to follow, it is implied that the analysis is being performed for a specific operating condition and a specific engine control mode.

If it can be assumed here that any gain scheduling leads to slowly time-varying gains, then the particular feedback system being considered can be treated as (approximately) time invariant. In this case, the system nonlinearities reside primarily outside the feedback loop, and the purpose of feedback is to force approximately linear behavior between y and y_c. The analysis framework that follows focuses only on the feedback portion of the system. However, this does not imply that the prefilters, gain scheduling, limit logic, etc., outside the feedback loop are not important to the system design, but that stability and performance of the feedback loops are fundamental to a successful design. Furthermore, since the feedback control loops for the airframe and engine are, under current practice, developed by different organizations, it could be argued that interactions in these loops would constitute the most difficult design challenge.

Now, more specifically, consider the aircraft dynamics isolated from the engine dynamics, with input/output characteristics defined in terms of a matrix of transfer functions $G_A^*(s)$, where

$$y_A(s) = G_A^*(s)u_A(s) \tag{1}$$

Likewise, let the isolated engine's input/output characteristics be defined in terms of a matrix of transfer functions $G_E^*(s)$, where

$$y_E(s) = G_E^*(s)u_E(s) \tag{2}$$

Consider that each of these systems will be acted on by feedback control compensation matrices $K_A(s)$ for the aircraft flight control system, and $K_E(s)$ for the engine control system. The associated engine feedback system is shown in Fig. 4 [note again that $K_E(s)$ and $G_E^*(s)$ are, in general, matrices].

The closed-loop quasilinear responses of this system are given by

$$y_E(s) = \left[I + G_E^*(s)K_E(s)\right]^{-1}G_E^*(s)K_E(s)\,y_{Ec}(s) \tag{3}$$

and the closed-loop characteristic polynomial is

$$\phi_{cl}(s) = \phi_{ol}(s)\det\left[I + G_E^*(s)K_E(s)\right] \tag{4}$$

where the roots of $\phi_{ol}(s)$ are an aggregate of the poles of $G_E^*(s)$ and $K_E(s)$.

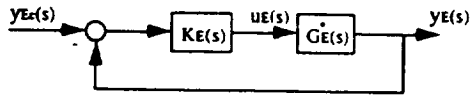

Fig. 4 Block diagram of the isolated engine feedback loop.

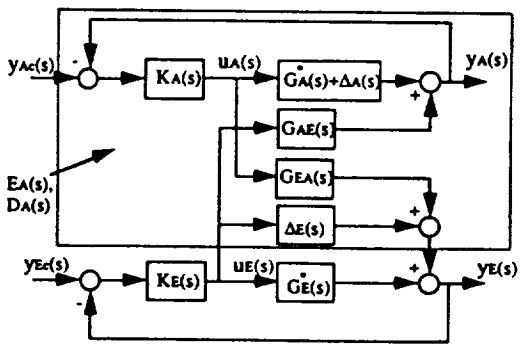

Fig. 5 Block diagram of the coupled airframe/engine system.

But since the airframe/engine system dynamics are in fact coupled, their input/output characteristics are more accurately represented as

$$\begin{bmatrix} y_A(s) \\ y_E(s) \end{bmatrix} = \begin{bmatrix} G_A(s) & G_{AE}(s) \\ G_{EA}(s) & G_E(s) \end{bmatrix} \begin{bmatrix} u_A(s) \\ u_E(s) \end{bmatrix} = [G(s)] \begin{bmatrix} u_A(s) \\ u_E(s) \end{bmatrix} \tag{5}$$

where, again, $G_A(s)$, $G_E(s)$, $G_{AE}(s)$, and $G_{EA}(s)$ are, in general, matrices. Note also that $G_A(s)$ and $G_E(s)$ may differ from the decoupled subsystem models $G_A^*(s)$ and $G_E^*(s)$ by some amounts $\Delta_A(s)$ and $\Delta_E(s)$, respectively, due to the cross-coupling actually present between the airframe and engine systems. That is,

$$\begin{aligned} G_A(s) &= G_A^*(s) + \Delta_A(s) \\ G_E(s) &= G_E^*(s) + \Delta_E(s) \end{aligned} \tag{6}$$

Further, $G_{AE}(s)$ and $G_{EA}(s)$ represent any input coupling that leads to the open-loop engine control inputs influencing airframe responses or the open-loop airframe control inputs influencing the engine responses, respectively. Now, if both $G_{AE}(s)$ and $G_{EA}(s)$ are "large," the system is said to exhibit two-directional coupling. If only one is "large," the coupling between the subsystems is primarily one-directional.

The actual coupled system, under the influence of the airframe and engine control feedback compensation $K_A(s)$ and $K_E(s)$, is then shown in Fig. 5. In this figure the lower portion of the block diagram is the original engine loop, but it is no longer isolated from the airframe as in Fig. 4.

Figure 5 reveals how, for example, the coupling dynamics $G_{AE}(s)$ and $G_{EA}(s)$ and the airframe dynamics $G_A(s)$, augmented with the airframe compensator $K_A(s)$, interact with the engine loops. (Note that a dual exists for the effects of the coupling and augmented engine dynamics on the airframe loops.) Through block diagram manipulation, the system in Fig. 5 may be represented as in Fig. 6, where

$$E_A(s) = \Delta_E - G_{EA}\left[I + K_A(G_A^* + \Delta_A)\right]^{-1} K_A G_{AE} \tag{7}$$

$$D_A(s) = G_{EA}\left[I + K_A(G_A^* + \Delta_A)\right]^{-1} K_A \tag{8}$$

(Note that functional dependence on s is not indicated in some of these terms to simplify notation.) Because of the manner in which these terms affect the engine loop, $E_A(s)$ will be referred to as the additive interaction matrix, and $D_A(s)$ will be referred to as the disturbance interaction matrix. Clearly, if $\Delta_A(s)$, $\Delta_E(s)$, $G_{AE}(s)$, and $G_{EA}(s)$ are not really zero, the engine loop is not actually that shown in Fig. 2 but rather that shown in Fig. 6

The critical expressions of Eqs. (7) and (8) reveal several key facts. First, Eq. (7) shows that the additive interaction matrix $E_A(s)$ depends on the weighted matrix product of the input coupling transfer matrices $G_{EA}(s)$ and $G_{AE}(s)$, the airframe dynamics $G_A^*(s) + \Delta_A(s)$, and the change in the engine transfer function matrix due to coupling $\Delta_E(s)$. $E_A(s)$ will therefore be "small" (for example, small maximum singular value) if Δ_E is "small" and if either $G_{AE}(s)$ or $G_{EA}(s)$ is "small." Thus, if only one-directional coupling is present, the additive interaction matrix will tend to be "small."

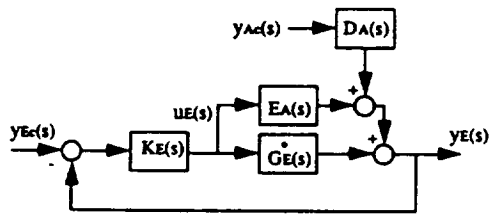

Fig. 6 Block diagram of the engine feedback loop interacting with the airframe subsystem.

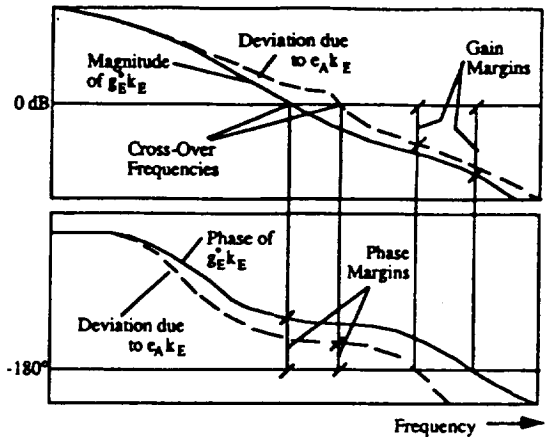

Fig. 7 Example noninteracting (solid line) and interacting (dashed line) systems' engine loop transfers.

Conversely, from Eq. (8), note that the disturbance interaction matrix $D_A(s)$ is independent of $G_{AE}(s)$. Hence, it may be "large" if $G_{EA}(s)$ is "large," even though $G_{AE}(s)$ is "small." That is, the disturbance interaction matrix can be "large" even if only one-directional coupling is present.

Finally, both the additive and disturbance interaction matrices depend explicitly on the airframe control laws $K_A(s)$. If the airframe loops are not closed [$K_A(s) = 0$], $E_A(s)$ reduces to $\Delta_E(s)$ and $D_A(s)$ reduces to zero. Consequently, the phenomenon of interest here is fundamentally one involving feedback.

To reveal the import of the additive and disturbance interaction matrices, note that the quasilinear responses of the engine system in Fig. 6 are

$$\begin{aligned} y_E(s) = &\left[I + (G_E^* + E_A)K_E\right]^{-1}(G_E^* + E_A)K_E y_{Ec}(s) \\ &+ \left[I + (G_E^* + E_A)K_E\right]^{-1} D_A y_{Ac}(s) \end{aligned} \tag{9}$$

Comparison of the decoupled engine system's input/output relationship of Eq. (3) with the truly coupled system's input/output relationship of Eq. (9) reveals that the additive interaction matrix $E_A(s)$ can affect both stability and performance of the engine feedback system. However, the disturbance interaction matrix $D_A(s)$ does not affect stability of the quasilinear system, since (as shown later) the characteristic polynomial of the closed-loop coupled system is independent of this matrix. Clearly, however, $D_A(s)$ has an impact on the engine control system performance. Commands into the flight control system $y_{Ac}(s)$ disturb the engine responses through $D_A(s)$ and appear as output disturbances to the engine control loops. Thus, if $D_A(s)$ is large, the closed-loop engine performance will suffer.

Quite significant is the fact that $E_A(s)$ can affect the interacting system's closed-loop stability. The closed-loop characteristic polynomial for the coupled system is

$$\phi_{cl}(s) = \phi_{ol}(s) \det\left\{I + \left[G_E^*(s) + E_A(s)\right]K_E(s)\right\} \tag{10}$$

Here the roots of $\phi_{ol}(s)$ are an aggregate of the poles of $K_E(s)$ and the poles of the system with only the airframe loops closed with $K_A(s)$, or the values of s for which $\det[I + G_A(s)K_A(s)] = 0$. These facts are derived in Appendix A. Now it can be shown from Nyquist stability theory[14] that the closed-loop system in Fig. 6 is assured to remain stable if the feedback loop is stable for $E_A(s) = 0$, and if

$$\det\left\{I + \left[G_E^*(j\omega) + \epsilon E_A(j\omega)\right]K_E(j\omega)\right\} \neq 0, \quad [0 < \epsilon < 1] \tag{11}$$

for all frequencies $\omega > 0$. It can further be shown that this is assured if

$$\bar{\sigma}\left[E_A(j\omega)K_E(j\omega)\right] < \underline{\sigma}\left[I + G_E^*(j\omega)K_E(j\omega)\right] \quad \text{for all } \omega > 0 \tag{12}$$

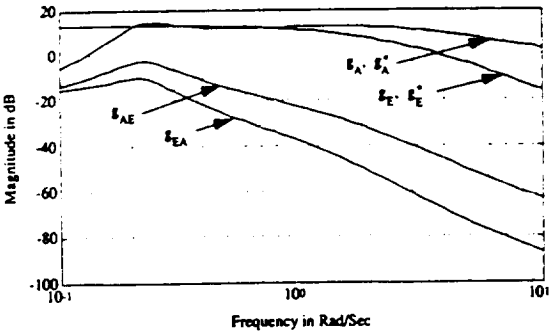

Fig. 8 Open-loop normalized transfer function magnitudes.

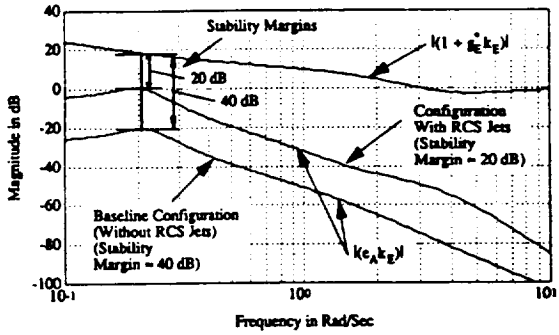

Fig. 9 Plot of Eq. (17), the scalar form of Eq. (12).

or if

$$\bar{\sigma}\left\{E_A(j\omega)\left[G_E^*(j\omega)\right]^{-1}\right\} < \underline{\sigma}\left\{I + \left[G_E^*(j\omega)K_E(j\omega)\right]^{-1}\right\} \quad \text{for all } \omega > 0 \tag{13}$$

where $\bar{\sigma}$ and $\underline{\sigma}$ denote the maximum and minimum singular values of a matrix, respectively.

These key inequalities are measures of the overall system's stability robustness with respect to uncertainties in airframe/engine interactions. In fact, the system's robustness can be indicated by plotting both sides of Eq. (12) or (13). It is evident that there will be loss of robustness at frequencies where $E_A(s)$ is "large" (i.e., if its maximum singular value is large). At these critical frequencies, a stability robustness margin may be defined as the distance between the left- and right-hand sides of Eq. (12) or (13). Since $E_A(s)$ is a strong function of the cross-coupling dynamics $G_{AE}(s)$ and $G_{EA}(s)$, small variations in elements of either $G_{AE}(s)$ or $G_{EA}(s)$ at some critical frequency may reduce this margin to zero and thus lead to the failure of the aforementioned stability criteria.

The significance of the preceding results may be seen more clearly by considering a single-input/single-output engine control system. Let the regulated engine response of interest be, for example, fan speed N_2, and, for a fixed nozzle area, let the control input be the main burner fuel flow rate w_F. In this case, the transfer function matrices $G_E^*(s)$, $\Delta_A(s)$, $K_E(s)$, and $E_A(s)$, as well as $D_A(s)$, reduce to scalars, denoted by $g_E^*(s)$, $\delta_A(s)$, $k_E(s)$, $e_A(s)$, and $d_A(s)$. Then Eq. (9) reduces to the scalar relationship

$$y_E(s) = \left[\frac{(g_E^* + e_A)k_E}{1 + (g_E^* + e_A)k_E}\right] y_{Ec} + \left[\frac{1}{1 + (g_E^* + e_A)k_E}\right] d_A y_{Ac} \tag{14}$$

Also, if all system transfer functions are assumed to be scalars, Eqs. (7) and (8) reduce to

$$e_A(s) = \delta_E - \frac{g_{EA}g_{AE}k_A}{1 + k_A(g_A^* + \delta_A)} \tag{15}$$

$$d_A(s) = \frac{g_{EA}k_A}{1 + k_A(g_A^* + \delta_A)} \tag{16}$$

Equation (15) shows clearly that $e_A(s)$ is a strong function of the frequency-dependent (weighted) product of $g_{EA}(s)$ and $g_{AE}(s)$. Hence, if either $g_{AE}(s)$ or $g_{EA}(s)$ (or both) are small and $\delta_E(s)$ is small at critical frequencies, then $e_A(s)$ will tend to be small at those frequencies.

The characteristic equations in Eq. (14) also show that if $e_A(s)$ is large, then gain and phase margins present in the decoupled engine loop transfer $[k_E(s)g_E^*(s)]$ may be eroded in the coupled engine loop transfer, as depicted in Fig. 7. However, from Eq. (12), stability of the coupled system is assured if

$$|e_A(j\omega)k_E(j\omega)| < |1 + g_E^*(j\omega)k_E(j\omega)| \quad \text{for all } \omega > 0 \tag{17}$$

which is the scalar form of Eq. (12).

Note that the focus of this analysis has been the effect of airframe dynamics on the engine loop. A dual analysis reveals how the interactions affect the airframe attitude loops. That is, the dual of Eq. (9) gives the airframe responses for the interacting system as

$$y_A(s) = \left[I + (G_A^* + E_E)K_A\right]^{-1}(G_A^* + E_E)K_A\, y_{Ac}(s) + \left[I + (G_A^* + E_E)K_A\right]^{-1}D_E\, y_{Ec}(s) \tag{18}$$

where the interaction matrices $E_E(s)$ and $D_E(s)$, given below, are the duals of $E_A(s)$ and $D_A(s)$:

$$E_E(s) = \Delta_A - G_{AE}\left[I + K_E(G_E^* + \Delta_E)\right]^{-1}K_E G_{EA} \tag{19}$$

$$D_E(s) = G_{EA}\left[I + K_E(G_E^* + \Delta_E)\right]^{-1}K_E \tag{20}$$

The airframe loops are assured to remain stable in the presence of interaction uncertainties as long as

$$\bar{\sigma}\left[E_E(j\omega)K_A(j\omega)\right] < \underline{\sigma}\left[I + G_A^*(j\omega)K_A(j\omega)\right] \quad \text{for all } \omega > 0 \tag{21}$$

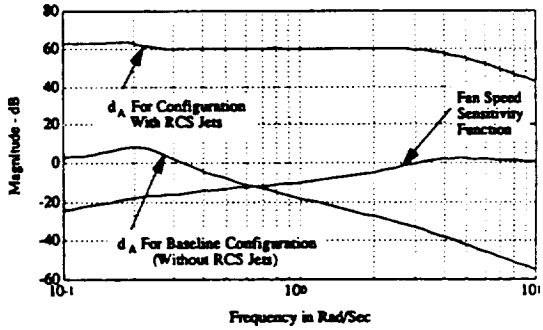

Fig. 10 Engine performance analysis.

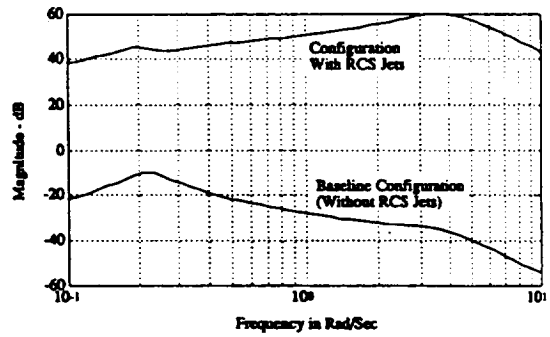

Fig. 11 Fan speed response from pilot pitch stick input (rpm/lb).

which is the dual of Eq. (12). Also, "large" $D_E(s)$, for example, will degrade the flying qualities of the flight control system due to disturbances arising from engine commands.

As a final note, this analysis does not necessarily require analytical models of the airframe and/or engine. Input/output mappings of the system could conceivably be experimentally obtained, and graphical data could be used exclusively to obtain plots of Eqs. (7), (8), and (12), for example.

Two Case Studies

The techniques just presented will now be used in the analysis of an airframe/engine system that has been the subject of several investigations of integrated flight and propulsion control.[1,3,4,14] The baseline vehicle to be considered is representative of a high-performance Short Takeoff and Landing (STOL) fighter aircraft equipped with a thrust-vectoring/thrust-reversing nozzle. The operating point under consideration is the approach-to-landing flight condition at an airspeed of $V_0 = 120$ kt and flight-path angle $\gamma_0 = -3$ deg. The quasilinear vehicle system model is that given in Refs. 10, 15, and 16. A second configuration will also be considered, which is identical to the baseline but with a high-pressure RCS added. Although significant airframe/engine coupling may be expected, the analysis will show that little critical interactions exist for the baseline configuration, and only one-directional coupling is present for the configuration that includes the RCS. Note also that, although the analysis herein involves only single-input/single-output systems, the last section presented a multivariable methodology and thus is not restricted to scalar systems.

For both cases the airframe's dynamics are aerodynamically unstable. The airframe flight control design objective is to stabilize the airframe's dynamics and obtain classical pitch rate and angle-of-attack responses from pilot pitch stick input δ_{stick}. The objective of the engine control law is to regulate the fan speed. The control laws for both cases are given in Appendix B.

Case 1

The open-loop system is described as

$$\begin{bmatrix} (K_{\delta\alpha}/K_{\delta q})\alpha + q \\ N_2 \end{bmatrix} = \begin{bmatrix} g_A(s) & g_{AE}(s) \\ g_{EA}(s) & g_E(s) \end{bmatrix} \begin{bmatrix} \delta_{pitch} \\ w_f \end{bmatrix} \tag{22}$$

where, for example,

$$g_A(s) = \frac{-14(s+0.03\pm0.07j)(s+0.6)(s+1.4)(s+3.6)(s+7)(s+90)}{(s+0.06\pm0.2j)(s+1.4)(s-1.5)(s+2)(s+3.6)(s+7)(s+90)}$$

$$g_E(s) = \frac{1.3(s+0.06\pm0.2j)(s-1.5)(s+2)(s+16\pm6j)(s+37)}{(s+0.06\pm0.2j)(s+1.4)(s-1.5)(s+2)(s+3.6)(s+7)(s+90)} \tag{23}$$

Note the unstable mode at 1.5 rad/s. From Appendix B, the control law is

$$\begin{bmatrix} \delta_{pitch} \\ w_f \end{bmatrix} = -\begin{bmatrix} K_{\delta q} & 0 \\ 0 & 6(s+\tfrac{1}{2})/s \end{bmatrix} \begin{bmatrix} (K_{\delta\alpha}/K_{\delta q})\alpha + q \\ N_2 \end{bmatrix} - \begin{bmatrix} K_{\delta st}/K_{\delta q} \\ 0 \end{bmatrix} \delta_{stick} \tag{24}$$

where w_f = fuel flow rate, and the pitch attitude control δ_{pitch}, the feedback gains $K_{\delta\alpha}$ and $K_{\delta q}$, and the pilot stick gain $K_{\delta st}$ are given in Appendix B. These control laws lead to gain crossover frequencies in the engine and aircraft pitch loops of approximately 3 and 5 rad/s, respectively.

Shown in Fig. 8 are the magnitudes of the input/output mappings in Eq. (22), as well as the mappings for the decoupled airframe and engine $g_A^*(s)$ and $g_E^*(s)$. To properly evaluate the relative sizes of the input/output relationships of the airframe and engine, the system must be normalized by, for example, estimates of the maximum values of the controls and responses. The values used to normalize this plant are given in Table 1 and are taken from Ref. 9.

Figure 8 reveals that the cross-coupling terms $g_{AE}(s)$ and $g_{EA}(s)$ are both smaller than the diagonal elements in Eq. (22) by approximately 40 dB for frequencies above 1 rad/s. (Recall that the loop gain cross-over frequencies are around 3-5 rad/s.) Also, since there are no visible differences in the plots of $g_A(s)$ and $g_A^*(s)$, and $g_E(s)$ and $g_E^*(s)$, $\Delta_A(s)$ and $\Delta_E(s)$ are quite small. Hence, from Eqs. (7), (8), (19), and (20), $e_A(s)$, $d_A(s)$, $e_E(s)$, and $d_E(s)$ should all be quite small, and it might be expected that airframe/engine interactions will be negligible. However, the complete analysis requires knowledge of candidate control laws, since feedback compensation could increase critical cross-coupling.

Shown in Fig. 9 are plots of both sides of the key inequality of the stability robustness analysis, Eq. (12) or (17). This figure shows that $|e_A k_E|$ for the baseline configuration is much less than $|1 + g_E^* k_E|$ throughout the frequency range shown. The stability margin, defined here as the minimum distance between the left- and right-hand sides of the inequality of Eq. (12) or (17), occurs near 0.2 rad/s and is approximately 40 dB for the baseline configuration. Therefore, the analysis indicates significant engine loop stability robustness against uncertainties in airframe/engine interactions.

Figure 10 presents the magnitude of the engine's fan speed sensitivity function $\{1/[1+(g_E+e_A)k_E]\}$ along with the magnitude of the engine loop disturbance interaction due to pilot input $d_A(j\omega)$ [Eq. (8) or (16)] for the baseline configuration. The spectrum of the engine response because of these disturbances, or N_2/δ_{stick}, is shown in Fig. 11, also labeled as the baseline configuration. This response is, of course, the product of the two terms plotted in Fig. 10. These plots reveal that the fan speed loop will reject disturbances arising from pilot pitch inputs, since $g_{EA}(j\omega)$ is small.

In summary, the analysis of this airframe/engine system description indicates that the additive and disturbance interaction effects $e_A(s)$ and $d_A(s)$ are small [and although not shown, $e_E(s)$ and $d_E(s)$ are small as well]. Hence, the coupling in this vehicle will not significantly degrade the closed-loop performance of both the airframe and engine subsystems; the system is therefore robust against interaction uncertainties and decentralized control laws appear quite adequate.

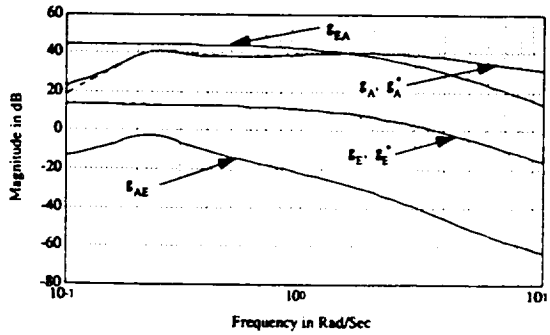

Fig. 12 Open-loop normalized transfer function magnitudes with pitch RCS control included.

Table 1 Estimates of maximum values of controls and responses

$q_{max} = 0.06$ rad/s
$\alpha_{max} = 3$ deg
$N_{2\,max} = 570$ rpm
$\delta_{TV\,max} = 10$ deg
$w_{f\,max} = 5000$ lb/h

Table 2 Additive perturbations of $g_{AE}(j\omega)$

Case	$\delta\lvert g_{AE}\rvert$, (rad/s)/(lb/h)
1	1.6
2	3.2
3	4.7
4	6.3
5	6.7

over the frequency range shown. Hence, strong one-directional coupling is indicated.

The large increase in the magnitude of $g_{EA}(j\omega)$ causes the magnitude of $d_A(j\omega)$ to significantly increase [see Eq. (16)], as shown in Fig. 10. This figure indicates that the engine loop can no longer effectively reject fan speed disturbances arising from pilot pitch stick inputs. In fact, Fig. 11 shows the significant increase in the magnitude of the fan speed response due to pilot pitch stick input over the baseline case.

Furthermore, the increase in magnitude of $g_{EA}(j\omega)$ causes an increase in magnitude of $e_A(j\omega)$ over the baseline configuration as well, as indicated in Fig. 9. Hence, stability robustness against uncertainties in airframe/engine interactions is reduced. Figure 9 shows that the stability margin is reduced from the baseline configuration to approximately 20 dB, again measured at 0.2 rad/s. It is worth noting that this critical frequency is well removed from the cross-over frequencies of the airframe and engine loops (3 and 5 rad/s). Note that in this situation small increases in the magnitude of $g_{AE}(j\omega)$ may cause a substantial increase in the additive interaction term $e_A(j\omega)$, since this term is a strong function of the product of $g_{AE}(j\omega)$ and $g_{EA}(j\omega)$ [Eq. (15)]. Hence, small variations in $g_{AE}(j\omega)$ may therefore cause significant degradation in stability robustness and/or performance. For these reasons, a sensitivity study will be performed on $g_{AE}(j\omega)$.

For this vehicle and control system configuration, the pitch trim occurs at a small thrust-vectoring angle δ_{TV}. Thus, engine

The airframe/engine system's closed-loop airframe transfer functions [see Eq. (18)] are

$$\alpha(s) = \frac{-0.1(s+0.06\pm0.2j)(s+30)}{(s+0.05\pm0.2j)(s+2.8\pm2.8j)}\,T_1(s)\left(\frac{\text{deg}}{\text{lb}}\right)\delta_{stick}(s) + \frac{-4e-4(s+2\pm0.6j)(s+4)(s+5)(s-76)}{(s+0.05\pm0.2j)(s+2.8\pm2.8j)}\,T_2(s)\left(\frac{\text{deg}}{\text{rpm}}\right)N_{2c}(s)$$

$$q(s) = \frac{-0.05s(s+0.07)(s+0.5)}{(s+0.05\pm0.2j)(s+2.8\pm2.8j)}\,T_1(s)\left(\frac{\text{rad/s}}{\text{lb}}\right)\delta_{stick}(s) + \frac{-4e-5(s+2)(s+3)(s+7\pm2j)(s-21)}{(s+0.05\pm0.2j)(s+2.8\pm2.8j)}\,T_2(s)\left(\frac{\text{rad/s}}{\text{rpm}}\right)N_{2c}(s)$$

where

$$T_1(s) = \frac{(s+0.4)(s+2\pm4j)(s+8)(s+90)}{(s+0.4)(s+2\pm4j)(s+8)(s+90)} \qquad T_2(s) = \frac{s}{(s+0.4)(s+2\pm4j)(s+8)(s+90)} \tag{25}$$

and where $T_1(s)$ is unity to the accuracy displayed, indicating that engine modes are essentially unobservable in the airframe responses. The transfer functions between the airframe responses and commanded fan speed N_{2c} are also quite small since the disturbance interaction effect $d_E(s)$ is small.

The closed-loop fan speed response [see Eq. (9) or (14)] for the airframe/engine system is

$$N_2(s) = \frac{-(s-2)(s+4\pm2j)(s+90)}{(s+0.4)(s+2\pm4j)(s+8)(s+90)}\,T_1(s)\left(\frac{\text{rpm}}{\text{rpm}}\right)N_{2c}(s) + \frac{-0.06(s-6)(s+7)(s-258)}{(s+0.4)(s+2\pm4j)(s+8)(s+90)}\,T_2(s)\left(\frac{\text{rpm}}{\text{lb}}\right)\delta_{stick}(s)$$

where

$$T_1(s) = \frac{(s+0.05\pm0.2j)(s+2.8\pm2.8j)}{(s+0.05\pm0.2j)(s+2.8\pm2.8j)} \qquad T_2(s) = \frac{s(s+0.4)(s+3\pm2j)}{(s+0.05\pm0.2j)(s+2.8\pm2.8j)} \tag{26}$$

As with the airframe responses, $T_1(s)$ is unity, indicating that airframe modes are essentially unobservable in the engine response. The fan speed response from pilot pitch stick input is quite small since $d_A(s)$ is small.

Case 2

Now consider the same vehicle with similar control laws but with pitch attitude control power enhanced by a combination of thrust vectoring and pitch RCS jets. RCS jets, which draw bleed flow from the engine's compressor, will directly influence the quality of airflow through the engine, thus increasing airframe/engine interactions. Models of the effects of bleed flow on the propulsion system were provided by the NASA Lewis Research Center. The control laws for this configuration are also detailed in Appendix B and are such that the airframe and engine control loops, cross-over frequencies, etc., are essentially the same as those for the baseline configuration.

The magnitudes of the elements of the plant transfer function matrix [Eq. (22)] are shown in Fig. 12. Again, the plant was normalized using the maximum values of control inputs and responses given in Table 1, and the maximum value of the pitch RCS jet nozzle area A_q was 1 in.^{2}. When compared with Fig. 8, this figure shows that the addition of pitch RCS control increases the magnitude of $g_{EA}(j\omega)$ by approximately 50 dB

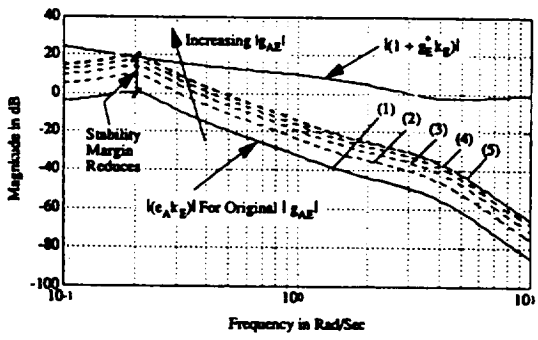

Fig. 13 Plot of Eq. (17) for various magnitudes of engine-to-airframe interactions, $|g_{AE}(j\omega)|$.

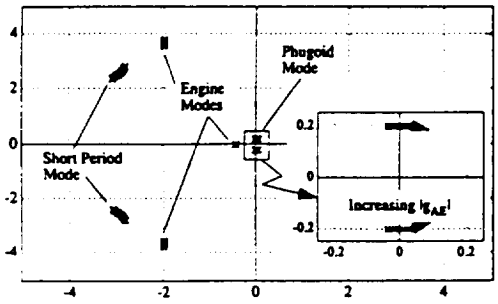

Fig. 14 Locus of the airframe/engine system's closed-loop poles as the magnitude of $g_{AE}(j\omega)$ is increased.

thrust transients will not generate large pitching moments, and this is the reason $g_{AE}(s)$ is small in this case. If the vehicle configuration was such that the trim thrust-vectoring angle were large, thus increasing the component of the thrust vector perpendicular to the airframe's longitudinal axis, engine thrust transients would create larger pitching moments. In such a case, $g_{AE}(s)$ would be larger.

Figure 13, like Fig. 9, shows the inequality of Eq. (17). This figure, however, displays $|e_A k_E|$ for various values of the magnitude of $g_{AE}(j\omega)$. Here,

$$g_{AE}(j\omega) = \left(|g_{AE}|_{\text{nominal}} + \delta|g_{AE}|\right) e^{j\phi_{AE}} \tag{27}$$

Table 2 lists the additive perturbations of the magnitude of $g_{AE}(j\omega)$ corresponding to the dashed curves in Fig. 13.

Figure 13 shows that $|e_A k_E|$ is much less than $|1 + g_E k_E|$ throughout the frequency range for the nominal magnitude of $g_{AE}(j\omega)$, and stability of the system is not in jeopardy. However, the stability margin reduces to zero ($|e_A k_E| = |1 + g_E^* k_E|$) at ≈ 0.2 rad/s when the magnitude of $g_{AE}(j\omega)$ is increased by only 6.7 (rad/s)/(lb/h) (case 5). From Fig. 12, note that $g_{AE}(j\omega)$, thus increased, would become comparable in magnitude to the other transfer functions in the system.

Figure 14 shows how the closed-loop eigenvalues of the system vary as the magnitude of $g_{AE}(j\omega)$ is increased. Higher frequency engine poles are not shown and do not vary to any great extent. However, this figure shows that a low-frequency (phugoid mode) instability does indeed occur at a frequency of 0.2 rad/s. Further, this instability occurs precisely for the increase in magnitude of $g_{AE}(j\omega)$ corresponding to case 5 in Fig. 13. It is also significant that the critical frequency of instability (0.2 rad/s) is not near the engine or airframe loop cross-over frequencies where phase margin is measured and that Eq. (17) correctly indicated that instability will first occur at this critical frequency due to variations in airframe/engine interactions.

Conclusions

Expressions were derived for additive and disturbance interaction matrices that may be used to quantify the significance of airframe/engine interactions on either the engine control loops or, for the dual analysis, the flight control loops. A technique for determining the stability robustness of the system against uncertainties in these interactions was presented. The size of the interaction matrices in critical frequency ranges, measured, for example, by their singular values, quantifies the effect of airframe/engine coupling on closed-loop stability and/or performance. The critical interaction matrices were shown to depend on the control compensation as well as the input/output characteristics of the airframe/engine system. If the system exhibits two-directional coupling, stability as well as performance may be compromised. Systems with one-directional coupling may preserve adequate stability robustness, although performance can be seriously affected.

This analysis was then applied to an airframe/engine system considered in previous integrated control studies, and two cases were presented. The baseline configuration was shown to exhibit few interactions. Classical decentralized control laws therefore appear quite suitable. However, the analysis revealed significant one-directional cross-coupling for a second control configuration with a reaction control system added. Inclusion of the RCS jets led to significant disturbances in the fan speed loop arising from pilot pitch inputs, and reduction in the stability robustness against variations in airframe/engine interactions was also recorded. The analysis accurately indicated the frequency at which instability would first occur due to these variations. Frequently, only engine-to-airframe interactions are thought to be of concern; however, this case clearly indicates strong airframe-to-engine coupling. In some previous IFPC studies only engine-to-airframe interactions were thought to be of concern. Although this may have been a valid assumption for the vehicle configurations examined, analysis methodologies should, in general, consider two-directional coupling.

Appendix A: Derivation of Eq. (10)

Let a state-space realization of the input/output mapping for the fully coupled aircraft/engine system be defined as

$$\begin{bmatrix}\dot{x}_A\\ \dot{x}_E\end{bmatrix} = \begin{bmatrix}A_A & A_{AE}\\ A_{EA} & A_E\end{bmatrix}\begin{bmatrix}x_A\\ x_E\end{bmatrix} + \begin{bmatrix}B_A & B_{AE}\\ B_{EA} & B_E\end{bmatrix}\begin{bmatrix}u_A\\ u_E\end{bmatrix}$$

$$\begin{bmatrix}y_A\\ y_E\end{bmatrix} = \begin{bmatrix}C_A & 0\\ 0 & C_E\end{bmatrix}\begin{bmatrix}x_A\\ x_E\end{bmatrix} \tag{A1}$$

and the mapping given as

$$\begin{bmatrix}y_A(s)\\ y_E(s)\end{bmatrix} = \begin{bmatrix}G_A(s) & G_{AE}(s)\\ G_{EA}(s) & G_E(s)\end{bmatrix}\begin{bmatrix}u_A(s)\\ u_E(s)\end{bmatrix} = [G(s)]\begin{bmatrix}u_A(s)\\ u_E(s)\end{bmatrix} \tag{A2}$$

with system characteristic polynomial

$$\phi_S(s) = \det\begin{bmatrix}sI - A_A & -A_{AE}\\ -A_{EA} & sI - A_E\end{bmatrix} \tag{A3}$$

Also let the state-space descriptions of the aircraft and engine compensation $K_A(s)$ and $K_E(s)$ be, respectively,

$$\dot{x}_{k_A} = A_{k_A}x_{k_A} + B_{k_A}\epsilon_{Ac}, \qquad u_A = C_{k_A}x_{k_A}$$

$$\dot{x}_{k_E} = A_{k_E}x_{k_E} + B_{k_E}\epsilon_{Ec}, \qquad u_E = C_{k_E}x_{k_E} \tag{A4}$$

where $\epsilon_{Ac}(s) = y_{Ac}(s) - y_A(s)$ and $\epsilon_{Ec}(s) = y_{Ec}(s) - y_E(s)$ are the inputs to the aircraft and engine compensators. The characteristic polynomials of these compensators are

$$\phi_{k_A}(s) = \det(sI - A_{k_A})$$

$$\phi_{k_E}(s) = \det(sI - A_{k_E}) \tag{A5}$$

Sought now is the state-space description of $G_E^*(s) + E_A(s)$, as presented in Fig. 6. Using Eqs. (A1) and (A4), and referring to Fig. 5, yields the desired result, or

$$\begin{bmatrix}\dot{x}_A\\ \dot{x}_E\\ \dot{x}_{k_A}\end{bmatrix} = \begin{bmatrix}A_A & A_{AE} & B_A C_{k_A}\\ A_{EA} & A_E & B_{EA}C_{k_A}\\ -B_{k_A}C_A & 0 & A_{k_A}\end{bmatrix}\begin{bmatrix}x_A\\ x_E\\ x_{k_A}\end{bmatrix}$$

$$+ \begin{bmatrix}B_{AE}\\ B_E\\ 0\end{bmatrix}u_E + \begin{bmatrix}0\\ 0\\ B_{k_A}\end{bmatrix}y_{Ac}$$

$$y_E = [0 \quad C_E \quad 0]\begin{bmatrix}x_A\\ x_E\\ x_{k_A}\end{bmatrix} \tag{A6}$$

Denoting this system as

$$\dot{x}_1 = A_1 x_1 + B_1 u_E + B_2 y_{Ac}$$
$$y_E = C_1 x_1 \tag{A7}$$

it can be shown[17] that the characteristic polynomial of this system $[G_E^*(s) + E_A(s)]$ is

$$\phi_1(s) = \det(sI - A_1) = \phi_S(s)\phi_{k_A}(s)\det\left[I + G_A(s)K_A(s)\right] \tag{A8}$$

Appending the state equation for the engine compensator $K_E(s)$ to the state equation for $G_E^*(s) + E_A(s)$ gives the state-space description of the open-loop system of Fig. 6 [or $[G_E^*(s) + E_A(s)]K_E(s)$] as

$$\begin{bmatrix}\dot{x}_1\\ \dot{x}_{k_E}\end{bmatrix} = \begin{bmatrix}A_1 & B_1C_{k_E}\\ 0 & A_{k_E}\end{bmatrix}\begin{bmatrix}x_1\\ x_{k_E}\end{bmatrix} + \begin{bmatrix}0\\ B_{k_E}\end{bmatrix}\epsilon_{Ec} + \begin{bmatrix}B_2\\ 0\end{bmatrix}y_{Ac}$$
$$y_E = [C_1 \quad 0]\begin{bmatrix}x_1\\ x_{k_E}\end{bmatrix} \tag{A9}$$

The characteristic polynomial of this system is

$$\phi_2(s) = \det\begin{bmatrix}sI - A_1 & -B_1C_{k_E}\\ 0 & sI - A_{k_E}\end{bmatrix} = \phi_1(s)\phi_{k_E}(s) \tag{A10}$$

Closing the (engine) loop in Fig. 6, the state-space equation for the entire closed-loop system is then

$$\begin{bmatrix}\dot{x}_1\\ \dot{x}_{k_E}\end{bmatrix} = \begin{bmatrix}A_1 & B_1C_{k_E}\\ -B_{k_E}C_1 & A_{k_E}\end{bmatrix}\begin{bmatrix}x_1\\ x_{k_E}\end{bmatrix} + \begin{bmatrix}0\\ B_{k_E}\end{bmatrix}y_{Ec} + \begin{bmatrix}B_2\\ 0\end{bmatrix}y_{Ac}$$
$$y_E = [C_1 \quad 0]\begin{bmatrix}x_1\\ x_{k_E}\end{bmatrix} \tag{A11}$$

and the characteristic polynomial for this closed-loop system is

$$\phi_{cl}(s) = \det\begin{bmatrix}sI - A_1 & -B_1C_{k_E}\\ B_{k_E}C_1 & sI - A_{k_E}\end{bmatrix}$$
$$= \phi_1(s)\phi_{k_E}(s)\det\left[I + (G_E^* + E_A)K_E\right] \tag{A12}$$

or

$$\phi_{cl}(s) = \phi_S(s)\phi_{k_A}(s)\det\left[I + G_A(s)K_A(s)\right]$$
$$\times \phi_{k_E}(s)\det\left[I + (G_E^* + E_A)K_E\right] \tag{A13}$$

Defining

$$\phi_{ol}(s) = \phi_S(s)\phi_{k_A}(s)\det\left[I + G_A(s)K_A(s)\right]\phi_{k_E}(s) \tag{A14}$$

gives

$$\phi_{cl}(s) = \phi_{ol}(s)\det\left[I + (G_E^* + E_A)K_E\right] \tag{A15}$$

which is the result presented as Eq. (10). Note that $\det[I + G_A(s)K_A(s)]$ is a rational function with denominator equal to $\phi_S(s)\phi_{k_A}(s)$. Thus, the roots of $\phi_{ol}(s)$ are the roots of $\phi_{k_E}(s)$, which are the poles of $K_E(s)$, and the values of s for which $\det[I + G_A(s)K_A(s)]$ equals zero.

Appendix B: Case Study Control Laws

The following defines the controls and measured responses for the case study vehicular system used in the analysis.

The aircraft control inputs are: δ_{TV} = nozzle thrust-vectoring angle, deg; A_q = pitch RCS jet nozzle area, in.^{2}; and δ_{flaps} = trailing-edge/leading-edge flap deflection angle, in.^{2}.

Table B1 Airframe control law gains

Gain	$\delta_{pitch} = \delta_{TV}$	$\delta_{pitch} = \delta_{TV} - 8A_q$
$K_{f\alpha}$, deg/deg	−2.9	−4.6
$K_{b\alpha}$, deg/deg	−3.7	−0.1
K_{bq}, deg/rad/s	−56.5	−2.3
$K_{b\delta st}$, deg/lb	−0.7	−0.5

The engine control input is w_f = main burner fuel flow rate, lb/h.

The aircraft responses are α = angle of attack, deg, and q = pitch rate, rad/s.

The engine response is N_2 = engine fan speed, rpm.

Two cases are presented with different control architectures for pitch attitude control, defined as δ_{pitch}. For the first case, pitch is controlled only by thrust vectoring, thus, $\delta_{pitch} = \delta_{TV}$. For the second case, pitch is controlled by a "blend" of both thrust vectoring and pitch RCS jet nozzle area, defined as $\delta_{pitch} = \delta_{TV} - 8A_q$.

The airframe's short period mode is unstable, and the control objective is to stabilize the short period mode and obtain a desired modal frequency near 4 rad/s and a damping ratio of 0.7. This is achieved by feeding back angle of attack and pitch rate to pitch control. The other airframe control objective is to increase the flight-path time constant (usually denoted as $1/\tau_{\theta 2}$) to approximately 0.5 rad/s. This is achieved by feeding back angle of attack to the flaps. Finally, the pilot stick force gain is adjusted to give an approximate Bode gain on $q(s)/\delta_{stick}(s)$ of 0.03 (rad/s)/lb. In summary, the airframe control laws are

$$\delta_{flaps} = -K_{f\alpha}\alpha$$
$$\delta_{pitch} = -K_{b\alpha}\alpha - K_{bq}q - K_{b\delta st}\delta_{stick} \tag{B1}$$

The values of the gains for both pitch control case are given in Table B1. Note that increased control power in using RCS jets led to the reduced feedback gains.

Finally, to regulate fan speed, fan speed is fed back through proportional plus integral compensation, with gains of −6 (lb/h)/rpm and −3 [(lb/h)s]/rpm, respectively.

The effects on system stability of the low gain flap loop are minimal. Therefore, the two-by-two system shown in Eq. (22) is obtained by first closing the flap loop and then combining the two aircraft attitude responses (α and q) to form one blended aircraft response.

Acknowledgments

This work was sponsored by the NASA Lewis Research Center under Grant NAG3-998. Peter Ouzts and Sanjay Garg have served as technical program managers.

References

[1]Smith, K., and Stewart, C., "A Survey of Control Law Options for Integrated Flight/Propulsion Control for Fighter STOL Approach," *Proceedings of the AIAA Guidance and Control Conference* (Seattle, WA), AIAA, New York, 1984 (AIAA Paper 84-1900).

[2]Shaw, P., Blumberg, K., Joshi, D., Anex, R., Vincent, J., and Skira, C., "Development and Evaluation of an Integrated Flight and Propulsion Control System," *Proceedings of the AIAA Joint Propulsion Conference* (Monterey, CA), AIAA, New York, 1985 (AIAA Paper 85-1423).

[3]Smith, K. L., "Design Methods for Integrated Control Systems," Aero Propulsion Lab., Air Force Wright Aeronautical Laboratories, AFWAL-TR-86-2103, Dayton, OH, Dec. 1986.

[4]Rock, S. M., Emami-Naeini, A., and Anex, R. P., "Propulsion Control Specifications in Integrated Flight/Propulsion Control Systems," *Proceedings of the AIAA/ASME/SAE/ASEE 24th Joint Propulsion Conference* (Boston, MA), AIAA, Washington, DC, 1988

(AIAA Paper 88-3236).

[5]Shaw, P. D., Rock, S. M., and Fisk, W. S., "Design Methods for Integrated Control Systems," Aero Propulsion Lab., Air Force Wright Aeronautical Laboratories, AFWAL-TR-88-2061, Dayton, OH, June 1988.

[6]Garg, S., Mattern, D. L., and Bullard, R. E., "Integrated Flight/Propulsion Control System Design Based on a Centralized Approach, *Proceedings of the AIAA Guidance, Navigation, and Control Conference* (Boston, MA), AIAA, Washington, DC, 1989 (AIAA Paper 89-3520).

[7]Berry, D., and Schweikhard, W., "Potential Benefits of Propulsion and Flight Control Integration for Supersonic Cruise Vehicles," based on SAE Paper 740478, 1974.

[8]Tape, R., Hartill, W., et al., "Vectoring Exhaust Systems for STOL Tactical Aircraft," *Journal of Engineering for Power, Transactions of the American Society of Mechanical Engineers*, July 1983.

[9]Garg, S., Mattern, D., Bright, M., and Ouzts, P., "*H*-Infinity Based Integrated Flight/Propulsion Control Design for a STOVL Aircraft in Transition Flight," NASA TM 103198, Aug. 1990.

[10]Schmidt, D., Schierman, J., and Garg, S., "Analysis of Airframe/Engine Interactions—An Integrated Control Perspective," *Proceedings of the AIAA/ASME/SAE/ASEE 26th Joint Propulsion Conference* (Orlando, FL), AIAA, Washington, DC, 1991 (AIAA Paper 90-1918).

[11]Peczkowski, J., and Stopher, S., "Nonlinear Multivariable Synthesis with Transfer Functions," *Proceedings of the 1980 Joint Automatic Control Conference*, Vol. 1, Pt. WA8-D, 1980.

[12]Sain, M., and Peczkowski, J., "Nonlinear Multivariable Design by Total Synthesis," Dept. of Electrical Engineering, Univ. of Notre Dame, Control System Technical Rept. 36, Notre Dame, IN, March 1985.

[13]Schmidt, D., and Schierman, J., "A Framework for the Analysis of Airframe/Engine Interactions and Integrated Flight/Propulsion Control," *Proceedings of the American Control Conference* (Boston, MA), June 1991, pp. 761–766.

[14]Doyle, J., and Stein, G., "Multivariable Feedback Design: Concepts for a Classical/Modern Synthesis," *IEEE Transactions on Automatic Control*, Vol. AC-26, No. 1, 1981, pp. 4–16.

[15]Schmidt, D., and Schierman, J., "Extended Implicit Model Following as Applied to Integrated Flight and Propulsion Control," *Proceedings of the AIAA Guidance, Navigation, and Control Conference* (Portland, OR), AIAA, Washington, DC, 1990 (AIAA Paper 90-3444).

[16]Schierman, J., and Schmidt, D., "Robust Control Synthesis for Integrated Flight and Propulsion Control," IEEE Conference on Decision and Control, Honolulu, HI, Dec. 1990.

[17]Kwakernaak, H., and Sivan, R., *Linear Optimal Control Systems*, Wiley-Interscience, New York, 1972.

ANALYSIS OF AIRFRAME/ENGINE INTERACTIONS - AN INTEGRATED CONTROL PERSPECTIVE

P/A
90A 40557

David K. Schmidt * and John D. Schierman**
Department of Mechanical and Aerospace Engr.
Arizona State University
Tempe, AZ 85287-6106

Sanjay Garg†
Lewis Research Center Group
Sverdrup Technology, Inc.
Cleveland, OH

Abstract

Techniques for the analysis of the dynamic interactions between airframe/engine dynamical systems are presented. Critical coupling terms are developed that determine the significance of these interactions with regard to the closed loop stability and performance of the feedback systems. A conceptual model is first used to indicate the potential sources of the coupling, how the coupling manifests itself, and how the magnitudes of these critical coupling terms are used to quantify the effects of the airframe/engine interactions. A case study is also presented involving an unstable airframe with thrust vectoring for attitude control. It is shown for this system with classical, decentralized control laws that there is little airframe/engine interaction, and the stability and performance with these control laws is not effected. Implications of parameter uncertainty in the coupling dynamics is also discussed, and effects of these parameter variations are also demonstrated to be small for this vehicle configuration.

Introduction

In the design of highly maneuverable fighter aircraft, or for those capable of short take off and vertical landing (STOVL), the propulsion system is frequently being considered for augmenting the lift and the maneuvering capabilities of the vehicle. Some designs include thrust vectoring to affect the attitude of the airframe and thrust reversing to quickly change flight velocity. Reaction control jets, drawing high pressure air from compressor bleed, can be used for attitude control of the aircraft. Compressor bleed can also be used for upper wing surface blowing to effect the boundary layer, thus the characteristics of the lifting surface. Changes within the engine that either effect the thrust or compressor pressure will therefore effect the airframe dynamics. Variable inlet geometry, used to effect the airflow through the engine can also effect the drag, pitch and yaw characteristics of the airframe.

On the other hand, the attitude dynamics of the airframe can effect the airflow at the inlet to the engine, thus effecting the quality of airflow the fan and compressor receive. Deflecting the thrust-vectoring nozzle angle or thrust reverser port can effect the back pressure on the turbine, especially if the nozzle is not choked. This change in back pressure propagates through the engine, and constitutes an unwanted disturbance.

Reference [1] presents particular examples of airframe/engine interactions from actual aircraft. This reference records that an F-104 airplane executing a rolling maneuver at Mach 1.87 experienced sideslip, which precipitated an engine surge. This sudden reduction in airflow caused the inlet shock to move forward, which then caused a diverging yawing motion. The phenomenon of engine unstart, in which the normal shock at the throat "pops" out of the inlet and causes large flow disturbances around the airframe is another example of airframe/engine interactions. Flight data was used to estimate that a double engine unstart, experienced by an XB-70 during a turn at Mach 3, would have produced a 2.5g acceleration and 30 deg/sec roll rate if the pilot had not taken corrective action. Data from a YF-12 airplane showed a yaw acceleration due to engine unstart was approximately 88% of the acceleration produced by maximum rudder deflection. The engine's bypass doors (BPD) were also seen to be as effective as the aileron and rudder controls in producing rolling and yawing accelerations. The rolling and yawing acceleration derivatives with respect to bypass door opening (measured as % of maximum opening) of the YF-12 at Mach 3 are 0.35 deg/sec^2/(percent max BPD) and 0.11 deg/sec^2/(percent max BPD), respectively. These derivatives with respect to aileron and rudder deflections (measured as % of maximum deflection) are 0.295 deg/sec^2/(percent max $\delta_{aileron}$) and 0.073 deg/sec^2/(percent max δ_{rudder}), respectively.

In the design of the control systems for such aircraft, as well as for the propulsion system, one must properly account for the dynamic coupling between the airframe and the engine, [2,3]. The purpose of this paper is not to discuss the design of a particular control system, but to indicate how the cross coupling dynamics between the airframe and engine can effect the airframe/engine system stability and performance, and to present methods for determining their significance from the perspective of control system design. This problem is similar to that discussed in [4], for example. However, this cited reference does not fully explore the problem of two-directional coupling between the airframe and engine systems. In this paper, the more general problem involving two-directional coupling is specifically treated. In the next section, the systems theory to be used will be developed and presented, followed by a demonstration of the theory and further discussion on the effects of the coupling. Finally, a classical decentralized control law, developed for a vehicle that has been the subject of several studies on integrated flight/propulsion control, will be evaluated, and it will be shown that for this vehicle system, critical cross coupling is not present.

System Analysis Preliminaries

Let the aircraft perturbation dynamics defined in the neighborhood of the relevant flight condition be described in terms of a matrix of transfer functions $G_A(s)$, where,

$$y_A(s) = G_A(s)u_A(s) \qquad (1)$$

with $y_A(s)$ the vector of aircraft responses (angle of attack, α, pitch rate, q, etc.), and $u_A(s)$ the vector of aircraft control inputs, (flap deflection, δ_F, thrust vector nozzle deflection, δ_{TV}, etc.) Likewise, let the engine dynamics defined in the neighborhood of the relevant operating condition be described in terms of a matrix of transfer functions $G_E(s)$, where,

* Professor, Assoc. Fellow, AIAA
** Doctoral Candidate, Student Member, AIAA
† Aerospace Technologist, Senior Member, AIAA

AIAA Paper No. 90-1918, presented at the Joint Propulsion Conf.

$$y_E(s) = G_E(s)u_E(s) \quad (2)$$

with $y_E(s)$ the vector of engine responses (turbine temperature, T_4, fan speed, N_2,etc.), and $u_E(s)$ the vector of engine control inputs, (fuel flow rate, w_F, nozzle area, A_7, etc.)

Each of these subsystems will be acted upon by feedback systems with control compensation matrix $K_A(s)$, for the aircraft flight control system, and $K_E(s)$, for the engine control system, as shown below, for example, where y_{E_c} is the vector of desired or commanded responses.

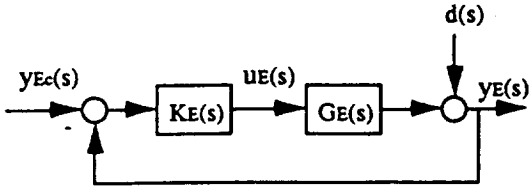

Figure 1 - Block Diagram of the Engine Feedback Loop

Here d(s) represents any outside disturbances acting on the system.

More generally, however, the aircraft/engine system input/output dynamics are

$$\begin{bmatrix} y_A(s) \\ y_E(s) \end{bmatrix} = \begin{bmatrix} G_A^*(s) & G_{AE}(s) \\ G_{EA}(s) & G_E^*(s) \end{bmatrix} \begin{bmatrix} u_A(s) \\ u_E(s) \end{bmatrix} = [G(s)] \begin{bmatrix} u_A(s) \\ u_E(s) \end{bmatrix} \quad (3)$$

where $G_A^*(s)$ and $G_E^*(s)$ are different from $G_A(s)$ and $G_E(s)$ above by the amounts $\Delta_A(s)$ and $\Delta_E(s)$, respectively, due to dynamic cross coupling between the engine and airframe subsystems. That is,

$$G_A^* = G_A + \Delta_A$$
$$G_E^* = G_E + \Delta_E \quad (3a)$$

Further, $G_{AE}(s)$ and $G_{EA}(s)$ represent input coupling also due to airframe/engine dynamic interactions. Specific examples of these coupling effects will follow. Note that $G_A^*(s)$, $G_E^*(s)$, $G_{AE}(s)$ and $G_{EA}(s)$ all have the same characteristic polynomial, denoted as $\phi_{ol}^*(s)$.

In the most general case, the control compensation matrix may have the form,

$$K(s) = \begin{bmatrix} K_A(s) & K_{AE}(s) \\ K_{EA}(s) & K_E(s) \end{bmatrix} \quad (4)$$

where the off-diagonal terms, $K_{AE}(s)$ and $K_{EA}(s)$, represent control cross-feeds between the airframe and engine subsystems. The entire system is then representable in the following block diagram.

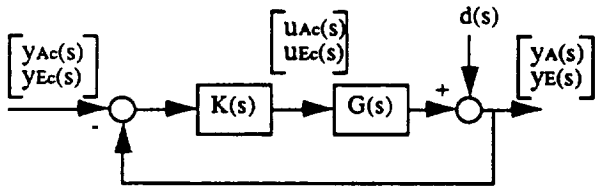

Figure 2 - Block Diagram of the Airframe/Engine Feedback System

Again, d(s) represents any disturbances acting on the system, such as atmospheric turbulence. This closed loop system is governed by the following input-output relationship, [5],

$$\begin{bmatrix} y_A(s) \\ y_E(s) \end{bmatrix} = [I + G(s)K(s)]^{-1}G(s)K(s) \begin{bmatrix} y_{Ac}(s) \\ y_{Ec}(s) \end{bmatrix} + [I + G(s)K(s)]^{-1}d(s) \quad (5)$$

For a tracking and regulation feedback system, the closed loop performance is defined in terms of how well the system's responses follow the commanded inputs and, at the same time, reject unwanted disturbances acting on the system. Thus, from the above equation, the performance objective of the control design is to make the matrix $[I + G(s)K(s)]^{-1}G(s)K(s)$ approximate the identity matrix in a certain frequency range, and make $[I + G(s)K(s)]^{-1} \approx 0$ over the frequency range where d(s) has significant power. Finally, the characteristic polynomial, $\Delta(s)$, for this closed loop system is, [5],

$$\Delta(s) = \phi_{ol}(s)\, \det[I + G(s)K(s)] \quad (6)$$

where the open loop system, G(s)K(s), has the characteristic polynomial $\phi_{ol}(s)$, which has roots equal to the poles of G(s) and K(s).

The above expressions represent a very general case. Typically, the approach used in the control design is simpler, in that control cross-feeds may be absent, (i.e. $K_{AE}(s)$ and $K_{EA}(s) = 0$). This implies the compensator matrix, K(s), is block diagonal. This situation may be represented as shown in the following block diagram, and will be the configuration considered in the remainder of this paper. The case with cross-feeds, although more complex algebraically, may be addressed in a manner similar to that presented here.

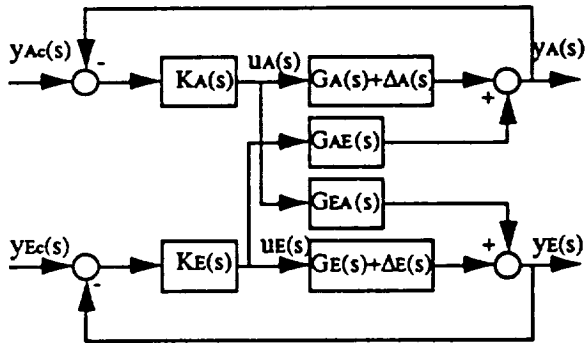

Figure 3 - Block Diagram of the Aircraft/Engine Loop With Diagonal K(s)

Each of the terms arising from the effects of the airframe/engine coupling are apparent in the above figure.

Note that if the compensation $K_A(s)$ and $K_E(s)$ are synthesized assuming that the system is decoupled, the engine loop would be as shown in Fig. 1. For this system, the responses would be given by

$$y_E(s) = [I + G_EK_E]^{-1}G_EK_E\, y_{Ec}(s) + [I + G_EK_E]^{-1}d(s) \quad (7)$$

which of course differ from those given by Eqn. (5) if coupling is present. Also, the closed loop characteristic polynomial for the system in Fig. 1 is

$$\Delta(s) = \phi_{ol}'(s)\, \det[I + G_E(s)K_E(s)] \quad (8)$$

where the roots of $\phi_{ol}'(s)$ are the poles of $G_E(s)$ and $K_E(s)$. Generally, the roots of this polynomial would not be a subset of

those for $\phi_{ol}(s)$ of Eqn. (6).

Figure 4 shows how the coupling dynamics, $G_{AE}(s)$ and $G_{EA}(s)$, and the airframe dynamics, $G_A^*(s)$, augmented with the airframe compensator, $K_A(s)$, can all be grouped together to form a transfer function that will be denoted as $E_A(s)$.

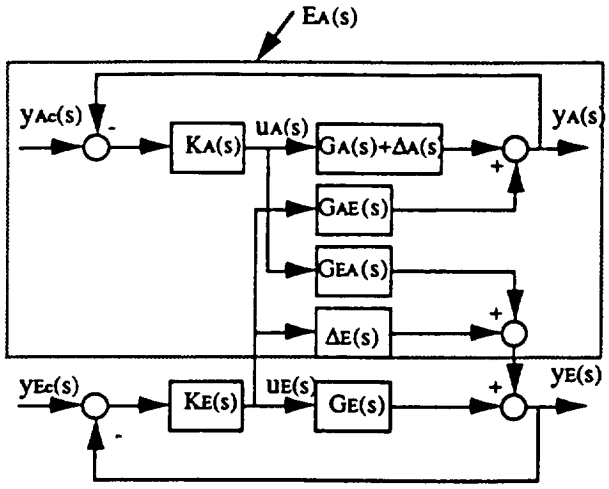

Figure 4 - Block Diagram of Aircraft/Engine Loop With the Airframe's Influences on the Engine Loop Grouped as $E_A(s)$

In other words, since $\Delta_A(s)$, $\Delta_E(s)$, $G_{AE}(s)$, and $G_{EA}(s)$ are not really zero, the engine loop is not that shown in Fig. 1, but rather that shown in the following figure.

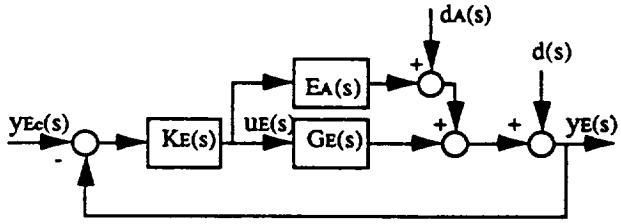

Figure 5 - Block Diagram of the Engine Loop for the Coupled Aircraft/Engine System

Here the effects of the actual coupling present are grouped into the terms $E_A(s)$ and $d_A(s)$. These expressions, given below, are obtained by block diagram manipulation of Fig. 4.

$$E_A(s) = \Delta_E - G_{EA}[I + K_A(G_A + \Delta_A)]^{-1}K_A G_{AE} \qquad (9)$$

$$d_A(s) = G_{EA}[I + K_A(G_A + \Delta_A)]^{-1}K_A y_{Ac}(s) \qquad (10)$$

The critical closed-loop coupling matrix $E_A(s)$ depends most importantly on the *product* of the input coupling transfer functions $G_{EA}(s)G_{AE}(s)$, as well as on the airframe control law, $K_A(s)$, the airframe dynamics, $G_A(s) + \Delta_A(s)$, and the change in the engine transfer function, $\Delta_E(s)$. Therefore, if Δ_E is "small", and if either $G_{AE}(s)$ or $G_{EA}(s)$ or both are "small," then $E_A(s)$ is "small." Also note that if the airframe subsystem includes no feedback ($K_A(s)=0$), $E_A(s)$ simply equals $\Delta_E(s)$, and $d_A(s)=0$. Note further that the disturbance $d_A(s)$ is independent of $G_{AE}(s)$. Hence this disturbance may be significant even though $G_{AE}(s)$ is small.

It can also be shown that the input/output characteristics of the system in Fig. 5, including the coupling effects, is

$$y_E(s) = [I + (G_E+E_A)K_E]^{-1}(G_E+E_A)K_E\, y_{Ec}(s) + [I + (G_E+E_A)K_E]^{-1}(d_A(s)+d(s)) \qquad (11)$$

and the closed loop characteristic polynomial for this system is

$$\Delta(s) = \phi_{ol}^{-1}(s)\det[I + (G_E + E_A)K_E] \qquad (12)$$

Here the roots of $\phi_{ol}^{-1}(s)$ are the poles of $K_E(s)$ and the poles of the system augmented with $K_A(s)$, or the values of s for which $\det[I + K_A G_A^*] = 0$. Eqn. (12) and this result are derived in Appendix A. Note here that $E_A(s)$ effects the characteristic polynomial, but $d_A(s)$ does not.

Eqn. (11) reveals how $E_A(s)$ can degrade engine control system performance. Also note how commands into the flight control system, $y_{Ac}(s)$, are transmitted to the engine responses through $d_A(s)$. Eqn. (11) also shows that this term enters into the engine responses the same way as any other disturbances, d(s). Thus, the commanded inputs into the aircraft (from the pilot) act as additional disturbances to the engine.

Perhaps more significant, Eqn. (12) shows that the system's closed-loop characteristic polynomial is affected by $E_A(s)$, thus $E_A(s)$ can clearly effect the stability. It can be shown from Nyquist stability theory, [5,6], that the closed loop system in Fig. 5 is assured to remain stable if the loop is stable for $E_A(s)=0$, and if

$$\det[I + (G_E + \varepsilon E_A)K_E] \neq 0\,,\ [0<\varepsilon<1] \qquad (13)$$

for all frequency. It can further be shown that Eqn. (13) is assured if

$$\sigma_{max}(E_A K_E) < \sigma_{min}(I+G_E K_E) \qquad (14)$$

for all frequency, where σ denotes the singular value of a matrix. Thus, it is evident from this inequality that there will be loss of stability robustness for "large" $E_A(s)$, (i.e., if its maximum singular value is large.)

Consider now a single-input/single-output engine control system. For example, the engine response of interest may be fan speed, N_2, and, for a fixed nozzle area, the input to control the fan speed may be the main burner fuel flow rate, w_F. In this case, the transfer function matrices $G_E(s)$, $K_E(s)$, and $E_A(s)$, as well as $d_A(s)$, reduce to scalars, denoted by $g_E(s)$, $k_E(s)$ and $e_A(s)$, etc. Then Eqn. (11) reduces to the scalar relationship

$$y_E(s) = \frac{(g_E + e_A)k_E}{1 + (g_E + e_A)k_E} y_{Ec}(s) + \frac{1}{1 + (g_E + e_A)k_E}(d_A(s) + d(s)) \qquad (15)$$

If all transfer functions are assumed for the moment to be scalars, Eqns. (9) and (10) reduce to,

$$e_A(s) = \delta_E - \frac{g_{EA}g_{AE}k_A}{1 + k_A(g_A+\delta_A)} \qquad (16)$$

$$d_A(s) = \frac{g_{EA}k_A}{1 + k_A(g_A+\delta_A)}\, y_{Ac}(s) \qquad (17)$$

Note again that if δ_E is small, and if either $g_{EA}(s)$ or $g_{AE}(s)$ or both are small, then $e_A(s)$ is small.

Eqn. (15) shows that if $e_A(s)$ is large, then gain and phase margins present in the $k_E(s)g_E(s)$ loop transfer may be eroded, as depicted in Fig. 6. But from Eqn. (14), this will not occur if

$$|e_A k_E| << |1 + g_E k_E| \qquad (18)$$

for all frequencies.

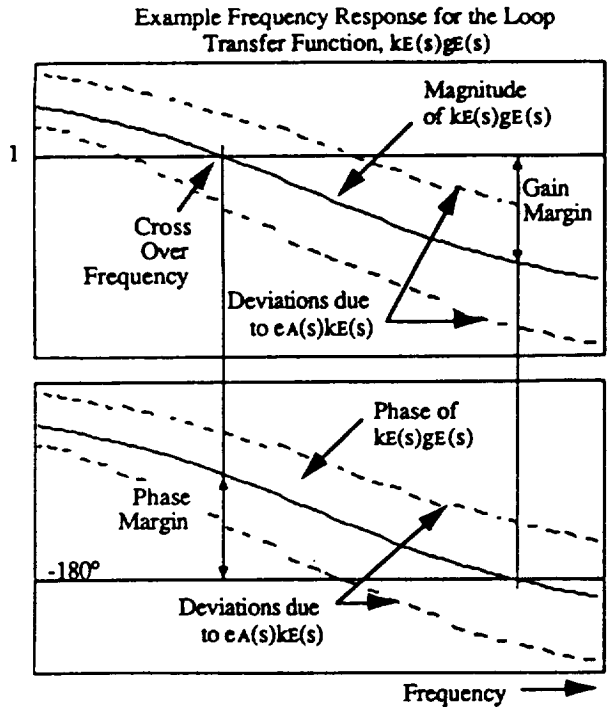

Figure 6- Example Loop Transfer Frequency Response or Open Loop Bode Plot

In all the above discussion, the focus has been on the effect of the airframe on the engine loop. Of course, a dual situation is present in that the engine also affects the airframe loop. In designing $K_A(s)$, the flight control designer must obtain airframe responses to pilot inputs that meet the flying quality specifications. These specifications require a pure aircraft-like modal response, and certain frequencies and dampings for these modes. Consider the dual of Eqn. (15), that is, the equation for the aircraft response,

$$y_A(s) = \frac{(g_A + e_E)k_A}{1+(g_A + e_E)k_A} y_{Ac}(s) + \frac{1}{1+(g_A + e_E)k_A}(d_E(s) + d(s))$$

where the coupling term $e_E(s)$ models the effect of the engine on the airframe attitude loop. If $e_E(s)$ is small, the aircraft response transfer functions will exhibit almost perfect pole-zero cancellations of the engine modes. Thus, only airframe modes will be dominant, as desired. This cannot be assured if $e_E(s)$ is large. Furthermore, if the disturbance from the engine, $d_E(s)$, is significant, it will degrade the flying qualities.

The final topic is that of model uncertainty, or uncertainty in all the system model transfer functions. Returning the focus to the engine loop, uncertainty can be modeled as additive dynamics just like $E_A(s)$. Hence, uncertainty just adds directly to $E_A(s)$ and therefore has the same effect on the loop. With modeling uncertainty, the engine loop in Fig. 5 may be considered changed to that shown below.

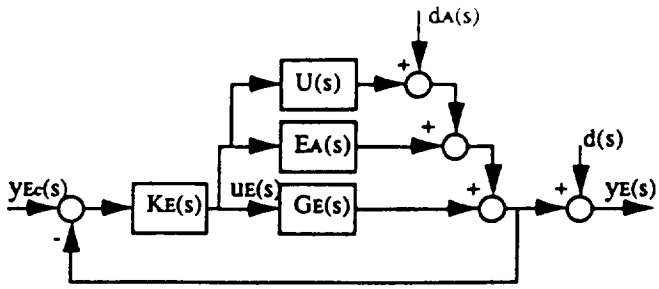

Figure 7 - Engine Loop with Coupling and Model Uncertainty

Here any additional model uncertainty is represented by the block U(s). The basic effect of this uncertainty is to merely increase the "effective" additive dynamics from $E_A(s)$ to $E_A(s)+U(s)$. But the problem of obtaining a model, or even a bound on U(s) is difficult, and currently is the subject of research.

Sources of Cross Coupling

Consider first a vehicle to be controlled with thrust vectoring, as shown in Fig. 8. The pitch attitude, θ, is to be controlled by the nozzle deflection angle δ_{TV}.

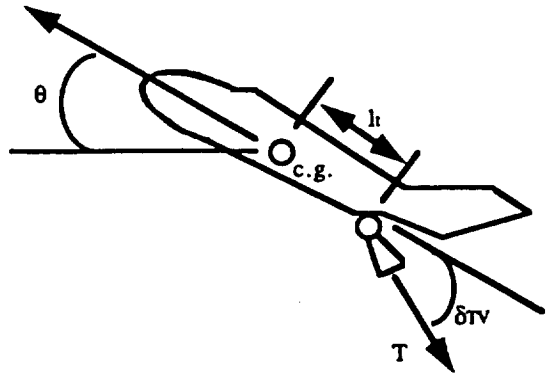

Figure 8 - Vehicle Pitch Attitude and Nozzle Thrust Vectoring Angle

Assuming some aerodynamic pitch damping, C_θ', is present, and ignoring the plunge degree of freedom, the attitude equation is

$$\Sigma M_{cg} = I_{yy}\ddot{\Theta} + C_\theta'\dot{\Theta} = -T\, l_t \sin(\delta_{tv}) \qquad (19)$$

where I_{yy} is the mass moment of inertia of the aircraft about its center of gravity.

Now consider the following block diagram for describing the possible interactions between the airframe and engine.

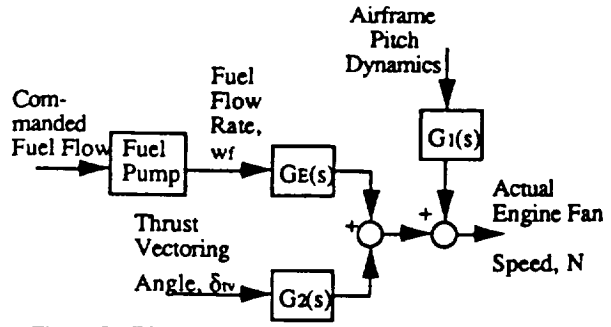

Figure 9 - Block Diagram of the Engine Influenced By the Airframe

The thrust vectoring is used to control the aircraft's pitching motion. However, if the nozzle is not choked and the augmentor pressure changes due to the re-directed engine exhaust, this may change the back pressure on the turbine, which will affect the fan speed. These dynamics are represented in the above figure by $G_2(s)$. The airframe pitching motion will effect the air flow at the inlet, which will effect the flow conditions at the compressor face. This effect is represented by $G_1(s)$. In this example, it is considered that the nozzle area is fixed so that the engine fan speed would be controlled by the fuel flow rate, w_f.

Let the fan speed dynamics be modeled here as a first order lag with a time constant of $1/\tau_E$, and let the fan speed equation of motion be

$$\dot{N} = -\tau_E N + \tau_{Eo} w_f + C_\delta \delta_{tv} + C_A \theta \tag{20}$$

where the parameter C_A reflects interactions from the pitching dynamics and the parameter C_δ reflects the effect of δ_{TV} on the fan speed. Although for this model these coupling terms are considered constants, these effects may actually turn out to have dynamics.

Considering the outputs of interest to be pitch angle and engine speed, the linearized model leads to the following

$$\begin{bmatrix} \dot{\theta}(s) \\ N(s) \end{bmatrix} = \begin{bmatrix} g_A^*(s) & g_{AE}(s) \\ g_{EA}(s) & g_E^*(s) \end{bmatrix} \begin{bmatrix} \delta_{TV} \\ w_f \end{bmatrix} \tag{21}$$

where,

$$g_A^*(s) = \frac{K_\delta s(s+\tau_E) + C_E C_\delta s}{\phi_{ol}^*(s)} \qquad g_{AE}(s) = \frac{C_E \tau_{Eo} s}{\phi_{ol}^*(s)}$$

$$g_{EA}(s) = \frac{C_A K_\delta + C_\delta s(s+C_\theta)}{\phi_{ol}^*(s)} \qquad g_E^*(s) = \frac{\tau_{Eo} s(s+C_\theta)}{\phi_{ol}^*(s)} \tag{22}$$

and the open loop characteristic polynomial is

$$\phi_{ol}^*(s) = s(s+C_\theta)(s+\tau_E) - C_A C_E \tag{23}$$

where:

$$C_\theta = C_\theta^{\cdot}/I_{yy}$$

$$K_\delta = -(T_o\, l_t \cos(\delta_{tv_o}))/I_{yy}$$

$$C_E = -(C_t\, l_t \sin(\delta_{tv_o}))/I_{yy}$$

T_o = trim thrust

δ_{tv_o} = trim thrust vectoring nozzle angle

$t = C_t N$ = small perturbation thrust

C_t = constant (assumed)

N = small perturbation engine fan speed

Note that the term C_E reflects the engine's influence on the airframe's dynamics.

Under the assumption that no interactions between the airframe's attitude dynamics and the engine dynamics exist, or C_A, C_E and C_δ are all zero, the input coupling dynamics, $g_{AE}(s)$ and $g_{EA}(s)$, are both zero, and the airframe transfer function reduces to

$$g_A(s) = \frac{K_\delta s}{s(s+C_\theta)} \tag{24}$$

Likewise, the engine transfer function reduces to

$$g_E(s) = \frac{\tau_{Eo}}{(s+\tau_E)} \tag{25}$$

Now take the following for the airframe pitch compensation:

$$k_A(s) = (\omega_{c\theta}/K_\delta)\frac{(s+C_\theta)}{s} \tag{26}$$

This leads to an augmented airframe transfer function that is a first order lag, with a pole at $-\omega_{c\theta}$. Finally, let the engine compensator, $k_E(s)$, be simply a gain k_E.

With the model and these control laws,

$$e_A(s) = \frac{-\omega_{c\theta} C_E(\tau_{Eo}/K_\delta)(s+C_\theta)[C_A K_\delta + C_\delta s(s+C_\theta)]}{\phi_{ol}^*(s)\phi_{ol}^*(s)\left[1 + \frac{\omega_{c\theta}(1/K_\delta)(s+C_\theta)(K_\delta(s+\tau_E)+C_E C_\delta)}{\phi_{ol}^*(s)}\right]} + \frac{\tau_{Eo} C_E C_A}{\phi_{ol}^*(s)(s+\tau_E)} \tag{27}$$

Clearly, if C_E is small, or if $g_{EA}(s)$ is small, then $e_A(s)$ is small. Note further that as the airframe crossover frequency $\omega_{c\theta}$ is increased, $e_A(s)$ is increased. Hence for all other things equal, a tighter airframe control loop can have a dilaterious effect on the engine loop.

Using the following numerical values, the system's open-loop transfer function magnitudes are shown in Fig. 10.

Model parameters: $K_\delta = -0.08$, $C_\theta = 1.1$, $\tau_{Eo} = 0.78$, $\tau_E = 1.4$

Design parameters: $\omega_{c\theta} = 6$, $k_E = 9$

Coupling parameters: $C_E = 1.e\text{-}05$, $C_A = 10$, $C_\delta = 0$

These parameter values were chosen by approximately matching the frequency responses of the more complete system model to be discussed in the case study of the next section. Note that $g_{AE}(s)$ is very small, as are $\Delta_A(s)$ and $\Delta_E(s)$.

The size of the product of the input coupling transfer functions, and the coupling transfer function $e_A(s)$ are shown in Fig. 11. Clearly both are small as expected, and hence, the coupling effects will not be significant. The size of $k_E e_A(s)$, compared to the loop transfer, or open loop Bode, for the engine loop is shown in Fig. 12. The fact that the loop transfer is much larger at all frequencies, along with Eqns. (15) and (18), assures that the coupling effects are truly small. The gain and phase margins of the engine loop are unaffected, as are the closed loop transfer functions, as shown below. For the completely decoupled system, the closed-loop transfer functions are

$$\frac{\theta(s)}{\delta_p(s)} = \frac{6(s+1.1)}{(s+1.1)(s+6)}$$

$$\frac{N(s)}{N_c(s)} = \frac{7.02}{(s+8.42)}$$

while with the parameter values given above, the closed loop transfer functions for the coupled system are

$$\frac{\theta(s)}{\delta_p(s)} = \frac{6(s+1.1)(s+8.42)}{(s+1.1)(s+6)(s+8.42)}$$

$$\frac{N(s)}{N_c(s)} = \frac{7.02(s+1.1)(s+6)}{(s+1.1)(s+6)(s+8.42)}$$

Clearly, for the parameter values selected for this system, the coupling is not significant.

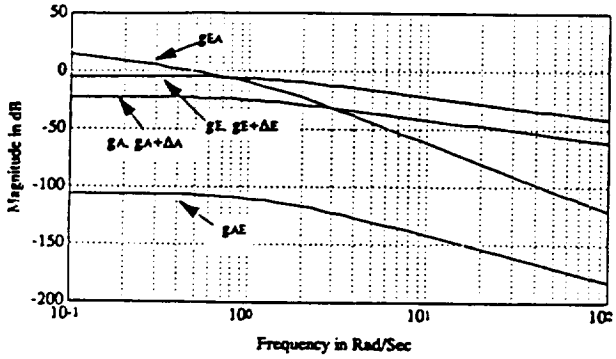

Figure 10 - Open Loop Transfer Function Magnitudes

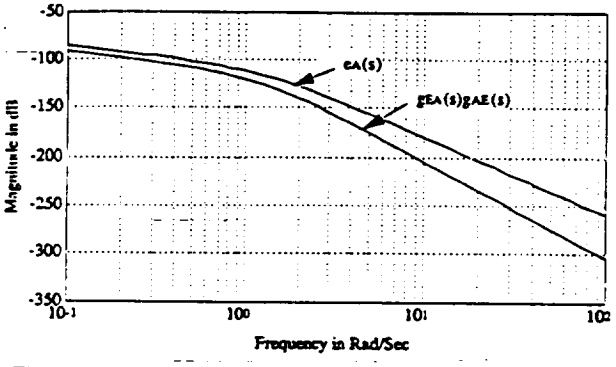

Figure 11 - Magnitudes of $e_A(s)$ and the Product $g_{EA}(s)g_{AE}(s)$

Now consider increasing the coupling parameters to

$$C_E = 0.025,\ C_A = 12,\ C_\delta = -3.5$$

The closed loop transfer functions become

$$\frac{\theta(s)}{\delta_p(s)} = \frac{6(s+1.1)(s+9.514)}{(s+1.093)(s+7.214\pm2.267j)}$$

$$\frac{N(s)}{N_c(s)} = \frac{7.02(s+1.1)(s+6)}{(s+1.093)(s+7.214\pm2.267j)}$$

Now, there is no longer accurate cancellations of the engine modes in the airframe response, and airframe modes in the engine response. However, in this case the stability robustness is still not greatly effected. As shown in Fig. 13, $e_A k_E(s)$ is still quite small near the engine loop cross-over frequency region (≈ 7 rad/sec,) so gain and phase margins of this loop would not be eroded.

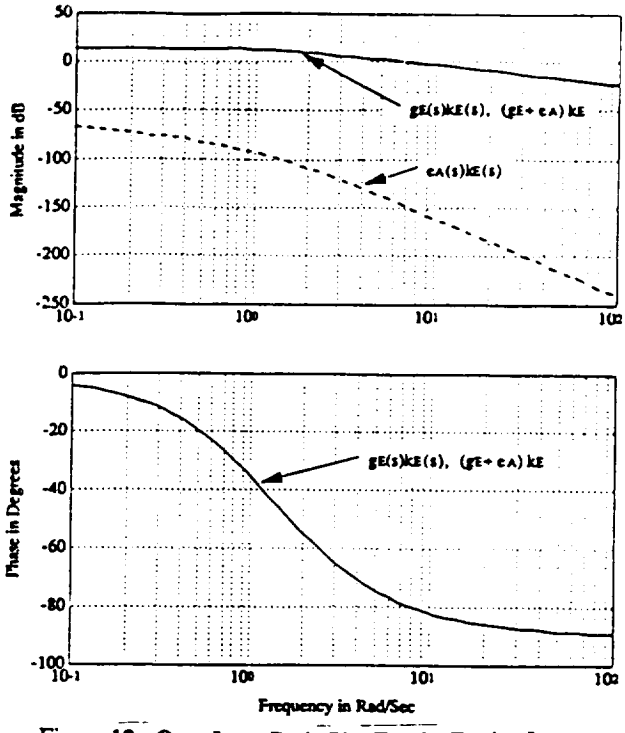

Figure 12 - Open Loop Bode Plot For the Engine Loop

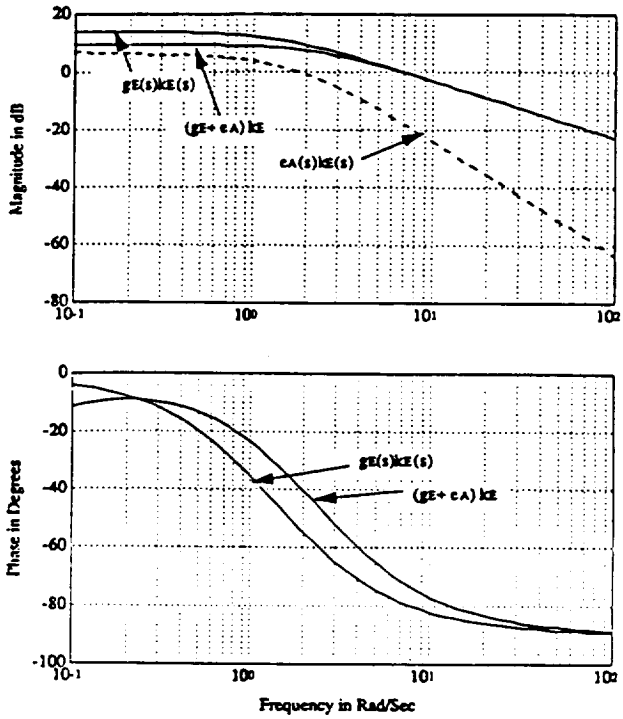

Figure 13 - Open Loop Bode Plot For the Engine Loop

A Case Study

Using the techniques just presented, attention will be directed to the analysis of an airframe/engine system that has been the subject of several studies of integrated flight and engine control, [e.g. 7]. The vehicle to be considered is representative of a high performance fighter aircraft with 2-D thrust vectoring and thrust reversing. The vehicle dynamics are linearized about the Short Take Off and Landing (STOL) approach-to-landing reference condition at an airspeed of V_o = 120 Knots and flight path angle γ_o = -3°. The system states are

$$\vec{x} = [u, w, q, \theta, N_2, N_{2.5}, P_6, T_{41B}]^T$$

where, the "aircraft" states are:

u = body axis forward velocity (ft/sec)
w = body axis plunge velocity (ft/sec)
q = pitch rate (rad/sec)
θ = pitch angle (radians)

and the "engine" states are:

N_2 = engine fan speed (rpm's)
$N_{2.5}$ = engine compressor speed (rpm's)
P_6 = engine mixing plane pressure (psia)
T_{41B} = high pressure turbine temperature (°R)

The control inputs used in this study are:

$$\vec{u} = [\delta_{flaps}, \delta_{TV}, w_f]^T$$

where,

δ_{flaps} = trailing edge and leading edge flap deflection (deg)
δ_{TV} = nozzle thrust vectoring angle (deg)
w_f = main burner fuel flow rate (#/hr)

The state space description for the system is given in Appendix B. The aircraft's attitude dynamics are to be controlled by thrust vectoring. For this model the nozzle throat area is not considered as an input, therefore, only the fuel flow rate is used to control the engine fan speed.

Classical feedback control laws were synthesized for the airframe and engine by considering each subsystem separately, and treating them as non-interacting. The open loop thrust vectoring angle to pitch rate and airframe plunge acceleration transfer functions are

$$\frac{q(s)}{\delta_{tv}(s)} = \frac{-0.0797s(s+0.1894\pm0.101j)}{(s+0.05681\pm0.2154j)(s-1.065)(s+1.472)} \left(\frac{rad/sec}{deg}\right)$$

$$\frac{N_z(s)}{\delta_{tv}(s)} = \frac{0.02127s(s+0.02456)(s+6.984)}{(s+0.05681\pm0.2154j)(s-1.065)(s+1.472)} \left(\frac{g's}{deg}\right)$$

The airframe dynamics are aerodynamically unstable. The flight control design objective is to obtain classical longitudinal aircraft responses given by,

$$\frac{q(s)}{\delta_{sl}(s)} = \frac{K_q\, s(s + 1/\tau_{\theta_1})\,(s + 1/\tau_{\theta_2})}{(s^2 + 2\zeta_{ph}\omega_{ph}\, s + \omega_{ph}^2)(s^2 + 2\zeta_{sp}\omega_{sp}\, s + \omega_{sp}^2)}$$

$$\frac{N_z(s)}{\delta_{sl}(s)} = \frac{K_{Nz}(s + 1/\tau_{N_1})\,(s + 1/\tau_{N_2})(s + 1/\tau_{N_3})}{(s^2 + 2\zeta_{ph}\omega_{ph}\, s + \omega_{ph}^2)(s^2 + 2\zeta_{sp}\omega_{sp}\, s + \omega_{sp}^2)}$$

(Phugoid Mode) (Short Period Mode) (28)

to stabilize the short period mode, and achieve a modal frequency of 4 rad/sec and a damping ratio of 0.707. This may be achieved by feeding back angle of attack and pitch rate with feedback gains of 3.934 (deg)/(deg) and 57 (deg)/(rad/sec), respectively, using the thrust vectoring control. Also, the flight path time constant, $1/\tau_{\theta 2}$, must be increased to approximately 0.52 rad/sec. This may be achieved by feeding back angle of attack, with a feedback gain of -2.897 (deg)/deg), to the flap. For the aircraft *decoupled* from the engine, these feedback gains give the following closed-loop aircraft transfer functions for pilot input, $\delta_p(s)$, to pitch rate and plunge acceleration,

$$\frac{q(s)}{\delta_p(s)} = \frac{-0.05369s(s+0.07352)(s+0.5231)}{(s+0.03065\pm0.1703j)(s+2.885\pm2.893j)} \left(\frac{rad/sec}{lbs}\right)$$

$$\frac{N_z(s)}{\delta_p(s)} = \frac{0.01687s(s+0.003983)(s+10.46)}{(s+0.03065\pm0.1703j)(s+2.885\pm2.893j)} \left(\frac{g's}{lbs}\right)$$

The objective of the engine control design is to regulate the fan speed. Proportional plus integral compensation will be used, with gains of -6 (lb/hr)/rpm and -3 ((lb/hr)sec)/rpm, respectively. With these control laws, the loop gain crossover frequencies for the thrust vectoring and the engine loops are both between 1 and 10 rad/sec, and gain and phase margins of the fuel flow rate loop appear adequate. The open-loop Bode plots for these loops are shown in Figs. 14 and 15 below.

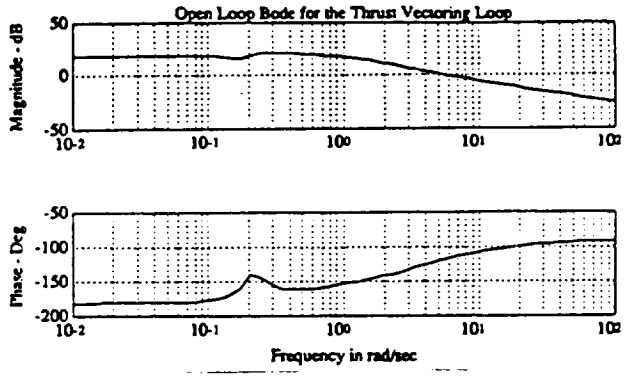

Figure 14 - Thrust Vectoring Loop Transfer Frequency Response

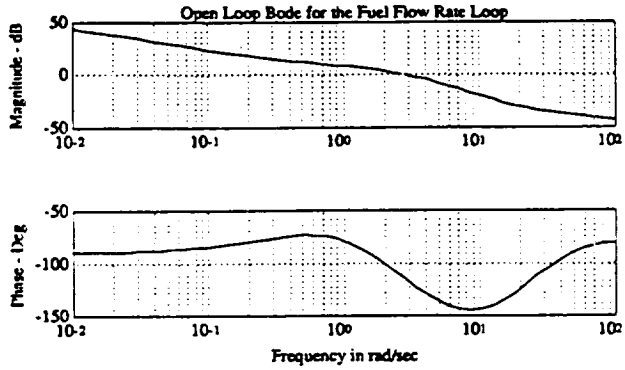

Figure 15 - Fuel Flow Rate Loop Transfer Frequency Response

With this decoupled design, the actual *coupled* aircraft/engine system will now be evaluated in terms of the significance of the subsystem interactions. First, the magnitudes of the four transfer functions, analogous to those in Eqn. (21), are shown in Fig. 16. Note, as with the simpler model discussed previously, the pitch-rate-to-fuel-flow transfer function, $g_{AE}(s)$, is small, along with $\Delta_A(s)$ and $\Delta_E(s)$. Shown in Fig. 17 is the critical cross-coupling transfer function $e_A(s)$, and its small magnitude is apparent. Finally, the size of $e_A(s)k_E(s)$ is compared to the engine loop transfer in Fig. 18. Clearly, the gain and phase margins in this loop will not be degraded due to this small term. Furthermore, the effects of cross coupling on

the closed-loop performance is likewise not expected to be significant for this system.

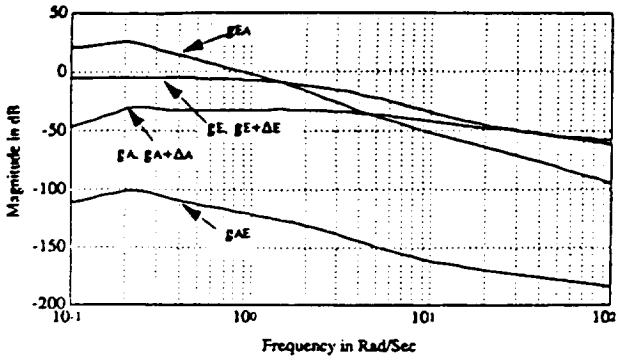

Figure 16 - Open Loop Transfer Function Magnitudes

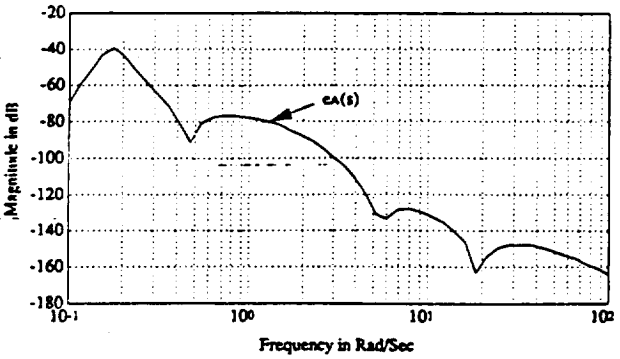

Figure 17 - Magnitude of the $e_A(s)$ Transfer Function

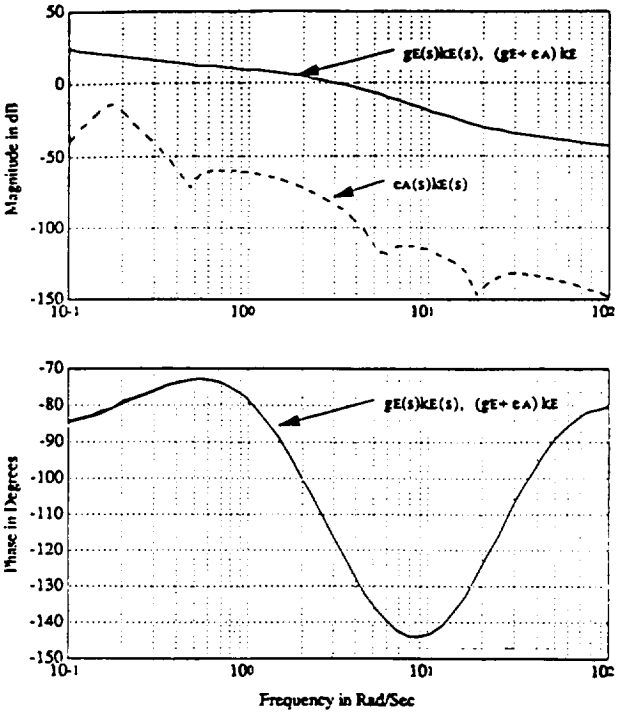

Figure 18 - Open Loop Bode Plot for the Engine Loop

The closed loop transfer functions for the airframe responses, for the *fully coupled* system and the decentralized control laws above are

$$\frac{q(s)}{\delta_p(s)} = \frac{-0.05369s(s+0.07279)(s+0.5232)}{(s+0.03029\pm0.1704j)(s+2.885\pm2.893j)}\,T(s)$$

$$\frac{N_z(s)}{\delta_p(s)} = \frac{0.01687s(s+0.003275)(s+10.46)}{(s+0.03029\pm0.1704j)(s+2.885\pm2.893j)}\,T(s)$$

where, (29)

$$T(s) = \frac{(s+0.4198)(s+1.99\pm3.535j)(s+8.014)(s+89.67)}{(s+0.4198)(s+1.99\pm3.535j)(s+8.014)(s+89.67)}$$

(Note that these transfer functions are 9th order. The additional pole is due to the integral control of engine fan speed.) The transfer function T(s) is essentially unity. The transfer function for the engine fan speed response to a commanded engine fan speed for the *decoupled* system is

$$\frac{N_2(s)}{N_{2c}(s)} = \frac{0.1469s(s+16.44\pm5.89j)(s+36.93)}{(s+0.4195)(s+1.99\pm3.535j)(s+8.014)(s+89.67)}$$

The companion transfer function for the same control laws on the *coupled* system is

$$\frac{N_2(s)}{N_{2c}(s)} = \frac{0.1469s(s+16.43\pm5.89j)(s+36.94)}{(s+0.4198)(s+1.99\pm3.535j)(s+8.014)(s+89.67)}\,T(s)$$

where, (30)

$$T(s) = \frac{(s+0.0303\pm0.1704j)(s+2.885\pm2.893j)}{(s+0.03029\pm0.1704j)(s+2.885\pm2.893j)}$$

Clearly for this system, no significant coupling between the engine and the airframe attitude dynamics is present, and the control systems suffer little performance degradation.

If model uncertainty is considered in the coupling dynamics, large effects of course are possible. This will be evaluated briefly below. Let the coefficient on the mixing plane pressure in the pitch-rate state equation of motion be varied from -0.03 to 0.01 (rad/sec^2)/(psia). Also let the coefficients on the plunge-velocity in all the engine state equations be varied ±20 times their nominal values. Finally, let the coefficient on the thrust vectoring angle input to the mixing plane pressure equation of motion be varied from -25 to 25 (psia/sec)/(deg).

The ranges of these parameter variations are only first order approximations, based on studies of other coupled aircraft/engine models as well as simple engineering considerations [8,9]. For example, the parameter C_E in the conceptual model of the last section is analogous to the coefficient on the mixing plane pressure in the pitch rate state equation. Since C_E is a function the trim thrust vectoring nozzle angle, it can therefore change sign depending on the trim value. These variations form a "three-dimensional parameter space" in which all the parameters are varied at the same time. Root loci of the full 8'th order closed loop system due to all these parameter variations shows that this range of variations will not cause instability, and the variation in the magnitude of the coupling transfer function is still quite small (though not shown).

The effect on the closed-loop system transfer functions will now be assessed. For example, selecting the following set of parameter variations,

-0.03 (rad/sec^2)/(psia), -20 times, and -25 (psia/sec)/(deg) (31)

the closed loop transfer functions become

$$\frac{q(s)}{\delta_p(s)} = \frac{-0.05369s(s+0.0656)(s+0.5346)}{(s+0.02811\pm0.1646j)(s+2.523\pm2.68j)}\,T(s)$$

$$T(s) = \frac{(s+0.4317)(s+2.009\pm3.485j)(s+8.055)(s+80.17)}{(s+0.4122)(s+2.124\pm3.585j)(s+7.999)(s+90.16)}$$

$$\frac{N_z(s)}{\delta_p(s)} = \frac{-0.09057s(s+0.001526)}{(s+0.02811\pm0.1646j)(s+2.523\pm2.68j)}\,T(s)$$

$$T(s) = \frac{(s+0.4175)(s+2.011\pm3.558j)(s+7.266\pm0.351j)(s-24.05)}{(s+0.4122)(s+2.124\pm3.585j)(s+7.999)(s+90.16)}$$

$$\frac{N_2(s)}{N_{2c}(s)} = \frac{0.1469s(s+15.87\pm6.145j)(s+38.64)}{(s+0.4122)(s+2.124\pm3.585j)(s+7.999)(s+90.16)}\,T(s)$$

$$T(s) = \frac{(s+0.02777\pm0.1649j)(s+2.598\pm2.719j)}{(s+0.02811\pm0.1646j)(s+2.523\pm2.68j)}$$

which differ from the transfer functions of Eqns. (29) and (30), and T(s) is now no longer unity. However, the effect of these parameter variations on the flying qualities has been evaluated, and they are minimal.

For the parameter variations selected as in Eqn. (31), the open-loop airframe/engine transfer functions are shown in Fig. 19, and the magnitude of the cross-coupling transfer function is shown in Fig. 20. Finally, $e_A k_E(s)$ is again compared to the engine loop transfer in Fig. 21. These plots show that although the coupling has increased from the nominal system, as presented in Figs. 16 through 18, it is still quite small. The performance, as measured by the closed-loop transfer functions is somewhat effected, but the stability robustness is not, for this case.

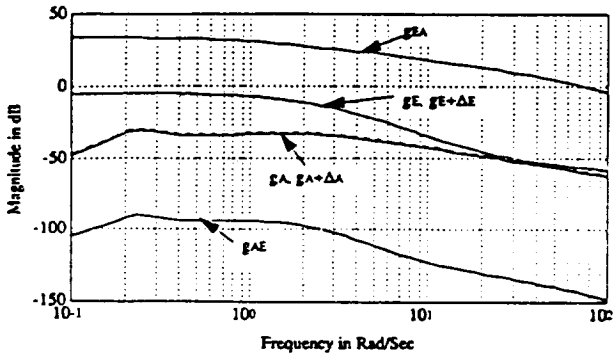

Figure 19 - Open Loop Transfer Function Magnitudes

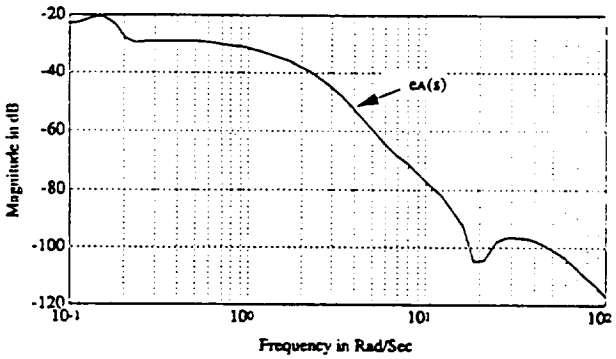

Figure 20 - Magnitude of the $e_A(s)$ Transfer Function

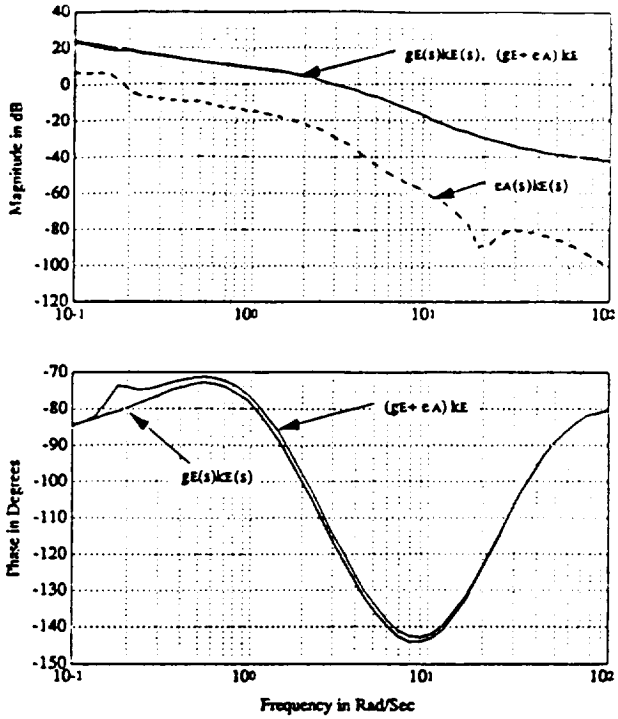

Figure 21 - Open Loop Bode Plot for the Engine Loop

Conclusions

Two coupling transfer function matrices were derived that quantify, in a meaningful way, the significance of airframe/engine interactions on the engine control loop. (These matrices each have duals for quantifying the effects on the flight control loop.) The size of these matrices, measured, for example, by their singular values, quantify the effect of coupling on closed-loop performance and stability robustness. These cross coupling terms were shown to depend on the control compensation transfer functions and the transfer functions for the airframe/engine system. In particular, they are functions of the off-diagonal transfer functions in the system's transfer function matrix. When the critical coupling terms are small compared to the magnitude of the loop transfer function (matrix), cross coupling effects are minimal. A conceptual model was offered to demonstrate the method. A case study of an airframe/engine system used in earlier studies of integrated control techniques was then presented. This study revealed that this particular vehicle, as modeled, exhibited very little critical interactions. A classical decentralized control system synthesized assuming the airframe and engine subsystems are totally non-interacting was quite suitable in this case. Other vehicle configurations, and/or more accurate models of the cross-coupling effects may reveal much more significant airframe/engine interactions. These interactions, however, may be evaluated with the analytical framework presented herein.

Appendix A - Derivation of Equation (12)

Let the state space description of the fully coupled aircraft/engine system presented be defined as

$$\begin{bmatrix}\dot{x}_A\\ \dot{x}_E\end{bmatrix} = \begin{bmatrix}A_A & A_{AE}\\ A_{EA} & A_E\end{bmatrix}\begin{bmatrix}x_A\\ x_E\end{bmatrix} + \begin{bmatrix}B_A & B_{AE}\\ B_{EA} & B_E\end{bmatrix}\begin{bmatrix}u_A\\ u_E\end{bmatrix}$$

$$\begin{bmatrix}y_A\\ y_E\end{bmatrix} = \begin{bmatrix}C_A & 0\\ 0 & C_E\end{bmatrix}\begin{bmatrix}x_A\\ x_E\end{bmatrix} \qquad (A1)$$

leading to

$$\begin{bmatrix} y_A(s) \\ y_E(s) \end{bmatrix} = \begin{bmatrix} G_A^*(s) & G_{AE}(s) \\ G_{EA}(s) & G_E^*(s) \end{bmatrix} \begin{bmatrix} u_A(s) \\ u_E(s) \end{bmatrix} = [G(s)] \begin{bmatrix} u_A(s) \\ u_E(s) \end{bmatrix} \quad \text{(A2)}$$

with characteristic polynomial,

$$\phi_{ol}^*(s) = \det \begin{bmatrix} sI-A_A & -A_{AE} \\ -A_{EA} & sI-A_E \end{bmatrix} \quad \text{(A3)}$$

Also let the state space descriptions of the aircraft and engine compensators, $K_A(s)$ and $K_E(s)$, be, respectively,

$$\begin{aligned} \dot{x}_{k_A} &= A_{k_A} x_{k_A} + B_{k_A} \dot{y}_{Ac} \\ u_A &= C_{k_A} x_{k_A} \\ \dot{x}_{k_E} &= A_{k_E} x_{k_E} + B_{k_E} \dot{y}_{Ec} \\ u_E &= C_{k_E} x_{k_E} \end{aligned} \quad \text{(A4)}$$

where $y_{Ac}'(s) = y_{Ac}(s) - y_A(s)$ and $y_{Ec}'(s) = y_{Ec}(s) - y_E(s)$ are the inputs to the aircraft and engine compensators. The characteristic polynomials of these compensators are

$$\begin{aligned} \phi_{k_A}(s) &= \det (sI - A_{k_A}) \\ \phi_{k_E}(s) &= \det (sI - A_{k_E}) \end{aligned} \quad \text{(A5)}$$

Sought now is the state space description of $G_E(s)+E_A(s)$, as presented in Fig. 5. Using Eqns. (A1) and (A4), and referring to Fig. 3, yields

$$\begin{bmatrix} \dot{x}_A \\ \dot{x}_E \\ \dot{x}_{k_A} \end{bmatrix} = \begin{bmatrix} A_A & A_{AE} & B_A C_{k_A} \\ A_{EA} & A_E & B_{EA} C_{k_A} \\ -B_{k_A} C_A & 0 & A_{k_A} \end{bmatrix} \begin{bmatrix} x_A \\ x_E \\ x_{k_A} \end{bmatrix} + \begin{bmatrix} B_{AE} \\ B_E \\ 0 \end{bmatrix} u_E + \begin{bmatrix} 0 \\ 0 \\ B_{k_A} \end{bmatrix} y_{Ac}$$

$$y_E = \begin{bmatrix} 0 & C_E & 0 \end{bmatrix} \begin{bmatrix} x_A \\ x_E \\ x_{k_A} \end{bmatrix} \quad \text{(A6)}$$

Denoting this system as

$$\begin{aligned} \dot{x}_1 &= A_1 x_1 + B_1 u_E + B_2 y_{Ac} \\ y_E &= C_1 x_1 \end{aligned} \quad \text{(A7)}$$

it can be shown, [10], that the characteristic polynomial of this system, $(G_E(s)+E_A(s))$, is

$$\phi_1(s) = \det (sI - A_1) = \phi_{ol}^*(s) \phi_{k_A}(s) \det \left[I + G_A^*(s) K_A(s) \right] \quad \text{(A8)}$$

Appending the state equation for the engine compensator, $K_E(s)$, to the state equation for $G_E(s)+E_A(s)$ gives the state space description of the open loop system of Fig. 5, $(G_E(s)+E_A(s))K_E(s)$,

$$\begin{bmatrix} \dot{x}_1 \\ \dot{x}_{k_E} \end{bmatrix} = \begin{bmatrix} A_1 & B_1 C_{k_E} \\ 0 & A_{k_E} \end{bmatrix} \begin{bmatrix} x_1 \\ x_{k_E} \end{bmatrix} + \begin{bmatrix} 0 \\ B_{k_E} \end{bmatrix} \dot{y}_{Ec} + \begin{bmatrix} B_2 \\ 0 \end{bmatrix} y_{Ac}$$

$$y_E = \begin{bmatrix} C_1 & 0 \end{bmatrix} \begin{bmatrix} x_1 \\ x_{k_E} \end{bmatrix} \quad \text{(A9)}$$

It can further be shown that the characteristic polynomial of this system is

$$\phi_{ol}(s) = \det \begin{bmatrix} sI-A_1 & -B_1 C_{k_E} \\ 0 & sI-A_{k_E} \end{bmatrix} = \phi_1(s) \phi_{k_E}(s) \quad \text{(A10)}$$

Closing the (engine) loop in Fig. 5, the state space equation for the closed loop system is

$$\begin{bmatrix} \dot{x}_1 \\ \dot{x}_{k_E} \end{bmatrix} = \begin{bmatrix} A_1 & B_1 C_{k_E} \\ -B_{k_E} C_1 & A_{k_E} \end{bmatrix} \begin{bmatrix} x_1 \\ x_{k_E} \end{bmatrix} + \begin{bmatrix} 0 \\ B_{k_E} \end{bmatrix} y_{Ec} + \begin{bmatrix} B_2 \\ 0 \end{bmatrix} y_{Ac}$$

$$y_E = \begin{bmatrix} C_1 & 0 \end{bmatrix} \begin{bmatrix} x_1 \\ x_{k_E} \end{bmatrix} \quad \text{(A11)}$$

and the characteristic polynomial for this closed loop system is

$$\Delta(s) = \det \begin{bmatrix} sI-A_1 & -B_1 C_{k_E} \\ B_{k_E} C_1 & sI-A_{k_E} \end{bmatrix} = \phi_1(s) \phi_{k_E}(s) \det \left[I + (G_E+E_A) K_E \right] \quad \text{(A12)}$$

or,

$$\Delta(s) = \phi_{ol}^*(s) \phi_{k_A}(s) \det \left[I + G_A^*(s) K_A(s) \right] \phi_{k_E}(s) \det \left[I + (G_E+E_A) K_E \right] \quad \text{(A13)}$$

Defining

$$\ddot{\phi}_{ol}(s) = \phi_{ol}^*(s) \phi_{k_A}(s) \det \left[I + G_A^*(s) K_A(s) \right] \phi_{k_E}(s) \quad \text{(A14)}$$

gives

$$\Delta(s) = \ddot{\phi}_{ol}(s) \det \left[I + (G_E+E_A) K_E \right] \quad \text{(A15)}$$

which is the result presented as Eqn. (12). Note that $\det \left[I + G_A^*(s) K_A(s) \right]$ is a rational function with denominator equal to $\phi_{ol}^*(s) \phi_{k_A}(s)$. Thus, the roots of $\phi_{ol}''(s)$ are the roots of $\phi_{k_E}(s)$, which are the poles of $K_E(s)$, and the values of s for which $\det \left[I + G_A^*(s) K_A(s) \right]$ equals zero.

Appendix B - State Space Model for the Case Study

Using Eqn. (A1), the airframe/engine system is modeled in the following form

$$\dot{x} = Ax + Bu$$

where, $A = \begin{bmatrix} A_A & A_{AE} \\ A_{EA} & A_E \end{bmatrix}$ and $B = \begin{bmatrix} B_A & B_{AE} \\ B_{EA} & B_E \end{bmatrix}$

with states, x = [u (ft/sec), w(ft/sec), q(rad/sec), θ(radians), N_2(rpm's), $N_{2.5}$(rpm's), P_6(psia), T_{41B}(°R)]^T
and inputs, u = [δn_{aps}(deg), δT_V(deg), w_f(#/hr)]^T
For the vehicle in question, the model is given below, [7].

$$A_A = \begin{bmatrix} -5.8930e-02 & 1.0670e-01 & -3.8600e+01 & -3.1840e+01 \\ -2.6590e-01 & -2.6650e-01 & 1.9480e+02 & -4.5990e+00 \\ -1.5410e-03 & 7.8060e-03 & -1.9490e-01 & -4.8180e-04 \\ 0 & 0 & 1.0000e+00 & 0 \end{bmatrix}$$

$$A_{AE} = \begin{bmatrix} 3.1440e-04 & 2.5990e-04 & 3.8190e-02 & 2.2500e-03 \\ -1.5780e-05 & -2.1060e-06 & 1.8260e-04 & -2.9570e-06 \\ 9.4600e-07 & 3.7440e-07 & 3.6680e-05 & 2.6760e-06 \\ 0 & 0 & 0 & 0 \end{bmatrix}$$

$$A_{EA} = \begin{bmatrix} 7.7820e-01 & 1.5420e-01 & 0 & 0 \\ 1.5180e-01 & 3.0080e-02 & 0 & 0 \\ 7.9340e-01 & 1.5720e-01 & 0 & 0 \\ -1.0050e-01 & -1.9920e-02 & 0 & 0 \end{bmatrix}$$

$$A_E = \begin{bmatrix} -4.1910e+00 & 6.0220e+00 & -3.4340e+02 & 1.1600e+01 \\ 4.2630e-01 & -5.7070e+00 & 2.7160e+01 & 1.0400e+01 \\ 2.2950e-01 & 1.1550e-01 & -9.0240e+01 & 8.4760e-01 \\ 3.7400e-02 & -1.0360e-01 & -7.9540e+00 & -1.0680e+00 \end{bmatrix}$$

$$B_A = \begin{bmatrix} -4.1830e\text{-}04 & -8.4280e\text{-}02 \\ -5.4520e\text{-}01 & -2.1475e\text{-}01 \\ -7.9700e\text{-}02 & 8.8132e\text{-}03 \\ 0 & 0 \end{bmatrix} \qquad B_{AE} = \begin{bmatrix} 3.4360e\text{-}05 \\ 1.2380e\text{-}08 \\ 5.5070e\text{-}08 \\ 0 \end{bmatrix}$$

$$B_{EA} = \begin{bmatrix} 0 & 0 \\ 0 & 0 \\ 0 & 0 \\ 0 & 0 \end{bmatrix} \qquad B_E = \begin{bmatrix} 1.4690e\text{-}01 \\ 5.3600e\text{-}02 \\ 1.8130e\text{-}02 \\ 1.6430e\text{-}01 \end{bmatrix}$$

Acknowledgements

This work was sponsored by the NASA Lewis Research Center under Grant # NAG3-998. Mr. Peter Ouzts is the technical program manager.

References

[1] Berry, D., Schweikhard, W., "Potential Benefits of Propulsion and Flight Control Integration for Supersonic Cruise Vehicles," based on SAE paper 740478, 1974.

[2] Shaw, P.D., Rock, S.M., and Fisk, W.S., "Design Methods for Integrated Control Systems," AFWAL -TR-88-2061, Aero Propulsion Laboratory, Air Force Wright Aeronautical Laboratories, Dayton, Ohio, June, 1988.

[3] Smith, K.L., "Design Methods for Integrated Control Systems," AFWAL-TR-86-2103, Aero Propulsion Laboratory, Air Force Wright Aeronautical Laboratories, Dayton, Ohio, December, 1986.

[4] Rock, S.M., Emami-Naeini, A., Anex, R.P., "Propulsion Control Specifications in Integrated Flight/Propulsion Control Systems," AIAA Paper No. 88-3236, AIAA/ASME/SAE/ASEE 24th Joint Propulsion Conference, Boston, Mass., 1988.

[5] Doyle, J., Stein, G., "Multivariable Feedback Design: Concepts for a Classical/Modern Synthesis," IEEE Transactions on Automatic Controls, Vol. AC-26, No. 1, pp. 4-16, Feb., 1981.

[6] Rosenbrock, H., "The Stability of Multivariable Systems," IEEE Transactions on Automatic Controls, Vol. AC-17, pp. 105-107, Feb., 1972.

[7] Garg, S., Mattern, D.L., and Bullard, R.E., "Integrated Flight/Propulsion Control System Design Based on a Centralized Approach," AIAA Paper No. 89-3520, AIAA Guidance, Navigation and Control Conference, Boston, Mass., 1989.

[8] Lancaster, E., *Jet Propulsion Engines*, Princeton University Press, Princeton, N.J., 1959.

[9] Tape, R., Hartill, W., et al., "Vectoring Exhaust Systems for STOL Tactical Aircraft," Journal of Engineering for Power, Transactions of the American Society of Mechanical Engineering, July, 1983.

[10] Kwakernaak, H., Sivan, R., *Linear Optimal Control Systems*, Wiley-Interscience, New York, 1972.

Extended Implicit Model Following As Applied To Integrated Flight and Propulsion Control*

David K. Schmidt† and John D. Schierman††

Department of Mechanical and Aerospace Engineering
Arizona State University
Tempe, AZ 85287-6106

Abstract

An extended model following control synthesis methodology, including loop transfer recovery, is presented and applied to synthesize control laws for integrated flight and propulsion control (IFPC). The vehicle considered is representative of an unstable modern fighter aircraft, with a 2D thrust-vectoring and thrust-reversing nozzle. The linearized design model includes both airframe and engine dynamics. The fact that it is necessary to regulate some responses as well as dynamically shape others is discussed, thus leading to a hybrid-control-problem formulation. A previously developed model-following formulation of the LQR problem is extended to handle this hybrid problem. Compensators are then obtained to realize an output-feedback control law, by using a loop-transfer-recovery procedure. The airframe and engine responses are decoupled, and perfect airframe response following is obtained. The loop transfers also reveal good stability robustness and reasonable loop cross-over frequencies that would not lead to excessive actuation requirements. The approach also yields compensators of dynamic order lower than the plant, thus easing their implementation. When compared to the results for a classically designed control law, the performance of the multivariable design was superior to that of the classical, while the loop shapes were quite similar.

Introduction

Enhancement of maneuvering capabilities of high performance aircraft by propulsion systems capable of delivering forces and moments to the flight control process is considered a viable engineering approach. For aircraft such as those capable of short take-off and vertical landing (STOVL), significant dynamic interactions between the airframe and the engine are present, and some configurations may lead to interactions in critical frequency ranges. Recently, Schmidt and Schierman[1] discussed the difference between the more common one-directional coupling between airframe and engine, and the critical two-dimensional variety. A measure of the critical interaction was developed that was expressed in terms of the size of an interaction matrix compared to the magnitude of the loop transfer. For aircraft/engine systems which do not have significant dynamical interactions, separate designs of the flight and propulsion control systems have been quite adequate. However, if this coupling is large and not taken into account when designing the control laws, then these dynamical interactions will lead to loss of system performance and stability robustness, or in severe cases to instabilities.

This problem is referred to here, and elsewhere, as the Integrated Flight and Propulsion Control (IFPC) problem. During the past several years, design integration methods[2-5] have been proposed that were intended to synthesize integrated control laws, while in a variety of ways dealing with the potential dynamic interactions.

In Ref. 2 a decentralized off-line approach was considered, by which the flight control laws for the airframe, plus the required generalized actuation bandwidths were obtained via Linear Quadratic Regulator (LQR) theory. The propulsion system was considered to be a component of these generalized actuators, and its control system was later designed, off line or independent of the airframe, to meet these required bandwidths. However, this approach can only directly account for one-directional dynamic interactions between the airframe and engine. It cannot directly take into account how the airframe's dynamics influence those of the engine. The allowable unmodeled or ignored interactions these designs can tolerate was the subject, for example, of Ref.3. Finally, although the resulting control laws were evaluated in a manned simulation, an analytical validation of the flying qualities was not performed, so compliance with the military specification was not considered.

In Ref. 4 a centralized approach was exercised that directly applied Linear Quadratic Gaussian/Loop Transfer Recovery (LQG/LTR) methodology, using a linear fully integrated airframe/propulsion dynamical model. This approach can account for two- directional dynamic coupling. The resulting control laws were not evaluated analytically in terms of the resulting flying qualities, due in part to the complexity of the closed-loop systems obtained via this method. It also tends to result in high order compensators that may be difficult to implement. Also, in both these studies, simulations revealed high actuation requirements, indicative of high loop-crossover frequencies.

The issue of simpler feedback compensation was the subject of Ref.5, in which LQG/LTR was again applied to synthesize full-order compensation.These compensators were then partitioned and simplified via order reduction. Except for the resulting loop shapes, these control laws have not been further evaluated.

In this paper a new synthesis approach is offered, and explored via a case study. The design objectives will be presented at the outset, the justification is given for considering this synthesis approach in light of these design goals, the synthesis methodology is presented, and the case study is addressed. A pseudo-classical design is also developed for the purposes of comparison. The results of this study will be discussed vis a vis the aforementioned design goals, and conclusions presented.

It will be shown that the two control laws so developed both satisfy the goals stated, and in fact lead to similar results for the vehicular system considered. This is considered a positive result since one goal of developing the new technique was to obtain somewhat classical-like control laws. The fact that the results for both control laws are similar is also due to the fact that, as shown in Ref. 1, this particular vehicle model possesses little of the critical two-directional coupling. This model was selected here in spite of this fact because it was used in Refs. 2 and 5, and further comparison of results is therefore possible.

Design Goals and Methodology Motivation

The goals or design objectives for control laws that are aimed at addressing the IFPC problem involve system performance, robustness, and implementation issues.

Performance - Foremost among the performance issues is the fact that the control systems must deliver excellent handling qualities, in spite of the potential airframe/engine dynamic coupling. The handling qualities criteria are quantified in terms of specified time constants, damping ratios and frequencies for the airframe modes, as well as closed-loop frequency from pilot input. Control laws that produce closed-

* As Presented at the 1990 AIAA GN&C Conference, Portland, OR

† Professor of Engineering; Associate Fellow, AIAA.

†† Doctoral Candidate; Student Member, AIAA.

AIAA PAPER NO. 90-3444

loop airframe responses that reflect classical airframe dynamics are desirable. In fact, how well the resulting airframe responses approximate certain frequency responses of a conventional aircraft with the desired modal characteristics is one step in meeting the military specifications[10]. One implication of this design goal is that the control system should decouple the airframe and engine responses. If the engine's dynamics are observable in the aircraft responses, then classical airframe dynamical properties are not obtained. Note that these design goals are not those of a regulator.

Engine control, on the other hand, requires regulation of responses about an operating point, with gain scheduling and transition control from one point to the next within the operating envelope. For example, in order to maintain stable combustion, it is important that the fan and compressor do not exceed their surge limits. For structural considerations, the main burner and the high pressure turbine should not exceed specified pressure and temperature limits. Therefore, stable, robust regulation of responses such as fan and compressor speeds, temperatures, and pressures, is a primary goal in the control design of the engine.

Finally, these performance objectives must be met with minimum actuation requirements, such that rate and deflection limits are avoided. Not only are high actuation requirements taxing on the hardware, rate and deflection limiting degrade both performance and stability by introducing unmodeled non-linear effects into the loops. Therefore, control bandwidths or crossover frequencies must be as low as possible.

Robustness - The system must possess adequate stability margins so that it is robust against unmodeled or inaccurately modeled dynamics. Usually, this requires minimum gain and phase margins in all loops, although singular-value-based[6] robustness analysis is currently popular. Also, the loop transfers must roll off sufficiently to handle high-frequency unmodeled dynamics or non-linearities.

Implementation - The compensation should be easily implementable. This implies that it should be of low dynamic order, and preferably should be similar to classical control laws. If so, the results can yield additional insight with regard to the control system's interactions with the overall airframe/engine system. Furthermore, the existing techniques for control law validation and verification, as well as the necessary gain scheduling may still be utilized.

The synthesis approach to be presented will be referred to as the Extended Implicit Model Following/Loop Transfer Recovery (EIMF/LTR) technique[6,7]. Model following is an integral part of the formulation so that the closed-loop airframe responses may be shaped to take on the desired dynamics. This method does not yield a regulator, and may not necessarily give loop transfers with classical (k/s) loop shapes. However, the design goals were not those for a regulator, and classical stability augmentors (e.g., pitch dampers) do not yield regulator loop shapes either. Implicit model following rather than explicit model following is utilized to eliminate the dynamic prefilter that is a integral part of the latter control structure. This leads to closed-loop airframe responses of lower dynamic order that are simpler and easier to evaluate in terms of handling-qualities assessments, and simpler to implement. Also, perfect model-following concepts[6] are exploited to minimize loop gains and crossover frequencies.

The implicit-model-following formulation of Refs. 6 and 7 are herein extended to address the hybrid problem of model following for some responses and regulation of others. As noted earlier, engine responses, as well as aircraft velocity in some cases, must be regulated. Consequently, for an integrated synthesis approach to the IFPC problem, regulation as well as model following must be admitted in the formulation.

Loop-transfer recovery is employed to synthesize the compensators, utilizing the state-feedback gains obtained from the solution to the EIMF problem. This may be accomplished by exploiting the asymptotic properties of the Kalman filter, as in the standard LQG/LQR approach[8], or by using a direct recovery technique as presented in Ref. 9. Either technique yields the compensators necessary to realize an output feedback structure, as depicted in Fig. 1. Since such LTR procedures recover the state-feedback loop shapes at the input to the plant, the robustness properties of the state-feedback control law are recovered there. Further, since the state-feedback control law is obtained via an LQR formulation of the model-following problem, compensators with the robustness properties of the LQR solution result.

Case Study Vehicular System

The vehicle to be considered in this investigation is the same as in Refs. 2 and 5. It is representative of a high performance fighter aircraft with the capabilities of 2-D thrust vectoring and thrust reversing. The vehicle dynamics are linearized about the Short Take Off and Landing (STOL) approach-to-landing reference condition at an airspeed of V_o = 120 Knots and flight path angle γ_o = -3°. The states, controls and responses are listed below. This model, with the *same* control and measurement vectors is used for both the classical design and the EIMF/LTR design presented in the nest sections.

The state vector is

$$\vec{x} = [u, w, q, \theta, N_2, N_{2.5}, P_6, T_{41B}]^T$$

where, the aircraft states are

u = body axis forward velocity (ft/sec)
w = body axis plunge velocity (ft/sec)
q = pitch rate (rad/sec)
θ = pitch angle (radians)

and the engine states are

N_2 = engine fan speed (rpm's)
$N_{2.5}$ = engine compressor speed (rpm's)
P_6 = engine mixing plane pressure (psia)
T_{41B} = high pressure turbine temperature (°R)

The control inputs to be considered are

$$\vec{u} = [A_{78}, \delta_{TV}, \delta_{flaps}, w_f]$$

where, the aircraft controls are

A_{78} = thrust reverser port area (in^2)
δ_{TV} = nozzle thrust vectoring angle (deg)
δ_{flaps} = trailing edge flap deflection angle minus leading edge flap deflection angle (deg) - see Reference [3]

and the single engine control to be considered here is

w_f = main burner fuel flow rate (#/hr)

(Note that the main nozzle throat area control used in Ref. 2 is not used in this study.) The aircraft's forward velocity is to be essentially regulated with the thrust reverser, while the attitude dynamics are controlled by thrust vectoring. The flaps are direct lift devices which are used to control the flight-path-to-attitude response, and the fuel-flow rate is used to control the engine fan speed. The measurements used for feedback are

$$\vec{y} = [u, w, q, N_2]^T$$

The vehicle model, partitioned in the following manner, is given in Appendix A,

$$\begin{bmatrix} \dot{x}_A \\ \dot{x}_E \end{bmatrix} = \begin{bmatrix} A_A & A_{AE} \\ A_{EA} & A_E \end{bmatrix} \begin{bmatrix} x_A \\ x_E \end{bmatrix} + \begin{bmatrix} B_A & B_{AE} \\ B_{EA} & B_E \end{bmatrix} \begin{bmatrix} u_A \\ u_E \end{bmatrix}$$

where the subscript A denotes aircraft subsystem and controls, and the subscript E denotes engine subsystem and controls. Results from a modal analysis are shown in Table 1. This table presents the open loop poles and the responses dominated by these modes.

Table 1 - Modal Analysis of the Open Loop System

Open Loop Poles	Mode Shapes
-0.0571 ± 0.2154j	phugoid mode (u)
-1.472 +1.065	short period mode (w,q,θ)
-1.401 -3.569 -6.958	highly coupled engine modes involving all the engine states
-89.28	mostly associated with P6

The open-loop thrust-vectoring-angle-to-pitch-rate, airframe plunge-acceleration (at the center of rotation) , as well as the fuel flow-to-fan-speed transfer functions are

$$\frac{q(s)}{\delta_{tv}(s)} = \frac{-0.0797s(s+0.1897\pm0.1013j)}{(s+0.05709\pm0.2153j)(s-1.065)(s+1.472)}\,T(s)\left(\frac{\text{rad/sec}}{\text{deg}}\right)$$

$$\frac{\alpha(s)}{\delta_{tv}(s)} = \frac{-0.1542(s+0.04249\pm0.1957j)(s+28.65)}{(s+0.05709\pm0.2153j)(s-1.065)(s+1.472)}\,T(s)\left(\frac{\text{deg}}{\text{deg}}\right)$$

$$T(s) = \frac{(s+1.401)(s+3.569)(s+6.958)(s+89.28)}{(s+1.401)(s+3.569)(s+6.958)(s+89.28)}$$

$$\frac{N_2(s)}{w_f(s)} = \frac{0.1469(s+16.43\pm5.89j)(s+36.94)}{(s+1.401)(s+3.569)(s+6.958)(s+89.28)}\,T(s)\left(\frac{\text{RPM}}{\#/\text{hr}}\right)$$

$$T(s) = \frac{(s+0.05646\pm0.2155j)(s-1.065)(s+1.472)}{(s+0.05709\pm0.2153j)(s-1.065)(s+1.472)}$$

From the above transfer functions and Table 1 it can be seen that the short period mode is unstable. Note that the poles of T(s) in the airframe transfer functions are predominantly those for the engine modes, and the engine dynamics are essentially unobservable in these airframe responses. The converse is true in the engine transfer function.

Performance Objectives

The flight control synthesis objective is to obtain classical longitudinal aircraft responses to pilot stick input, given by,

$$\frac{q(s)}{\delta_p(s)} = \frac{K_q\, s(s + 1/\tau_{\theta_1})\,(s + 1/\tau_{\theta_2})}{(s^2 + 2\zeta_{ph}\omega_{ph}\, s + \omega_{ph}^2)(s^2 + 2\zeta_{sp}\omega_{sp}\, s + \omega_{sp}^2)}$$

$$\frac{\alpha(s)}{\delta_p(s)} = \frac{K_\alpha(s + 1/\tau_{\alpha_1})\,(s + 1/\tau_{\alpha_2})}{(s^2 + 2\zeta_{ph}\omega_{ph}\, s + \omega_{ph}^2)(s^2 + 2\zeta_{sp}\omega_{sp}\, s + \omega_{sp}^2)}$$

(Phugoid Mode) (Short Period Mode) (1)

The short-period mode must be stabilized, achieving a specified frequency and damping ratio. Also, a desirable value for the real flight-path time constant, $1/\tau_{\theta 2}$, (not present in the open-loop transfer function) should be obtained. Table 2 lists the desired values selected for these parameters in this analysis, and are believed to be consistent with the military specification[10].

Table 2 - Desired Attitude Modal Parameters

ω_{sp}	2 Rad/Sec
ζ_{sp}	0.707
$1/\tau_{\theta 2}$	0.52 Rad/Sec

The value for the flight path time constant is driven by handling requirements, but is also consistent with Ref. 5, which states that it should not be increased above this value due to excessive flap deflections.

The requirements on the phugoid mode will be met by achieving some modest damping for this mode, and by rendering this mode essentially unobservable in the attitude response. The desired attitude response may be defined in terms of the following dynamic model.

$$\frac{q_m(s)}{\delta_p(s)} = \frac{M_\delta(s + 1/\tau_{\theta_2})}{s^2 + 2\zeta_{sp}\omega_{sp}s + \omega_{sp}^2}$$

$$\frac{\alpha_m(s)}{\delta_p(s)} = \frac{Z_\alpha}{s^2 + 2\zeta_{sp}\omega_{sp}s + \omega_{sp}^2} \qquad (2)$$

or, in state space form:

$$\begin{bmatrix}\dot{x}_1\\ \dot{x}_2\end{bmatrix} = \begin{bmatrix}0 & 1\\ -\omega_{sp}^2 & -2\zeta_{sp}\omega_{sp}\end{bmatrix}\begin{bmatrix}x_1\\ x_2\end{bmatrix} + \begin{bmatrix}0\\ 1\end{bmatrix}\delta_p$$

$$\begin{bmatrix}\alpha_m\\ q_m\end{bmatrix} = \begin{bmatrix}Z_\alpha & 0\\ M_\delta/\tau_{\theta_2} & M_\delta\end{bmatrix}\begin{bmatrix}x_1\\ x_2\end{bmatrix} \qquad (3)$$

Here, δ_P is the input from the pilot (e.g., stick deflection). The remaining terms to be selected are

$$Z_\alpha = -4.42 \text{ deg/(slug-ft/sec)}$$
$$M_\delta = -0.0797 \text{ /lbs}$$

These terms are obtained from the short-period approximation for the study vehicle. With this approximation, the model in Appendix A yields

$$\frac{\alpha(s)}{\delta_{tv}(s)} \approx \frac{-0.1542(s+28.67)}{(s-1.003)(s+1.464)} \approx \frac{-4.42 \text{ (for s=0)}}{(s-1.003)(s+1.464)}$$

and

$$\frac{q(s)}{\delta_{tv}(s)} \approx \frac{-0.0797(s+0.3199)}{(s-1.003)(s+1.464)}$$

The objective of the engine control design taken here is to regulate the fan speed. However, quantitative specifications on disturbance responses of the fan speed, such as maximum overshoot allowed or desired settling time, have not been formulated at this time. The response characteristics will be selected to yield engine-loop crossover frequencies close to those in the attitude loop, thereby maximizing the potential for dynamic interactions, the basic issue in this research

The following block diagram presents the closed loop system and shows the measurement and control vectors.

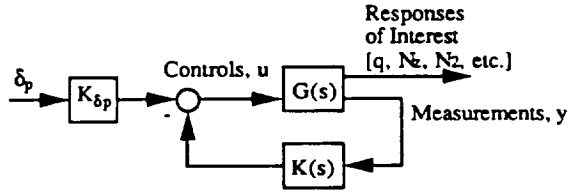

Figure 1 - Block Diagram of the Feedback Control Structure

where,

$$\begin{bmatrix}A_{78}\\ \delta_{tv}\\ \delta_{flap}\\ w_f\end{bmatrix} = -\begin{bmatrix}k_{11} & k_{12} & k_{13} & k_{14}\\ k_{21} & k_{22} & k_{23} & k_{24}\\ k_{31} & k_{32} & k_{33} & k_{34}\\ k_{41} & k_{42} & k_{43} & k_{44}\end{bmatrix}\begin{bmatrix}u\\ w\\ q\\ N_2\end{bmatrix} - K_{\delta p}\delta_p$$

$$u = -K(s)\, y - K_{\delta p}\delta_p \qquad (4)$$

Note that the structure of the compensator, K(s), will be the same for both the classical and EIMF/LTR designs presented in the next sections. Also note, $K_{\delta p}$ will be a 4x1 vector of constant gains (for both designs) on the pilot stick input, δ_p. Finally, because the plunge velocity, w, is a state used in the vehicular model, it is used, instead of angle of attack, α, in the measurement vector. The response of interest, α, may be obtained simply by the relationship, $\alpha = w/V_o$.

Classical Control Law Synthesis

First, the desired $1/\tau_{\theta_2}$ can be obtained via augmenting the lift effectiveness of the airframe, or by increasing Z_α. This may be achieved by feeding back angle of attack to the flaps, with a gain corresponding to k_{32}/V_o in Eq. 4. The necessary Z_α is obtained with a feedback gain of 2.9 (deg/deg). Next, to stabilize the attitude response, angle-of-attack (or w/V_o) will be fed back to the thrust-vectoring nozzle, with gain k_{22}/V_o in Eq. 4. A root locus of this transfer function (with the flap loop closed) would reveal that such a loop closure would yield the desired short-period frequency with a gain of 1.32 (deg)/(deg). Then, to augment the damping of the resulting short-period mode, pitch rate will also be fed back to the thrust-vectoring nozzle, with gain k_{23}. Again, a root locus for this loop closure would reveal that the required gain is 24.7 (deg)/(rad/sec). Finally, feeding back forward speed with a small gain to the thrust-reverser port area can be used to help regulate forward speed, which will help damp the phugoid mode, force a front-side response, and eliminate a non-minimum phase flight path. At the slow flight velocity, the vehicle's trim condition is "on the back side of the power curve," as shown in Fig. 2.

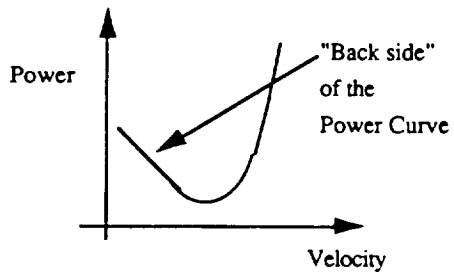

Figure 2 - Example Power-vs-Velocity Curve

This leads to nonminimum phase behavior associated with a right-half plane transmission zero in the attitude transfer function, or a right-half plane $1/\tau_{\theta_1}$, (see Eq. (1)). It turns out that the airframe transfer function matrix considered later in the multivariable case also has a transmission zero at the same location. This feature limits robustness recovery in the LTR procedure[8,11]. Regulation of forward velocity eliminates this problem. A speed-loop gain on the thrust reversing loop, or k_{11} of 0.5 (in^2)/(ft/sec) is selected here.

Finally, the engine response must be regulated to reject disturbances. A simple proportional-plus-integral loop is used, with gains of -6 (lb/hr)/rpm and -3 ((lb/hr)sec)/rpm, respectively, to close the loop on engine speed to fuel flow. So $k_{44}(s)$ is 6(s+.5)/s. Designs with additional engine loop closures are currently under investigation.

The closed-loop airframe response transfer functions using this control law are

$$\frac{q(s)}{\delta_p(s)} = \frac{-0.0795s(s+0.2048)(s+0.6266)}{(s+0.08664\pm0.09438j)(s+1.408\pm1.409j)}\,T(s)\left(\frac{rad/sec}{\#}\right)$$

$$T(s) = \frac{(s+0.4052)(s+1.985\pm3.532j)(s+8.016)(s+89.68)}{(s+0.4104)(s+1.985\pm3.531j)(s+8.016)(s+89.67)}$$

$$\frac{\alpha(s)}{\delta_p(s)} = \frac{-4.086(s+0.1067\pm0.1714j)}{(s+0.08664\pm0.09438j)(s+1.408\pm1.409j)}\,T(s)\left(\frac{deg}{\#}\right)$$

$$T(s) = \frac{(s+0.4117)(s+1.985\pm3.531j)(s+8.015)(s+89.65)}{(s+0.4104)(s+1.985\pm3.531j)(s+8.016)(s+89.67)} \qquad (5)$$

where T(s), which reflects the effects of the engine dynamics, is approximately unity for each response. Therefore, the engine response is decoupled from that of the airframe's attitude and flight-path response. The closed loop $1/\tau_{\theta 2}$ achieved is about 0.63 (1/s), and the short-period damping and frequency achieved are 0.7075 and 1.99 rad/sec, respectively. Thus these design goals all appear to be adequately met.

Figs. 3 and 4 present the closed-loop frequency responses for angle of attack and pitch rate from pilot stick input. Also plotted in the dashed lines are the responses of the desired dynamics presented earlier.

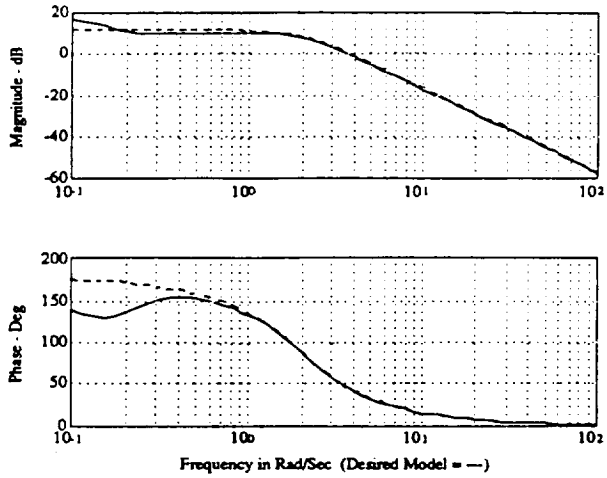

Figure 3 - Closed Loop Frequency Response of Angle of Attack-to-Pilot Stick Input (Deg/lbs)

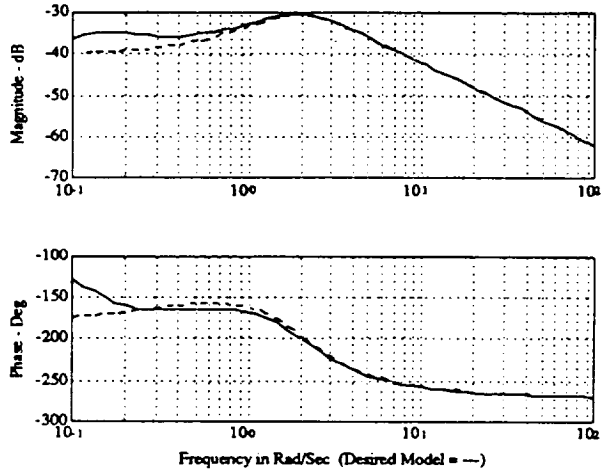

Figure 4 - Closed Loop Frequency Response of Pitch Rate-to-Pilot Stick Input ((Rad/Sec)/lbs)

These responses show good agreement, especially in the critical frequency range between 0.5 and 10 rad.sec.

Fig. 5 shows the disturbance rejection performance, in terms of the closed-loop sensitivity function relating engine speed to a speed disturbance, or mag[1/(1+kg)] at the engine speed output.

Engine speed disturbances will be rejected below about 4 rad/sec. Fig. 6 shows the response of the fan speed to a one RPM step disturbance. This plot shows good regulation performance with a settling time to 2% of the final value of approximately 5 seconds.

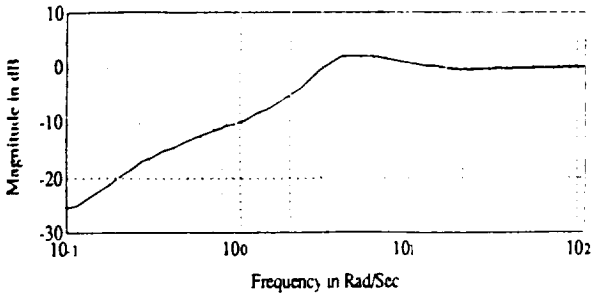

Figure 5 - Sensitivity Function of Measured Fan Speed-to-Fan Speed Disturbance (RPM/RPM)

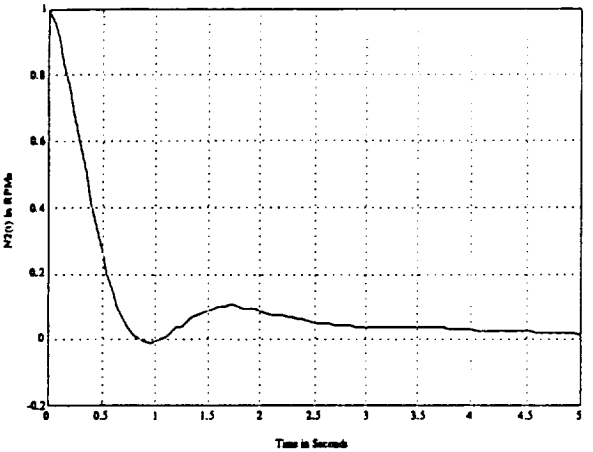

Figure 6 - Measured Fan Speed Unit Step Disturbance Response

The open-loop Bode plots for these control laws are shown in Figs. 7 through 10, where each loop transfer shown reflects the fact that all other loops are closed.

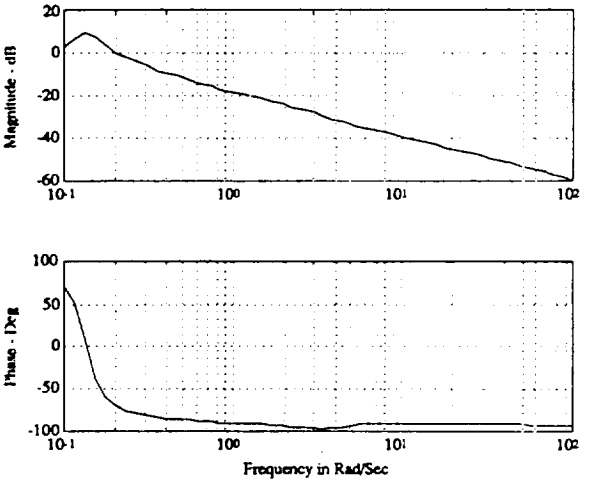

Figure 7 - Thrust Reverser Port Area Loop Transfer - With All Other Loops Closed

The thrust-reverser loop has a gain cross-over frequency of 0.2 rad/sec, a phase margin of 110°, and an infinite gain margin. The thrust-vectoring loop has a gain cross-over frequency of 2.2 rad/sec, a phase margin of 45°, and a low-gain margin of approximately -6 dB. The flap loop has a magnitude less than one for all frequency, and a gain margin of approximately 6 dB. Finally, the fuel-flow-rate loop has a cross-over frequency of 3 rad/sec, a phase margin of 64°, and infinite gain margin.

These results can be compared with those for the LQG/LTR control design recorded in Ref. 5. For the fuel-flow-rate loop, for example, that design had a 15 dB gain margin and 50° phase margin. The cross-over frequencies of the thrust-reverser, thrust-vectoring and fuel-flow-rate loops from the same study were 1.7, 6.2 and 3.2 rad/sec, respectively.

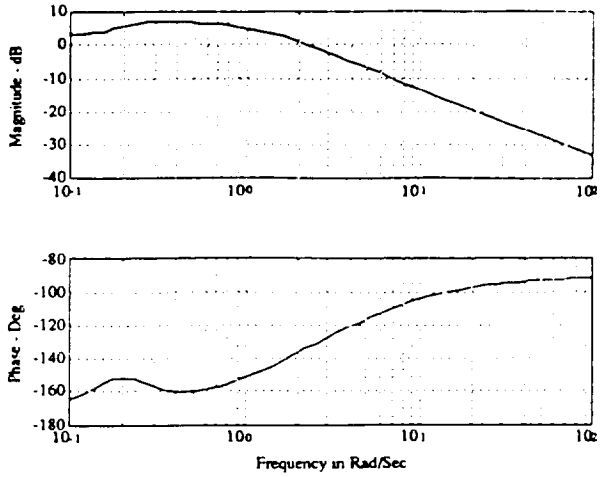

Figure 8 - Thrust Vectoring Angle Loop Transfer - With All Other Loops Closed

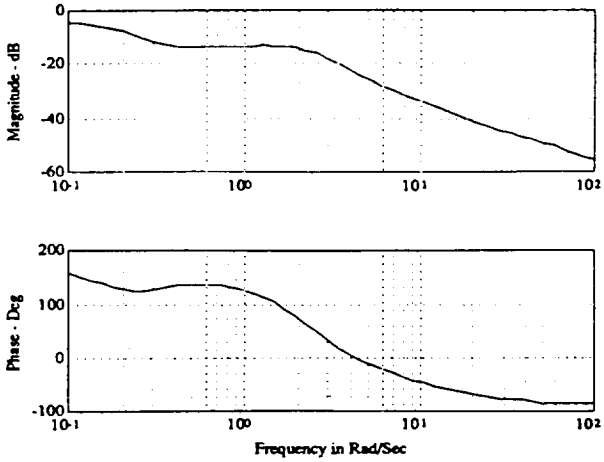

Figure 9 - Flap Angle Loop Transfer - With All Other Loops Closed

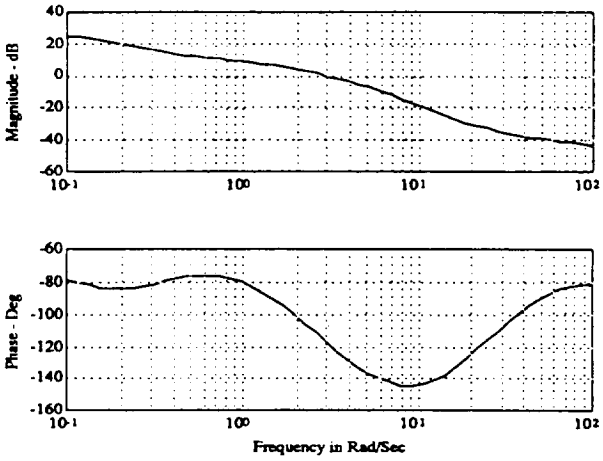

Figure 10 - Fuel Flow Rate Loop Transfer - With All Other Loops Closed

EIMF/LTR Control Synthesis Methodology[6,7]

Consider the control of the linear time-invariant aircraft/engine dynamic system modeled as

$$\dot{x} = Ax + Bu$$
$$y = Cx \tag{6}$$

The model of the desired dynamics to be followed is represented as

$$\dot{x}_m = A_m x_m + B_m \delta_p$$
$$y_m = C_m x_m \tag{7}$$
$$\dot{\delta}_p = -100.\ \delta_p$$

where δ_p is the stick input from the pilot.

The error vector to be chosen is

$$e = y - y_m \tag{8}$$

and the error dynamics to be selected in the synthesis are

$$\dot{e} = -G_e e \tag{9}$$

Defining the quadratic loss function to be:

$$J = \int_0^\infty \{(\dot{e}+G_e e)^T Q(\dot{e}+G_e e) + u^T R u\} dt \tag{10}$$

the solution of this linear quadratic problem is the state-feedback control law

$$u = -K_{fb}x - K_{ff}x_m - K_{\delta_p}\delta_p \tag{11}$$

Implicit model following results when the gains on the model states are zero. This can be assured if C_m is chosen to be square and invertible, and the error dynamics are chosen to be

$$G_e = -C_m A_m C_m^{-1} \tag{12}$$

Perfect model following results when the error vector is exactly zero for all time, and is achievable when CB is full rank. If perfect model following is achievable and the system has no non-minimum phase transmission zeros, the above LQ formulation will asymptotically approach the perfect model following result as $R \rightarrow 0$. Fig. 11 presents the closed-loop system implied by Eq. (11), for implicit model following.

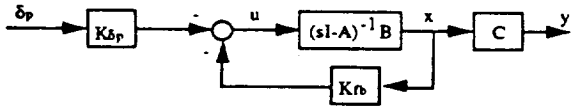

Figure 11 - Model Following State-Feedback Control Block Diagram

Although the matrices Q and R in the above loss function can be used to adjust the gains, it must be emphasized that the choice of desired dynamics to be followed and the error vector to be minimized is the most critical part of the synthesis. The transmission zeros of the system are determined by the choice of inputs and followed responses, thus, by the choice of the error vector. As Reference [6] states, for a square system, some of the closed-loop poles approach the finite open loop transmission zeros, and, under the conditions of perfect model following, the rest of the closed loop poles approach the poles of the error dynamics, G_e. Further, for implicit model following Eq. 12 reveals how the error dynamics are directly related to the desired model dynamics. The choice of desired dynamics and error vector can also greatly influence the shapes of the loop transfers. Finally, formulating the problem such that perfect model-following is achievable keeps the loop gains and crossover frequencies down. If perfect model following is not achievable the performance is achieved via arbitrarily high gains.

The synthesis approach just described must now be extended to allow regulation of some of the system's responses. Regulation is incorporated into the model following synthesis by simply defining the desired model to be followed by the regulated responses as the constant zero. For example, if responses y_1 and y_2 are to follow a desired model with responses y_m, while responses y_3 and y_4 are to be regulated, then the error vector becomes simply

$$\vec{e} = \begin{bmatrix} y_1 - y_{1_m} \\ y_2 - y_{2_m} \\ \hline y_3 \\ y_4 \end{bmatrix} \tag{13}$$

Otherwise, the formulation and solution to the LQ problem proceeds as above.

Once the EIMF state-feedback gains are found from this procedure, compensators may then be synthesized using the loop-transfer-recovery procedures of Ref. 5, 9 or 11. The approach of Ref. 9 yields a closed-form solution and exact recovery, while the more familiar approach of Ref. 5 or 11 yields asymptotic recovery. Proceeding as in Ref. 9, a singular value decomposition of the control input matrix for the plant, B, is used to formulate a reduced order observer, described as:

$$\dot{\hat{x}} = \hat{A}\hat{x} + \hat{B}y$$
$$u = \hat{C}\hat{x} + \hat{D}y \tag{14}$$

from which the LTR compensator matrix is obtained as shown below.

$$K(s) = K_{fb}(\hat{C}(sI - \hat{A})^{-1}\hat{B} + \hat{D}) \tag{15}$$

The algorithm to obtain this compensator is presented in Appendix A. Note that via standard LQG/LTR, the compensator is of the same order as the plant and order reduction may be considered. In this LTR procedure, a reduced order observer is obtained directly. However, it does not guarantee any high-frequency roll off, so this would be added, if necessary, as the final step in the synthesis.

With the compensation K(s) so obtained, and the pilot-input gains taken from Eq. 11, the augmented system becomes that shown in Fig. 1.

EIMF Control Law Synthesis

The desired dynamic model to be followed by the aircraft's attitude response is, consistent with Eq. 2,

$$\frac{q_m(s)}{\delta_p(s)} = \frac{M_\delta(s + 1/\tau_{\theta_2})}{s^2 + 2\zeta_{sp}\omega_{sp}s + \omega_{sp}^2}$$
$$\frac{\alpha_m(s)}{\delta_p(s)} = \frac{Z_\alpha}{s^2 + 2\zeta_{sp}\omega_{sp}s + \omega_{sp}^2} \tag{16}$$

or

$$\begin{bmatrix}\dot{x}_1 \\ \dot{x}_2\end{bmatrix} = \begin{bmatrix} 0 & 1 \\ -\omega_{sp}^2 & -2\zeta_{sp}\omega_{sp}\end{bmatrix}\begin{bmatrix}x_1 \\ x_2\end{bmatrix} + \begin{bmatrix}0 \\ 1\end{bmatrix}\delta_p$$
$$\begin{bmatrix}\alpha_m \\ q_m\end{bmatrix} = \begin{bmatrix} Z_\alpha & 0 \\ M_\delta/\tau_{\theta_2} & M_\delta\end{bmatrix}\begin{bmatrix}x_1 \\ x_2\end{bmatrix} \tag{17}$$

with

$\omega_{sp} = 2$ rad/sec

$\zeta_{sp} = 0.707$

$1/\tau_{\theta_2} = 0.52$

$Z_\alpha = -4.42$

$M_\delta = -0.0797$

With regulation of forward speed and engine fan speed also desired, the error vector is:

$$\vec{e} = \begin{bmatrix} u \\ w - w_m \\ q - q_m \\ N_2 + \int N_2 \end{bmatrix} \qquad (18)$$

Note that integral of fan speed is added in the above. Addition of this term is associated with the fact that integral action on N_2 is desired. Again, note that plunge velocity is used, where $w=\alpha/V_o$. With this error vector, the finite transmission zeros of the open-loop system are shown in Table 3.

Table 3 - Finite Transmission Zeros of the Open Loop System

Transmission Zeros
-68.612
-13.0491 ± 5.5632j
-1.0
0.0

The transmission zero at -1 is due to the inclusion of the integral of engine fan speed in the error vector, as explained in Appendix C. The transmission zero at the origin is due to the fact that pitch-rate is used in the error vector. If pitch rate plus integral of pitch rate, or θ, were used, this zero would move into the left half of the complex plane.

The error dynamics are now selected to be

$$G_e = \begin{bmatrix} g_{e_u} & 0 & 0 \\ 0 & -C_m A_m C_m^{-1} & 0 \\ 0 & 0 & g_{e_{N2}} \end{bmatrix} \qquad (19)$$

This choice of error dynamics reflects the desire to decouple the attitude dynamics from the engine speed and forward speed, as well as implicitly model follow the desired short period model. Finally, the forward-speed and engine-speed responses will include a mode with time constants g_{e_u} and $g_{e_{N2}}$, respectively. Values for these time constants were chosen to be 0.1 and 1 rad/sec, respectively.

EIMF Results

Before synthesizing the dynamic compensation via the LTR procedure, the frequency responses of the loop transfers, using state feedback gains obtained from the EIMF control laws, $K_{fb}(sI-A)^{-1}B$, are investigated. This is done, for example, to check the performance, controller bandwidths, and stability robustness. Since loop transfer recovery will be used later, the bandwidths and robustness of the state-feedback control laws will be recovered, by definition. Also, for the control laws implemented as in Fig. 1, it can be shown[12] that the responses to pilot input are unchanged due to the inclusion of estimation in the manner described herein.

For the results presented below, the values of Q and R in the loss function of Eq. (10) are

$$Q = 1\text{x}10^5(\text{diag}[0.4,1,100,0.1])$$

and

$$R = 1\text{x}10^{-4}\,(\text{diag}[1,0.2,0.2,1\text{e-}03])$$

These values were chosen primarily on the basis of the resulting Bode loop shapes, with special attention to stability margins and loop cross-over frequencies. The resulting EIMF control gains, $K_{\delta p}$ and K_{fb}, are listed in Appendix C.

Figs. 12 through 15 show the individual loop transfers.

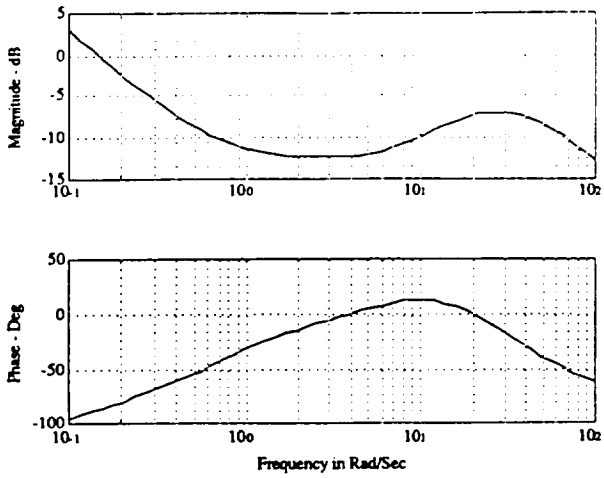

Figure 12 - Thrust Reverser Port Area Loop Transfer - With All Other Loops Closed

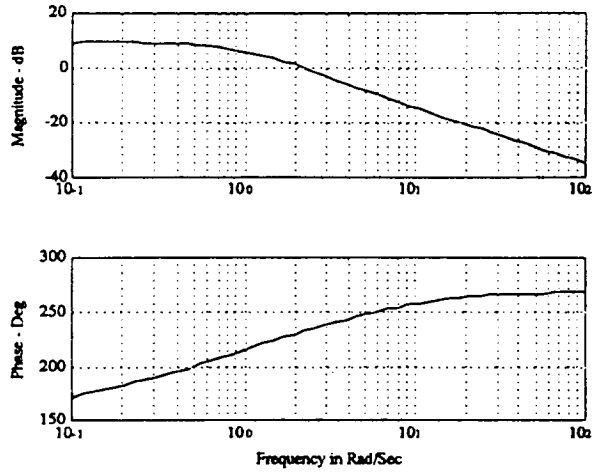

Figure 13 - Thrust Vectoring Angle Loop Transfer - With All Other Loops Closed

The thrust-reverser loop has a cross-over frequency of 0.15 rad/sec, a phase margin of 90°, and an infinite gain margin. The thrust-vectoring loop has a cross-over frequency of 2.1 rad/sec, a phase margin of 55°, and a gain margin of -10 dB. The flap loop has a magnitude less than one for all frequency, and a gain margin of approximately 10 dB. The fuel-flow-rate loop has a cross-over frequency of 10.2 rad/sec, a phase margin of 70°, and a gain margin of 12 dB. These results show that the EIMF design gives loop shapes, loop cross-over frequencies and stability margins that are very similar to those of the classical design presented earlier.

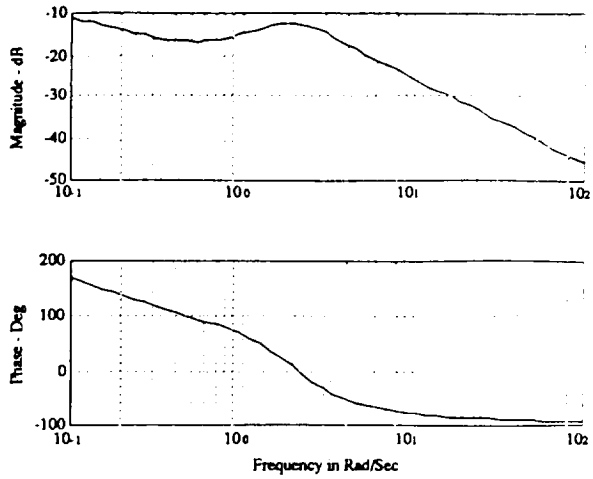

Figure 14 - Flap Angle Loop Transfer - With All Other Loops Closed

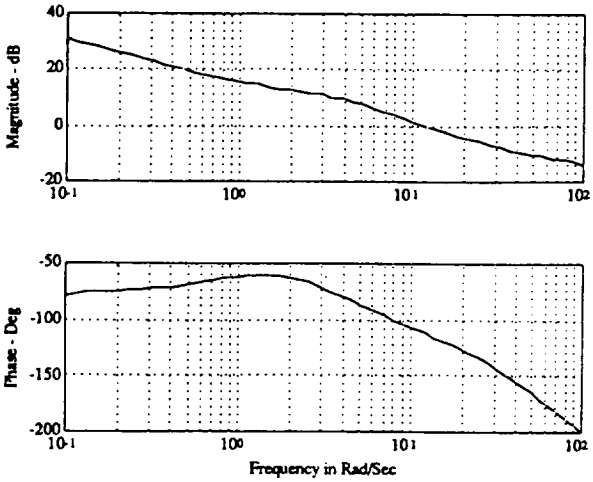

Figure 15 - Fuel Flow Rate Loop Transfer - With All Other Loops Closed

EIMF/LTR Results

With the state-feedback gains now available, the compensation is synthesized as outlined in Appendix D. The responses taken for feedback are u, w, q and N_2, identical to the classical case. Again, this leads to a 4x4 compensator matrix, K(s), as in Fig. 1, which describes the closed-loop system.

Recalling that the desired pitch rate and angle-of-attack-to-pilot input transfer functions are

$$\frac{q_m(s)}{\delta_p(s)} = \frac{-0.0797(s+0.52)}{(s+1.414\pm1.414j)}\left(\frac{rad/sec}{\#}\right)$$

$$\frac{\alpha_m(s)}{\delta_p(s)} = \frac{-4.422}{(s+1.414\pm1.414j)}\left(\frac{deg}{\#}\right)$$

the closed-loop transfer functions obtained using this control law are,

$$\frac{q(s)}{\delta_p(s)} = \frac{-0.0797(s+0.52)}{(s+1.414\pm1.414j)}T(s)\left(\frac{rad/sec}{\#}\right)$$

$$\frac{\alpha(s)}{\delta_p(s)} = \frac{-4.422}{(s+1.414\pm1.414j)}T(s)\left(\frac{deg}{\#}\right)$$

$$T(s) = \left(\frac{s(s+0.1)(s+1)^3(s+13.05\pm5.563j)}{(s+0.0001511)(s+0.1)(s+1)^3(s+13.05\pm5.563j)}\right)\left(\frac{(s+13.05\pm5.563j)(s+68.62)^2}{(s+13.05\pm5.563j)(s+68.61)(s+68.62)}\right)$$

Near-perfect model following is evident in these responses.

Figs. 16 and 17 present the closed-loop frequency responses for pitch rate and angle of attack to pilot stick input. Also plotted are the desired frequency responses. Since they are essentially the same, and considering the closed-loop transfer functions given above, one must conclude that the desired handling qualities would be achieved.

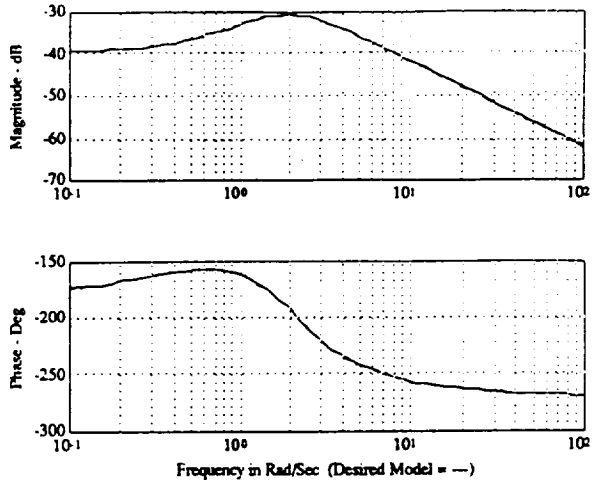

Figure 16 - Closed Loop Pitch Rate-to-Pilot Stick Input Frequency Response

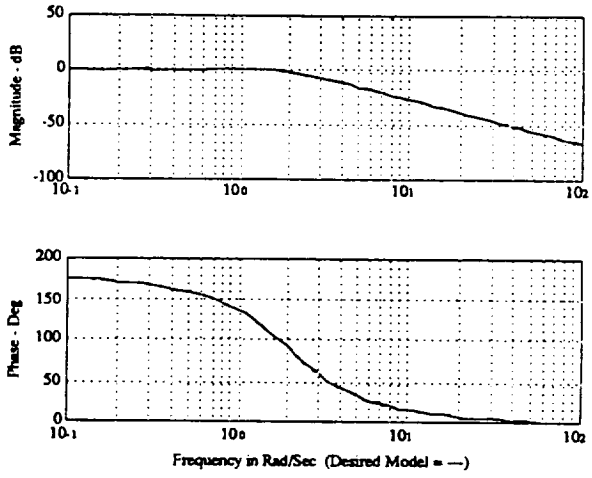

Figure 17 - Closed Loop Frequency Response of Angle of Attack from Pilot Stick Input (Deg/lbs)

Shown in Fig. 18 is the performance of the control law in rejecting fan speed disturbances, again expressed in terms of the magnitude of the sensitivity function for fan speed mag[1/(1+gk)]. It is noted that speed disturbances will be rejected below about 15 rad/sec. This performance is better than that shown for the classical control law.

Fig. 19 shows the response of the fan speed to a one RPM step fan speed disturbance.

Very accurate pole-zero cancellations in the closed-loop transfer function leads to the following transfer function for this disturbance response.

$$\frac{N_2(s)}{d(s)} \approx \frac{s(s+1.251)(s+3.518)(s+6.805)(s+97.64)}{(s+1)(s+1)(s+13.05\pm5.563j)(s+68.61)}\left(\frac{RPM}{RPM}\right)$$

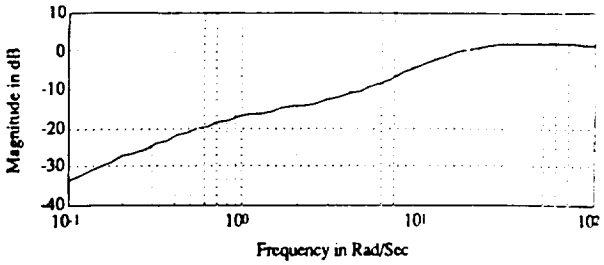

Figure 18 - Sensitivity Function of Measured Fan Speed-to-Fan Speed Disturbance (RPM/RPM)

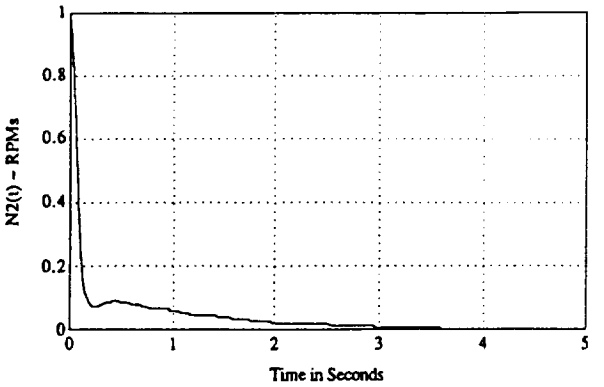

Figure 19 - Measured Fan Speed Unit Step Disturbance Response

Clearly the steady state value of $N_2(t)$ to a step disturbance goes to zero. One pole at -1 is the error pole, g_{ex2}, as discussed in Ref.6. The remaining poles are transmission zeros arising due to the loop-transfer recovery. Note that all these parameters were chosen directly or indirectly in the synthesis, and therefore may be adjusted as desired.

Comparisons of singular value plots of the loop transfers using the state feedback control law, $K_{fb}(sI-A)^{-1}B$, and the LTR compensation, $K(s)C(sI-A)^{-1}B$, as well as the loop transfers of each loop, with all other loops closed, revealed complete robustness recovery, as promised by this exact recovery method, Ref. 9. Consequently, the loop transfers for the loops broken at the control input are identical to those for the EIMF state-feedback control law. Specifically, the individual loop transfers are as shown in the previous section.

The state-space realization for the compensators is given in Appendix E. The compensator transfer-function matrix, or K(s) in Fig. 1, is given in Table 4. Note that $K_{14}(s)$, $K_{24}(s)$, and $K_{34}(s)$ are essentially zero, so they are not listed. These transfer functions are all fifth order, with poles at the transmission zeros of the plant.

Conclusions

A control law synthesis technique was presented that was developed to achieve excellent handling qualities, decoupling the engine and airframe dynamics, with modest control bandwidths or crossover frequencies. The robustness properties of the LQR solution were exploited by formulating the implicit model following problem in the LQ framework, and utilizing a novel loop transfer recovery procedure to obtain the feedback compensation. The methodology was applied to the integrated flight and propulsion control problem in the form of a case study, utilizing the linear model of an unstable fighter aircraft, with engine dynamics and a 2D thrust-vectoring and thrust-reversing nozzle. A classically designed control law was developed for comparison.

The results revealed that both control laws would appear to deliver adequate performance, as defined herein, with modest gain crossover frequencies, thus keeping actuation requirements to a minimum. Although the airframe responses obtained using the new technique were somewhat superior to those for the classical design, the individual loop transfers of the two control laws were quite similar. Both of these are considered to be positive attributes of the new procedure offered. The airframe responses with the new control law were exactly those desired, thus demonstrating the performance achievable, subject to actuation bandwidth, with this approach. Finally, engine control laws were simultaneously synthesized, along with those for the airframe, and would appear to deliver good disturbance-rejection performance. This was also accomplished with reasonable crossover frequencies. The simplicity of the classically designed compensators was superior to the new controller, the latter being fourth-order while the former consisted primarily of constants. If different vehicle configurations ultimately exhibit more bi-directional coupling than that considered here, a classical control synthesis may, however, encounter considerably more difficulty than that demonstrated here. Whether the difficulty involved with the newer approach is significantly increased as well is an open question.

Table 4 - EIMF/LTR Compensation Matrix

Numerators for the Individual Compensator Transfer Functions	Bode Gain	Units of Compensator
N_{K11} = -122(0) (0.6)(1)[0.94,9.9]	-0.6	in^2/(ft/sec)
N_{K12} = 37(0) (-0.6)(1)[0.94,10]	-0.2	in^2/(ft/sec)
N_{K13} = -89(1)(1.5)(14)(29)(32)	+121	in^2/(rad/sec)
N_{K21} = -0.3(0) (1)[0.92,12](-33)	+0.1	deg/(ft/sec)
N_{K22} = -0.2(0) (1)[0.92,14](133)	-0.3	deg/(ft/sec)
N_{K23} = -21(-0.1)(1)[0.92,14](67)	+1.9	deg/(rad/sec)
N_{K31} = 2.1(0) (1)[0.89,17](23)	+0.4	deg/(ft/sec)
N_{K32} = -0.7(0) (1)[0.91,16](29)	-0.4	deg/(ft/sec)
N_{K33} = 59(0.3)(1)[0.92,14](68)	+16.0	deg/(rad/sec)
N_{K41} = -4.9e5(1)[-0.42,1.5][0.95,4.1]	-1284	#/hr/(ft/sec)
N_{K42} = 1.5e5[0.07,0.78](1)(3.3)(3.8)	+82.5	#/hr/(ft/sec)
N_{K43} = -1.03e6(0.6)(1)(1.7)(4.6)(47)	-16488	#/hr/(rad/sec)
N_{K44} = -85(1)(-3.7)(4)(10)(-92)	-85.1	#/hr/(RPM)
Characteristic Polynomial of Compensator : $\Delta(s)$ = (0) (1)[0.92,14.2](68.6)		

Note: (a) = (s+a), and [a,b] = complex mode with damping ratio = a, and frequency = b

Appendix A. Linear Model for the Case-Study Vehicle

The states are defined as

$x = [u\ (ft/sec),\ w(ft/sec),\ q(rad/sec),\ \theta(radians),\ N_2(rpm's),\ N_{2.5}(rpm's),\ P_6(psia),\ T_{41B}(°R)]^T$

with inputs,

$u = [A_{78}(in^2),\ \delta_{flaps}(deg),\ \delta_{TV}(deg),\ w_f(\#/hr)]^T$

For the vehicle in question, the model is

$A_A =$

-5.8930e-02	1.0670e-01	-3.8600e+01	-3.1840e+01
-2.6590e-01	-2.6650e-01	1.9480e+02	-4.5990e+00
-1.5410e-03	7.8060e-03	-1.9490e-01	-4.8180e-04
0	0	1.0000e+00	0

A_{AE} =

3.1440e-04	2.5990e-04	3.8190e-02	2.2500e-03
-1.5780e-05	-2.1060e-06	1.8260e-04	-2.9570e-06
9.4600e-07	3.7440e-07	3.6680e-05	2.6760e-06
0	0	0	0

A_{EA} =

7.7820e-01	1.5420e-01	0	0
1.5180e-01	3.0080e-02	0	0
7.9340e-01	1.5720e-01	0	0
-1.0050e-01	-1.9920e-02	0	0

A_E =

-4.1910e+00	6.0220e+00	-3.4340e+02	1.1600e+01
4.2630e-01	-5.7070e+00	2.7160e+01	1.0400e+01
2.2950e-01	1.1550e-01	-9.0240e+01	8.4760e-01
3.7400e-02	-1.0360e-01	-7.9540e+00	-1.0680e+00

$[B_A \; B_{AE}]$ =

-2.0550e-01	-4.1830e-04	-8.4280e-02	3.4360e-05
-2.9360e-04	-5.4520e-01	-2.1475e-01	1.2380e-08
1.0680e-04	-7.9700e-02	8.8132e-03	5.5070e-08
0	0	0	0

$[B_{EA} \; B_E]$ =

0	0	0	1.4690e-01
0	0	0	5.3600e-02
-4.3020e+01	0	0	1.8130e-02
0	0	0	1.6430e-01

Appendix B. Transmission Zeros

Given an output to a linear system as:

$$y = c_1x_1 + c_2x_2$$

with,

$$x_2 = \int x_1 dt$$

then one of the finite transmission zeros of the system is:

$$z = -c_2/c_1$$

Limited Proof:

For the following system

$$\begin{bmatrix}\dot{x}_1\\ \dot{x}_2\end{bmatrix} = \begin{bmatrix}a_1 & a_2\\ 1 & 0\end{bmatrix}\begin{bmatrix}x_1\\ x_2\end{bmatrix} + \begin{bmatrix}b\\ 0\end{bmatrix}u$$

$$y = [c_1 \; c_2]\begin{bmatrix}x_1\\ x_2\end{bmatrix}$$

it can be shown that the transmission zero, z, solves the following generalized eigenvalue/eigenvector problem, (Reference [13]):

$$z\begin{bmatrix}1 & 0 & 0\\ 0 & 1 & 0\\ 0 & 0 & 0\end{bmatrix}\begin{bmatrix}m_1\\ m_2\\ v\end{bmatrix} = \begin{bmatrix}a_1 & a_2 & b\\ 1 & 0 & 0\\ c_1 & c_2 & 0\end{bmatrix}\begin{bmatrix}m_1\\ m_2\\ v\end{bmatrix}$$

from which it can be seen that:

$$m_1 = z\, m_2$$
$$c_1m_1 + c_2m_2 = 0$$

which implies that $z = -c_2/c_1$. Note that this proof can be extended to a general nth order system.

Appendix C. Gains From EIMF Synthesis

K_{fb} =

(Columns 1 through 5)

-5.8088e-01	-3.6615e-01	1.6462e+02	1.4829e+02	-4.0719e-03
1.2147e-01	-3.1857e-01	-2.0023e+01	1.9819e+00	-1.4838e-05
9.3060e-01	-3.7123e-01	5.6713e+01	1.6195e+01	1.1593e-04
5.2975e+00	1.0497e+00	-3.2672e-05	-3.4348e-05	-1.4915e+01

(Columns 6 through 9) $K_{\delta p}$ =

5.6152e-03	-5.7903e-01	2.2713e-03	1.1439e-03	-8.1261e-01
2.4741e-05	-2.2436e-03	2.0137e-05	4.7736e-06	-7.8155e-01
-5.8529e-05	5.5120e-03	-3.6180e-05	-1.3315e-05	1.9853e+00
4.0994e+01	-2.3376e+03	7.8965e+01	6.8074e+00	2.2454e-08

Note that the gains in the 9th column are the gains on the integral of fan speed.

Appendix D. Algorithm for Obtaining the EIMF/LTR Compensator of Fig. 1

Under the assumption that CB is of full rank, obtain the singular value decomposition of B,

$$B = [\,U_1 \quad U_2]\begin{bmatrix}\Sigma_B\\ 0\end{bmatrix}V_1^T$$

Defining,

$$\begin{bmatrix}U_2^T\\ C\end{bmatrix}^{-1} = [\,L_1 \quad L_2]$$

the state space matrices for the LTR compensator of Eqns. (14) and (15) are,

$$\hat{A} = U_2^T A\, L_1 \qquad \hat{B} = U_2^T A\, L_2$$
$$\hat{C} = K_{fb}L_1 \qquad \hat{D} = K_{fb}L_2$$

$$K(s) = K_{fb}(\hat{C}(sI - \hat{A})^{-1}\hat{B} + \hat{D})$$

Appendix E. EIMF/LTR Compensator State Space Realization

$\hat{A}$ =

5.7226e+04	2.0882e+04	-4.2212e+04	6.4002e+04	9.4118e+00	0
-2.2824e+04	-8.3294e+03	1.6822e+04	-2.5505e+04	-1.3850e+01	0
2.3632e+01	8.6205e+00	-1.1212e+01	2.6424e+01	5.5470e-03	0
-4.3788e+04	-1.5978e+04	3.2286e+04	-4.8980e+04	-3.9126e+00	0
0	0	0	0	-1.0000e+00	0
0	0	0	0	0	0

$\hat{B}$ =

-4.1865e+04	1.2836e+04	-8.7611e+04	-9.4118e+00
1.6689e+04	-5.1168e+03	3.4906e+04	1.3850e+01
-1.6144e+01	4.9111e+00	-1.4672e+01	-5.5470e-03
3.2034e+04	-9.8216e+03	6.6991e+04	3.9126e+00
0	0	0	1.0000e+00
0	0	0	1.0000e+00

$\hat{C}$ =

(Columns 1 through 5)

2.0736e+02	7.5653e+01	1.1425e+01	2.3188e+02	4.3601e-02
1.1963e+00	4.3648e-01	1.3142e+00	1.3379e+00	1.5458e-04
2.9408e+00	1.0731e+00	1.5779e+01	3.2895e+00	-4.7652e-04
6.6995e+05	2.4446e+05	-4.9409e+05	7.4930e+05	9.1941e+01

(Column 6) $\hat{D}$ =

-4.2457e-02	-1.2198e+02	3.6856e+01	-8.9368e+01	-4.2457e-02
-1.4980e-04	-3.4894e-01	-1.7434e-01	-2.1007e+01	-1.4980e-04
4.6320e-04	2.0863e+00	-7.2555e-01	5.9131e+01	4.6320e-04
-8.5134e+01	-4.9011e+05	1.5027e+05	-1.0254e+06	-8.5134e+01

Acknowledgements

This work was sponsored by NASA Lewis Research Center under Grant No. NAG3-998. Mr. Peter Ouzts is the technical monitor.

References

[1] Schmidt, D.K., Schierman, J.D., "Analysis of Airframe/Engine Interactions - An Integrated Control Perspective," AIAA Paper No. 90-1918, presented at the 26th AIAA Joint Propulsion Conference, Orlando, Fl, July, 1990.

[2] Shaw, P.D., Rock, S.M., and Fisk, W.S., "Design Methods for Integrated Control Systems," AFWAL -TR-88-2061, Aero Propulsion Laboratory, Air Force Wright Aeronautical Laboratories, Dayton Ohio, June, 1988.

[3] Rock, S.M., Emami-Naeini, A., Anex, R.P., "Propulsion Control Specifications in Integrated Flight/Propulsion Control Systems," AIAA Paper No. 88-3236, AIAA/ASME/SAE/ASEE 24th Joint Propulsion Conference, Boston, Mass., 1988.

[4] Smith, K.L., "Design Methods for Integrated Control Systems," AFWAL-TR-86-2103, Aero Propulsion Laboratory, Air Force Wright Aeronautical Laboratories, Dayton Ohio,December, 1986.

[5] Garg, S., Mattern, D.L., and Bullard, R.E., "Integrated Flight/Propulsion Control System Design Based on a Centralized Approach," AIAA Paper No. 89-3520, AIAA Guidance, Navigation and Control Conference, Boston, Massachusetts, 1989.

[6] Anderson, M.R., Schmidt, D.K., "The Significance of Error Dynamics in Model-Following For Flight Control Design," AIAA Paper No. 87-2311, AIAA Guidance, Navigation and Control Conference, Monterey, California, 1987.

[7] Schmidt, D. K., "Flight Control Design Research to Meet Handling Qualities Requirements, Phase II," final report for the McDonnell Aircraft Co., performed at Arizona State Univ., Dept. of Mech and Aero Engr., Tempe, AZ, July, 1989.

[8] Doyle, J., Stein, G., "Multivariable Feedback Design: Concepts for a Classical/Modern Synthesis," IEEE Transactions on Automatic Controls, Vol. AC-26, No. 1, pp. 4-16, Feb., 1981.

[9] Bacon, B.J., "Closed-Form Solution for Loop Transfer Recovery Via Reduced-Order Observers," AIAA Paper No. 89-3455, AIAA Guidance, Navigation and Control Conference, Boston, Massachusetts, 1989.

[10] Anon., MIL-8785C, Flying Qualities for Piloted Airplanes, USAF, Flight Dynamics Laboratory, WPAFB, Dayton, Ohio.

[11] Ridgely, D.B., Banda, S.S., "Introduction to Robust Multivariable Control," AFWAL-TR-85-3102, Flight Dynamics Laboratory, Air Force Wright Aeronautical Laboratories, Dayton Ohio, February, 1986.

[12] Schmidt, D.K., and Foxgrover, J.A., "Multivariable Flight Control Synthesis Approaches to Meet Handling Qualities Objectives," AIAA paper no. 84-1831, GN&C Conf., Seattle, August, 1984.

[13] Sinha, P.K., *Multivariable Control,* Marcel Dekker, Inc., New York, 1984.

Robust Control Synthesis for Integrated Flight and Propulsion Control

John D. Schierman and David K. Schmidt

Aerospace Research Center
College of Engineering and Applied Sciences
Arizona State University
Tempe, AZ 85287-8006

Abstract

Two control synthesis methodologies are presented and applied to synthesize control laws for integrated flight and propulsion control (IFPC). The vehicle considered is representative of an unstable modern fighter aircraft equipped with a 2D thrust-vectoring and thrust-reversing nozzle. The linearized model of this vehicle includes both airframe and engine dynamics. It is necessary to regulate some responses and dynamically shape others, thus leading to a hybrid control problem formulation. A linear quadratic (LQ) model following formulation is the first approach to this hybrid problem. Compensators are then obtained to realize an output-feedback control law, by using standard loop-transfer-recovery procedures. An H^∞ formulation is also presented. For the LQ formulation, near-perfect airframe response following can be obtained while good stability robustness and reasonable loop cross-over frequencies are found in the individual loop transfers. The trade-off between model following performance and multivariable stability robustness, as measured by singular value tests, is specifically addressed. Results obtained via the H^∞ control formulation are shown to be similar to those from the LQ formulation.

As Presented at the December 1990 IEEE Conference on Decision and Control Honolulu, Hawaii.

Robust Control Synthesis for Integrated Flight and Propulsion Control*

John D. Schierman† and David K. Schmidt††

Aerospace Research Center
College of Engineering and Applied Sciences
Arizona State University
Tempe, AZ 85287-6106

1. Introduction

Conventional aircraft typically do not experience significant dynamical interactions between the airframe and propulsion subsystems. Separate control designs of these subsystems are quite adequate. However, new aircraft configurations are under development in which the propulsion systems are capable of delivering forces and moments to the flight control process to enhance the maneuvering capabilities. For such aircraft, significant dynamic interactions between the airframe and the engine can occur and some configurations may experience interactions in critical frequency ranges. If this coupling is large and not taken into account when designing the control laws, then these dynamical interactions can lead to loss of system performance and stability robustness, or to instabilities, as discussed in Ref. 1.

This problem is referred to here, and elsewhere, as the Integrated Flight and Propulsion Control (IFPC) problem. During the past several years, design integration methods[2-5] have been proposed that were intended to synthesize integrated control laws, while in a variety of ways dealing with the potential dynamic interactions.

In this paper a design approach different from those in Refs. 2-5 is offered, and explored via a case study. This new approach will be referred to as Extended Implicit Model Following (EIMF). Two design methodologies will be presented which implement this new approach. First, EIMF control laws will be synthesized by linear quadratic (LQ) with Loop Transfer Recovery (LTR) techniques, designated as the EIMF/LTR design[6]. Then, a unique H^∞ formulation will be developed and used to synthesize a second set of control laws, referred to as the EIMF/H^∞ design.

The design objectives will be presented at the outset, the justification is given for considering this design approach in light of these goals. Then the synthesis methodologies are presented, and the case study is addressed. The results will then be discussed vis a vis the aforementioned design goals, and conclusions presented.

2. Design Goals and Methodology Motivation

The design objectives for the IFPC problem involve system performance, stability robustness, and implementation issues.

Performance - Foremost among the performance issues is the fact that the control systems must deliver excellent handling qualities, in spite of the potential airframe/engine dynamic coupling. The handling qualities criteria are quantified in terms of specified time constants, damping ratios and frequencies for the airframe modes, as well as closed-loop frequency responses from pilot input. Control laws that produce closed-loop airframe responses that reflect classical

---

* As Presented at the December 1990 IEEE Conference on Decision and Control, Honolulu, Hawaii.

† Doctoral Candidate and Research Associate.

†† Professor of Engineering and Acting Director; Member, IEEE.

airframe dynamics are desirable. In fact, how well the resulting airframe responses approximate certain frequency responses of a conventional aircraft with the desired modal characteristics is one step in meeting the military specifications[7]. One implication of this design goal is that the control system should decouple the airframe and engine responses. If the engine's dynamics are observable in the aircraft responses to pilot inputs, then classical airframe dynamical properties are not obtained. Note that these design goals are not those of a regulator.

Engine control, on the other hand, requires regulation of responses about an operating point, with gain scheduling and transition control from one point to the next within the operating envelope. For example, in order to maintain stable combustion, it is important that the fan and compressor do not exceed their surge limits. For structural considerations, the main burner and the high pressure turbine should not exceed specified pressure and temperature limits. Therefore, stable, robust regulation of responses such as fan and compressor speeds, temperatures, and pressures, is a primary goal in the control design of the engine.

Finally, these performance objectives must be met with minimum actuation requirements such that rate and deflection limits are avoided. Not only are high actuation requirements taxing on the hardware, but rate and deflection limiting also degrade both performance and stability by introducing unmodeled non-linear effects into the loops. Therefore, control bandwidths or crossover frequencies must be as low as possible.

Robustness - The system must possess adequate stability margins so that it is robust against unmodeled or inaccurately modeled dynamics. Usually, this requires minimum gain and phase margins in all loops, although singular value based[8,9] robustness analysis can be performed as well. The results in this paper include both single-loop and multivariable robustness margins. Also, the loop transfers must roll off sufficiently to handle high-frequency unmodeled dynamics or non-linearities.

Implementation - The compensation should be easily implementable. This implies that it should be of low dynamic order, and preferably should be similar to classical control laws. If so, the results can yield additional insight with regard to the control system's interactions with the overall airframe/engine system. Furthermore, the existing techniques for control law validation and verification, as well as the necessary gain scheduling may still be utilized.

Motivation - Model following is an integral part of the formulation considered here so that the closed-loop airframe responses may be shaped to take on desired dynamics. Model following design goals are not those for a regulator and this method may not necessarily yield loop transfers with classical (k/s) loop shapes, just as classical stability augmentors (e.g., pitch dampers) do not yield regulator loop shapes. Implicit rather than explicit model following is utilized to eliminate the dynamic pre-filter that is present in the latter control structure. This leads to closed-loop airframe responses of lower dynamic order that are easier to evaluate in terms of handling-qualities assessments, and simpler to implement. Also, perfect model-following concepts[10] are exploited to minimize loop gains and crossover frequencies.

For an integrated synthesis approach to the IFPC problem, regulation as well as model following must be admitted in the formulation. Typically, engine responses, and perhaps aircraft velocity must be regulated. The implicit-model-following formulation of Refs. 10 and 11 are herein extended to address the hybrid problem of model following for some responses and regulation of others.

The standard LTR procedure[8,9] is employed to synthesize compensators necessary to realize an output feedback structure, utilizing the state-feedback gains obtained from the LQ solution to the EIMF problem. This LTR procedure recovers the state-feedback loop shapes, and hence robustness, at the input to the plant.

Compensators are also directly synthesized by a new H^∞ formulation to realize an EIMF/H^∞ control law design. It will be shown that the control laws developed by the EIMF/LTR and EIMF/H^∞ methods have similar characteristics. It will be shown that with both synthesis techniques there is an explicit trade-off between model-following performance and stability robustness. This interesting result is one of the more significant theoretical aspects of this research and is currently under further consideration.

3. Case Study Vehicular System

The vehicle to be considered in this investigation is the same as in Ref. 6. It is representative of a high performance fighter aircraft with the capabilities of 2-D thrust vectoring and thrust reversing. The vehicle dynamics are linearized about the Short Take Off and Landing (STOL) approach-to-landing reference condition at an airspeed V_o = 120 Knots and flight path angle γ_o = -3°. The states, controls and responses are listed below. This model, with the *same* control and measurement vectors is used for both the EIMF/LTR and EIMF/H^∞ designs.

The state vector of the model, and the control inputs to be considered are, respectively,

$$\vec{x} = [u, \alpha, q, \theta, N_2, N_{2.5}, P_6, T_{41B}]^T \quad \text{and} \quad \vec{u} = [A_{78}, \delta_{TV}, \delta_{flaps}, w_f]^T$$

These variables are defined in the following table.

Table 3.1 - States and Controls of the Case Study Vehicular System

The aircraft states are:
- u = body axis forward velocity (ft/sec)
- α = angle of attack (deg)
- q = pitch rate (rad/sec)
- θ = pitch angle (radians)

The engine states are:
- N_2 = engine fan speed (rpm's)
- $N_{2.5}$ = engine compressor speed (rpm's)
- P_6 = engine mixing plane pressure (psia)
- T_{41B} = high pressure turbine temperature (°R)

The aircraft controls are:
- A_{78} = thrust reverser port area (in^2)
- δ_{TV} = nozzle thrust vectoring angle (deg)
- δ_{flaps} = trailing edge flap deflection angle minus leading edge flap deflection angle (deg) - see Ref. [5]

The single engine control is:
- w_f = main burner fuel flow rate (#/hr)

The aircraft's forward velocity is to be regulated essentially with the thrust reverser, while the attitude dynamics are controlled by thrust vectoring. The flaps are direct lift devices which are used to control the flight-path-to-attitude response, and the fuel-flow rate is used to control the engine fan speed. The measurements used for feedback are

$$\vec{y} = [\, u, \alpha, q, N_2]^T$$

The vehicle model, partitioned in the following manner, is given in Appendix A,

$$\begin{bmatrix} \dot{x}_A \\ \dot{x}_E \end{bmatrix} = \begin{bmatrix} A_A & A_{AE} \\ A_{EA} & A_E \end{bmatrix} \begin{bmatrix} x_A \\ x_E \end{bmatrix} + \begin{bmatrix} B_A & B_{AE} \\ B_{EA} & B_E \end{bmatrix} \begin{bmatrix} u_A \\ u_E \end{bmatrix} \tag{3.1}$$

where the subscript A denotes aircraft subsystem and controls, and the subscript E denotes engine subsystem and controls. Results from a modal analysis are shown in Table 3.2. This table presents the open loop poles and the responses dominated by these modes. Note that the short period mode is unstable.

Table 3.2 - Modal Analysis of the Open Loop System

Open Loop Poles	Mode Shapes
-0.0571 ± 0.2154j	phugoid mode (u)
-1.472 +1.065	short period mode (w,q,θ)
-1.401 -3.569 -6.958	highly coupled engine modes involving all the engine states
-89.28	mostly associated with P6

4. Performance Objectives for the Case Study

The flight control synthesis objective is to obtain classical fourth-order longitudinal aircraft responses to pilot stick input, given by,

$$\frac{q(s)}{\delta_p(s)} = \frac{K_q\, s(s + 1/\tau_{\theta_1})\,(s + 1/\tau_{\theta_2})}{(s^2 + 2\zeta_{ph}\omega_{ph}\, s + \omega_{ph}^2)(s^2 + 2\zeta_{sp}\omega_{sp}\, s + \omega_{sp}^2)}$$

$$\frac{\alpha(s)}{\delta_p(s)} = \frac{K_\alpha(s + 1/\tau_{\alpha_1})\,(s + 1/\tau_{\alpha_2})}{(s^2 + 2\zeta_{ph}\omega_{ph}\, s + \omega_{ph}^2)(s^2 + 2\zeta_{sp}\omega_{sp}\, s + \omega_{sp}^2)}$$

(Phugoid Mode) (Short Period Mode) (4.1)

This implies the engine modes should not contribute to these responses. The short-period mode must be stabilized, achieving a specified frequency and damping ratio. Also, a desirable value for the real flight-path time constant, $1/\tau_{\theta 2}$, should be obtained. Table 4.1 lists the desired values selected for these parameters in this analysis, and are believed to be consistent with the military specification[7].

Table 4.1 - Desired Attitude Modal Parameters

ω_{sp}	2 Rad/Sec
ζ_{sp}	0.707
$1/\tau_{\theta 2}$	0.52 Rad/Sec

The value for the flight path time constant is driven by handling requirements, but is also consistent with Ref. 5, which states that it should not be increased above this value due to excessive flap deflections.

The requirements on the phugoid mode will be met by achieving some modest damping for this mode, and by rendering this mode essentially unobservable in the attitude response. Therefore, the desired attitude response may be defined in terms of the following dynamic model in state space form:

$$\begin{bmatrix}\dot{x}_1\\ \dot{x}_2\end{bmatrix}=\begin{bmatrix}0 & 1\\ -\omega_{sp}^2 & -2\zeta_{sp}\omega_{sp}\end{bmatrix}\begin{bmatrix}x_1\\ x_2\end{bmatrix}+\begin{bmatrix}0\\ 1\end{bmatrix}\delta_p$$

$$\begin{bmatrix}\alpha_m\\ q_m\end{bmatrix}=\begin{bmatrix}Z_\alpha & 0\\ M_\delta/\tau_{\theta_2} & M_\delta\end{bmatrix}\begin{bmatrix}x_1\\ x_2\end{bmatrix} \qquad (4.2)$$

which yields the following transfer functions:

$$\frac{\alpha_m(s)}{\delta_p(s)}=\frac{Z_\alpha}{s^2+2\zeta_{sp}\omega_{sp}s+\omega_{sp}^2}$$

$$\frac{q_m(s)}{\delta_p(s)}=\frac{M_\delta(s+1/\tau_{\theta_2})}{s^2+2\zeta_{sp}\omega_{sp}s+\omega_{sp}^2} \qquad (4.3)$$

Here, δ_P is the input from the pilot (e.g., stick deflection). The remaining terms to be selected are Z_α and M_δ. These values are obtained from the short-period approximation for the study vehicle. This approximation yields

$$\frac{\alpha(s)}{\delta_{tv}(s)}\approx\frac{-0.1526(s+28.67)}{(s-1.003)(s+1.464)}\approx\frac{-4.376\ \ (\text{for } s\approx 0)}{(s-1.003)(s+1.464)}$$

and

$$\frac{q(s)}{\delta_{tv}(s)}\approx\frac{-0.0797(s+0.3199)}{(s-1.003)(s+1.464)}$$

from which,

$$Z_\alpha = -4.376\ \text{deg/(slug-ft/sec)}$$
$$M_\delta = -0.0797\ \text{/lbs}$$

Therefore, Eqn. (4.3) becomes:

$$\frac{\alpha_m(s)}{\delta_p(s)}=\frac{-4.376}{(s+1.414\pm 1.414j)}\left(\frac{\text{deg}}{\text{lbs}}\right)$$

$$\frac{q_m(s)}{\delta_p(s)}=\frac{-0.0797(s+0.52)}{(s+1.414\pm 1.414j)}\left(\frac{\text{rad/sec}}{\text{lbs}}\right) \qquad (4.4)$$

The objective of the engine control design here is to simply regulate the fan speed. Quantitative specifications on the disturbance response of the fan speed, such as maximum overshoot allowed or desired settling time, have not been formulated at this time. So, the response characteristics will be selected to yield engine-loop crossover frequencies close to those in the attitude loop, thereby maximizing the potential for dynamic interactions, the basic issue in this research.

5. Control Law Structure for the Case Study

The following block diagram represents the closed-loop system,

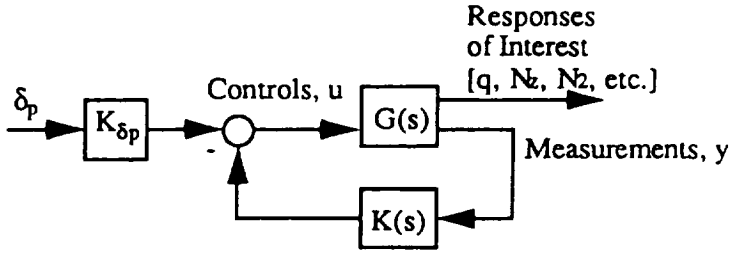

Figure 5.1 - Block Diagram of the Feedback Control Structure

where, the control law is

$$u = -K(s)\, y \; -K_{\delta p}\delta_p$$

or, (5.1)

$$\begin{bmatrix} A_{78} \\ \delta_{tv} \\ \delta_{flap} \\ w_f \end{bmatrix} = - \begin{bmatrix} k_{11} & k_{12} & k_{13} & k_{14} \\ k_{21} & k_{22} & k_{23} & k_{24} \\ k_{31} & k_{32} & k_{33} & k_{34} \\ k_{41} & k_{42} & k_{43} & k_{44} \end{bmatrix} \begin{bmatrix} u \\ \alpha \\ q \\ N_2 \end{bmatrix} - K_{\delta p}\delta_p$$

Note that the structure of the compensator, K(s), will be the same for both the EIMF/LTR and EIMF/H^∞ designs. Also note, $K_{\delta p}$ will be a 4x1 vector of constant gains (for both designs) on the pilot stick input, δ_p.

6. EIMF/LTR Control Synthesis Methodology[10,11]

Model Following - Consider the control of the aircraft/engine modeled as linear time-invariant dynamical system, or

$$\begin{aligned} \dot{x} &= Ax + Bu \\ y &= Cx \end{aligned} \tag{6.1}$$

The model of the desired dynamics to be followed is represented as

$$\begin{aligned} \dot{x}_m &= A_m x_m + B_m \delta_p \\ y_m &= C_m x_m \\ \dot{\delta}_p &= A_p \delta_p \end{aligned} \tag{6.2}$$

where δ_p represents the (unknown) stick input from the pilot. Since δ_p is not known a priori, it is modeled as low-pass white noise.

The model following error vector is the difference between the vehicle's responses and the responses of the desired model,

$$e = y - y_m \tag{6.3}$$

with error dynamics

$$\dot{e} = -G_e e \tag{6.4}$$

The error dynamics matrix, G_e, is selected by the designer. The quadratic loss function to be minimized is

$$J = \int_0^\infty \left\{(\dot{e}+G_e e)^T Q (\dot{e}+G_e e) + u^T R u\right\} dt \tag{6.5}$$

where the weighting matrices on the error dynamics and control inputs, Q and R, are also to be selected .

The solution of this LQ problem is the constant-gain control law,

$$u = -K_{fb}x - K_{ff}x_m - K_{\delta_p}\delta_p \tag{6.6}$$

Perfect model following results when the error vector is zero for all time, and is guaranteed achievable when CB is square and of full rank. The perfect model following control law can be obtained by algebraically solving for u which yields $\dot{e} + G_e e = 0$. However, this control law will result in closed loop pole-zero cancellations of any right half plane transmission zeros. The above LQ control law will asymptotically approach the perfect model following control law as R approaches zero, if perfect model following is achievable and the system has no right half plane transmission zeros[12]. If right half plane transmission zeros are present, the LQ formulation will give closed loop poles located at the stable mirror images of the right half plane transmission zeros.

Implicit model following results when the gains on the model states, K_{ff}, are zero. This can be assured if C_m is chosen to be square and invertible, and the error dynamics are chosen to be

$$G_e = -C_m A_m C_m^{-1} \tag{6.7}$$

The matrices Q and R in the above loss function can be used to adjust the control law design, but the choice of desired dynamics to be followed and the error dynamics are the most critical part of the synthesis.

The synthesis approach just described must now be extended to allow regulation of some of the system's responses. Regulation is incorporated into the model following synthesis by defining the desired responses to be "followed" by the regulated responses as the constant zero. For example, if responses y_1 and y_2 are to follow a desired model with responses y_{1m} and y_{2m}, while responses y_3 and y_4 are to be regulated, then the error vector becomes:

$$\vec{e} = \begin{bmatrix} y_1 - y_{1_m} \\ y_2 - y_{2_m} \\ \hline y_3 \\ y_4 \end{bmatrix} \tag{6.8}$$

Otherwise, the formulation and solution to the LQ problem proceeds as above.

Robustness - In Appendix B, one form of the LQ guaranteed singular-value-robustness margin is presented. Unfortunately, the model following linear quadratic design does not deliver such a guarantee. The solution of the state-feedback gain matrix, K_{fb}, of Eqn. (6.6) is,

$$K_{fb} = \hat{R}^{-1}[(CB)^T Q C_1 + B^T P_1] \tag{6.9}$$

where,

$$\hat{R} = R + (CB)^T Q CB, \quad C_1 = CA + G_e C$$

and P_1 is the solution to the following matrix Riccati equation,

$$0 = P_1 A_1 + A_1^T P_1 - P_1 B \hat{R}^{-1} B^T P_1 + C_1^T Q_1 C_1 \tag{6.10}$$

with,

$$A_1 = A - B\hat{R}^{-1}(CB)^T Q C_1 \quad \text{and} \quad Q_1 = Q - QCB\hat{R}^{-1}(CB)^T Q$$

Now, just as Kalman's Inequality, Eqn. (B.6), can be derived from the associated LQR Riccati Eqn. (B.5), the following inequality can be derived from the above Riccati equation:

$$[I + \hat{R}^{1/2} K_{fb} \bar{\phi}(I+Z) B \hat{R}^{-1/2}]^T [I + \hat{R}^{1/2} K_{fb} \phi (I+Z) B \hat{R}^{-1/2}] \geq I \tag{6.11}$$

where,

$$Z = P_1^{-1} C_1^T Q C = P_1^{-1}(CA + G_e C)^T Q C \tag{6.12}$$

Note, $\phi = (sI-A)^{-1}$ is the resolvent matrix of the system of Eqn. (6.1) evaluated at $s=j\omega$ (ω = frequency), and $\bar{\phi}$ is its complex conjugate. The following guarantee results from this inequality:

$$\underline{\sigma}\left[\hat{R}^{1/2}\left(I + \left(K_{fb}\phi(I+Z)B\right)^{-1}\right)\hat{R}^{-1/2}\right] \geq 1/2 \text{ (-6 dB) for all } \omega \tag{6.13}$$

where, $\underline{\sigma}$ = minimum singular value.

Although the guaranteed stability robustness of this system is less than that for LQ regulators, when $\hat{R} \approx r_o I$, where r_o = scalar, and $\bar{\sigma}(Z) << 1$, Eqn. (6.13) will approach the LQR robustness guarantee of Eqn. (B.7).

The above reveals the trade-off between multivariable robustness and model following performance. Model following performance may be improved by either increasing Q or decreasing R. Increasing Q will directly increase Z. Decreasing R will decrease P_1, increasing P_1^{-1}, thus also increasing Z. As Z gets larger the guarantee offered by Eqn. (6.13) moves further away from the LQR guarantees. Recall that if R is set to zero, and if there are no right half plane transmission zeros, then perfect model following results. In this case, Q_1 in the above Riccati equation becomes zero. Hence, $P_1 = 0$, Z becomes infinite, and no guarantees can be given by Eqn. (6.13).

If R is chosen to be $r_o I$, and Q is decreased, then Eqn. (6.13) will approach the LQR robustness guarantees. However, reducing Q degrades the model following performance.

Scaling Effects - Since the loss function J, of Eqn. (6.5) is a scalar, the minimization of J must be formulated so that it will appropriately minimize the model following errors and control efforts according to their relative sizes of units. This may be achieved by normalizing or scaling the control inputs and system responses by dividing each by their maximum value, and choosing $Q = q_o I$, and $R = r_o I$. For example, nominal values of fan speed are of the order of 10,000 RPM's, and nominal values of angle of attack are of the order of less than 10°. Therefore, a unity change in fan speed is insignificant, whereas a unity change in angle of attack can be a large perturbation. By scaling, a unity change in fan speed will be equivalent in size to a unity change in angle of attack.

It can be shown that the following choice of weighting matrices is equivalent to scaling the control inputs and system responses.

$$Q = q_o Q', \quad q_o = \text{scalar}, \quad Q' = S_e^2$$
$$R = r_o R', \quad r_o = \text{scalar}, \quad R' = S_u^2 \tag{6.14}$$

where,

$$S_e = \text{diag}\{1/(e_i)_{max}\} \qquad S_u = \text{diag}\{1/(u_i)_{max}\} \tag{6.15}$$

$(e_i)_{max}$ is the maximum allowable magnitude of the i'th model following error, and $(u_i)_{max}$ is the maximum control effort available from the i'th control. This choice of Q and R is effectively Bryson's rule[13] for choosing weights in the LQR quadratic loss function. It may be a difficult task to choose the matrices S_e and S_u from a trial and error approach. These values should be chosen in an intelligent manner from an understanding of the system.

Once Q' and R' are fixed, the only design "dial" left is the ratio q_o/r_o. It has been found that only the ratio, not the individual values of q_o and r_o, determines the robustness/performance trade-off in the design. If this ratio is decreased, the guarantee given by Eqn (6.13) approaches the LQR robustness guarantees, but model following performance degrades.

LTR - Assuming that weighting matrices Q and R can be found that give a satisfactory trade-off between performance and robustness using the EIMF state-feedback gains, compensators may then be synthesized using the standard LTR procedure[8,9] to obtain output feedback control laws. With the compensation K(s) so obtained, and the pilot-input gains, K_δ, taken from Eqn. (6.6), the augmented system becomes that shown in Fig. 5.1.

7. EIMF/LTR Control Law Synthesis for the Case Study

With the desired attitude model to follow, presented previously, and the desire to regulate forward speed and engine fan speed, the error vector is:

$$\vec{e} = \begin{bmatrix} \alpha - \alpha_m \\ q - q_m \\ \hline u \\ N_2 + \int N_2 \end{bmatrix} \tag{7.1}$$

Note that integral of fan speed is added in the above. Addition of this term is associated with the fact that integral action on N_2 is desired. With this error vector, the finite transmission zeros of the open-loop system are shown in Table 7.1.

Table 7.1 - Finite Transmission Zeros of the Open Loop System

Transmission Zeros
-68.612
-13.0491 ± 5.5632j
-1.0
0.0

The transmission zero at -1 is due to the inclusion of the integral of engine fan speed in the error vector, as explained in Ref. 6. The transmission zero at the origin is due to the fact that pitch-rate is used in the error vector. If pitch rate plus integral of pitch rate, or θ, were used, this zero would move into the left half of the complex plane.

The error dynamics are now selected to be

$$G_e = \begin{bmatrix} -C_m A_m C_m^{-1} & 0 & 0 \\ 0 & g_{e_u} & 0 \\ 0 & 0 & g_{e_{N2}} \end{bmatrix} \tag{7.2}$$

This choice of error dynamics reflects the desire to decouple the attitude dynamics from the engine speed and forward speed, as well as implicitly follow the desired short period model, (A_m and C_m are given by Eqn. (4.2).) Finally, the forward-speed and engine-speed responses will include a mode with time constants g_{e_u} and $g_{e_{N2}}$, respectively. Values for these time constants were chosen to be 0.1 and 1 rad/sec, respectively.

Some design results are given for two different values of the ratio q_o/r_o. Note that for the vehicular case study, the scaling matrices S_y and S_u, used in the weighting matrices Q and R, have been chosen, from Ref. 5, to be

$$\begin{aligned} S_y &= \text{diag}[0.05,\ 0.3,\ 17.189,\ 1.7446\text{x}10^{-3}] \\ S_u &= \text{diag}[0.02,\ 0.1,\ 0.1,\ 2.0\text{x}10^{-4}] \end{aligned} \tag{7.3}$$

8. EIMF/LTR Design Results

The first results presented are for the ratio $q_o/r_o = 1\text{x}10^4$. Using the EIMF state feedback gains, K_{fb}, the compensator is obtained from the standard LTR procedure[9]. Comparisons of singular value plots of the loop transfers using the state feedback control law, or $K_{fb}(sI\text{-}A)^{-1}B$, and the LTR compensation, or $K(s)C(sI\text{-}A)^{-1}B$, revealed complete robustness recovery. The compensator transfer-function matrix, or K(s) in Fig. 5.1, is given in Table 8.1 for this control law after some straight forward order reduction. The transfer functions presented in this table are all fifth order, with poles at the finite transmission zeros of the plant, plus one additional pole at the origin due to integral control on fan speed. Note that many of these compensators can be simplified further.

For $q_o/r_o = 1\text{x}10^4$, near-perfect model following performance is achieved. The closed-loop transfer functions obtained using the above feedback compensation are,

$$\begin{aligned} \frac{\alpha(s)}{\delta_p(s)} &= \frac{-4.389}{(s+1.414\pm1.414j)}\, T_1(s) \left(\frac{\text{deg}}{\text{lbs}}\right) \\ \frac{q(s)}{\delta_p(s)} &= \frac{-0.0797(s+0.521)}{(s+1.414\pm1.414j)}\, T_2(s) \left(\frac{\text{rad/sec}}{\text{lbs}}\right) \end{aligned} \tag{8.1}$$

where the poles $T_1(s)$ and $T_2(s)$ are the poles of the phugoid mode and all engine modes. Both $T_1(s)$ and $T_2(s)$ are very close to unity due to accurate pole-zero cancellations. Comparing these results to the desired responses given by Eqn. (4.4), near-perfect model following is evident.

Figs. 8.1 and 8.2 present the closed-loop frequency responses for angle of attack and pitch rate from pilot stick input. Also plotted are the desired frequency responses, which are not visible, since they are essentially the same as the closed-loop responses.

The fan speed disturbance rejection performance is indicated by the magnitude of the engine loop's sensitivity function, shown in Figure 8.3. It can be seen that disturbances with frequency content below 20 rad/sec will be rejected.

Table 8.2 summarizes the cross-over frequencies, phase margins and gain margins for all four individual loops, with each loop broken at the input to the plant, and all others closed. Note that the magnitude of the flap loop is less than one throughout the frequency range.

Table 8.1 - EIMF/LTR Compensation Matrix

Con-trols	Numerators for the Individual Compensator Transfer Functions	Bode Gain	Measure-ments	Units of Compensator
A78	-123.3(0)(0)(0.90)[0.93,9.5]	-0.7	u	sq-in/(ft/sec)
	142.3(0)(-1.8e-04)(-0.61)[0.93,10.1]	-0.6	α	sq-in/deg
	-110.3(0)(1.5)(13.2)(-25.2)(31.1)	120.0	q	sq-in/(rad/sec)
	-0.04[-0.2,0.4][-0.06,8.5](13.4)	-3.8e-4	N2	sq-in/(RPM)
δ_{tv}	-0.4(0)(0)[0.9,11.8](-29.5)	0.1	u	deg/(ft/sec)
	-84.8(0)(0)[0.92,13.6]	-1.1	α	deg/deg
	-21.1(0)(-0.1)[0.92,14.0](67.2)	2.1	q	deg/(rad/sec)
	1.2e-05(-0.5)[0.7,1.0](17.2)(26.1)(35.6)	-6.5e-6	N2	deg/(RPM)
δflap	1.6(0)(0)[0.9,13.9](50.4)	1.1	u	deg/(ft/sec)
	-1.9(0)(-1.2e-05)[0.9,13.9](51.3)	-1.4	α	deg/deg
	58.8(0)(0.3)[0.9,14.2](68.3)	17.9	q	deg/(rad/sec)
	-3.4e-05(0.4)[0.01,2.3][0.9,13.8](63.4)	5.7e-5	N2	deg/(RPM)
wf	-4.6e+05(0)(2.9e-05)(-0.06)(2.2)(4.3)	-20.0	u	(#/hr)/(ft/sec)
	5.4e+05(0)(-4.0e-05)(0.7)(2.2)(4.3)	250.0	α	(#/hr)/deg
	-1.0e+06(0)(0.3)(2.2)(4.3)(46.9)	-1.1e+4	q	(#/hr)/(rad/sec)
	8269(0.005)[1.0,1.1](10.4)	7.1	N2	(#/hr)/(RPM)
	Characteristic Polynomial of Compensator : $\Delta(s)$ = (0)(0)[0.9,14.2](68.6)			

Note: (a) = (s+a), and [a,b] = complex mode with damping ratio = a, and frequency = b

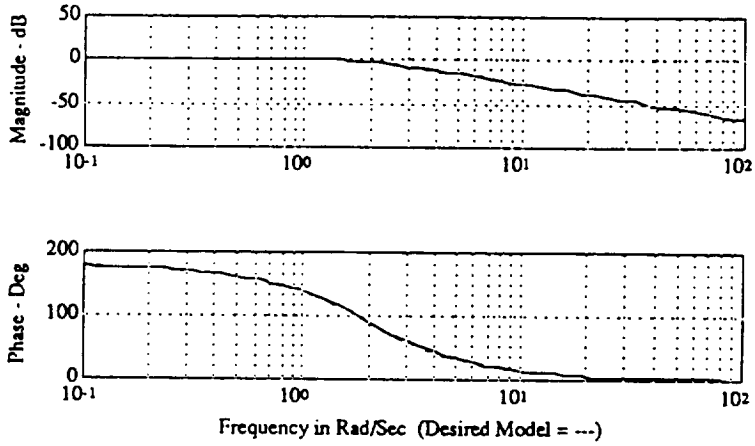

Figure 8.1 - Closed Loop Frequency Response of Angle of Attack from Pilot Stick Input (Deg/lbs)

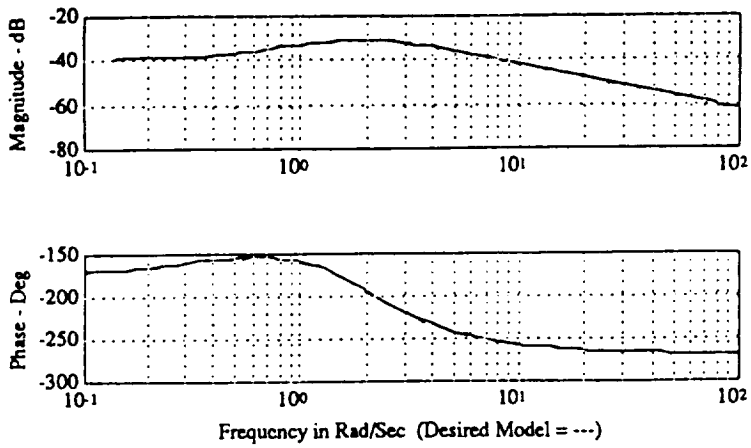

Figure 8.2 - Closed Loop Frequency Response of Pitch Rate from Pilot Stick Input ((Rad/Sec)/lbs)

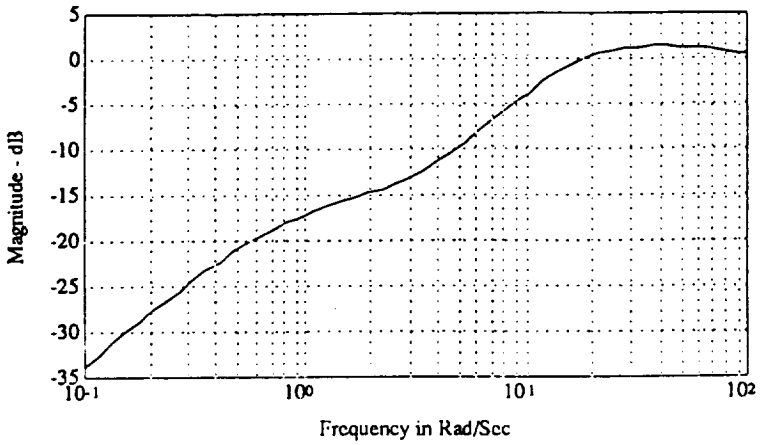

Figure 8.3 - Sensitivity Function of Measured Fan Speed-to-Fan Speed Disturbance (RPM/RPM)

Table 8.2 - Individual Loop Characteristics

Loop	Cross-Over Frequency (rad/sec)	Phase Margin (degrees)	Gain Margin (dB)
Thrust Reversing	0.18	90	∞
Thrust Vectoring	2.0	50	-10
Flaps	——	——	-10
Fuel Flow	10.2	75	12

The cross-over frequencies and stability margins in all the loops are quite good. The thrust vectoring and fuel flow loop transfers are presented below, for example.

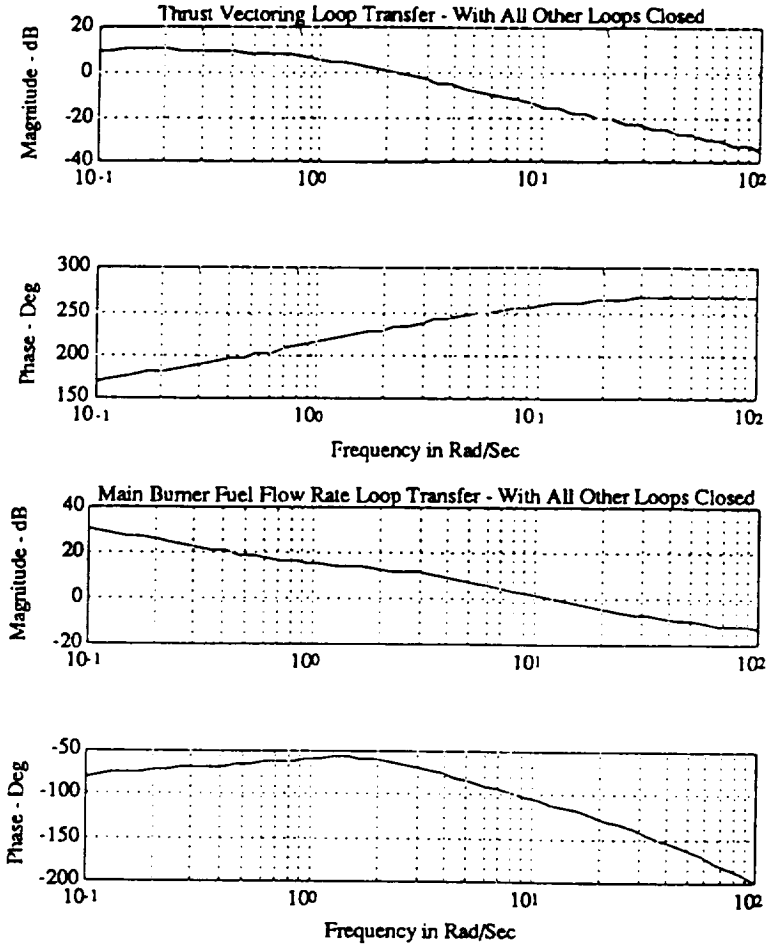

Figure 8.4 - Individual Loop Transfers - Loops Broken One at a Time, With All Other Loops Closed

The following figure presents $\underline{\sigma}(I + (KG)^{-1})$, scaled at each frequency to obtain the least conservative results, as discussed in Appendix B. Again, since full robustness recovery was obtained, this plot is the same whether implemented with full state-feedback or LTR compensation.

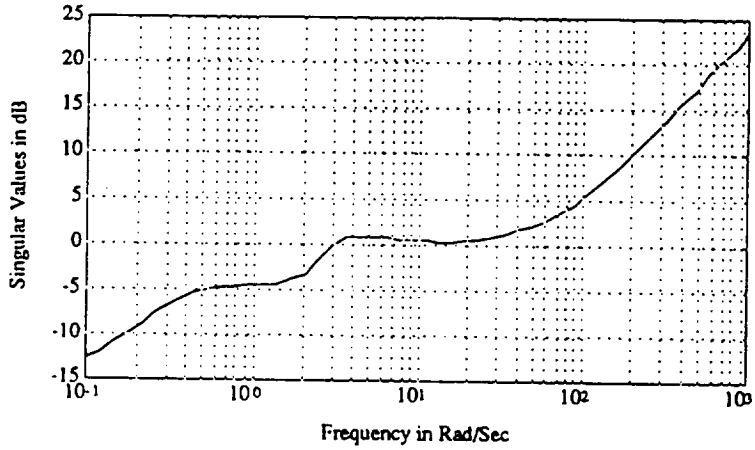

Figure 8.5 - Scaled Multivariable Singular Value Robustness Test $q_o/r_o = 10{,}000$

This plot shows that this system has "LQ-like" multivariable robustness for frequencies above ≈ 0.3 rad/sec. For piloted aircraft, loss of robustness in the low-frequency range, or the phugoid mode is not as critical as loss of robustness at higher frequencies.

It is noted that the results (not shown) for the unscaled singular value test are quite poor. The original units led to widely separated singular values of the loop transfer, and previous work[14] has shown that these multivariable robustness tests work best when plant and loop transfer singular values are closely spaced. Recall that scaling the controls by the matrix S_u gives approximate equivalence in the sizes of the units on the controls. This produces singular values of the scaled loop transfer that are much closer together, and the singular value robustness test, which plots $\underline{\sigma}(I + (S_u K G S_u^{-1})^{-1})$, shows much improved results compared to the unscaled singular value test.

Decreasing the q_o/r_o ratio from $1x10^4$ to 2/3 leads to improved low-frequency robustness, with singular values greater than the LQ guarantee. However, the high-frequency robustness degrades. The results using frequency dependent scaling are shown below.

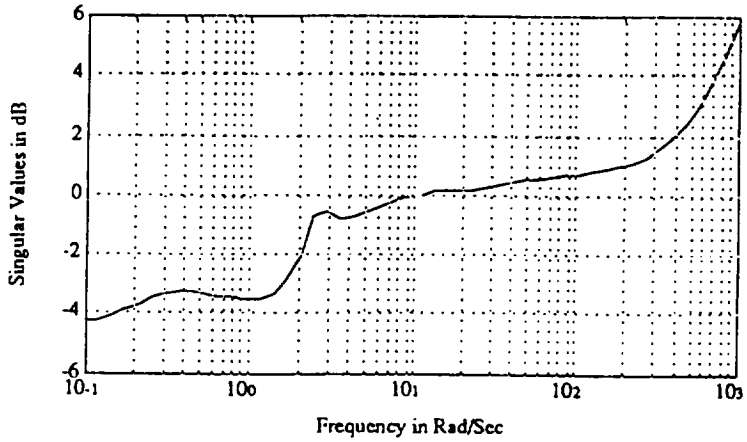

Figure 8.6 - Scaled Multivariable Singular Value Robustness Test
$q_o/r_o = 2/3$

The model following performance also degrades. The corresponding closed loop responses are,

$$\frac{\alpha(s)}{\delta_p(s)} = \frac{-0.1376(s+32.27)}{(s+1.352\pm1.323j)} T_1(s) \left(\frac{\text{deg}}{\text{lbs}}\right) \quad \text{(Note: } 0.1376x32.27 = 4.44\text{)}$$

$$\frac{q(s)}{\delta_p(s)} = \frac{-0.07897s(s+0.2738\pm0.1479j)}{(s+0.1241\pm0.1477j)(s+1.352\pm1.323j)} T_2(s) \left(\frac{\text{rad/sec}}{\text{lbs}}\right) \tag{8.2}$$

and $T_1(s)$ and $T_2(s)$ are only approximately unity. Comparing these results with the desired responses (Eqn. (4.4)) and the responses of the previous case (Eqn. (8.1)) it can be seen that the short period and phugoid modes are no longer decoupled, there is no longer a real $1/\tau_{\theta 2}$ zero, and the desired short period mode's frequency and damping are not achieved. Note, however, the engine's disturbance rejection performance, as measured by the fan speed sensitivity function (not shown), remains approximately the same as that shown in Fig. 8.3.

The individual thrust-vectoring and flap loop transfers also remain approximately the same. The cross-over frequency of the fuel flow loop, on the other hand, decreased to 0.5 rad/sec.

In summary, the first control law gives near perfect model following performance at the expense of low frequency multivariable robustness, and larger cross-over frequency in the fuel

flow loop. The second case led to improved low-frequency multivariable robustness at the expense of both model following performance and high frequency multivariable robustness.

9. H^∞ Theory[15]

An EIMF control synthesis technique can also be formulated using an H^∞-norm minimization framework. The following figure displays the general H^∞ control block diagram structure.

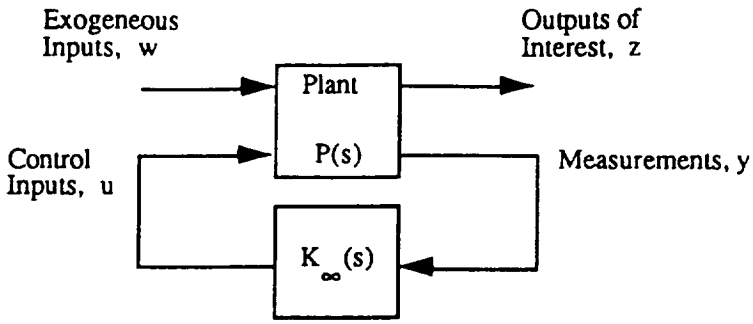

Figure 9.1 - General Block Diagram for the H^∞ Control Problem

Here, the plant P(s) represents the plant dynamics, plus any frequency dependent weighting functions. The exogenous inputs, w, represent external inputs to the system, which may include commanded inputs, low frequency disturbances, and high frequency measurement noises. The outputs of interest, z, are those variables to be controlled, which may include plant responses as well as control inputs, u.

The design objective is to find a compensator, $K_\infty(s)$ that stabilizes the closed loop system and minimizes the H^∞-norm of the transfer function matrix from the outputs of interest, z, to the exogenous inputs, w. The H^∞-norm of a matrix $T(j\omega)$ is defined as

$$\|T\|_\infty \equiv \sup_\omega \left[\bar{\sigma}(T(j\omega))\right] \tag{9.1}$$

Typically, the H^∞ control methodology is used as a multivariable control approach to meet classical control design objectives, namely, loop shaping. Weightings $W_1(s)$ and $W_2(s)$, in the figure below, are chosen, for example, to shape the singular values of the sensitivity and complementary sensitivity matrices.

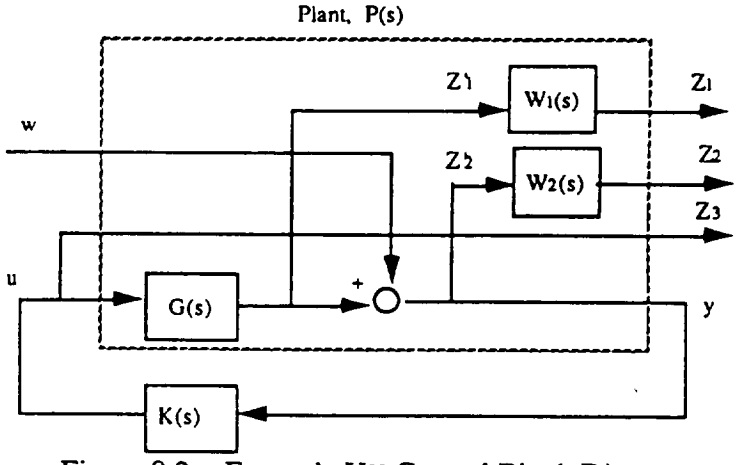

Figure 9.2 - Example H^∞ Control Block Diagram

Once all weighting functions are defined, the "plant," P(s) is defined and the H^∞ compensator can be obtained from Ref. 15. This involves iteratively solving two Riccati equations.

10. EIMF/H^∞ Control Law Methodology and Synthesis

In Section 6 the EIMF control law design methodology utilized LQR theory to minimize the quadratic loss function involving model-following errors, regulation errors, and control inputs. The EIMF design objectives can also exploit H^∞ theory to minimize the H^∞-norm of a transfer function, again involving model-following errors, regulation errors, and control inputs.

Here, an approximate equivalence will be developed between the EIMF/LTR and the EIMF/H^∞ procedures so that comparisons can be made. The following block diagram presents just one EIMF/H^∞ formulation.

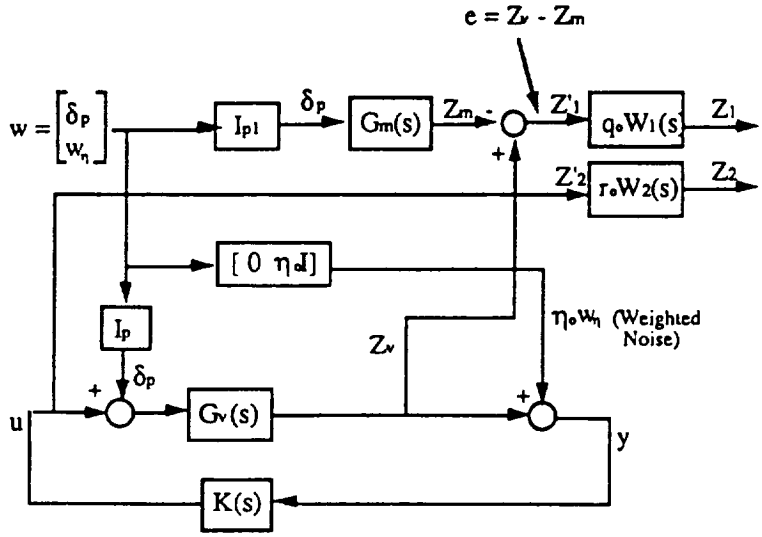

Figure 10.1 - EIMF/H^∞ Control Design Block Diagram

$G_v(s)$ represents the airframe/engine system, Eqn. (6.1), and $G_m(s)$ represents the desired model to follow, Eqn. (6.2). A vector of fictitious measurement noise inputs, w_η, must be included in the vector of exogenous inputs, w. This noise is weighted by some small number, η_o. The matrices I_p and I_{pl} are used so that the only exogenous input into both the desired model and the vehicle model is the pilot stick input, δ_p. For the case study, since the pilot stick input is a scalar, and there are four measurements, ($y = [u, \alpha, q, N_2]^T$) and four controls, ($u = [A_{78}, \delta_{tv}, \delta_{flaps}, w_f]^T$) then,

$$I_p = \begin{bmatrix} 1 & 0 & 0 & 0 & 0 \\ 1 & 0 & 0 & 0 & 0 \\ 1 & 0 & 0 & 0 & 0 \\ 1 & 0 & 0 & 0 & 0 \end{bmatrix} \qquad I_{pl} = [\,1 \;\; 0 \;\; 0 \;\; 0 \;\; 0\,] \tag{10.1}$$

The model following error is formed by subtracting the responses of the vehicle and desired model,

$$e = Z_v - Z_m \tag{10.2}$$

Thus, the intermediate output vector is the model following errors and the control inputs, or,

$$z' = [Z_1' \;\; Z_2']^T = [\, e \;\; u \,]^T \tag{10.3}$$

Note from the block diagram that implicit model following is a result. This formulation will not, however, produce stick gains, such as $K_{\delta p}$ in Eqn. (6.6). Stick gains could possibly be incorporated into the matrices I_p and I_{pl} above. To date, these have been simply chosen to be unity "gains."

The intermediate output vector, z', is then weighted as shown in Fig. 10.1 to form the final output vector, z. Note that q_o and r_o are scalars, and $W_1(s)$ and $W_2(s)$ are matrices which may contain frequency dependent weighting functions. Some parallel can be drawn between the weighting scheme used in the EIMF/LTR design method (see Eqns. (6.14) and (6.15)) here, by choosing

$$q_o W_1(s) = q_o S_y^2, \quad r_o W_2(s) = r_o S_u^2 \tag{10.4}$$

However, for the results presented in the next section, the control inputs and responses are scaled according to:

$$y_{new} = S_y y, \qquad u_{new} = S_u u \tag{10.5}$$

where S_y and S_u are given in Eqn. (7.3). Then the following weightings are used in conjunction with this scaled system:

$$q_o W_1(s) = q_o I, \quad r_o W_2(s) = r_o I, \quad \eta_o = 1 \times 10^{-8} \tag{10.6}$$

This implementation is closely related to that of Eqn. (10.4), and, for numerical reasons, gives improved results.

From the block diagram, the state space description for this H^∞ model following formulation is,

$$\begin{bmatrix} \dot{x}_v \\ \dot{x}_m \end{bmatrix} = \begin{bmatrix} A_v & 0 \\ 0 & A_m \end{bmatrix} \begin{bmatrix} x_v \\ x_m \end{bmatrix} + \begin{bmatrix} B_v I_p \\ B_m I_{pl} \end{bmatrix} \begin{bmatrix} \delta_p \\ w \end{bmatrix} + \begin{bmatrix} B_v \\ 0 \end{bmatrix} u$$

$$\begin{bmatrix} \dot{z}_1 \\ \dot{z}_2 \end{bmatrix} = \begin{bmatrix} C_v & -C_m \\ 0 & 0 \end{bmatrix} \begin{bmatrix} x_v \\ x_m \end{bmatrix} + \begin{bmatrix} 0 \\ I \end{bmatrix} u \tag{10.7}$$

$$y = [\; C_v \quad 0 \;] \begin{bmatrix} x_v \\ x_m \end{bmatrix} + [\; 0 \quad \eta_o I \;] \begin{bmatrix} \delta_p \\ w \end{bmatrix}$$

Frequency-dependent weighting functions can also be augmented to this realization, as desired, and the H^∞ compensator can then be obtained from Ref. 15.

11. EIMF/H^∞ Results

Some results are presented below for two different values of q_o/r_o. For the first case, $q_o/r_o = 1 \times 10^6$, and the compensator transfer-function matrix for this case is given in Table 11.1, after some straight-forward order reduction. The transfer functions presented in this table are seventh order, with some poles at the finite transmission zeros of the plant. Again, inclusion of integral control on fan speed leads to one additional pole at the origin.

Table 11.1 - EIMF/H$^{\infty}$ Compensation Matrix

Con-trols	Numerators for the Individual Compensator Transfer Functions	Bode Gain	Measure-ments	Units of Compensator
A78	0.01(0)(0.08)(1.0)(-1.4)(8.4)[0.9,14.1](69.6)	-0.3	u	sq-in/(ft/sec)
	0.05(0)(0.2)(1.0)(1.3)(-8.0)[0.9,15.7](61.1)	-0.2	α	sq-in/deg
	1.4(0)(2.9e-03)(1.0)[0.2,4.9][0.9,14.3](68.8)	76.0	q	sq-in/(rad/sec)
	-3.0e-04(0.04)(0.9)(1)[1.0,3.0][0.9,13.7](82.0)	-6.9e-3	N2	sq-in/(RPM)
δ_{tv}	2.0e-03(0)(8.0e-03)(1)(-1.8)(4.9)[0.9,14.2](68.6)	-0.04	u	deg/(ft/sec)
	8.3e-03(0)(-0.02)(0.4)(1)[0.9,14.1](28.3)(68.3)	0.18	α	deg/deg
	0.2(0)(9.3e-04)(1)[0.6,2.4][0.9,14.2](68.6)	2.70	q	deg/(rad/sec)
	-4.8e-05(6.8e-03)(1.0)(1)[-0.04,2.1][0.9,14.2](68.9)	-4e-3	N2	deg/(RPM)
δflap	4.6e-05(0)[0.8,0.2](1)[0.9,14.2](-14.5)(68.6)	4.7e-5	u	deg/(ft/sec)
	0.02(0)(-0.02)(0.5)(1)[0.9,14.2](68.2)	0.02	α	deg/deg
	5.1e-03(0)[0.5,0.1](1)(2.2)[0.9,14.2](68.6)	4.4e-4	q	deg/(rad/sec)
	-1.1e-06[-0.2,0.3](1.0)(1)(3.0)[0.9,14.2](68.1)	4.5e-7	N2	deg/(RPM)
wf	39.9(0)[-0.5,0.3](1.0)(6.5)[0.5,15.3]	0.6	u	(#/hr)/(ft/sec)
	3.3e+04(0)[1.0,0.3](1.0)[0.9,4.4]	6.8	α	(#/hr)/deg
	41.9(0)(-0.02)(0.8)[0.8,1.9][0.9,13.4](85.3)	276.0	q	(#/hr)/(rad/sec)
	-5.2(-0.02)(0.7)(1)(1.0)(5.9)[0.7,8.0]	0.2	N2	(#/hr)/(RPM)
	Characteristic Polynomial of Compensator : $\Delta(s)$ = (0)(0)(0.5)(1)[0.9,14.2](68.6)			
Note: (a) = (s+a), and [a,b] = complex mode with damping ratio = a, and frequency = b				

Comparing this table of compensators with Table 8.1, the Bode gains of the compensators for the thrust reverser and thrust vectoring controls are quite similar for both designs. However, the Bode gains above are much smaller for the flap and fuel flow compensators. The poles at (0)[0.9199,14.19](68.61), the transmission zeros of the plant, are present for both designs. However, they are approximately cancelled in all but the fuel flow compensators above, whereas they are only cancelled in the fan speed-to-thrust vectoring and flap compensators in the EIMF/LTR design. Also, the above design contains the additional poles at (0.5)(1).

These differences in compensation lead to differences in the individual loop transfers. For this design, the thrust vectoring loop transfer has large gain at high frequencies. However, the other three are all low-gain loops. The cross-over frequencies, and stability margins of the other three loops are summarized in the table below.

Table 11.2 - Individual Loop Characteristics

Loop	Cross-Over Frequency (rad/sec)	Phase Margin (degrees)	Gain Margin (dB)
Thrust Reversing	1.08	80	-6
Flap	——	——	+11
Fuel Flow	0.2	40	-35/ω=0.13r/s +10/ω=0.35r/s

Further research involving other weighting schemes may help add roll-off to the thrust vectoring loop shape and increase the magnitudes of the other loops.

This value of q_o/r_o gives near-perfect model following and the results match those of the EIMF/LTR design given by Eqn. (8.1) and Figs. 8.1 and 8.2.

Although the performance is excellent, the multivariable robustness is quite poor, as seen in the next figure.

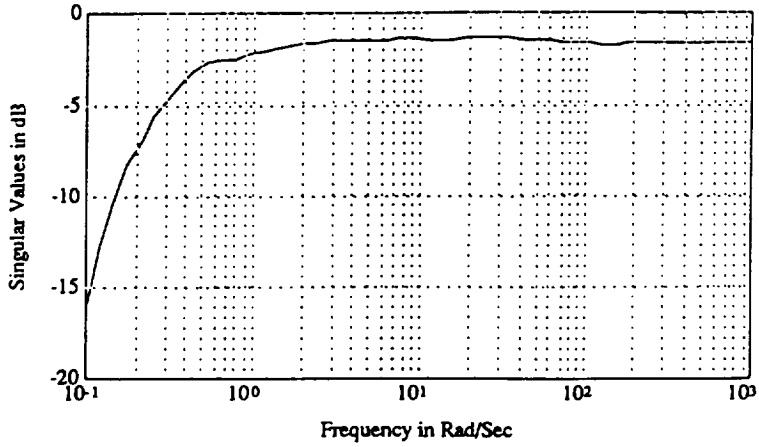

Figure 11.1 - Scaled Multivariable Singular Value Robustness Test
$q_o/r_o = 1x10^6$

Similarities in the design results between the EIMF/LTR method and the EIMF/H^∞ method have been found. Just as in the EIMF/LTR design method, once the weightings $W_1(s)$ and $W_2(s)$ are fixed, the ratio q_o/r_o determines the model following performance and multivariable robustness achieved. Decreasing this ratio will increase the multivariable robustness. If this ratio is made small enough, the robustness can be made as large as the LQR guaranteed margins, however, the model following performance degrades.

Reducing the q_o/r_o ratio to a value of 0.05 dramatically improves the multivariable robustness, as shown in the figure below.

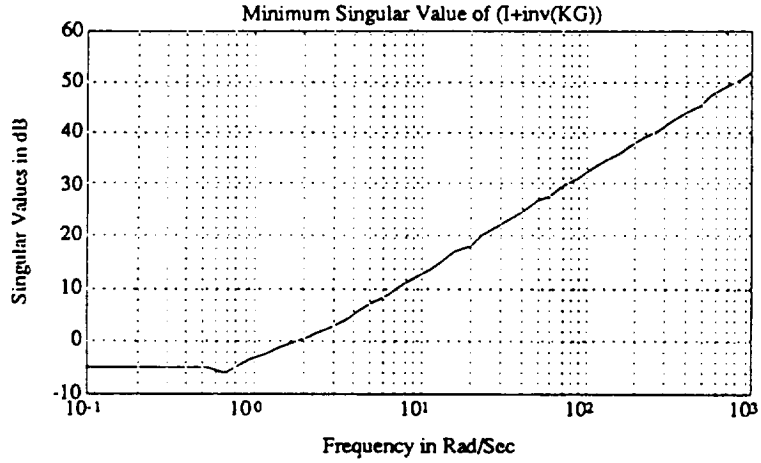

Figure 11.2 - Scaled Multivariable Singular Value Robustness Test
$q_o/r_o = 0.05$

It can be seen that, not only does the robustness satisfy the guarantees of LQ regulators, but the high frequency robustness (roll-off) is excellent. Thus, unlike the EIMF/LTR design (Fig. 8.6), decreasing the q_o/r_o ratio here seems to improve the multivariable robustness for all frequencies. Also, the individual loop shapes all have low cross-over frequencies and good gain and phase margins.

Unfortunately, improvement in the robustness comes at the cost of the model following performance, as seen in the next two plots.

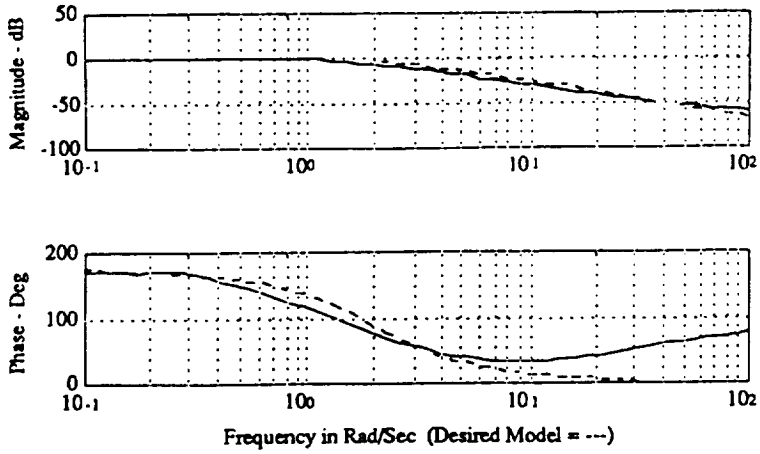

Figure 11.3 - Closed Loop Frequency Response of Angle of Attack from Pilot Stick Input (Deg/lbs)

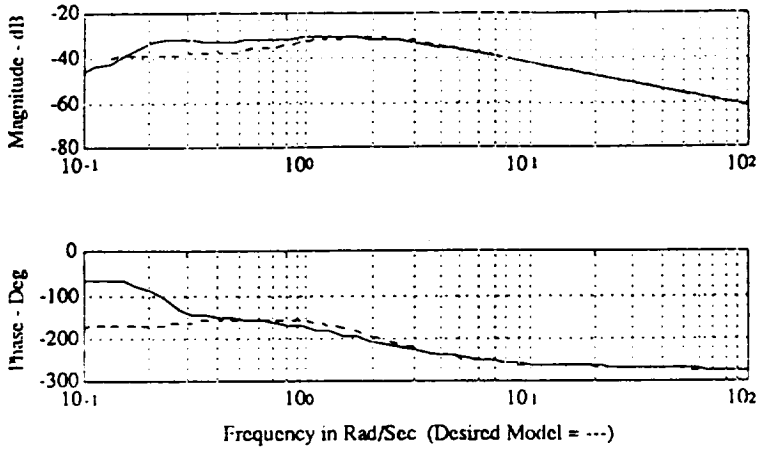

Figure 11.4 - Closed Loop Frequency Response of Pitch Rate from Pilot Stick Input ((Rad/Sec)/lbs)

Conclusions

Control law synthesis techniques were presented that were developed to achieve excellent handling qualities, decoupling the engine and airframe dynamics. However, a clear trade-off between performance and multivariable robustness has been recognized and discussed. The methodology was applied to an integrated flight and propulsion control case study.

The EIMF/LTR approach led to control laws that deliver excellent model following and regulation performance with modest gain crossover frequencies, thus keeping actuation requirements to a minimum. The airframe responses were exactly those desired, thus demonstrating the performance achieved. The engine control laws were simultaneously synthesized, along with those for the airframe, and would appear to deliver good disturbance-rejection performance. The results also indicate reasonable multivariable robustness, as defined herein. However, an increase in low frequency robustness comes at the cost of decreases in both model following performance and high frequency robustness.

The EIMF/H^∞ approach led to control laws that also deliver excellent model following performance. However, the multivariable robustness was poor. As with the EIMF/LTR design, the multivariable robustness can be improved, yet this reduces the model following performance. Other H^∞ formulations which may, for example, take advantage of loop shaping techniques, offer future areas of research.

Appendix A. Linear Model for the Case-Study Vehicle

The states are defined as

$$x = [u\ (ft/sec),\ \alpha(deg),\ q(rad/sec),\ \theta(radians),\ N_2(rpm's),\ N_{2.5}(rpm's),\ P_6(psia),\ T_{41B}(^\circ R)]^T$$

with inputs,

$$u = [A_{78}(in^2),\ \delta_{flaps}(deg),\ \delta_{TV}(deg),\ w_f(\#/hr)]^T$$

For the vehicle in question, the model is

$A_A =$

-3.6523e-02	3.8161e-01	-3.8600e+01	-3.1840e+01
-8.7843e-02	-2.8897e-01	5.6739e+01	5.8886e-01
9.8260e-05	2.7918e-02	-1.9490e-01	-4.8180e-04
0	0	1.0000e+00	0

$A_{AE} =$

3.1440e-04	2.5990e-04	3.8190e-02	2.2500e-03
-2.2924e-05	-1.5892e-05	-2.1976e-03	-1.3331e-04
9.4600e-07	3.7440e-07	3.6680e-05	2.6760e-06
0	0	0	0

$A_{EA} =$

8.1058e-01	5.5150e-01	0	0
1.5812e-01	1.0758e-01	0	0
8.2641e-01	5.6223e-01	0	0
-1.0468e-01	-7.1244e-02	0	0

$A_E =$

-4.1910e+00	6.0220e+00	-3.4340e+02	1.1600e+01
4.2630e-01	-5.7070e+00	2.7160e+01	1.0400e+01
2.2950e-01	1.1550e-01	-9.0240e+01	8.4760e-01
3.7400e-02	-1.0360e-01	-7.9540e+00	-1.0680e+00

$[B_A\ B_{AE}] =$

-2.0550e-01	-4.1830e-04	-8.4280e-02	3.4360e-05
1.2018e-02	-1.5241e-01	-5.5082e-02	-2.0197e-06
1.0680e-04	-7.9700e-02	8.8132e-03	5.5070e-08
0	0	0	0

$[B_{EA}\ B_E] =$

0	0	0	1.4690e-01
0	0	0	5.3600e-02
-4.3020e+01	0	0	1.8130e-02
0	0	0	1.6430e-01

Appendix B. Multivariable Singular Value Robustness

Several singular value tests are often used to measure the stability robustness of multivariable systems[8,9]. For example, the following test may be used to measure the robustness of the system to multiplicative uncertainty at the plant input. First, it is assumed that the nominal closed loop system is stable, and multiplicative perturbations, E, in the loop do not change the encirclement requirements of the critical point in the Nyquist plot. Under these assumptions, if

$$\bar{\sigma}(E) < \underline{\sigma}(I + (KG)^{-1}) \text{ for all frequency, } \omega \qquad (B.1)$$

then the closed loop system is guaranteed to be stable in the presence of E, at the input to the plant, where the true plant is G(I+E). Note that $\bar{\sigma}$ = maximum singular value, and $\underline{\sigma}$ = minimum singular value.

Linear quadratic regulators guarantee a minimum value for the right hand side of the above inequality[9]. Given the following linear time-invariant system,

$$\dot{x} = Ax + Bu$$
$$y = Cx \qquad (B.2)$$

minimization of the quadratic loss function,

$$J = \int_0^\infty [y^T Q y + u^T R u]\, dt \qquad (B.3)$$

leads to the following state-feedback control law,

$$u = -K_{fb}x, \quad K_{fb} = R^{-1}B^{T}P \tag{B.4}$$

where K_{fb} is the matrix of regulator state feedback gains, and P is the solution to the algebraic Riccati equation,

$$0 = A^{T}P + PA - PBR^{-1}B^{T}P + C^{T}QC \tag{B.5}$$

Kalman's Inequality,

$$[I + R^{1/2}K_{fb}\bar{\phi}BR^{-1/2}]^{T}\,[I + R^{1/2}K_{fb}\phi BR^{-1/2}] \geq I \tag{B.6}$$

is derived from this Riccati equation. Note, $\phi = (sI - A)^{-1}$ is the resolvent matrix of the plant, evaluated at $s = j\omega$, and $\bar{\phi}$ is its complex conjugate. Under the assumption that R is diagonal and that the inputs can be scaled such that $R = \rho I$, the guaranteed singular value robustness margin for LQ regulators can then be derived from the Kalman Inequality, and is given as

$$\underline{\sigma}(I + (K_{fb}\phi B)^{-1}) \geq 1/2 \text{ (-6 dB) for all } \omega \tag{B.7}$$

Thus, in the absence of a model for the uncertainty, E, it may be desirable to find control laws that make the right hand side of Eqn. (B.1) as large as possible, and LQ regulators guarantee the above minimum value.

Furthermore, singular values of a transfer function matrix are not independent of the units of that matrix. Therefore, the choice of units for the system will directly influence the results of the singular value test of Eqn. (B.1). The following block diagram shows the inclusion of a scaling matrix S_u at the input to the plant, with input multiplicative uncertainty.

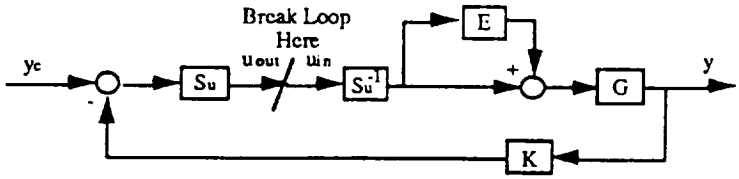

Figure B.1 - Addition of Control Input Scaling to the Loop

If S_u is diagonal, this is equivalent to defining a new set of units for the control inputs. Breaking the loop at the point shown in the figure, the following scaled robustness test may be derived. If,

$$\bar{\sigma}(S_u E S_u^{-1}) < \underline{\sigma}\left(I + (S_u K G S_u^{-1})^{-1}\right)^{-1} \text{ for all } \omega \tag{B.8}$$

then the system is guaranteed to be stable under the same assumptions stated for Eqn. (B.1).

The conservatism of the robustness test of Eqn. (B.1) can therefore be reduced by finding diagonal scaling matrices, equivalent to finding a new set of units for the control inputs, such that the left hand side of the above inequality is made smaller, and the right hand side is made larger. The robustness test is made independent of the units of the system by finding a diagonal scaling matrix *at each frequency* that maximizes the distance between the left and right hand sides of the inequality. In the absence of any models of the uncertainty, it may be desirable to find scaling matrices at each frequency that just make the right hand side as large as possible. This technique is referred to as the "scaled multivariable singular value robustness test," shown in Figs. 8.5, 8.6, 11.1, and 11.2.

Acknowledgements

This work was sponsored by NASA Lewis Research Center under Grant No. NAG3-998. Mr. Peter Ouzts is the technical monitor.

References

[1] Schmidt, D., Schierman, J., "Analysis of Airframe/Engine Interactions - An Integrated Control Perspective," AIAA # 90-1918, 26th AIAA Joint Prop. Conf., Orlando, July, 1990.

[2] Shaw, P., Rock, S., Fisk, W., "Design Methods for Integrated Control Systems," AFWAL-TR-88-2061, Aero Propulsion Laboratory, Air Force Wright Aeronautical Labs, Dayton, June, 1988.

[3] Rock, S., Emami-Naeini, A., Anex, R., "Propulsion Control Specifications in Integrated Flight/Propulsion Control Systems," AIAA # 88-3236, AIAA 24th Joint Prop.Conf., Boston, 1988.

[4] Smith, K., "Design Methods for Integrated Control Systems," AFWAL-TR-86-2103, Aero Propulsion Labs, Air Force Wright Aeronautical Labs, Dayton, December, 1986.

[5] Garg, S., Mattern, D., Bullard, R., "Integrated Flight/Propulsion Control System Design Based on a Centralized Approach," AIAA # 89-3520, AIAA GN&C Conf., Boston, 1989.

[6] Schmidt, D., Schierman, J., "Extended Implicit Model Following As Applied To Integrated Flight and Propulsion Control," AIAA # 90-3444, GN&C Conf., Portland, August, 1990.

[7] Anon., MIL-8785C, Flying Qualities for Piloted Airplanes, USAF, Flight Dynamics Lab, WPAFB, Dayton.

[8] Doyle, J., Stein, G., "Multivariable Feedback Design: Concepts for a Classical/Modern Synthesis," IEEE Trans. on Automatic Controls, Vol. AC-26, No. 1, pp. 4-16, Feb., 1981.

[9] Ridgely, D., Banda, S., "Introduction to Robust Multivariable Control," AFWAL-TR-85-3102, Flight Dynamics Lab, Air Force Wright Aeronautical Labs, Dayton, February, 1986.

[10] Anderson, M., Schmidt, D., "The Significance of Error Dynamics in Model-Following For Flight Control Design," AIAA # 87-2311, AIAA GN&C Conf., Monterey, 1987.

[11] Schmidt, D., "Flight Control Design Research to Meet Handling Qualities Requirements, Phase II," final report for the McDonnell Aircraft Co., performed at Arizona State Univ., Dept. of Mech and Aero Engr., Tempe, AZ, July, 1989.

[12] Kreindler, E., Rothschild, D., "Model-Following in Linear-Quadratic Optimization," AIAA Journal, pp 835-842, Vol. 14, No. 7, July, 1976.

[13] Bryson, A.E., Ho, Y., *Applied Optimal Control*, John Wiley & Sons, Inc., New York, 1975.

[14] Garg, S., "Turbofan Engine Control System Design Using the LQG/LTR Methodology," NASA CR-182303, June, 1989.

[15] Doyle, J., Glover, K., "State-Space Formulae for All Stabilizing Controllers That Satisfy an H_∞-Norm Bound and Relations to Risk Sensitivity," Systems & Control Letters 11, pp. 167-172, North-Holland, 1988.

A Framework for the Analysis of Airframe/Engine Interactions and Integrated Flight/Propulsion Control†

David K. Schmidt [1] and John D. Schierman[2]
Aerospace Research Center
College of Engineering and Applied Sciences
Arizona State University
Tempe, AZ 85287-8006

Abstract

Potential sources of airframe/engine interactions are explored for aircraft subject to the study of integrated flight/propulsion control. A quasi-linear framework for the analysis of these dynamical interactions between the airframe and engine systems is presented. This analysis can be used to quantify, in a meaningful way, the magnitude of the interactions between the airframe and engine systems, determine if these interactions are significant to warrant further consideration in the control law synthesis, and if so, what are the critical frequency ranges where problems may occur due to these interactions. Justification for the use of this method, along with the assumptions, conditions and restrictions that apply are discussed. Sample results of this analysis are used to illustrate issues brought forth in its development. Also, a comparison is made between another framework for analysis in integrated flight and propulsion control, reported elsewhere, and the framework presented in this paper.

1. Introduction

In the design of highly maneuverable fighter aircraft, such as those capable of short take off and vertical landing, the propulsion system is frequently being considered for augmenting the lift and the maneuvering capabilities of the vehicle. Some designs include vectoring of the engine's aft nozzle to control the attitude of the airframe.[1] Thrust from a reaction control system (RCS) may also be used for attitude control of the aircraft.[2] The engine may be equipped with a ventral nozzle to enhance pitch control and augment lift.[3] Left and right ejectors, drawing primary thrust from the engine and secondary thrust from intakes over the top of the fuselage can augment lift and enhance pitch and roll control.[2] Thrust reversing nozzles can be used to improve forward speed control of the aircraft.[4] Upper wing surface blowing or blown flaps can be used to alter the boundary layer, thus the lifting characteristics of the wing.[5]

In the design of the control systems for such aircraft and their propulsion systems, the significance of the interactions between the airframe and the engine must be assessed. This is a fundamental issue in the so-called Integrated Flight and Propulsion Control (IFPC) problem.[1]

The main objective of the paper is to present a quasi-linear system analysis framework for assessing the significance of the cross-coupling dynamics between the airframe and engine, to justify that this analysis produces meaningful results, and to state the conditions and restrictions that apply to this methodology. The other objectives of the paper are to contrast this approach to another in the literature, and to describe potential sources of airframe/engine interactions.

The discussion on airframe/engine interactions is given next, in Section 2. In Section 3 the justification for why a quasi-linear analysis is valid, given that the airframe/engine system dynamics are nonlinear, is presented. The quasi-linear analysis is described in Section 4. Sample results of this analysis are then presented in Section 5. Section 6 is devoted to presenting a different analysis framework used in several studies[3,6] and how it is related to the framework presented in Section 4.

2. Potential Sources of Airframe/Engine Interactions

The purpose of this section is to detail dynamical interactions between the airframe and propulsion systems. In particular, these new designs used to improve the maneuvering abilities of the aircraft may impart significant coupling between the systems. Discussed is both how engine dynamics can influence the airframe, and how airframe dynamics can influence the engine. Refs. 2, 3, 4, and 6 through 9 also elaborate on these interactions.

In conventional aircraft, changes in aft thrust cannot be delivered instantaneously by the engine, introducing time delay in the airframe's forward speed response. Thrust reversing may be used to improve the speed of response, but disturbances in engine thrust may then be more significant in the forward speed dynamics.

Thrust vectoring of the aft nozzle can produce moments to control the attitude of the airframe. Thrust from a ventral nozzle can produce pitching moment as well as lift. The primary thrust for left and right ejectors may come from the mixed flow (core and by-pass flow) of the engine and is used to produce not only lift, but rolling moments as well. Effects from disturbances in the mixed flow that produce the engine thrust will therefore be seen in the lift and attitude responses of the airframe. On the other hand, commands in thrust reversing, thrust vectoring, ventral and ejector thrust may cause pressure disturbances in the augmentor or mixing plane. If the nozzle is operating in an unchoked condition, these pressure disturbances may propagate through the fan by-pass duct and cause a reduction in fan surge margin (margin between normal operating fan pressure ratio and stall pressure ratio) or possibly a fan stall itself. This, in turn, effects thrust disturbances by disturbing engine flow. Therefore, commands to control the airframe responses may influence the engine dynamics.

The secondary flow of the ejectors is produced when air is drawn through the ejector intakes by the primary flow from the engine. Secondary flow effects may significantly influence the airframe aerodynamics.

The thrust from both RCS jets, used to control the pitch, roll and yaw of the aircraft, as well as upper wing surface blowing, used to augment lift, is usually bleed air from the engine's compressor. Thus, the dynamics of the core flow can affect the lift and the attitude responses of the airframe. However, commands in RCS thrust will cause reduced core pressure due to compressor bleed, effecting engine flow disturbances. Also, airframe aerodynamic parameters such as dynamic pressure, angle of attack and sideslip angle can influence the effectiveness of the RCS control jets, possibly calling for increased control power, thus, increased compressor bleed flow.

Pressure disturbances at the inlet to the engine can alter the drag characteristics of the airframe. Sudden reduction in airflow caused by fan or compressor surge can cause the inlet shock to move or pop out of the inlet which can produce rolling or yawing moments. Variable inlet geometry used to control the position of the inlet shock can affect the drag and produce pitching and yawing moments. On the other hand, the attitude dynamics may significantly influence the airflow at the inlet causing flow disturbances throughout the engine.

The coupling between the airframe and engine may be viewed as in the Fig. 2.1. This figure indicates the engine can influence the airframe, which, in turn, influences the engine.

3. Justification for Quasi-Linear Analysis of Nonlinear Airframe/Engine Systems

Airframe and engine systems are highly nonlinear.[10-13] In light of this, the validity of quasi-linear analysis procedures, along with the applicable conditions and restrictions for such procedures are explored in this section.

Many points of operation for the airframe/engine system occur at some steady state trim or equilibrium condition where accelerations are small or zero, and rates or velocities are constant.[10,14] Large numbers of these reference or operating points can be defined throughout the flight envelopes of the airframe and engine. Usual practice involves feedback control design and stability and performance analysis at each operating point via quasi-linear or linear methodologies. Why linear methodology at certain operating points is a viable approach, and how nonlinearities are accounted for in transitioning between operating points is discussed first. Then, quasi-linear methods are investigated for use at operating conditions and during transitional phases of operation where linear assumptions are not strictly valid.

Given that feedback gains are synthesized by quasi-linear or linear methods, they can be scheduled on parameters that define the

† To be presented at the American Control Conference, Boston, June, 1991.

[1] Acting Director and Professor of Aerospace Engineering.

[2] Research Associate and Doctoral Candidate.

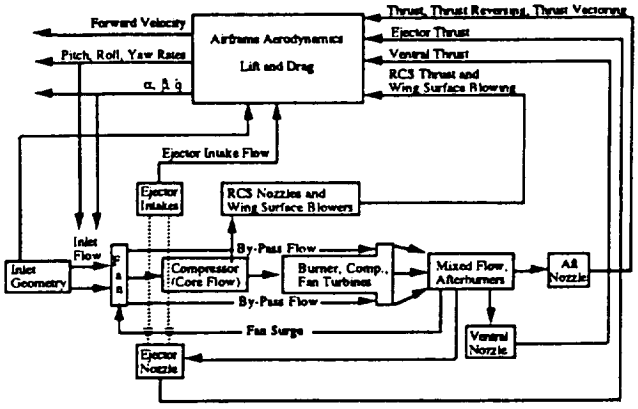

Figure 2.1 - Some Coupling Paths Between Airframe and Engine Systems

reference points. Some examples of flight steady state operation are constant speed-wings level-forward flight, climb-at-constant climb rate, steady-coordinated-banked turn, and approach-to-landing. Thus, feedback gains may be, in part, scheduled on pitch, roll and yaw rates, and their integrals, which define the attitude of the airframe. The gains may also be scheduled on parameters that determine the aerodynamic forces on the airframe, such as Mach number, dynamic pressure, and altitude, or ambient temperature and pressure.

Feedback gains on the engine may be scheduled using highly nonlinear tabulated data that take flight envelope information such as power lever angle, which defines the requested power level, and Mach number and ambient temperatures and pressures, which define inlet flow conditions.[14]

However, the system must be able to transition from one operating point to the next in a smooth and stable fashion without great loss of performance. The design of the gain schedules during these transitions can be a difficult and time consuming process. One example may be to use linear or nonlinear on-line interpolation procedures.[12-14]

The transition gain schedules may open some feedback loops and close others depending on the control objectives at the reference point in question. For example, during steady state operation, engine control is one of regulating thrust for performance and fan speed to keep the engine at the operating point. Engine switching logic, using accel/deccel schedules, is used during transitions through power level operating points to regulate on limit variables, such as main burner pressure or compressor turbine inlet temperature, to avoid engine limits, at the expense of engine performance.[19]

Figure 3.1 shows the airframe/engine nonlinear system viewed in the manner just described. Here, $\mathcal{G}$ and $\mathcal{K}$ represent the family of quasi-linear or linear airframe/engine models and control laws defined throughout the flight envelope.

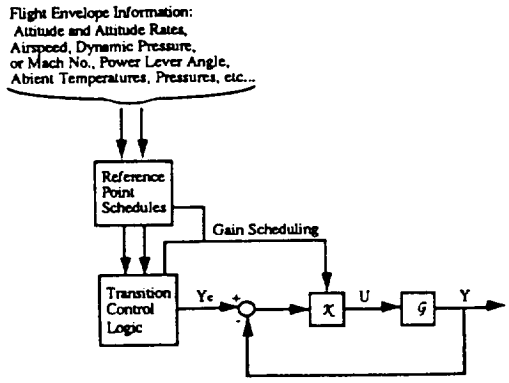

Figure 3.1 - Airframe/Engine Nonlinear System Viewed as a Family of Operating Points

Linear time-invariant analysis at particular operating points can accurately predict the stability of the equilibrium point of the nonlinear system given that transient motions from the steady state consist only of small perturbations. Lyapunov stability theory states that as long as the small perturbations remain within a certain domain of validity the stability of the linear system implies stability of the nonlinear system.[15-17] At operating points where linear analysis is performed, the system responses, Y, control inputs, U, and commanded inputs, Y_c, in Fig. 3.1 consist of the sum of the reference values and small perturbations. Sain, Peczkowski, and others[12,13] give a similar description for nonlinear engine systems.

Fig. 3.2 considers only the linear time-invariant small perturbation system model and control laws, G(s) and K(s), at a particular operating point. The assumptions implied here are that the feedback portion of the system behaves in a linear time-invariant fashion, and that the system responses, y, control inputs, u, and commanded inputs, y_c, are all small perturbation quantities. Note that the objective of the feedback loop is to regulate the error signal, e, or to keep it small. Linear control synthesis and analysis is frequently justifiable given that: (1) the error signal is kept small so that the small perturbation assumption is not violated, (2) the gain scheduling leads to slowly time-varying gains so that the system can be considered time-invariant at each operating point, and (3) observing from the figure, that nonlinearities of the system are outside the feedback loop, thus cannot affect its stability.

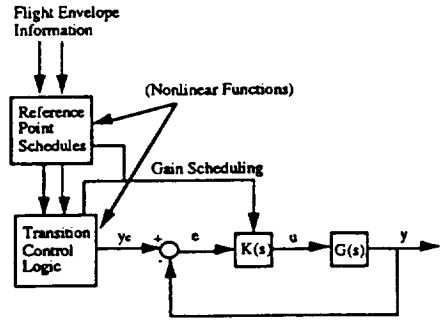

Figure 3.2 - Small Perturbation Linear Feedback System At One Particular Operating Point

An important use of linear control synthesis is that stability robustness will be provided to the actual nonlinear system as control laws are designed to provide more robustness for the linear system approximation.

Much experience exists using this approach in airframe control synthesis and analysis.[10] Linear airframe models are considered in design specifications given in Ref. 18. This document gives, for example, natural frequencies, damping ratios and time constants of various modes that should be met at different phases of operation so that the airframe dynamics reflect good classical flying qualities. Linear airframe control objectives typically require stabilizing or augmenting the stability of these various modes.

This linear approach has also often been considered for control synthesis and analysis of the nonlinear engine system, as discussed in, for example, Refs. 12-14. Sain, Peczkowski, and others[12,13] offer a systematic control law synthesis procedure for the total nonlinear engine system by utilizing a linear control law synthesis procedure at each operating point. Here, nonlinear plant and plant inverse models generate scheduled control inputs and response commands into the linear feedback loop.

Often, however, the small perturbation assumption may be too restrictive. For example, as stated in Refs. 3 and 19, the engine system is usually nonlinear during transient operation. Ref. 2 investigates a configuration involving RCS jets which lead to an absolute value nonlinearity due to the fact that an increase in compressor bleed flow is required for both positive and negative pitch, roll and yaw moments. The dynamics that couple the airframe and engine, discussed in the last section, may also include nonlinearities. Quasi-linear analysis, using the describing function technique, may be especially useful when nonlinearities in the system cannot be ignored, yet are "small," or can be isolated, such as in saturated actuators, or components with thresholds or hysteresis.[15]

In this case, the input/output relationship of the nonlinearities are modeled as linear describing functions plus a remnant. Unlike linear models, which are independent of the type of input to the system, quasi-linear models of nonlinear systems may differ for each input into the system. Step, sinusoid, and statistical inputs are often used in describing function analysis. Thus, sinusoidal input

describing functions may accurately model the nonlinear input/output behavior of systems subjected to nearly sinusoidal periodic inputs, but are invalid for systems subjected to, for example, step inputs. What type of input is used in the analysis depends on the important nonlinear features that need to be accurately modeled. The sinusoidal input describing function, used in limit cycle analysis, is equal to the complex ratio of the fundamental frequency component of the output to the input. The remnant models the effects of all higher harmonics. Higher order quasi-linear approximations must be performed until the remnant is small enough to be considered negligible. First or second order quasi-linear approximations are usually acceptable due to the attenuation characteristics of physical systems.

An important advantage of quasi-linear analysis is the ability to obtain describing function models by experiment. If accurate math models of the dynamics of the system being analyzed are not available, describing function models of the system can be experimentally derived by measuring and tabulating the outputs of the system for given inputs. For example, sinusoidal describing functions of the system can be generated by varying the frequency of the input sinusoid and measuring the response of the system. The results may then be analyzed to obtain, for example, "transfer function" like models or "Bode plots." It must be recognized, however, that, unlike linear systems, the resulting models obtained here are dependent on the amplitude of the input sinusoid.

As discussed in Refs. 15 and 20, equivalence can be drawn between robustness analysis involving limit cycles in quasi-linear approximations to nonlinear systems and stability robustness analysis using linear tools based on Nyquist stability theory. That is, margins to limit cycles for quasi-linear systems can be measured in the same way as gain and phase stability margins in, for example, Bode or Nyquist plots for linear systems.

Because of this, it is believed that the linear analysis to study the airframe/engine interactions presented in Ref. 21 can be directly extended to a quasi-linear analysis of nonlinear systems. That is, it is believed that the analysis of Ref. 21 is *not* restricted to those operating points where the airframe/engine system's dynamics are linear. The next section will present the quasi-linear viewpoint of this analysis. Thus, from now on, the coupled airframe/engine system and control laws, G(s) and K(s), shown in the block diagram of Fig. 3.2, are considered to be quasi-linear systems.

In summary, implicit in this representation is that only one operating point is considered, and is not intended to embody the system's characteristics throughout the entire flight envelope. That is, each operating point manifests a particular control architecture and system model. Note also that, although quasi-linear analysis is not restricted to the small perturbation assumptions of linear analysis, for each class of inputs to be analyzed, a different quasi-linear representation of the system must be obtained. For limit cycle analysis, sinusoidal input describing functions are used to define the quasi-linear system.

One final note is that the analysis to be presented is not intended to replace the high order complex nonlinear integration techniques involved in any final analysis and design iterations of the airframe/engine control laws. These complex techniques must be used for certain flight phases where the nonlinearities are extremely large, such as encountered in violent combat maneuvering. However, linear and quasi-linear control synthesis and analysis techniques are invaluable tools in obtaining control laws for a large portion of the flight envelope, as well as in acquiring more physical understanding of the complex nonlinear system.

4. The Quasi-Linear Analysis Framework

The following analysis closely follows that presented in Ref. 21. The analysis is conceptually extended here to include quasi-linear approximations to nonlinear systems. Let the quasi-linear aircraft model, defined at a particular flight condition be described in terms of the matrix of sinusoidal input describing functions, $G_A(s)$, where,

$$y_A(s) = G_A(s)u_A(s) \tag{4.1}$$

with $y_A(s)$ the vector of aircraft responses (angle of attack, α, pitch rate, q, etc.), and $u_A(s)$ the vector of aircraft control inputs, (flap deflection, δ_F, thrust vector nozzle deflection, δ_{TV}, etc.) Likewise, let the matrix of sinusoidal input describing functions defining the engine dynamics be described as $G_E(s)$, where,

$$y_E(s) = G_E(s)u_E(s) \tag{4.2}$$

with $y_E(s)$ the vector of engine responses (turbine temperature, T_4, fan speed, N_2, etc.), and $u_E(s)$ the vector of engine control inputs, (fuel flow rate, w_F, nozzle area, A_7, etc.)

Each of these subsystems will be acted upon by feedback systems with control compensation matrix $K_A(s)$, for the aircraft flight control system, and $K_E(s)$, for the engine control system, which is shown below, for example.

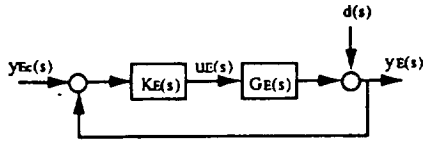

Figure 4.1 - Block Diagram of the Engine Feedback Loop

Here y_{E_c} is the vector of desired or commanded responses, and d(s) represents any exogenous disturbances acting on the system. If the above system were linear, the responses would be given by

$$y_E(s) = [I + G_EK_E]^{-1}G_EK_E\, y_{Ec}(s) + [I + G_EK_E]^{-1}d(s) \tag{4.3}$$

Note that often the compensation $K_A(s)$ and $K_E(s)$ are synthesized and implemented while essentially treating the subsystems as decoupled. Such control laws are defined here as *decentralized* controllers.

More generally, however, the aircraft/engine system dynamics may be defined at a particular flight condition as shown in the following matrix of sinusoidal input describing functions:

$$\begin{bmatrix} y_A(s) \\ y_E(s) \end{bmatrix} = \begin{bmatrix} G_A^*(s) & G_{AE}(s) \\ G_{EA}(s) & G_E^*(s) \end{bmatrix} \begin{bmatrix} u_A(s) \\ u_E(s) \end{bmatrix} = [G(s)] \begin{bmatrix} u_A(s) \\ u_E(s) \end{bmatrix} \tag{4.4}$$

where $G_A^*(s)$ and $G_E^*(s)$ are different from $G_A(s)$ and $G_E(s)$ above by the amounts $\Delta_A(s)$ and $\Delta_E(s)$, respectively, due to dynamic cross-coupling between the engine and airframe subsystems. That is,

$$\begin{aligned} G_A^* &= G_A + \Delta_A \\ G_E^* &= G_E + \Delta_E \end{aligned} \tag{4.5}$$

Further, $G_{AE}(s)$ and $G_{EA}(s)$ represent input coupling between the airframe and engine. This situation describes *two-directional* coupling. That is, the airframe control inputs affect the engine responses, and, likewise, the engine control inputs affect the airframe responses.

Note that this representation of the fully coupled system may not be strictly valid depending on the particular configuration under study. It can be seen in Fig. 2.1 that the coupling, in general, is manifested due to airframe responses entering as inputs to the engine system, and engine responses entering as inputs to the airframe system. The analysis should have analagous derivations for the different frameworks of the coupled airframe/engine systems. This topic is discussed further in Section 6.

A *centralized* synthesis/*decentralized* implementation approach is defined here as one in which control laws are synthesized with some knowledge of the coupling that exists between the airframe and engine subsystems, yet contain independent control compensation for each subsystem. That is, this approach is defined as one in which $K_A(s)$ and $K_E(s)$, discussed previously, are designed with knowledge of the system given by Eqn. 4.4.

Finally, control laws both designed with knowledge of airframe/engine interactions and implemented using cross-feedback paths between the airframe and engine loops are defined here as *centralized* controllers. The following control law is one such centralized approach:

$$\begin{bmatrix} u_A(s) \\ u_E(s) \end{bmatrix} = \begin{bmatrix} K_A(s) & K_{AE}(s) \\ K_{EA}(s) & K_E(s) \end{bmatrix} \begin{bmatrix} y_A(s) - y_{Ac}(s) \\ y_E(s) - y_{Ec}(s) \end{bmatrix} \tag{4.6}$$

The off-diagonal terms, $K_{AE}(s)$ and $K_{EA}(s)$, represent control cross-feeds between the airframe and engine subsystems. It is argued in Ref. 3 that it may be desirable to implement the airframe and engine

control laws separately because a fully centralized control law implementation may be quite difficult to perform. However, the question of the best approach to take in the IPFC problem is still under debate.

For simplicity, the analysis will assume the control cross-feeds are absent (i.e. $K_{AE}(s) = K_{EA}(s) = 0$.) This situation may be represented as shown in Fig. 4.2. For the linear analysis, the case with control cross-feeds, although more complex algebraically, may be addressed in a manner similar to that presented here, and it is believed that extensions to quasi-linear analysis may also be derived.

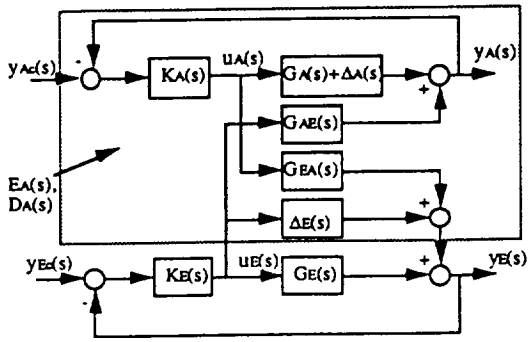

Figure 4.2 - Block Diagram of the Coupled Airframe/Engine System

Each of the terms arising from the effects of the airframe/engine coupling are apparent. This figure suggests that the coupling dynamics, $G_{AE}(s)$ and $G_{EA}(s)$, and the airframe dynamics, $G_A^*(s)$, augmented with the airframe compensator, $K_A(s)$, can all be grouped together to form the describing function matrices $E_A(s)$ and the $D_A(s)$. In other words, since $\Delta_A(s)$, $\Delta_E(s)$, $G_{AE}(s)$, and $G_{EA}(s)$ are not really zero, the engine loop is not that shown in Fig. 4.1 where airframe/engine interactions are ignored, but rather that shown in the Fig. 4.3. Here the effects of the actual coupling present are grouped into the terms $E_A(s)$ and $D_A(s)y_{Ac}$. Ref. 21 gives, through block diagram algebra, expressions for both $E_A(s)$ and $D_A(s)$, and this representation of the system is valid for linear systems. The validity of this representation is still under investigation for analysis of nonlinear systems. However, at this point, it is assumed that describing functions, $E_A(s)$ and $D_A(s)$, can be found by some manner so that the input/output relationships of the systems shown in Figs. 4.2 and 4.3 are equivalent.

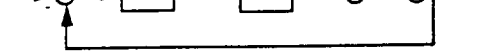

Figure 4.3 - Block Diagram of the Engine Loop for the Coupled Airframe/Engine System

Fig. 4.2 shows that the critical closed-loop coupling matrix $E_A(s)$ depends most importantly on the input coupling sinusoidal describing functions $G_{EA}(s)$ and $G_{AE}(s)$, as well as on the airframe control law, $K_A(s)$, the airframe dynamics, $G_A(s) + \Delta_A(s)$, and the change in the engine sinusoidal describing function, $\Delta_E(s)$. Therefore, if Δ_E is "small," and if $G_{AE}(s)$ and/or $G_{EA}(s)$ are "small," then $E_A(s)$ is "small."

For the linear analysis, the input/output characteristics of the system in Fig. 4.3, including the coupling effects, is

$$y_E(s) = [I + (G_E+E_A)K_E]^{-1}(G_E+E_A)K_E\, y_{Ec}(s) + [I + (G_E+E_A)K_E]^{-1}(D_A\, y_{Ec}+d(s)) \quad (4.7)$$

Note how commands into the flight control system, $y_{Ac}(s)$, are transmitted to the engine responses through $D_A(s)$, and this term enters into the engine responses the same way as any other disturbances, d(s). Thus, the commanded inputs into the aircraft (from the pilot) act as additional disturbances to the engine.

Ref. 21 points out that, for a linear analysis, $E_A(s)$ can affect the stability of the engine's closed loop system. This can be seen by comparing the engine's nominal response, given by Eqn. (4.3), and the true system's response of Eqn. (4.7). It can be shown from Nyquist stability theory[22,23] that, for a linear analysis, the closed loop system in Fig. 4.3 is assured to remain stable if the loop is stable for $E_A(s)=0$, and if

$$\det[I + (G_E + \varepsilon E_A)K_E] \neq 0\,,\ [0<\varepsilon<1] \quad (4.8)$$

for all frequency, which is assured if

$$\sigma_{max}(E_A K_E) < \sigma_{min}(I+G_E K_E) \quad (4.9)$$

for all frequency, where σ denotes the singular value of a matrix. Thus, it is evident from this inequality that there will be loss of stability robustness for "large" $E_A(s)$, (i.e., if its maximum singular value is large.) As stated in the previous section, an equivalence can be drawn between limit cycle analysis for quasi-linear systems and stability analysis for linear systems. It is the contention here that as the "size" of the describing function $E_A(s)$ grows larger, the closed loop engine system will approach a limit cycle. Rigorous justification of this assertion is currently being addressed.

The utility this analysis is that the results can be used to determine if significant cross-coupling between the airframe and engine systems exists, at the reference point under study, and if it needs to be addressed when synthesizing control laws. Another benefit from this analysis should be to determine the amount of coupling introduced into the system by the addition of devices, such as RCS jets, that use the propulsion system to enhance the airframe attitude control power. Also, more physical insight into the system's coupling dynamics may be obtained by observing the critical frequency ranges where $E_A(s)$ grows "large."

Ref. 21 also discusses how the effects of coupling can degrade the engine system's performance. Similar performance analysis for quasi-linear systems is currently under investigation.

Note too, that the focus of this analysis has been the effect of the airframe dynamics on the engine loop. A dual analysis is present in that the engine also affects the airframe loop.

5. Sample Results of the Quasi-Linear Analysis Procedure

Using the techniques just presented, attention will be directed to the analysis of an airframe/engine system that has been the subject of several studies of integrated flight and engine control.[1,3,4] The vehicle considered is representative of a high performance fighter aircraft with 2-D thrust vectoring, thrust reversing and RCS jets at the approach to landing flight condition. A more complete description of the vehicle and the control laws used can be found in Ref. 21. Although obtained from a linear analysis, the results presented in this section will be considered quasi-linear input/output relationships to underscore the aspects of the quasi-linear analysis of the last section.

The airframe/engine plant is defined as the matrix of sinusoidal input describing functions given by Eqn 4.4. The airframe response is a linear combination of angle of attack and pitch rate, and the engine response is fan speed. The control inputs are thrust vectoring angle and fuel flow rate. The control law considered here is decentralized. That is, no control cross-feeds are present and the airframe and engine control laws, $k_A(s)$ and $k_E(s)$ are designed only with the knowledge of $g_A(s)$ and $g_E(s)$. Note that lower case g is used to signify that these are scalar describing functions.

Fig. 5.1 shows the magnitudes of the four describing functions of the plant. This figure shows that the cross-coupling dynamics are both smaller than the main diagonal describing functions by approximately 40 dB for frequencies above one rad/sec. Therefore, since $e_A(s)$ is a function of the cross-coupling dynamics, the size of $e_A k_E$ will be quite small compared to the nominal engine loop describing function, $g_E k_E$, and airframe/engine interactions, as modeled here, will not instigate a limit cycle in the engine loop.

Fig. 5.2 compares the size of $e_A k_E$ to the nominal engine loop describing function, $g_E k_E$, when RCS jets are added to the system to aid in pitch control. Although not shown, this produces an increased magnitude in the g_{EA} describing function. In Section 2 it was discussed that RCS jets draw bleed flow from the engine's compressor, hence, control of the pitch attitude of the airframe directly influences the quality of the airflow through the engine. Although the system would not experience a limit cycle due to the addition of pitch

RCS control, it can be seen that the critical frequency in which a limit cycle could first occur from additional changes in the system dynamics would be at approximately 0.2 rad/sec. Note also that the phase angle of the true system begins to differ from the nominal engine system in this region.

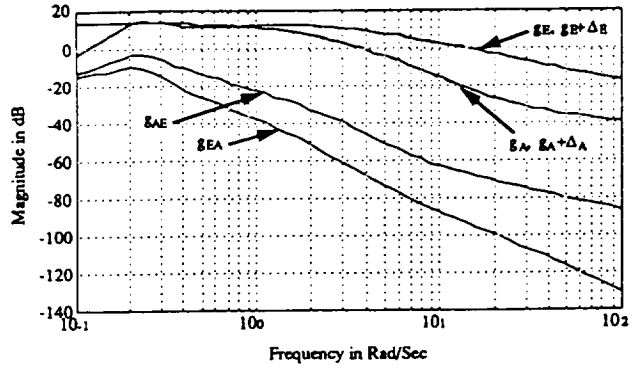

Figure 5.1 - Open Loop Describing Function Magnitudes

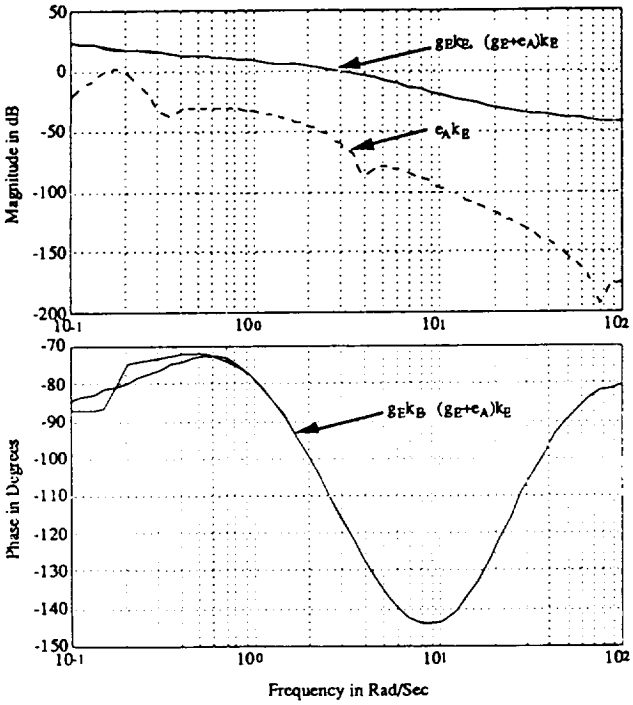

Figure 5.2 - Engine Loop Describing Function With Pitch RCS Control Added

These results show that this system, as modeled, will not be significantly affected by airframe/engine interactions and decentralized control synthesis may be adequate. However, note that the question of performance degradation due to these interactions has not yet been addressed for quasi-linear systems. The linear analysis for this configuration showed that the disturbance rejection performance of the engine was seriously degraded due to the additional disturbances from aircraft commanded inputs through $D_A(s)$. Analogies to quasi-linear performance analysis are under study.

6. A Related Analysis Framework

This section relates the framework of the analysis developed by Rock, Emami-Naeini, Shaw and others in Refs. 3 and 6 with the framework for the quasi-linear analysis of Section 4. In Section 4, it is modeled that the airframe control inputs affect the engine responses and the engine control inputs affect the airframe responses. This viewpoint seems natural if considering such interactions as RCS thrust commands (airframe control inputs for attitude control) drawing engine compressor bleed air, thus affecting engine flow (engine responses.)

However, in Refs. 3 and 6 the example vehicle under study for their analysis used varying magnitudes of aft and ventral thrust (engine responses) to effect pitching moments. Thus, a natural viewpoint for their model of how the airframe and engine interact is to consider that the engine responses are control inputs to the airframe system. That is, that the engine act as an attitude actuator to the airframe, (as well, of course, as a forward speed actuator.)

Fig. 6.1 displays the airframe/engine system framework as viewed by Refs. 3 and 6. Here, R(s) represents generalized actuators, that is, both airframe actuators and the engine system. K_S represents the airframe actuators and engine compensation, or the "subsystem" control laws. u_S, then, is the "subsystem" control inputs, and u_{mc} is the commanded inputs into the closed loop actuator/engine subsystems. P(s) models the "mission level" airframe system, and the "mission level" control laws are denoted as K_m. As defined in Section 4, y_A represents the airframe responses, and y_{Ac} represents the airframe commands to follow.

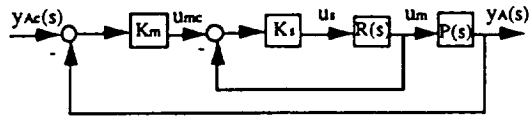

Figure 6.1 - Airframe/Engine System Framework of Refs. 3 and 6

Fig. 6.2 shows this framework with the engine system separated from airframe control inputs. Note that, for simplicity, the airframe actuator dynamics are modeled as the identity matrix. In comparing the system in Fig. 6.2 with the system of Fig. 4.2, it follows that

$$y_A = P(s)\begin{bmatrix} u_A \\ y_E \end{bmatrix} = \begin{bmatrix} G_A & G_{AE}G_E^{-1} \end{bmatrix}\begin{bmatrix} u_A \\ y_E \end{bmatrix} \tag{6.1}$$

$$\begin{bmatrix} u_A \\ y_{Ec} \end{bmatrix} = -K_m(y_A - y_{Ac}) = -\begin{bmatrix} K_A \\ K_{mE} \end{bmatrix}(y_A - y_{Ac}) \tag{6.2}$$

These equations can be used to draw the block diagram in Fig. 6.3, which shows more clearly the relationships between the two frameworks.

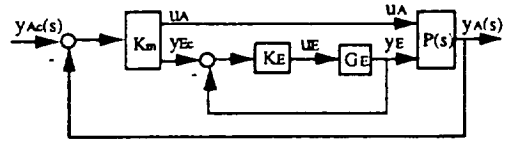

Figure 6.2 - Airframe/Engine System Framework With Engine System Explicitly Shown

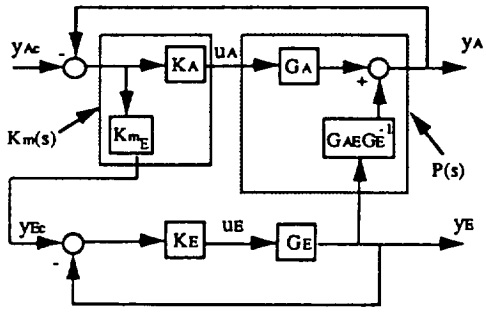

Figure 6.3 - System Framework of Refs. 3 and 6 as it Relates to the Framework of Section 4

The path from the engine responses to the aircraft responses through $G_{AE}G_E^{-1}$ is equivalent to the path from engine control inputs to airframe responses through G_{AE} alone, as given in Fig. 4.2, for $G_{EA} = 0$. Notice that for this framework, the commands into the closed loop engine system are no longer independent commands, as modeled in Section 4, but rather a function of the airframe responses and commanded inputs due to K_{mE}. Also note that differences between the nominal dynamics and the dynamics that include coupling effects of the airframe and engine, Δ_A and Δ_E, are assumed zero here.

as this issue was not addressed in Refs. 3 and 6. More significantly, however, is that the input coupling dynamics from the airframe to the engine, G_{EA}, is assumed to be zero. Because of this, this framework only considers *one-directional* coupling. Fig. 6.3 shows that the airframe dynamics cannot affect the stability (if linear) or susceptibility to limit cycles (if quasi-linear) of the engine loop. As discussed in Ref. 3, two-directional coupling was not considered. From the viewpoint of their framework, two-directional coupling would be modeled as engine responses-to-airframe inputs/airframe responses-to-engine inputs.

For quasi-linear analysis of nonlinear systems, it is important to realize that block diagram manipulation of systems may not keep the input/output relationships of the actual system. Therefore, it is imperative to model the coupled airframe/engine system properly when deriving critical coupling terms, such as $E_A(s)$. The frameworks presented in Section 4 and Refs. 3 and 6, are two possible models of how the engine and airframe couple. Which framework should be used may depend on the configuration under study.

7. Conclusions

The linear analysis of Ref. 21 was conceptually expanded here to embody quasi-linear approximations of nonlinear systems. A sinusoidal input describing function matrix was derived that quantifies, in a meaningful way, the significance of airframe/engine interactions on the engine control loop. The size of this matrix quantifies the effect of airframe/engine coupling on the susceptibility of the closed loop system to encounter a limit cycle. It was shown that the off-diagonal describing functions in the system's describing function matrix play a significant role in determining any critical cross-coupling between the airframe and engine. When the critical coupling terms are small compared to the magnitude of the nominal engine system's describing function, for which cross-coupling is ignored, effects of airframe/engine interactions are minimal. A dual analysis exists for determining the coupling effects of the engine dynamics in the nominal airframe loop.

Sample results of this analysis from a case study of an airframe/engine system used in earlier studies of integrated control techniques was then presented. This study revealed that the vehicle, as modeled at that particular operating point, exhibited very little critical interactions as far as encountering limit cycles. A classical decentralized control system synthesized assuming the airframe and engine subsystems are totally non-interacting was quite suitable in this case. However, the analysis shows how the inclusion of pitch RCS control jets in the model does increase the amount of cross-coupling. Not examined, at this time, is the effect cross-coupling has on the closed loop performance for nonlinear systems. Previous studies involving linear analysis show that coupling can have a significant detrimental effect on the performance, and it is believed that this will be the case with a quasi-linear analysis approach to study nonlinear system performance, if possible.

Comparison of the framework for the analysis presented in this paper with the framework developed in Refs. 3 and 6 showed that their framework does not consider two-directional coupling between the airframe and engine. In their analysis, the airframe dynamics cannot affect the engine loop. This assumption may lead to erroneous conclusions if the system in question has significant two-directional coupling between the airframe and engine. From the discussion on potential sources of airframe/engine interactions it can be observed that two-directional coupling may be present in the configurations under study for the IFPC problem.

Acknowledgements

This work was sponsored by the NASA Lewis Research Center under Grant # NAG3-998. Mr. Peter Ouzts is the technical program manager. Appreciation is expressed to Mr. Brett Newman for his material regarding nonlinear systems, and to Mr. Duane Mattern for his expertise in engine dynamics.

References

[1] Garg, S., Mattern, D.L., and Bullard, R.E., "Integrated Flight/Propulsion Control System Design Based on a Centralized Approach," AIAA Paper No. 89-3520, AIAA Guidance, Navigation and Control Conference, Boston, Ma., 1989.

[2] Garg, S., Mattern, D., Bright, M., Ouzts, P., "H-Infinity Based Integrated Flight/Propulsion Control Design for a STOVL Aircraft in Transition Flight," NASA TM 103198, NASA Lewis Research Center, Ohio, August, 1990.

[3] Rock, S.M., Emami-Naeini, A., Anex, R.P., "Propulsion Control Specifications in Integrated Flight/Propulsion Control Systems," AIAA Paper No. 88-3236, AIAA/ASME/SAE/ASEE 24th Joint Propulsion Conference, Boston, Mass., 1988.

[4] Smith, K., Stewart, C., "A Survey of Control Law Options for Integrated Flight/Propulsion Control for Fighter STOL Approach," AIAA Paper No. 84-1900CP, AIAA Guidance, Navigation and Control Conference, Seattle, Washington, August, 1984.

[5] Shaw, P., et al., "Development and Evaluation of an Integrated Flight and Propulsion Control System," AIAA Paper No. 85-1423, AIAA Joint Propulsion Conference, Monterey, California, July, 1985.

[6] Shaw, P.D., Rock, S.M., and Fisk, W.S., "Design Methods for Integrated Control Systems," AFWAL -TR-88-2061, Aero Propulsion Laboratory, Air Force Wright Aeronautical Laboratories, Dayton, Ohio, June, 1988.

[7] Smith, K.L., "Design Methods for Integrated Control Systems," AFWAL-TR-86-2103, Aero Propulsion Laboratory, Air Force Wright Aeronautical Laboratories, Dayton, Ohio, December, 1986.

[8] Berry, D., Schweikhard, W., "Potential Benefits of Propulsion and Flight Control Integration for Supersonic Cruise Vehicles," based on SAE paper 740478, 1974.

[9] Tape, R., Hartill, W., et al., "Vectoring Exhaust Systems for STOL Tactical Aircraft," Journal of Engineering for Power, Transactions of the American Society of Mechanical Engineering, July, 1983.

[10] Roskam, J., *Airplane Flight Dynamics and Automatic Flight Controls, Part II*, Roskam Aviation and Engineering Corp., Ottawa, Kansas, 1979.

[11] McRuer, D., Ashkenas, I., Graham, D., *Aircraft Dynamics and Automatic Control*, Princeton University Press, Princeton, New Jersey, 1973.

[12] Peczkowski, J., Stopher, S., "Nonlinear Multivariable Synthesis With Transfer Functions," Proceedings of the 1980 Joint Automatic Control Conference, Vol 1, Pt. WA8-D.

[13] Sain, M., Peczkowski, J., "Nonlinear Multivariable Design By Total Synthesis," Control System Technical Report #36, Department of Electrical Engineering, University of Notre Dame, Notre Dame, Indiana, March, 1985.

[14] DeHoff, R., et. al, "F100 Multivariable Control Synthesis Program," AFAPL-TR-77-35, Air Force Aero-Propulsion Lab, Wright Patterson Air Force Base, Dayton, Ohio, June, 1977.

[15] Graham, D., McRuer, D., *Analysis of Nonlinear Control Systems*, John Wiley & Sons, Inc., New York, 1961.

[16] Minorsky, N., *Introduction to Nonlinear Mechanics*, J. W. Edwards, Ann Arbor, Mich., 1947.

[17] Vidyasagar, M., *Nonlinear Systems Analysis*, Prentice-Hall Inc., New Jersey, 1978.

[18] Anon., MIL-8785C, Flying Qualities for Piloted Airplanes, USAF, Flight Dynamics Laboratory, WPAFB, Dayton, Ohio.

[19] Correspondence with Mr. Duane Mattern, Sverdrup Technology, Inc., Lewis Research Center Group, NASA Lewis Research Center, Cleveland Ohio.

[20] Thaler, G., Pastel, M., *Analysis and Design of Nonlinear Feedback Control Systems*, McGraw-Hill Inc., New York, 1962.

[21] Schmidt, D., Schierman, J., Garg, S., "Analysis of Airframe/Engine Interactions - An Integrated Control Perspective," AIAA # 90-1918, presented at the 26th Joint Propulsion Conference, Orlando, Fl., July, 1990.

[22] Doyle, J., Stein, G., "Multivariable Feedback Design: Concepts for a Classical/Modern Synthesis," IEEE Transactions on Automatic Controls, Vol. AC-26, No. 1, pp. 4-16, Feb., 1981.

[23] Rosenbrock, H., "The Stability of Multivariable Systems," IEEE Transactions on Automatic Controls, Vol. AC-17, pp. 105-107, Feb., 1972.

Analysis of Airframe/Engine Interactions in Integrated Flight and Propulsion Control†

John D. Schierman[1] and David K. Schmidt[2]
Aerospace Research Center
College of Engineering and Applied Sciences
Arizona State University
Tempe, AZ 85287-8006

Abstract

An analysis framework for the assessment of dynamic cross-coupling between airframe and engine systems from the perspective of integrated flight/propulsion control is presented. This analysis involves to determining the significance of the interactions with respect to deterioration in stability robustness and performance, as well as critical frequency ranges where problems may occur due to these interactions. The analysis illustrated here investigates both the airframe's effects on the engine control loops and the engine's effects on the airframe control loops in two case studies. The second case study involves a multi-input/multi-output analysis of the airframe. Sensitivity studies are performed on critical interactions to examine the degradations in the system's stability robustness and performance. Magnitudes of the interactions required to cause instabilities, as well as the frequencies at which the instabilities occur are recorded. Finally, the analysis framework is expanded to include control laws which contain cross-feeds between the airframe and engine systems.

1. Introduction

The Integrated Flight and Propulsion Control (IFPC) problem addresses interactions between airframe and engine systems in control law synthesis and analysis for configurations that use the propulsion system to augment the lift and improve maneuvering capabilities of the vehicle.[1-7] These configurations may give rise to significant coupling between the systems. Formulation of methods for assessing the significance of interactions between the systems, from the perspective of control design is to be addressed.

Ref. 8 initially presented an analysis framework to assess if cross-coupling dynamics between the airframe and engine are of sufficient "magnitude" to cause significant loss in stability robustness and/or performance, and thus warrant special consideration in the control law design.

The purpose of this paper is fourfold:

(1) Present case studies that not only analyze the airframe's effects on the engine, but also consider the *dual* analysis of the engine's effects on the airframe.

(2) Perform a multivariable analysis of the airframe control loops.

(3) Investigate the system stability and performance sensitivity to increases in critical coupling terms identified by the analysis.

(4) Expand the analysis framework to include control cross-feeds.

First, the basic analysis framework is reviewed in Section 2. Then, two case studies of a vehicle with different control configurations are presented in Sections 3 and 4. This airframe and engine was considered in several earlier studies of the integrated airframe and engine control problem.[1,2,4,5] In both control configurations the airframe's influence on the engine is shown to be significant, but it is also shown to constitute coupling in only one direction. Then a sensitivity analysis of the system's stability and performance is performed on critical interaction effects identified by the analysis. Finally, Section 5 extends the analysis methodology to control laws with cross-feeds between the airframe and engine systems.

2. Review Of Analysis Framework

A framework to analyze airframe/engine interactions was introduced in Ref. 8. Although the key features of the framework are reviewed here, more emphasis is placed on some aspects of the analysis that are pertinent to the case studies presented in the next sections. This analysis framework focuses on the feedback portion of the nonlinear airframe/engine system. Each operating point of the system elicits a particular quasi-linear system model and control architecture, G(s) and K(s). Ref. 8 presented one viewpoint of how the airframe and engine systems at one operating point interact. The treatment of nonlinear effects, such as engine limits, is presented in Ref. 9. The airframe/engine feedback system is considered as shown in Fig. 2.1.

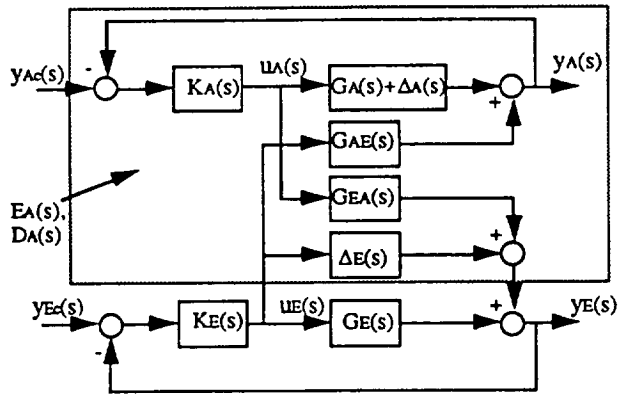

Figure 2.1 - Block Diagram of the Coupled Airframe/Engine System

In this figure, y_{Ac} is the vector of desired or commanded airframe responses, perhaps from pilot inputs, and y_{Ec} is the vector of commanded (or limited) engine responses. u_A is the vector of aircraft control inputs and u_E the vector of operative engine control inputs. Finally, y_A is the vector of aircraft responses and y_E is the vector of engine responses compatable with y_{Ec}.

Under the assumption that no coupling exists between the two systems, the airframe and engine input/output characteristics are defined in terms of the matrices $G_A(s)$ and

---

†As presented at the 1991 AIAA GN & C Conference, New Orleans
[1]Doctoral Candidate, Student Member, AIAA
[2]Acting Director, Prof. of Aero. Eng., Assoc. Fellow, AIAA

$G_E(s)$, respectively. These will be referred to as the *nominal* systems. The systems in which dynamic cross-coupling between the engine and airframe systems is considered differ from the decoupled nominal system models by the amounts $\Delta_A(s)$ and $\Delta_E(s)$, respectively. The following notation will be used to relate the plant descriptions :

$$G_A^* = G_A + \Delta_A \qquad G_E^* = G_E + \Delta_E \tag{2.1}$$

In the coupled system airframe responses are affected by engine control inputs either indirectly, or directly through $G_{AE}(s)$, and engine responses are affected by airframe control inputs either indirectly, or directly through $G_{EA}(s)$.

Finally, the system is acted upon by feedback control compensation matrices $K_A(s)$, for the aircraft flight control system, and $K_E(s)$, for the engine control system.

Refs. 8 and 9 suggest that the coupling dynamics, $G_{AE}(s)$ and $G_{EA}(s)$, and the airframe dynamics, $G_A^*(s)$, augmented with the airframe compensator, $K_A(s)$, be grouped together to form the matrices $E_A(s)$ and the $D_A(s)$, which capture the effects of the actual coupling present on the engine loop. This new representation of the coupled system is shown in Fig. 2.2. Note that in this figure d(s) represents any additional exogenous disturbances acting on the system.

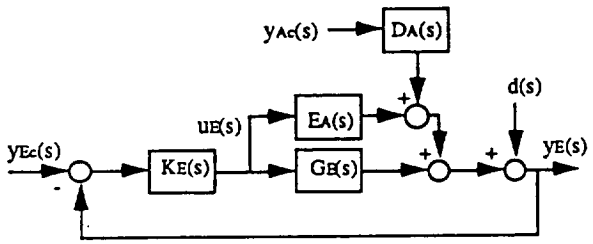

Figure 2.2 - Block Diagram of the Engine Feedback Loop For the Coupled Airframe/Engine System

If coupling does not exist between the airframe and engine, $E_A(s)$ and $D_A(s)$ are zero. Thus, if $E_A(s)$ and $D_A(s)$ are "small," as measured, for example, by singular values, this would indicate weak interactions between the airframe and engine systems. These expressions, given below, can be obtained by block diagram manipulation of Fig. 2.1, and are principal to this analysis.

$$E_A(s) = \Delta_E - G_{EA}[I + K_A(G_A + \Delta_A)]^{-1}K_A G_{AE} \tag{2.2}$$

$$D_A(s) = G_{EA}[I + K_A(G_A + \Delta_A)]^{-1}K_A \tag{2.3}$$

Eq. (2.2) shows that the "size" of the *product* $G_{EA}(s)G_{AE}(s)$ is critical in determining the "size" of $E_A(s)$. $E_A(s)$ will probably be "small" if Δ_E is "small" and if either $G_{AE}(s)$ and $G_{EA}(s)$ are "small." However, as illustrated in the case studies in the next sections, when $G_{EA}(s)$ is "large," the "size" of $E_A(s)$ becomes sensitive to small changes in the "size" of $G_{AE}(s)$. Note further that the "size" of $D_A(s)$ is independent of $G_{AE}(s)$, but may be significant if $G_{EA}(s)$ is "large." Finally, note that if loop closures on the airframe are not present ($K_A(s)=0$) then $E_A(s) = \Delta_E$, and $D_A(s)=0$.

The input/output characteristics of the engine system including coupling effects are

$$y_E(s) = [I + (G_E+E_A)K_E]^{-1}(G_E+E_A)K_E\, y_{Ec}(s) + [I + (G_E+E_A)K_E]^{-1}(D_A\, y_{Ac}(s)+d(s)) \tag{2.4}$$

This reveals how airframe/engine interactions can affect the stability and performance of the system. Airframe commanded responses, $y_{Ac}(s)$, are transmitted to the engine responses through $D_A(s)$, and act as additional disturbances to the engine. Thus, a key result of this analysis is that if $D_A(s)$ is large, the closed loop performance will suffer.

Note that large $E_A(s)$ can degrade the performance as well. However, since $E_A(s)$ is present in the return difference matrix, it also affects the system's closed loop stability. It can be shown,[10,11] for example, that the closed loop system in Fig. 2.2 is assured to remain stable if the loop is stable for $E_A(s)=0$, and if

$$\sigma_{max}(E_A K_E) < \sigma_{min}(I+G_E K_E) \quad \forall\, \omega \tag{2.5}$$

where ω = frequency, and σ denotes the singular value of a matrix. It is evident from this inequality that there will be loss of stability robustness for "large" $E_A(s)$.

Note that the focus of this analysis so far has been the effect of airframe dynamics on the engine loop. A dual is present and the engine loops clearly also affect the airframe loops, as shown in Fig. 2.3.

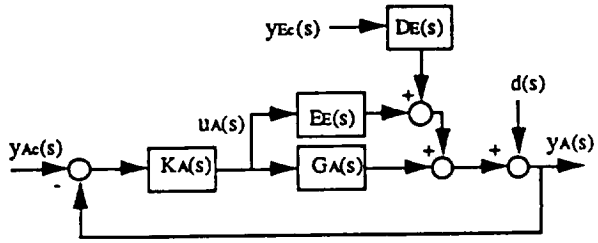

Figure 2.3 - Block Diagram of the Airframe Feedback Loop for the Coupled Airframe/Engine System

The dual of Eq. (2.4) gives the airframe responses as

$$y_A(s) = [I + (G_A+E_E)K_A]^{-1}(G_A+E_E)K_A\, y_{Ac}(s) + [I + (G_A+E_E)K_A]^{-1}(D_E\, y_{Ec}(s)+d(s)) \tag{2.6}$$

where

$$E_E(s) = \Delta_A - G_{AE}[I + K_E(G_E + \Delta_E)]^{-1}K_E G_{EA} \tag{2.7}$$

$$D_E(s) = G_{AE}[I + K_E(G_E + \Delta_E)]^{-1}K_E \tag{2.8}$$

Large $D_E(s)$ and/or $E_E(s)$ can degrade the flying qualities of the airframe control system. Further, the closed loop system in Fig. 2.3 is assured to remain stable if the loop is stable for $E_E(s)=0$, and if

$$\sigma_{max}(E_E K_A) < \sigma_{min}(I+G_A K_A) \quad \forall\, \omega \tag{2.9}$$

which is the dual of the key result of Eq. (2.5).

Two airframe/engine system configurations will now be considered in the next sections to assess the effects of cross-coupling between the airframe and engine systems.

3. First Case Study - Scalar Airframe and Engine Systems

The airframe/engine system used for this analysis has been the subject of several studies of integrated flight and propulsion control.[1,2,4,5] The vehicle to be considered is representative of a high performance Short Take Off and Landing (STOL) fighter aircraft equipped with a thrust vectoring/thrust reversing nozzle and a reaction control system (RCS). The operating point under consideration is the approach-to-landing flight condition. At this operating point the airframe dynamics are aerodynamically unstable. The vehicle model was

obtained from Ref. 1, and this particular system plant and control architecture was first presented in Ref. 9. The following table defines the controls and measurements used for this configuration.

Table 3.1 - Controls and Measurements
For The Case Study Vehicular System

The aircraft controls are:

δ_{TV} = nozzle thrust vectoring angle (deg)

A_q = pitch RCS control jet nozzle area (in^2)

δ_{flaps} = trailing edge - leading edge flap deflection angle (in^2)

The engine control is:

w_f = main burner fuel flow rate (#/hr)

The aircraft measurements are:

α = angle of attack (deg)

q = pitch rate (rad/sec)

The engine measurement is:

N_2 = engine fan speed (rpm's)

The vehicle's leading and trailing edge flaps are direct lift devices which are used to control the flight-path-to-attitude response. A combination of thrust vectoring and pitch RCS jet nozzle area is used to control the pitch attitude dynamics. This control "blend" is defined as q_c. Only the fuel flow rate is used to regulate engine fan speed.

Classical feedback control laws were synthesized. The flight control design objective is to stabilize the airframe dynamics and obtain classical pitch rate and angle-of-attack responses from pilot stick input, δ_p, that meet flying qualities requirements. The objective of the engine control law is to hold the operating point by regulating the fan speed. The control design is detailed in Refs. 8, 9, 12 and 13.

With this *decentralized* design, attention will now be directed towards evaluating the *coupled* system. The effects on system stability of the low gain flap loop are minimal.[8] Therefore, a two-by-two system can be obtained by closing the flap loop and combining the two aircraft measurements to form one blended aircraft pitch response. This open loop system is

$$\begin{bmatrix} (K_{\delta\alpha}/K_{\delta q})\,\alpha+q \\ N_2 \end{bmatrix} = \begin{bmatrix} g_A^*(s) & g_{AE}(s) \\ g_{EA}(s) & g_E^*(s) \end{bmatrix} \begin{bmatrix} q_c \\ w_f \end{bmatrix} \qquad (3.1)$$

where $K_{\delta\alpha}$ and $K_{\delta q}$ are feedback gains on angle-of-attack and pitch rate, respectively.

In order to properly evaluate the relative sizes of the input/output relationships of the airframe and engine, the system must be normalized by, for example, estimates of the maximum values of the (small perturbation) controls and responses.[1] The following estimates of these maximum values were used to normalize the plant.[13]

Table 3.2 - Maximum Values of Controls and Responses

q_{max} = 0.06 rad/sec	$\delta_{tv\,max}$ = 10 deg
α_{max} = 3 deg	$A_{q\,max}$ = 1 in^2
N_{2max} = 570 RPM's	$w_{f\,max}$ = 5,000 lbs/hr

Fig. 3.1 shows the magnitudes of the four normalized input/output mappings in Eq. 3.1, as well as the nominal airframe and engine models, $g_A(s)$ and $g_E(s)$. (Lower case letters indicate scalar transfer functions.)

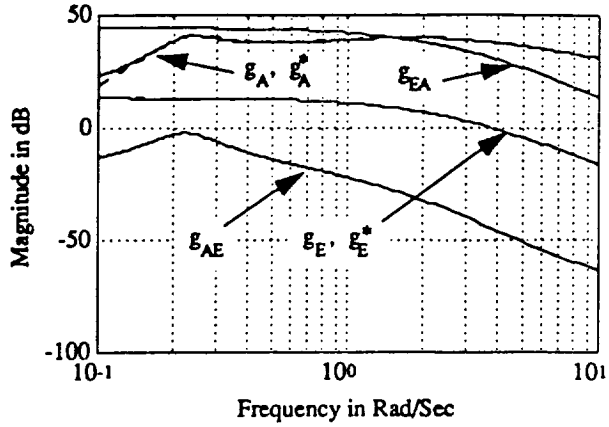

Figure 3.1 - Open Loop Normalized Input/Output Mappings

This figure shows that since there are little visible differences in the plots of $g_A(s)$ and $g_A^*(s)$, and $g_E(s)$ and $g_E^*(s)$, $\Delta_A(s)$ and $\Delta_E(s)$ are quite small. However, although $g_{AE}(s)$ is smaller than the diagonal terms in Eq. 3.1 throughout the frequency range plotted, $g_{EA}(s)$ is larger than both diagonal terms below 2 rad/sec. This is due to the RCS pitch attitude control. Recall that $g_{EA}(s)$ reflects how the engine responses are affected by airframe control inputs. The pitch RCS jets draw bleed air from the engine's compressor to enhance pitch attitude control power. $g_{EA}(s)$ will be even smaller than $g_{AE}(s)$ shown above when RCS jet control is not used.[9]

Analysis of the airframe/engine interactions requires some knowledge of candidate control laws since the feedback compensation ($K_A(s)$ or $K_E(s)$) appears explicitly in the interaction matrices (for example, $E_A(s)$.) However, even without knowledge of the control laws, investigation of the open loop plant can still reveal the nature of the airframe/engine interactions. Large $g_{EA}(s)$ in critical frequency ranges where cross-over is anticipated indicates the potential for significant airframe/engine interactions. From Eq. (2.3), $d_A(s)$ may therefore be large. Fig. 3.2 presents the engine's fan speed sensitivity function along with the magnitude of $d_A(s)$ for this system, and $d_A(s)$ is indeed large due to large $g_{EA}(s)$. This figure shows that the fan speed loop will not effectively reject disturbances from pilot pitch stick inputs. Fig. 3.3 shows the significant fan speed disturbance due to pilot stick input. Thus, cross-feed compensation between the airframe and engine may be required to reduce this effect.

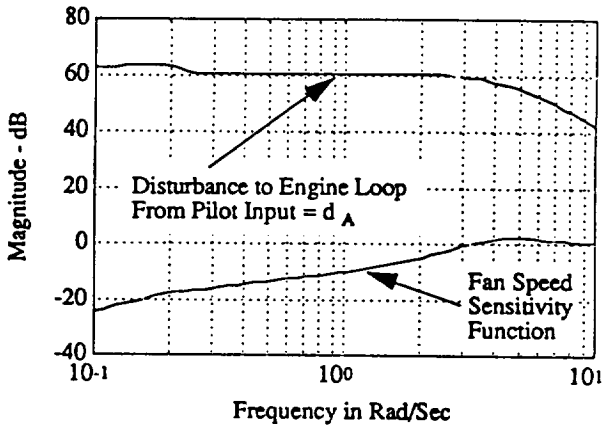

Figure 3.2 - Fan Speed Sensitivity Function and Engine Loop Disturbance From Airframe Commanded Responses

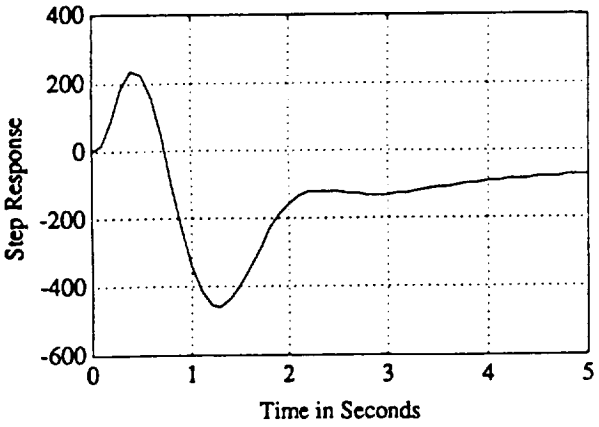

Figure 3.3 - Fan Speed Response From A One Pound Pilot Step Input (RPM's/lbs)

For this vehicle and control system configuration, the trim point occurs at a small thrust vectoring angle, δ_{tv}, thus engine thrust transients will not generate large pitching moments, and this is the reason $g_{AE}(s)$ is small. If the trim thrust vectoring angle is larger, thus increasing the component of the thrust vector perpendicular to the airframe's longitudinal axis, engine thrust transients would create larger pitching moments. In such a case, $g_{AE}(s)$ will be increased. The plant input/output mappings in Fig. 3.1 indicate that $g_{EA}(s)$ is large below 10 rad/sec. Thus, small increases in $g_{AE}(s)$ in this frequency range can increase the size of $g_{AE}(s)g_{EA}(s)$. From Eqs. (2.2) and (2.7), $e_A(s)$ and $e_E(s)$ may therefore be large, thereby degrading stability robustness and performance. For these reasons a *sensitivity* study will be performed on $g_{AE}(s)$.

Figure 3.4 shows how the closed loop eigenvalues of the system vary as the magnitude of $g_{AE}(s)$ is increased. Higher frequency engine poles are not shown and do not vary to any great extent. It can be seen, however, that the short period eigenvalues vary significantly. Although not shown, critical zeros also vary as $g_{AE}(s)$ is increased. This reflects a degradation in the flight control system's closed loop performance. Fig. 3.4 also shows the locus of phugoid roots, from which it can be seen that increasing $g_{AE}(s)$ will cause a low frequency instability.

Fig. 3.5 shows plots of both sides of the key inequality in the engine loop analysis, Eq. (2.5). This figure shows that $|e_A k_E|$ is indeed much less than $|1+g_E k_E|$ throughout the frequency range for the original value of $g_{AE}(s)$, and stability of the system is not in jeopardy. A *stability margin* for this analysis is defined here as the minimum distance between $|e_A k_E|$ and $|1+g_E k_E|$. For the original value of $g_{AE}(s)$ this margin is approximately 20 dB, and the minimum distance occurs at 0.2 rad/sec, the frequency at which the phugoid mode goes unstable when $g_{AE}(s)$ is increased, (see Fig. 3.4.)

Fig. 3.5 also shows $|e_A k_E|$ as the magnitude of $g_{AE}(s)$ is increased. First, the original value of $g_{AE}(s)$ was multiplied by 20 dB, and $|e_A k_E|$ and $|1+g_E k_E|$ touch at 0.2 rad/sec causing the stability margin to reduce to zero. At this point the stability test of Eq. (2.5) can no longer guarantee the closed loop system is stable. Instability actually occurs when $g_{AE}(s)$ is increased by a factor of approximately 40 dB. From Fig. 3.1, note that $g_{AE}(s)$, thus increased, takes on a magnitude comparable to the other transfer functions in the system.

Fig. 3.6 displays the Bode plots for both the nominal (i.e. decoupled) engine loop transfer, $g_E k_E$, and the engine loop transfer for the coupled system, $(g_E+e_A)k_E$. For the original value of $g_{AE}(s)$ there is almost no difference in these plots. This loop has an infinite gain margin and a 60° phase margin occurring at a cross-over frequency of approximately 3 rad/sec. As $g_{AE}(s)$ is increased, it can be seen that at 0.2 rad/sec the

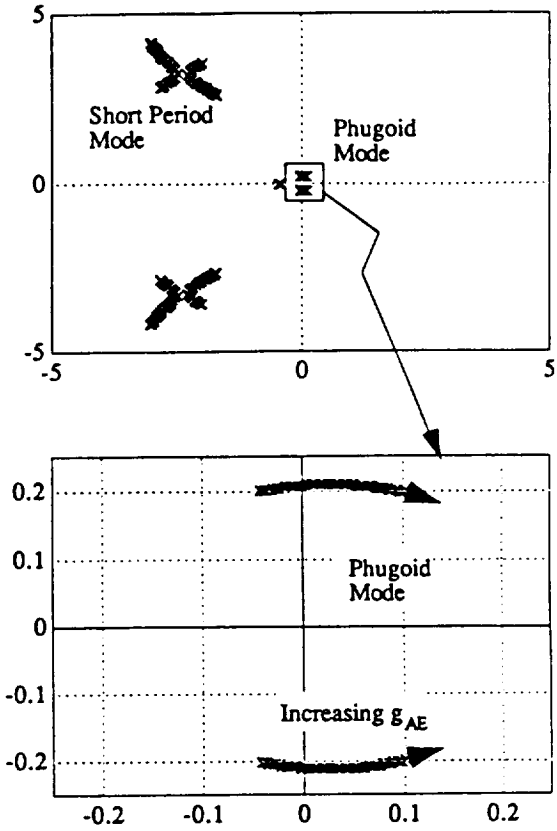

Figure 3.4 - Locus of the Airframe/Engine System's Closed Loop Poles As $g_{AE}(s)$ Is Increased

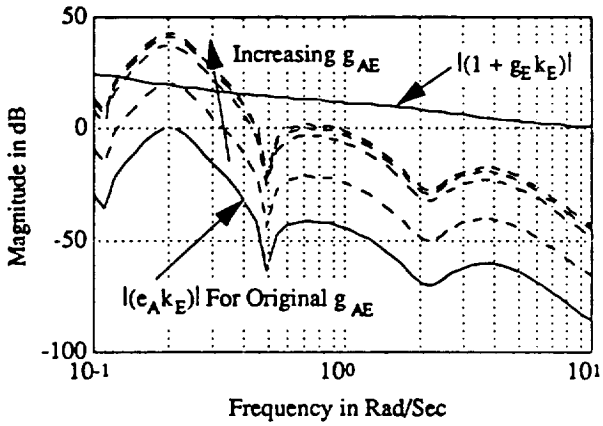

Figure 3.5 - Plot of Eq. (2.5)

magnitude of the loop transfer $(g_E+e_A)k_E$ approaches 0 dB as its phase approaches -180° A similar result is indicated in Fig. 3.8 (the dual of Fig. 3.6) which shows the Bode plot for the airframe loop. It is considered significant that the critical frequency of instability (0.2 rad/sec) is not near the nominal loop cross-over frequency (3 rad/sec) and that Eq. (2.5)correctly indicated that the minimum stability margin occurs at this frequency.

Unfortunately, however, this stability test was conservative in that a stability margin of 20 dB was indicated, whereas the actual margin was approximately 40 dB. However, shown in Fig. 3.7 is the dual of this stability test for the airframe loop, namely Eq. (2.9). Note that the various plots of $|e_E k_A|$ correspond to the same values of $g_{AE}(s)$ as in Fig. 3.5. Again, the minimum stability margin distance occurs at approximately

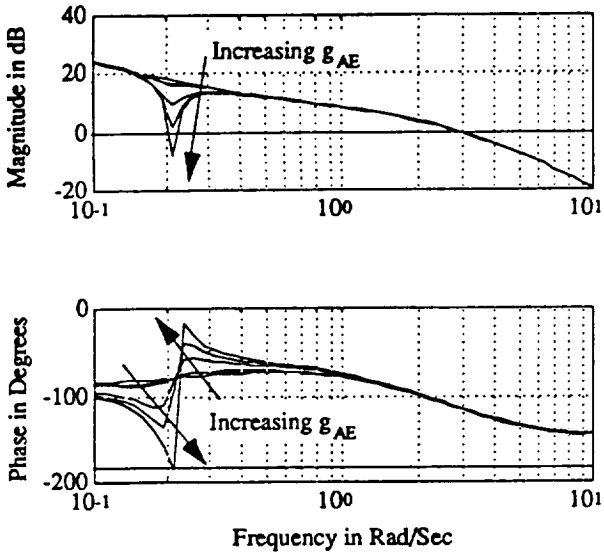

Figure 3.6 - Engine Loop Transfer Frequency Responses of Nominal ($g_E k_E$) and Coupled ($(g_E+e_A)k_E$) Systems

0.2 rad/sec, and when $|e_E k_A|$ is increased by 40 dB it just touches $|1+g_A k_A|$. That is, the stability test for the airframe loop gives a more accurate indication of the stability margin of approximately 40 dB. Thus, the stability test must be performed for both the airframe and engine loops, and the system's actual stability is more accurately predicted by the larger of the two stability margins as indicated by Eq. (2.5) or Eq. (2.9).

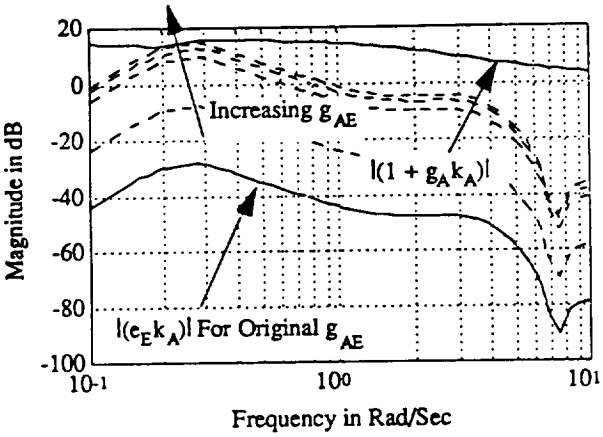

Figure 3.7 - Plot of Eq. (2.9)

Finally, closed loop "flight control" performance is evaluated in Fig. 3.9. This figure shows the magnitude of the closed loop pitch rate frequency response from pilot stick input. For the original value of $g_{AE}(s)$ the response of the coupled airframe/engine system closely resembles that of the nominal system which is considered to possess good flying qualities. As $g_{AE}(s)$ is increased, the response significantly deviates from the nominal near 0.2 rad/sec, as the damping in the phugoid mode approaches zero. Note that performance requirements, not closed loop stability, may be much more limiting.

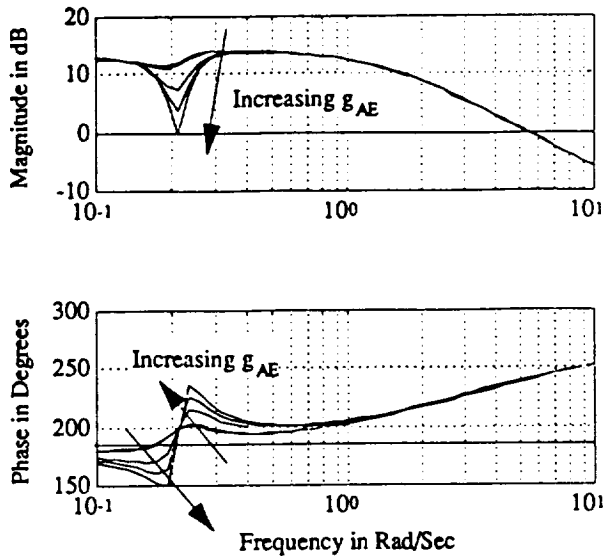

Figure 3.8 - Airframe Loop Transfer Frequency Responses of Nominal ($g_A k_A$) and Coupled ($(g_A+e_E)k_A$) Systems

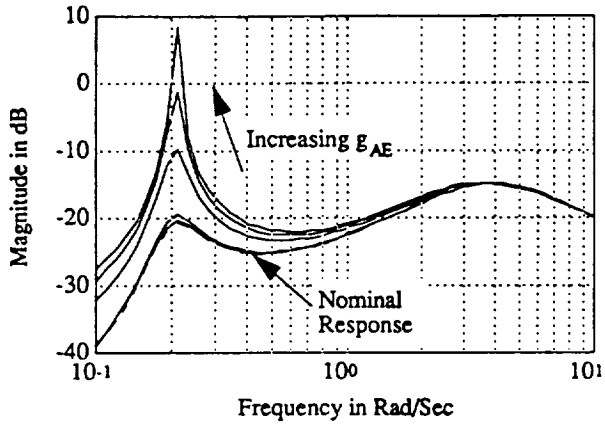

Figure 3.9 - Closed Loop Pitch Rate Response From Pilot Stick Input

At this time, only the angle-of-attack and pitch rate responses to pilot inputs have been evaluated with regards to flight control performance. However, from Eq. (2.8), note that as $g_{AE}(s)$ increases, $d_E(s)$ will certainly increase, hence disturbance rejection performance in the airframe loops will also degrade.

In summary, the analysis revealed:

1) Disturbances to the engine loop from airframe commanded responses are large - due to large $g_{EA}(s)$.

2) Sensitivity to $g_{AE}(s)$ in terms of stability robustness.

3) The frequency at which instability occurs due to increased $g_{AE}(s)$.

4) Closed loop airframe performance degradation due to increased $g_{AE}(s)$.

4. Second Case Study - Multivariable Airframe System

The airframe/engine system considered in this case is the same as in the last section. However, RCS jets are no longer included and only thrust vectoring is used to control pitch attitude. Flying qualities requirements are better met by feeding back forward speed, u (ft/sec), to thrust reverser port area, A_{78} (in^2), as first discussed in Ref. 12. The control law design for this configuration is presented in Refs. 8, 9, 12 and 13. Again closing the flap loop and combining angle-of-attack and pitch rate measurements to form one blended aircraft pitch response, gives the following three-by-three system:

$$\begin{bmatrix} u \\ (K_{\delta\alpha}/K_{\delta q})\,\alpha+q \\ N_2 \end{bmatrix} = \begin{bmatrix} g_{11} & g_{12} & g_{13} \\ g_{21} & g_{22} & g_{23} \\ g_{31} & g_{32} & g_{33} \end{bmatrix} \begin{bmatrix} A_{78} \\ \delta_{tv} \\ w_f \end{bmatrix} \quad (4.1)$$

With the exception that pitch control no longer includes RCS jets, the following physical "equivalence" in notation can be drawn between this system and that of the last section.

$$\begin{bmatrix} g_{22}(s) & g_{23}(s) \\ g_{32}(s) & g_{33}(s) \end{bmatrix} \leftrightarrow \begin{bmatrix} g_A^*(s) & g_{AE}(s) \\ g_{EA}(s) & g_E^*(s) \end{bmatrix} \quad (4.2)$$

Now, however, the airframe has two control inputs and two responses. Thus, the plant input/output descriptions are now expanded to

$$G_A^*(s) = \begin{bmatrix} g_{11} & g_{12} \\ g_{21} & g_{22} \end{bmatrix} \quad G_{AE}(s) = \begin{bmatrix} g_{13} \\ g_{23} \end{bmatrix}$$

$$G_{EA}(s) = [\, g_{31} \quad g_{32} \,] \quad g_E^*(s) = [g_{33}] \quad (4.3)$$

Fig. 4.1 displays the magnitudes of the plant input/output mappings. Again, the control inputs and system responses are normalized to their maximum values. The system maximum perturbation forward speed and thrust reverser port area are taken as

$$u_{max} = 20 \text{ ft/sec} \quad A_{78max} = 50 \text{ in}^2 \quad (4.4)$$

The other values were given in Table 3.2.

Fig. 4.1 shows that since RCS jets are no longer used, $g_{32}(s)$ is quite small, as expected. Also, both $g_{13}(s)$ and $g_{23}(s)$ are small, hence, $G_{AE}(s)$ is "small". However, $g_{31}(s)$ is quite large and of the same order of magnitude as $G_A^*(s)$ and $g_E^*(s)$. Thus, $G_{EA}(s)$ is not "small" for this configuration either. $g_{31}(s)$ is large due to the fact that changes in thrust reverser port area can influence the back pressure on the engine fan through the by-pass duct. Thus, closing the loop on forward speed to thrust reversing leads to large $G_{EA}(s)$ and perhaps significant airframe/engine interactions.

Again, from Eq. (2.3), $d_A(s)$ can be expected to be large since $G_{EA}(s)$ is "large." Fig. 4.2 presents the engine's fan speed sensitivity function along with the magnitude of $d_A(s)$ for this case. This figure shows, however, that $d_A(s)$ is not as large as in the previous case due in part to different airframe feedback compensation, $K_A(s)$.

Attention is now directed towards a sensitivity analysis similar to that presented in the first case study. An investigation of Eq. (2.2) would show that $g_{31}(s)$ multiplies both $g_{13}(s)$ and $g_{23}(s)$, while investigation of Eq. (2.7) also indicates that $g_{31}(s)$ multiplies $g_{13}(s)$ in the (1,1) element of $E_E(s)$, and multiplies $g_{23}(s)$ in the (2,1) element of $E_E(s)$. Hence, the system is potentially sensitive to deviations in $g_{13}(s)$ and/or $g_{23}(s)$. Thus, the following results present the sensitivity analysis increasing

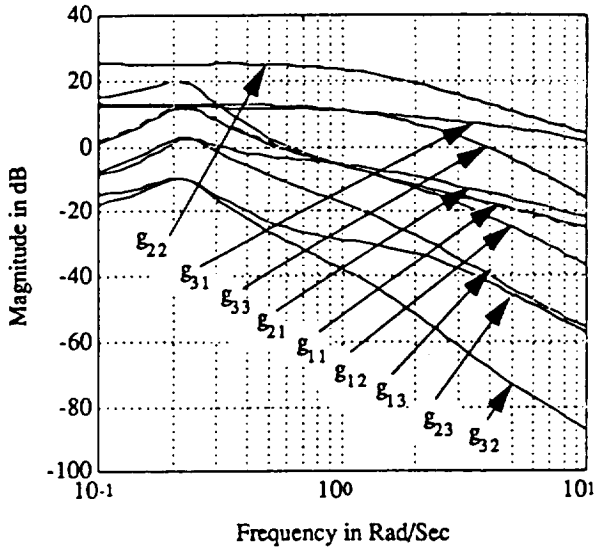

Figure 4.1 - Open Loop Normalized Input/Output Mappings

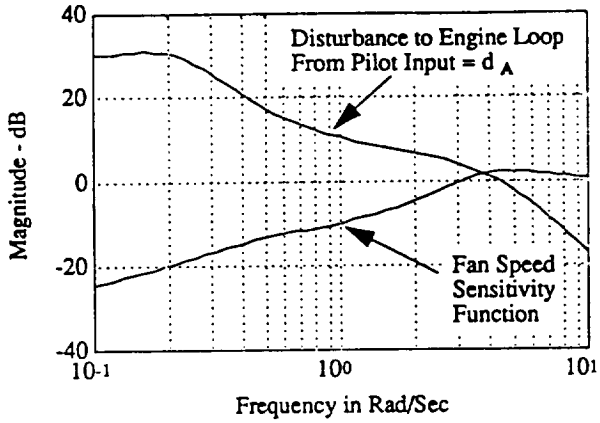

Figure 4.2 - Fan Speed Sensitivity Function and Engine Loop Disturbance From Airframe Commanded Responses

both elements of $G_{AE}(s)$ at the same time. Physically, $g_{23}(s)$ is equivalent to $g_{AE}(s)$ (pitch response-to-fuel flow rate) of the previous case study. $g_{13}(s)$ models the effects of fuel flow rate on the forward speed. Consequently, this term is sensitive to the vehicle's thrust-to-weight rating.

Fig. 4.3 shows plots of both sides of the key inequality for the engine loop analysis, Eq. (2.5). This figure shows that the stability margin with the original value of $G_{AE}(s)$ is approximately 20 dB measured at 0.2 rad/sec.

Fig. 4.3 also shows $|e_A k_E|$ for "larger" $G_{AE}(s)$. Instability actually occurs for the increase in $G_{AE}(s)$ leading to the largest $|e_A k_E|$ shown in the figure. In this case, both $g_{13}(s)$ and $g_{23}(s)$ were increased by 46 dB. Although this gain margin may seem large, at the frequency in which the system goes unstable, this is equal to an additive (rather than multiplicative) perturbation of only 3.6 (ft/sec)/(lbs/hr).

Fig. 4.4 displays the frequency responses of both the nominal and coupled system's engine loop transfers. As in the previous case study, this loop has infinite gain margin and 60° of phase margin occurring at a cross-over frequency of approximately 3 rad/sec. As the magnitude of $G_{AE}(s)$ is increased, the phase margin is reduced to zero and system instability occurs. Note here that instability in this case occurs near 3 rad/sec.

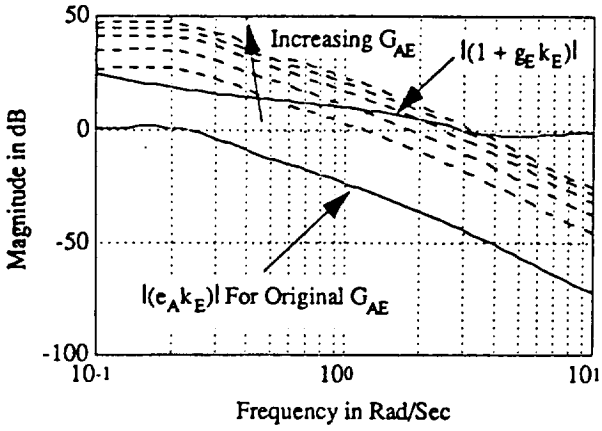

Figure 4.3 - Plot of Eq. (2.5)

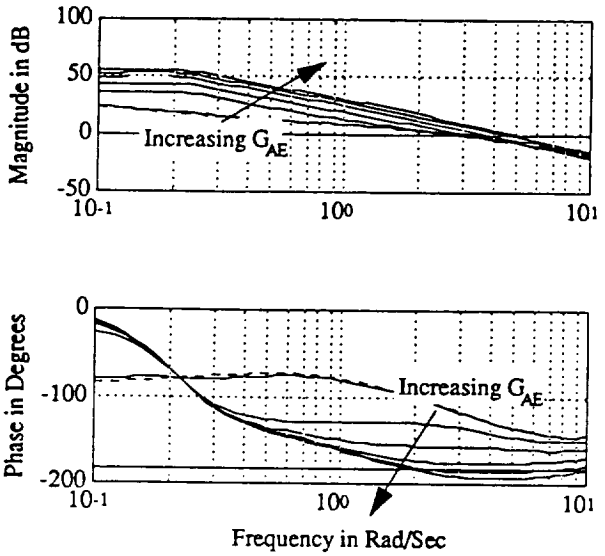

Figure 4.4 - Nominal and Coupled System's Engine Loop Transfer Frequency Responses

The dual stability test for the airframe loop is shown in Fig. 4.5. Note here that singular values are plotted since this is a multivariable system analysis. The stability margin indicated in this figure is approximately 30 dB measured at a frequency of 0.2 rad/sec. Thus, it can be seen that this test is less conservative in that a larger stability margin is guaranteed.

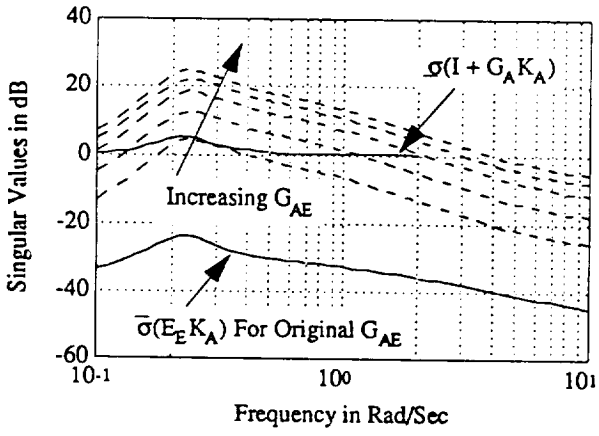

Figure 4.5 - Plot of Eq. (2.9)

Now consider the Bode plot in Fig. 4.6 showing the speed-to-thrust reverser loop with the pitch response-to-thrust vectoring loop closed. Note in this loop, stability margins are decreasing as the "magnitude" of $G_{AE}(s)$ is increased, but in the frequency range near 0.2 rad/sec rather than near 3 rad/sec indicated in Fig. 4.4. This is not unusual for a multivariable system, and underscores the need for singular value analysis, along with consideration of individual loops. What Fig. 4.5 indicates is that the "smallest" $E_E K_A$ for which stability is assured is of the order of 30 dB, and the instability for this worst-case matrix should occur at a frequency near 0.2 rad/sec. Hence, although sensitivity to $g_{13}(s)$ and $g_{23}(s)$ is indicated in Eqs. (2.5) and (2.9), the worst-case combination of changes in $g_{13}(s)$ and $g_{23}(s)$ was probably not found in the above analysis.

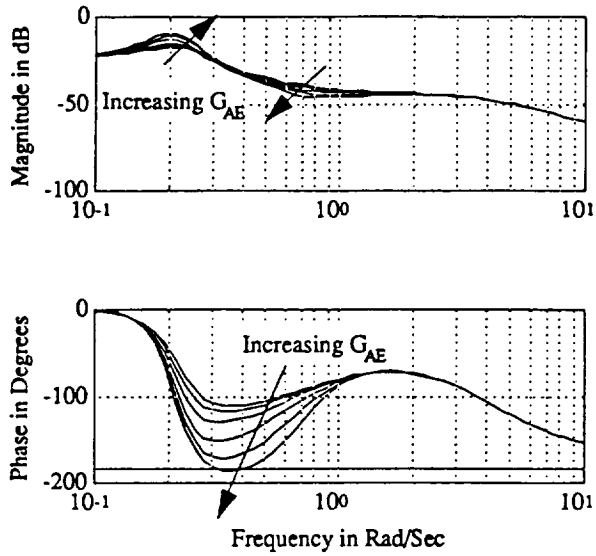

Figure 4.6 - Airframe Forward Speed-To-Thrust Reverser Loop Transfer Frequency Responses of Nominal and Coupled Systems (With Pitch-To-Thrust Vectoring Loop Closed)

5. Analysis Framework With Control Cross-Feeds

The control laws $K_A(s)$ and $K_E(s)$ in the case studies just presented are defined here as *decentralized* controllers in that they involve no cross-feeds between airframe responses and engine control inputs, or between engine responses and airframe control inputs. The method of analysis presented in Ref. 8 considered only systems with decentralized control laws. *Centralized* control laws may arise, for example, from application of multivariable synthesis approaches, and may well include control cross-feeds between the two systems. The purpose of this last section is to extend the analysis framework to allow for these cross-feeds.

Fig. 5.1 displays the system analogous to that in Fig. 2.1, but with the control cross-feeds $K_{AE}(s)$ and $K_{EA}(s)$ present.

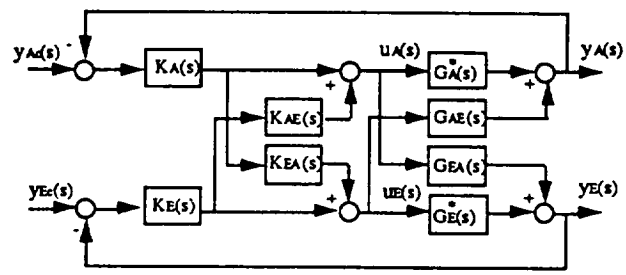

Figure 5.1 - Airframe/Engine System With Control Cross-Feeds

This system may also be represented as shown in Fig. 2.2 and 2.3. However, the complexity of the coupling expressions increases significantly, as shown below. Note that the indication of functional dependence on s is not carried through on the right hand sides of some of these expressions for simplicity of notation. It can be shown that, for the system in Fig. 5.1, the expressions for $E_A(s)$ and $D_A(s)$ in Fig 2.2 become

$$E_A(s) = \Delta_E + E_{A1}(s) + E_{A2}(s) + E_{A3}(s) + E_{A4}(s)$$
$$D_A(s) = D_{A1}(s) + D_{A2}(s) \tag{5.1}$$

$$E_{A1}(s) = -G_{EA}\,\phi_A\,K_A\,G_{AE},\quad E_{A2}(s) = G_{EA}\,\phi_A\,K_{AE}$$
$$E_{A3}(s) = -T_A\,\dot{\phi}_A\,G_{AE},\quad E_{A4}(s) = -T_A\,G_A^*\phi_A\,K_{AE} \tag{5.2}$$

$$D_{A1}(s) = G_{EA}\,\phi_A\,K_A,\quad D_{A2}(s) = T_A\,\dot{\phi}_A \tag{5.3}$$

where,

$$\phi_A(s) = \left(I + K_A\,G_A^*\right)^{-1},\quad \dot{\phi}_A(s) = \left(I + G_A^*\,K_A\right)^{-1}$$
$$T_A(s) = (G_E^* + E_{A1})\,\Phi_A\,K_{EA}\,K_A \tag{5.4}$$
$$\Phi_A(s) = \left(I + K_{EA}\,K_A\,\dot{\phi}_A\,G_{AE}\right)^{-1}$$

$\Delta_E(s)+E_{A1}(s)$ is identical to the original $E_A(s)$ given in Eq. (2.2). That is, $E_A(s)$ in Eq. (5.1) reduces to this when the cross-feeds $K_{AE}(s)$ and $K_{EA}(s)$ are zero. $E_{A2}(s)$ arises from the "K_{AE}-G_{EA}" path in the block diagram in Fig. 5.1. That is, $E_A(s)$ reduces to $E_{A2}(s)$ when $K_{EA}(s)$ and $G_{AE}(s)$ are zero. $E_{A3}(s)$ arises from the "G_{AE}-K_{EA}" path, or $E_A(s)$ reduces to $E_{A3}(s)$ when $K_{AE}(s)$ and $G_{EA}(s)$ are zero. Finally, $E_{A4}(s)$ arises from the "K_{AE}-K_{EA}" path, or $E_A(s)$ reduces to $E_{A4}(s)$ when $G_{EA}(s)$ and $G_{AE}(s)$ are zero. Dual results arise when considering the effects on the airframe loop. In this case, the results are the same as those in Eq. (5.1) - (5.4), but with all subscripts (A and E) interchanged. Thus, the dual expressions are

$$E_E(s) = \Delta_A + E_{E1}(s) + E_{E2}(s) + E_{E3}(s) + E_{E4}(s)$$
$$D_E(s) = D_{E1}(s) + D_{E2}(s) \tag{5.5}$$

$$E_{E1}(s) = -G_{AE}\,\phi_E\,K_E\,G_{EA},\quad E_{E2}(s) = G_{AE}\,\phi_E\,K_{EA}$$
$$E_{E3}(s) = -T_E\,\dot{\phi}_E\,G_{EA},\quad E_{E4}(s) = -T_E\,G_E^*\phi_E\,K_{EA} \tag{5.6}$$

$$D_{E1}(s) = G_{AE}\,\phi_E\,K_E,\quad D_{E2}(s) = T_E\,\dot{\phi}_E \tag{5.7}$$

where,

$$\phi_E(s) = \left(I + K_E\,G_E^*\right)^{-1},\quad \dot{\phi}_E(s) = \left(I + G_E^*\,K_E\right)^{-1}$$
$$T_E(s) = (G_A^* + E_{E1})\,\Phi_E\,K_{AE}\,K_E \tag{5.8}$$
$$\Phi_E(s) = \left(I + K_{AE}\,K_E\,\dot{\phi}_E\,G_{EA}\right)^{-1}$$

Note that solving for the control cross-feed that will force $D_A(s)=0$ gives:

$$K_{EA} = -(G_E^*)^{-1}\,G_{EA} \tag{5.9}$$

Hence, this cross-feed minimizes the disturbance from the airframe to the engine loop. By duality arguments, $D_E(s)=0$ when:

$$K_{AE} = -(G_A^*)^{-1}\,G_{AE} \tag{5.10}$$

Note that this solution requires inversion of the airframe and engine plants, which is not advisable if right half plane transmission zeros are present. Also, the above solutions unfortunately do not lead to $E_A(s)=0$ and $E_E(s)=0$.

6. Summary and Conclusions

Two case studies were presented in this paper that addressed the analysis of airframe/engine interactions. For both open loop airframe/engine configurations considered, the airframe's influence on the engine loop was significant. Commands to the flight control system resulted in significant undesirable fan speed disturbances. The engine's effect on the airframe loop, however, was "small" in both case studies, and thus the interactions between the airframe and engine were one-directional. Consequently, analysis revealed good stability robustness and closed loop flight control performance.

However, the analysis also indicated the system's potential sensitivity in engine-to-airframe interactions. The stability test used in the analysis of the airframe loop (Eq. (2.9)) more accurately predicted the actual coupling "stability margin" for both cases considered. This underscores the need for analyzing *both* the airframe and engine systems to accurately evaluate the significance of their interactions. For the second case study, which involved a multivariable airframe system, sensitivity to engine-to-airframe coupling was also explored. Again it was shown that instability could occur. However, a more extensive sensitivity study is required with multivariable systems, and worst-case combinations of plant variations is sought.

Finally, extension of the analysis method to allow for cross-feeds between the airframe and engine systems was presented.

Acknowledgements

This work was sponsored by the NASA Lewis Research Center under Grant # NAG3-998. Dr. Sanjay Garg is the technical program manager.

References

[1] Garg, S., Mattern, D.L., and Bullard, R.E., "Integrated Flight/Propulsion Control System Design Based on a Centralized Approach," AIAA Paper No. 89-3520, AIAA Guidance, Navigation and Control Conference, Boston, Ma., August, 1989.

[2] Rock, S.M., Emami-Naeini, A., Anex, R.P., "Propulsion Control Specifications in Integrated Flight/Propulsion Control Systems," AIAA Paper No. 88-3236, AIAA/ASME/SAE/ASEE 24th Joint Propulsion Conference, Boston, Mass., July, 1988.

[3] Smith, K., Stewart, C., "A Survey of Control Law Options for Integrated Flight/Propulsion Control for Fighter STOL Approach," AIAA Paper No. 84-1900CP, AIAA Guidance, Navigation and Control Conference, Seattle, Washington, August, 1984.

[4] Shaw, P., et al., "Development and Evaluation of an Integrated Flight and Propulsion Control System," AIAA Paper No. 85-1423, AIAA Joint Propulsion Conference, Monterey, California, July, 1985.

[5] Shaw, P.D., Rock, S.M., and Fisk, W.S., "Design Methods for Integrated Control Systems," AFWAL -TR-88-2061, Aero Propulsion Laboratory, Air Force Wright Aeronautical Laboratories, Dayton, Ohio, June, 1988.

[6] Smith, K.L., "Design Methods for Integrated Control Systems," AFWAL-TR-86-2103, Aero Propulsion Laboratory, Air Force Wright Aeronautical Laboratories, Dayton, Ohio, December, 1986.

[7] Berry, D., Schweikhard, W., "Potential Benefits of Propulsion and Flight Control Integration for Supersonic Cruise Vehicles," based on SAE paper 740478, 1974.

[8] Schmidt, D., Schierman, J., Garg, S., "Analysis of Airframe/Engine Interactions - An Integrated Control Perspective," AIAA # 90-1918, presented at the 26th Joint Propulsion Conference, Orlando, Fl., July, 1990.

[9] Schmidt, D., Schierman, J., "A Framework for the Analysis of Airframe/Engine Interactions and Integrated Flight/Propulsion Control," presented at the American Control Conference, Boston, Mass., June, 1991.

[10] Doyle, J., Stein, G., "Multivariable Feedback Design: Concepts for a Classical/Modern Synthesis," IEEE Transactions on Automatic Controls, Vol. AC-26, No. 1, pp. 4-16, Feb., 1981.

[11] Rosenbrock, H., "The Stability of Multivariable Systems," IEEE Transactions on Automatic Controls, Vol. AC-17, pp. 105-107, Feb., 1972.

[12] Schmidt, D., Schierman, J., "Extended Implicit Model Following As Applied To Integrated Flight and Propulsion Control," AIAA Paper No. 90-3444, AIAA Guidance, Navigation and Control Conference, Portland, Oregon, August, 1990.

[13] Schierman, J., Schmidt, D., "Robust Control Synthesis For Integrated Flight and Propulsion Control," IEEE Conference on Decision and Control, Honolulu, Hawaii, December, 1990.

P/A
92A55300

Analysis Of Airframe/Engine Interactions For A STOVL Aircraft With Integrated Flight/Propulsion Control†

John D. Schierman‡, T. Alan Lovell* and David K Schmidt**
Aerospace Research Center
College of Engineering and Applied Sciences
Arizona State University

Abstract

This paper presents new results from a multivariable analysis technique applied to an advanced STOVL configuration with highly interactive airframe and propulsion subsystems and uncertainty in the interactions between the subsystems. This analysis method is used to assess the effects of the dynamic cross-coupling between the airframe and engine subsystems. The analysis framework addresses two-directional dynamic cross-coupling, and also allows for cross-feeds between the subsystem controllers. The issue of stability and performance robustness is addressed, and the utility of singular value stability robustness criteria is presented. The configuration analyzed includes a thrust vectoring/thrust reversing aft nozzle, powered lift through the use of a ventral nozzle and ejectors, and Reaction Control System jets. Investigation of the open-loop dynamics indicates that significant interactions between the airframe and engine are generated as a consequence of the propulsive augmentation. A critical frequency range where instability would first occur due to small variations in the coupling dynamics is also indicated by the analysis. A stability sensitivity analysis reveals that the interactions between the engine and the airframe's flight path response are critical with regard to stability and performance robustness.

Introduction

The main objective of this paper is to present new results of an analysis method that examines the effects of interactions between airframe and engine subsystems. This analysis technique was first introduced in [1], and further developed in [2] and [3]. The procedure is applied for analysis of a particular vehicle configuration that has been the subject of several studies involved in the Integrated Flight and Propulsion Control (IFPC) problem [4]-[6]. The central issues of the airframe/engine interaction analysis methodology presented herein are to reveal how the interactions between the airframe and engine are manifested, and to assess their significance. The "size" of the interactions are quantified in a meaningful way to indicate their effect on reductions in stability robustness, and degradations in closed loop performance. The analysis method presently developed has proven useful in identifying critical frequencies where the system is lacking in stability robustness. The analysis also quantifies disturbances encountered in each loop due to the interactions between the airframe and engine. Analyzing these interactions should help to further understand how they should be addressed in the context of integrated control of the flight and propulsion subsystems.

The main focus in the IFPC problem is control synthesis and analysis of advanced concepts of highly maneuverable aircraft which utilize the propulsion subsystem for enhancing the lifting and maneuvering capabilities of the airframe [1]-[8]. Fig. 1 illustrates some of these new design concepts such as aft and ventral nozzle vectoring, Reaction Control System (RCS) jets, and left and right ejectors. Vectoring of the engine's nozzles generates moments that enhance the attitude control of the airframe. A ventral nozzle is located underneath the fuselage and redirects the engine's thrust for both pitch attitude control and lift augmentation. Thrust from RCS jets is drawn from engine compressor bleed flow and is also used to enhance attitude control. Primary ejector flow is due to the mixed flow of the engine (core and bypass flow) and secondary flow is generated by ejector intake doors over the top of the fuselage. If the ejectors act in unison, they provide propulsive lift at low speeds and hover. However, differential use of the left and right ejectors can enhance roll control of the aircraft.

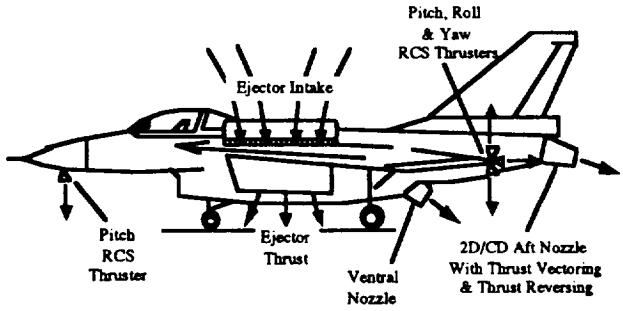

Figure 1 - IFPC Vehicle Configuration

Traditional aircraft only utilize engine thrust to affect forward velocity, and there is little need to address dynamic interactions between the airframe and engine subsystems. Conversely, for these new aircraft design concepts, the potential *two-directional interactions* between the airframe and engine subsystems are of major concern. Engine thrust will not only affect the forward velocity of the airframe, but will also influence the lift and attitude motion of the airframe as well. However, the inlet flow to the engine, which affects the thrust produced by the engine is, in turn, affected by the the dynamic motion of the airframe. Although the airframe and engine subsystem dynamics are usually reasonably well modeled, the dynamic interactions between these subsystems are frequently difficult to accurately predict and model early in the design cycle, and

---

† Presented At The AIAA GN&C Conf., Hilton Head, 1992.

‡ Doctoral Candidate, Student Member, AIAA.

* Graduate Fellow.

** Director, Prof. of Aero. Eng., Assoc. Fellow, AIAA.

AIAA PAPER NO. 92-4623

are often a significant source of uncertainty in the model of the system's dynamics. Therefore, a key focus of the analysis presented in this paper is system stability and performance robustness to uncertainties in the airframe/engine interactions. The stability and performance robustness of the system is most sensitive to certain critical interactions, and the analysis seeks to identify these critical interactions.

System Description And Control Law Architecture

The overall system's input-output characteristics are defined at one operating point by the matrix of transfer functions

$$\begin{bmatrix} y_A \\ y_E \end{bmatrix} = \begin{bmatrix} G_A & G_{AE} \\ G_{EA} & G_E \end{bmatrix} \begin{bmatrix} u_A \\ u_E \end{bmatrix}, \quad \text{or} \quad y(s) = G(s)u(s) \tag{1}$$

where $G_A(s)$ represents the airframe dynamics, and $G_E(s)$ represents the engine dynamics. Two-directional dynamic interactions between the airframe and engine are modeled by the off-diagonal transfer function matrices, $G_{AE}(s)$ and $G_{EA}(s)$. $G_{AE}(s)$ will be referred to as the engine-to-airframe coupling or interaction matrix, and $G_{EA}(s)$ will be referred to as the airframe-to-engine coupling or interaction matrix. The responses of each subsystem are affected by the control inputs of the other due to the presence of these interactions. $y_A(s)$ is the vector of airframe responses, and $y_E(s)$ is the vector of engine responses. Likewise, $u_A(s)$ is the vector of airframe control inputs, and $u_E(s)$ the vector of operative engine control inputs.

It is considered that the system is acted upon by either *centralized* or *decentralized* controllers. Centralized controllers are synthesized to address the design objectives of the overall system, and employ two-directional cross-feeds between the interacting subsystems to aid in this effort. Decentralized controllers are designed, built and tested separately for each subsystem. Therefore, utilization of control cross-feeds is limited.

The centralized control law architecture is defined here as

$$\begin{bmatrix} u_A \\ u_E \end{bmatrix} = \begin{bmatrix} K_A & K_{AE} \\ K_{EA} & K_E \end{bmatrix} \begin{bmatrix} y_{Ac} - y_A \\ y_{Ec} - y_E \end{bmatrix}$$

$$\text{or } u(s) = K(s)\{y_c(s) - y(s)\}) \tag{2}$$

$K_A(s)$ and $K_E(s)$ are the feedback control compensation matrices associated with the airframe and the engine control subsystems, respectively. Note the presence of the two-directional control cross-feeds indicated by $K_{AE}(s)$ and $K_{EA}(s)$. $y_{Ac}(s)$ is the vector of desired or commanded airframe responses, perhaps from pilot inputs, and $y_{Ec}(s)$ is the vector of commanded (or limited) engine responses, from either pilot inputs or commands from an outer-loop system.

Hierarchical decentralized control law architectures were all proposed in [5]-[8]. The objective of the work presented in these references was to develop a centralized control law *synthesis* technique with a decentralized *implementation* methodology. The centralized control laws are obtained by various multivariable control law synthesis methods. Then, decentralized control laws are developed that will "approximate" the centralized control in some manner to yield approximately the same closed-loop performance.

The hierarchical decentralized control law architecture is defined here as

$$\begin{bmatrix} u_A \\ u_E \end{bmatrix} = \begin{bmatrix} K_A & 0 \\ K_{EA} & K_E \end{bmatrix} \begin{bmatrix} y_{Ac} - y_A \\ y_{Ec} - y_E \end{bmatrix} \tag{3}$$

One-directional control cross-feed is utilized in the hierarchical decentralized controller, brought about by the presence of $K_{EA}(s)$. The term "hierarchical" conveys that the airframe is viewed as the "higher level" subsystem, and the "lower level" engine subsystem is a "thrust actuator" generating forces and moments on the airframe. Fig. 2 displays the airframe/engine system framework viewed in this manner. It can be seen that the airframe controller is responsible for not only generating aerodynamic control surface inputs, $u_A(s)$, but also for generating engine thrust commands, $y_{Tc}(s)$, to the engine subsystem. *This invokes the one-directional control cross-feed.* However, the decentralized propulsion system controller is designed and built separately. $y_T(s)$ is the vector of engine thrust responses, such as RCS, ejector, ventral, and aft thrusts. These responses act as control inputs to the airframe. $y_E(s)$ is the vector of internal regulated engine responses, such as fan and compressor speeds, and pressures and temperatures at various stages of the engine. The objective of the closed-loop propulsion system is to deliver the required thrust responses to the flight control loops for attitude and lift augmentation.

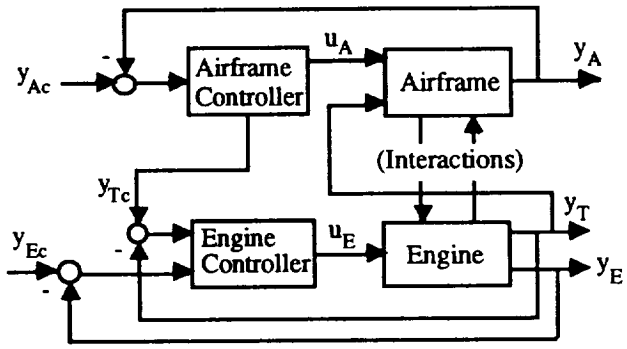

Figure 2 - Hierarchical Decentralized Control Law Architecture

Finally, another class of decentralized controllers that employ no cross-feeds between the subsystems can also be addressed by the analysis technique. In this case, both $K_{AE}(s)$ and $K_{EA}(s)$ are zero, and the matrix K(s) is block diagonal.

In summary, the analysis methodology may address systems with two-directional dynamic interactions between

the airframe and engine, and which employ either centralized or decentralized control laws.

Description Of The Vehicle Dynamics And Control Law

The vehicle configuration to be considered is representative of an E7-D delta wing supersonic aircraft, powered by a high bypass turbofan engine, with STOVL capabilities. The linear dynamic model and control law were provided by the NASA Lewis Research Center, and further details of the vehicle configuration are presented in [5] and [6]. The control law to be investigated in this analysis is documented in [5], which provides a detailed account of the design methodology and the system requirements. The focus of this study is on the longitudinal dynamics of the vehicle. The reference point about which the nonlinear model is linearized is the steady-state wings-level decelerating transition while approaching the hover landing flight phase. The forward flight speed is 80 knots. At this slow speed the forces and moments controlling the aircraft are transitioning from those generated by the aerodynamic control surfaces to those generated by the propulsion system. Table 1 presents the open-loop eigenvalues of the engine dynamics and longitudinal airframe dynamics. Note that the airframe's short period mode is unstable for this configuration and flight condition.

Table 1 - Airframe/Engine Modes

Eigenvalues (rad/sec)	Modes
-200	Pressure Mode
-38 -29	Temperature Modes
-7.1 -4.1	Rotor Speed Modes
1.3	Unstable Short Period
-2.1	Stable Short Period
-0.1+ 0.3i -0.1 - 0.3i	Phugoid Mode

Aerodynamic pitch control is provided by collective elevon deflection. Pitching moments are also provided by aft and ventral nozzle vectoring, and Reaction Control System (RCS) jets. The vehicle is also equipped with left and right ejectors which act in unison, and along with ventral nozzle thrust, provide propulsive lift at low speeds and hover. An ejector butterfly valve angle controls the amount of engine flow to the ejectors, thus the amount of ejector thrust.

The state space descriptions of the linear dynamic model and control law are given in Appendix A. The responses and control inputs are defined in Table 2. The first seven responses are airframe responses, while the fan speed, N_2, is a critical engine response. Therefore, the airframe and engine response vectors are (see Eq. (1))

$$y_A(s) = [Q_V, q, \theta, \gamma, V_V, \dot{V}, V]^T$$
$$y_E(s) = N_2 \qquad (4)$$

In [5] it is noted that the blended responses V_V and Q_V are utilized by the controller to provide good handling qualities in transition flight.

The plant and controller transfer function matrices were normalized by estimates of the maximum allowable perturbations of the responses and controls from their reference values. The maximum allowable perturbations in these responses and controls were provided by NASA Lewis, and are also presented in Table 2. The units of all inputs and outputs are normalized so that the magnitudes of the transfer functions could be meaningfully compared. Unless otherwise stated, all results are presented in these normalized units.

Table 2(a) - Airframe/Engine System Responses And Estimates Of Their Maximum Values

System Responses	Estimate Of Maximum Value
$Q_V = q + 0.3\theta$	6.3 deg/sec
q - pitch rate (deg/sec)	6.3 deg/sec
θ - pitch attitude (deg)	21 deg
γ - long. flight path angle (deg)	4.0 deg
$V_V = \dot{V} + 0.1V$	7.6 ft/sec^2
$\dot{V}$ - total acceleration (ft/sec^2)	7.6 ft/sec^2
V - true airspeed (ft/sec)	76 ft/sec
N_2 - fan speed (rpm's)	120 rpm's

Table 2(b) - Airframe/Engine Control Inputs And Estimates Of Their Maximum Values

System Control Inputs	Estimate Of Maximum Value
δ_E - elevon deflection (deg)	5.0 deg
A_q - pitch RCS area (in^2)	0.7 in^2
$\angle_8$ - aft nozzle vectoring angle (deg)	10 deg
η - ejector butterfly valve angle (deg)	8.0 deg
$\angle_{79}$ - ventral nozzle vectoring angle (deg)	10 deg
A_{78} - ventral nozzle area (in^2)	45 in^2
A_8 - aft nozzle throat area (in^2)	20 in^2
w_f - fuel flow rate (lbm/hr)	1000 lbm/hr

The engine's fan speed responses are shown in Fig. 3, and the magnitude of the airframe's pitch attitude, flight path angle, and forward velocity frequency responses are

shown in Figs. 4 through 6. (The airframe responses Q_V, q, V_V, and $\dot{V}$, are not shown but are directly related to the pitch attitude and forward velocity responses (Table 2(a)).)

It is clear that the airframe/engine system is quite multivariable in nature in that each response is significantly influenced by several controls. With the response vector defined in Eq. (4), it is desirable to select control input vectors such that the plant transfer function matrix in Eq. (1) be approximately diagonally dominant. However, due to the significant multivariable nature of the system, this could not be fully achieved. Fig. 3 shows that the engine's fan speed response from fuel flow rate is approximately 2 dB larger in magnitude than its response from ventral nozzle area, A_{78}, below 7 rad/sec. However, both w_f and A_{78} may be considered primary fan speed controls. Figs. 4 and 6 show that the airframe's pitch attitude and forward velocity responses from A_{78} are generally larger in magnitude than their responses from fuel flow rate. Therefore, for this initial study, the fuel flow rate will be considered the single engine control, and the airframe control vector will be ordered as listed in Table 2(b). Hence,

$$u_A(s) = [\delta_E, A_q, \angle_8, \eta, \angle_{79}, A_{78}, A_8]^T$$
$$u_E(s) = w_f \qquad (5)$$

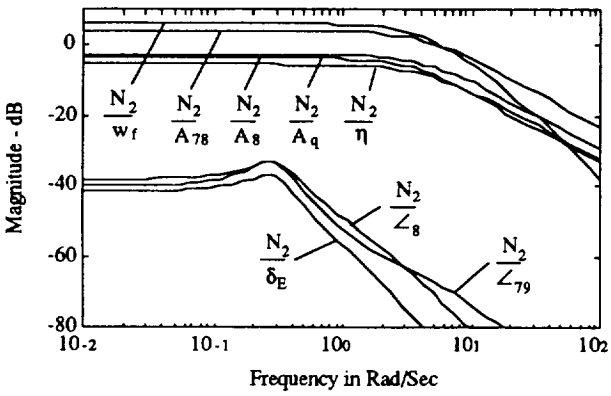

Figure 3 - Engine Fan Speed Frequency Response Magnitudes

With this selection, referring to Eq. (1), the airframe transfer matrix, $G_A(s)$, is 7x7, and the engine transfer function, $G_E(s)$, is a scalar. Thus, the engine-to-airframe coupling transfer matrix, $G_{AE}(s)$, is 7x1, and the airframe-to-engine coupling transfer matrix, $G_{EA}(s)$, is 1x7. (Note that the results of the analysis to follow are dependent on the selection of airframe and engine controls, and different selections have not been fully explored for this vehicle.) The partitioning of the control law matrix follows from the response vector (Eq. (4)) and the selection of airframe and engine controls (Eq. (5)). $K_A(s)$ is therefore 7x7, and $K_E(s)$ is a scalar. The control cross-feed matrices, $K_{AE}(s)$ and $K_{EA}(s)$ are 7x1 and 1x7, respectively.

With the choice of fuel flow rate as the engine control, the engine-to-airframe and airframe-to-engine coupling transfer functions in $G_{AE}(s)$ and $G_{EA}(s)$ are comparatively large in magnitude. Figs. 4 and 5 show that the fuel flow rate may significantly affect the airframe's pitch attitude and flight path angle responses. In turn, due to the *two-directional coupling*, Fig. 3 shows that the engine's fan speed may be significantly affected by the vehicle's utilization of the propulsion system to enhance attitude control and augment lift.

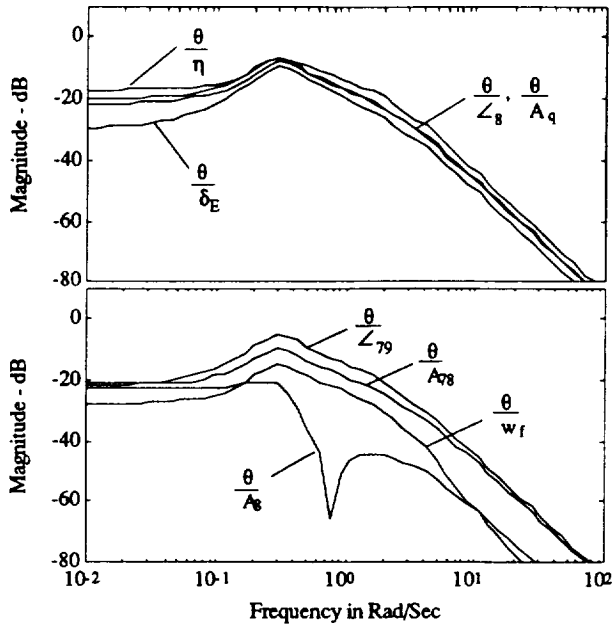

Figure 4 - Pitch Attitude Frequency Response Magnitudes

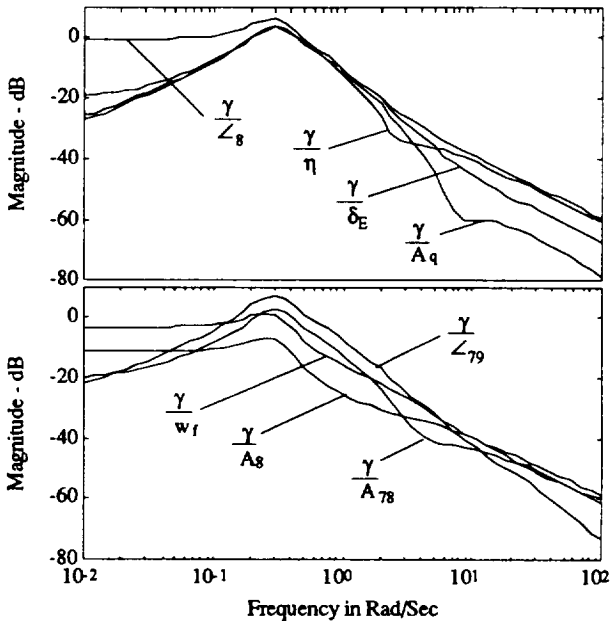

Figure 5 - Flight Path Angle Frequency Response Magnitudes

Stability Robustness Analysis

It is assumed here that the airframe and engine plants are reasonably well modeled, and hence any uncertainties in $G_A(s)$ and $G_E(s)$ at the design point are negligible. Recall, however, that the dynamic interactions between the airframe and engine are difficult to accurately model, and may contribute a considerable source of uncertainty in the model of the system's dynamics. Because the plant uncertainty is

structured in this manner, the structured singular value stability robustness criterion [9,10] may be utilized.

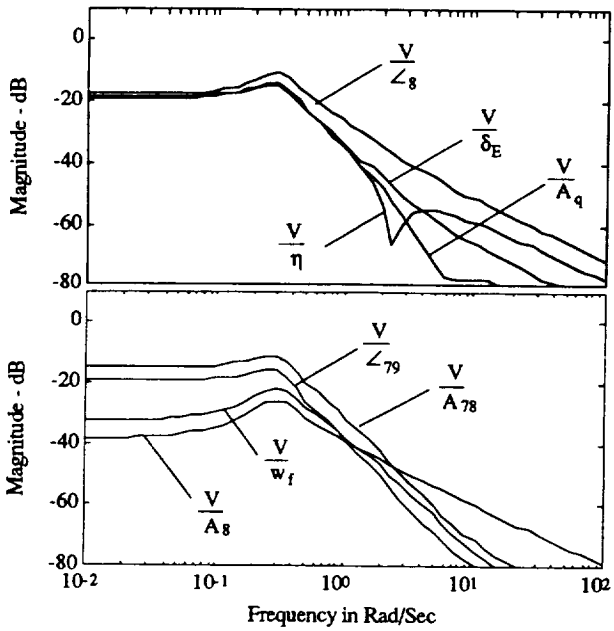

Figure 6 - Forward Velocity Frequency Response Magnitudes

Additive uncertainty in the coupling dynamics is defined here as

$$G_{AE} = G^*_{AE} + \Delta_{AE} \text{ and } G_{EA} = G^*_{EA} + \Delta_{EA} \quad (6)$$

where G^*_{AE} and G^*_{EA} represent nominal models of the interactions. Therefore, with these uncertainties, the "true" plant description is

$$G(s) = G^*(s) + \Delta(s), \text{ where}$$

$$G^*(s) = \begin{bmatrix} G_A & G^*_{AE} \\ G^*_{EA} & G_E \end{bmatrix}, \text{ and } \Delta(s) = \begin{bmatrix} 0 & \Delta_{AE} \\ \Delta_{EA} & 0 \end{bmatrix} \quad (7)$$

The feedback loop for the overall interacting system may now be represented as shown in Fig. 7, with the uncertainties in the coupling dynamics expressed in the following block-diagonal form:

$$\Delta_D(s) = \begin{bmatrix} \Delta_{AE} & 0 \\ 0 & \Delta_{EA} \end{bmatrix} \quad (8)$$

Q(s) in Fig. 7 represents the nominal *closed-loop* system, and it can be shown that

$$\begin{bmatrix} y \\ u' \end{bmatrix} = \begin{bmatrix} Q_{11} & Q_{12} \\ Q_{21} & Q_{22} \end{bmatrix} \begin{bmatrix} y_c \\ y' \end{bmatrix} \quad (9)$$

where,

$$Q_{11} = G^*K(I+G^*K)^{-1}, \quad Q_{12} = (I+G^*K)^{-1}$$
$$Q_{21} = P\,(I+KG^*)^{-1}K, \quad Q_{22} = -P\,(I+KG^*)^{-1}K$$

and the matrix P relates the off-diagonal uncertainty matrix, $\Delta(s)$, to the block-diagonal uncertainty matrix, $\Delta_D(s)$. That is,

$$\Delta(s) = \Delta_D(s)\,P, \quad P = \begin{bmatrix} 0 & I \\ I & 0 \end{bmatrix} \quad (10)$$

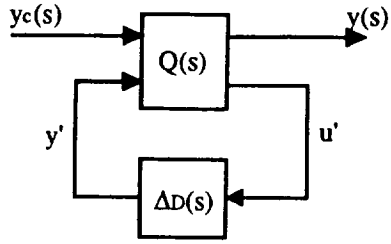

Figure 7 - System Description With Block-Diagonal Uncertainty

From [9] and [10], the system of Fig. 7 remains stable if and only if

$$\|\Delta_D\|_\infty < \frac{1}{\|Q_{22}\|_\mu} \quad (11)$$

where,

$$\|Q_{22}\|_\mu = \sup_\omega \left[\mu(Q_{22}(j\omega))\right], \quad \|\Delta_D\|_\infty = \sup_\omega \left[\sigma_{max}(\Delta_D(j\omega))\right] \quad (12)$$

Here $\mu(Q_{22}(j\omega))$ is the structured singular value of $Q_{22}(j\omega)$, and $\sigma_{max}(\Delta_D(j\omega))$ is the maximum singular value of $\Delta_D(j\omega)$.

Fig. 8 presents the inverse of $\mu(Q_{22}(j\omega))$ for the vehicle and control laws described in the previous section. This figure indicates that

$$\frac{1}{\|Q_{22}\|_\mu} = -19 \text{ dB} \quad (13)$$

Hence, closed-loop stability is assured if and only if $\|\Delta_D\|_\infty$ is less than -19 dB. Due to the structure of $\Delta_D(j\omega)$, this also implies that stability is assured if both $\|\Delta_{AE}\|_\infty$ and $\|\Delta_{EA}\|_\infty$ are less than -19 dB [10]. But without a model or estimate of the uncertainty matrix, $\Delta_D(j\omega)$, $\sigma_{max}(\Delta_D(j\omega))$ cannot be calculated, and hence particularly critical frequency ranges cannot be identified more precisely.

Another stability robustness criterion was developed and presented in [1]-[3] and will also be utilized here. As presented in [1]-[3], the airframe/engine system with the control law architecture of Eq. (2) may be described as shown in Fig. 9. Note that with reference to Eq. (2) and this figure,

$$K_{AE}(s) = \mathcal{K}_{AE}(s)K_E(s), \quad K_{EA}(s) = \mathcal{K}_{EA}(s)K_A(s) \quad (14)$$

Manipulating the block diagram of Fig. 9 into that shown in Fig. 10 gives rise to what [1]-[3] define as *multiplicative*

and disturbance interaction matrices, $M_A(s)$ and $D_A(s)$. These interaction terms capture the effects of the airframe's influence on the engine's control loops.

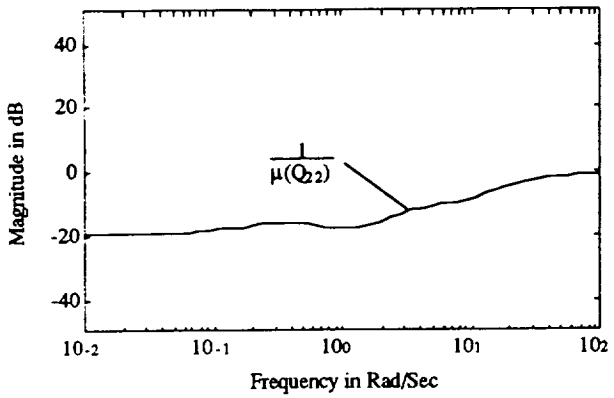

Figure 8 - Structured Singular Value Stability Criterion

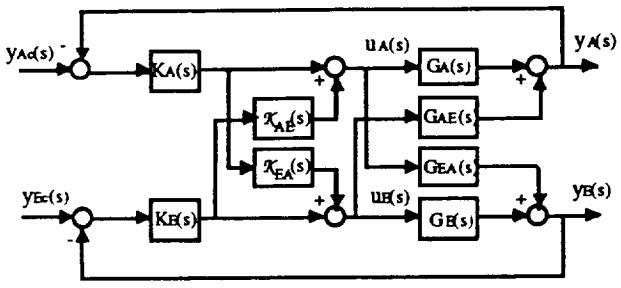

Figure 9 - Fully Interacting Airframe/Engine System

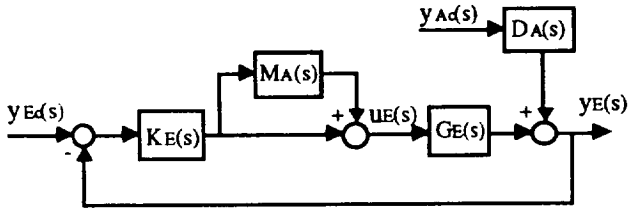

Figure 10 - Engine Loop With Multiplicative And Disturbance Interaction Effects From The Airframe

Specifically, it can be shown that

$$M_A(s) = G_E^{-1}\{G_{EA}\mathcal{K}_{AE} - (G_{EA}+G_E\mathcal{K}_{EA})K_A [I+(G_A+G_{AE}\mathcal{K}_{EA})K_A]^{-1}(G_{AE}+G_A\mathcal{K}_{AE})\} \quad (15)$$

$$D_A(s) = (G_{EA}+G_E\mathcal{K}_{EA})K_A[I+(G_A+G_{AE}\mathcal{K}_{EA})K_A]^{-1}$$

(Note that the engine affects the airframe in a dual manner, and the dual expressions for these interaction terms can be found by interchanging all subscripts A and E in the above expressions.)

Now the determinant of the return difference matrix for the system may be expanded as

$$\det[I+GK] = \det[I+(G_A+G_{AE}\mathcal{K}_{EA})K_A]\det[I+G_E(I+M_A)K_E] \quad (16)$$

Given that K(s) stabilizes the system, the $\det[I+G(j\omega)K(j\omega)]$ is nonzero for all frequency, ω. Therefore a *necessary* condition for stability is that the $\det[I+G_E(I+M_A)K_E]$ is nonzero for all frequency, ω. This is assured if the engine control law $K_E(s)$ stabilizes the (non-interacting) engine loop (in which case the $\det[I+G_EK_E]\neq 0$), and if [1],[12]

$$\sigma_{max}(M_A(j\omega)) < \sigma_{min}(I+(K_E(j\omega)G_E(j\omega))^{-1}) \quad \text{for all } \omega > 0 \quad (17)$$

Therefore, if $\sigma_{max}(M_A(j\omega))$ is equal to or greater than $\sigma_{min}(I+(K_E(j\omega)G_E(j\omega))^{-1})$, the $\det[I+G_E(I+M_A)K_E]$ can no longer be assured to be nonzero. If this determinant is in fact zero, then the closed-loop system is unstable.

For the airframe/engine system in question, the fuel flow rate is the single engine control, and the engine dynamic model, $G_E(s)$, is simply the fan speed-to-fuel flow rate transfer function, $N_2(s)/w_f(s)$. $K_E(s)$ is then, fuel flow rate-to-measured fan speed, or, $w_f(s)/N_2(s)$. Also, the non-interacting engine system $(I+G_EK_E)$ is stable here. Fig. 11 shows the plot of the stability robustness criterion of Eq. (17) for this system.

Although Fig. 11 shows that the criterion of Eq. (17) is satisfied for all frequencies, it can be seen that the magnitude of $M_A(j\omega)$ is only approximately 2 dB below the magnitude of $I+(K_EG_E)^{-1}$ in a critical frequency range between 0.4 and 1.0 rad/sec. Note further from Eq. (15) that $M_A(s)$ is a strong function of the coupling matrices $G_{AE}(s)$ and $G_{EA}(s)$, which are considered uncertain here. Hence, *a significant amount of uncertainty arises in the multiplicative interaction matrix*, and Fig. 11 indicates that frequencies between 0.4 and 1.0 rad/sec appear to be critical.

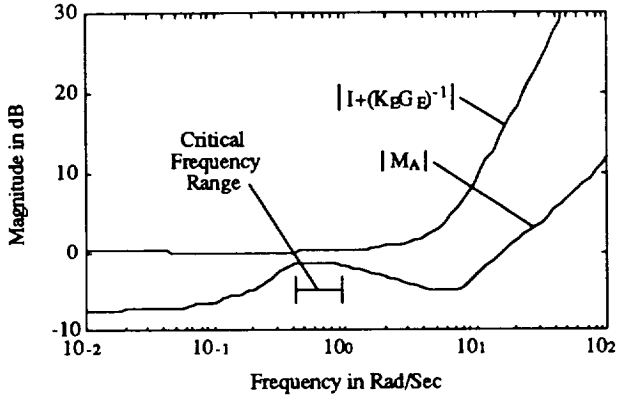

Figure 11 - Plot Of The Stability Robustness Criterion Of Eq. (17)

The sensitivity of the multiplicative interaction matrix $M_A(s)$ to uncertainties in the coupling dynamics shall now be addressed. Sought were those coupling transfer functions within $G_{AE}(s)$ and/or $G_{EA}(s)$ that if varied would produce the largest variations in the magnitude of $M_A(j\omega)$. Each coupling transfer function was varied (one at a time) by multiplying the nominal magnitude of the coupling transfer function by the same magnitude variation, δ_m. Then, at each frequency, the phase of the coupling transfer function was allowed to vary from nominal by an amount

δ_ϕ, which ranged from -60 degrees to +60 degrees. The "worst case" phase variation was defined as the δ_ϕ which caused the largest difference (in dB) in $|M_A(j\omega)|$.

All 14 coupling transfer functions (recall that $G_{AE}(s)$ is 7x1 and $G_{EA}(s)$ is 1x7) were varied, and the respective $|M_A(j\omega)|$ for each case is shown in Fig. 12. In this figure, the nominal magnitude of $M_A(j\omega)$ is plotted in the solid line. Each dashed line is a plot of $|M_A(j\omega)|$ for a magnitude variation δ_m=3 (≈10 dB) and the "worst case" phase variation at each frequency in one particular coupling transfer function. It can be seen from this figure that the magnitude of the multiplicative interaction matrix is most sensitive to magnitude and phase perturbations in four coupling transfer functions. These coupling transfer functions are fan speed-to-ventral nozzle area, N_2/A_{78}, fan speed-to-aft nozzle area, N_2/A_8, fan speed-to-ejector butterfly valve angle, N_2/η, and flight path angle-to-fuel flow rate, γ/w_f. Perturbations in the other ten coupling transfer functions caused negligible variations in $|M_A(j\omega)|$. It can be seen from Fig. 12 that, although perturbations in N_2/A_{78}, N_2/A_8 and N_2/η caused variations in $|M_A(j\omega)|$ at all frequencies, the perturbation in flight path angle-to-fuel flow rate caused the largest variation in $|M_A(j\omega)|$, and further, this occurred in the critical frequency range indicated in Fig. 11.

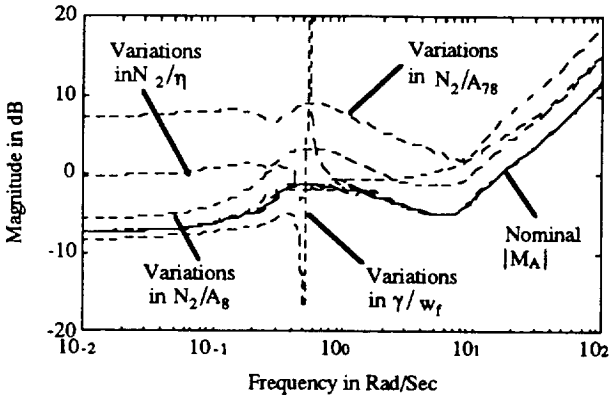

Figure 12 - Sensitivity Of Multiplicative Interaction Matrix To Perturbations In Coupling Transfer Functions

The magnitudes and phases of all 14 coupling transfer functions were also varied until instability occurred. Listed in Table 3 are those transfer functions for which the smallest magnitude and phase variations, δ_m and δ_ϕ, would lead to instability. For each transfer function, the table lists the magnitude and phase variations required to cause instability, and the frequency at which the instability occurs. Note that the combination of magnitude and phase variation required to cause instability is not unique. That is, more magnitude variation and less phase variation (or vice-versa) can also cause instability, and Table 3 simply lists example combinations. The first four transfer functions listed are engine-to-airframe ($G_{AE}(s)$) interactions, and the last three listed are airframe-to-engine ($G_{EA}(s)$) interactions. All coupling transfer functions not listed in this table required over 20 dB of magnitude variation and/or over 180 degrees of phase variation before instability would occur.

Table 3 - Variations In Coupling Transfer Functions Required To Cause Instability

Coupling Transfer Function	Magnitude Variation (dB)	Phase Variation (degrees)	Frequency At Instability (rad/sec)
q/w_f	16	-115	1.3
θ/w_f	18	-85	0.8
γ/w_f	10	-37	0.52
V/w_f	20	-120	0.38
N_2/A_{78}	20	-125	10
N_2/A_8	19	-138	1.3
N_2/η	20	-132	0.3

The flight path angle-to-fuel flow rate transfer function, γ/w_f, is the most critical interaction, with both the smallest magnitude variation (10 dB) and the smallest phase variation (-37 degrees) required to cause instability. For this perturbation, instability occurs at 0.52 rad/sec. Note that $|M_A(j\omega)|$ is greater than $|I+(K_E G_E)^{-1}|$ for this perturbation at 0.52 rad/sec, indicating the conservatism of the stability robustness criterion of Eq. (17). However, for this perturbation, $\sigma_{max}(\Delta_D(j\omega))$=10 dB for all ω, indicating that the structured singular value criterion shown in Fig. 8 is conservative as well.

Instability was determined by plotting the Nyquist plot of the determinant of $I+G(j\omega)K(j\omega)$ with perturbations in the coupling transfer functions. Fig. 13 presents the plot of the $\det(I+G(j\omega)K(j\omega))$ for both the nominal system, and the system with the variations in the flight path angle-to-fuel flow rate transfer function that caused instability. Although Fig. 13 only shows the Nyquist plot near the origin, it can be shown that there are two ensuing clockwise encirclements of the origin for the perturbed system. This implies that a pair of closed-loop eigenvalues lies on the $j\omega$-axis at $\pm$ 0.52j.

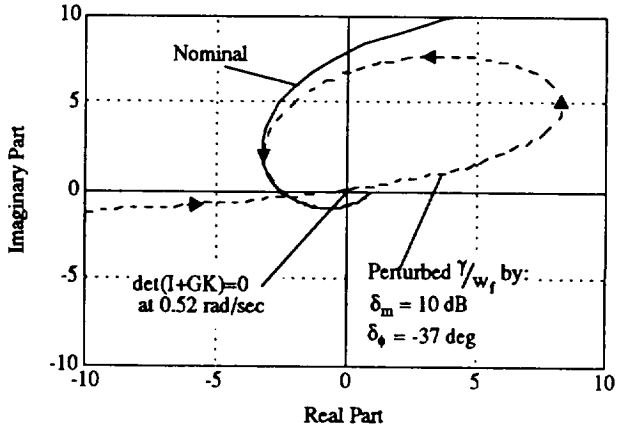

Figure 13 - Plot Of Airframe/Engine System's $\det[I+G(j\omega)K(j\omega)]$ With Variations In Flight Path Angle-To-Fuel Flow Rate Transfer Function

The significance of the uncertainty leading to the instability is depicted in Fig. 14. In the figure, the nominal flight path angle-to-fuel flow rate transfer function is shown along with magnitude and phase variations of 10 dB and -37 degrees. It can be seen that the magnitude of uncertainty that causes instability is actually quite "small" in the physical units of deg/(lbm/hr). At the frequency of instability (0.52 rad/sec) the nominal magnitude is -56 dB (0.0016 deg/(lbm/hr)) and the perturbed magnitude is -46 dB (0.0050 deg/(lbm/hr)). This is a difference of only 0.0034 deg/(lbm/hr).

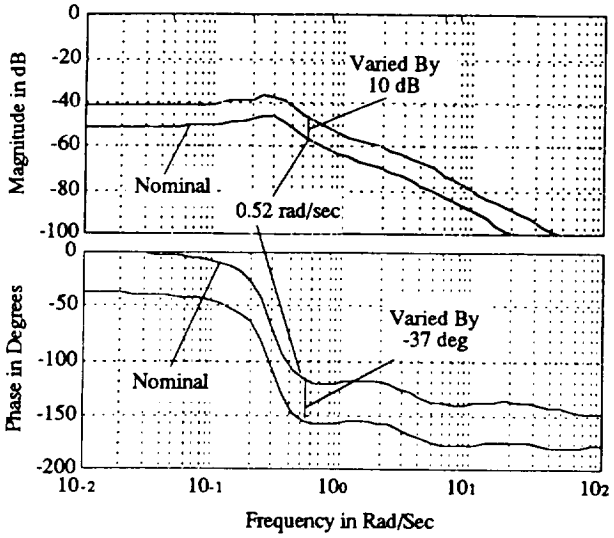

Figure 14 - Frequency Response Of Flight Path Angle-To-Fuel Flow Rate Transfer Function With Variations That Cause Instability

Finally, Fig. 15 presents the Bode plot of the engine fan speed loop (with all other loops closed). It can be seen that this loop nominally has infinite gain margin and 80 degrees of phase margin at a cross-over frequency of 5.5 rad/sec. However, the instability that occurs at 0.52 rad/sec due to the critical variations in the flight path angle-to-fuel flow rate coupling transfer function is also shown. It is clear that the classical phase margin defined at the gain cross-over frequency does *not* indicate this critical frequency. The structured singular value of the closed-loop matrix $Q_{22}(j\omega)$ (Eq. (9)), shown in Fig. 8, also failed to indicate this critical frequency. However, as indicated by Fig. 11, the robustness criterion of Eq. (17) correctly indicated the frequency range in which instability would occur for the *smallest* variations in magnitude and phase of one transfer function in $G_{AE}(s)$ or $G_{EA}(s)$. Furthermore, this criterion is most sensitive to variations in γ/w_f within the critical frequency range, which is consistent with the results in Fig. 12.

Performance Analysis

Referring back to Fig. 10, the *decoupled* or *non-interacting* engine system's closed-loop responses are

$$y_E(s) = [I + G_E K_E]^{-1} G_E K_E y_{Ec}(s) \qquad (18)$$

However, with airframe/engine interactions, the engine system's responses are

$$y_E(s) = [I + G_E(I+M_A)K_E]^{-1} G_E(I+M_A)K_E\, y_{Ec}(s) + [I + G_E(I+M_A)K_E]^{-1} D_A\, y_{Ac}(s) \qquad (19)$$

It be can seen that disturbances to the engine responses from airframe commands, $y_{Ac}(s)$ (for example, pilot stick inputs), arise unless the disturbance interaction matrix, $D_A(s)$, is zero. For this case study, $D_A(s)$ is a 1x7 matrix and $y_{Ac}(s)$ in Fig. 10 is

$$y_{Ac}(s) = [Q_{Vc}, q_c, \theta_c, \gamma_c, V_{Vc}, \dot{V}_c, V_c]^T \qquad (20)$$

However, in [5] and [6] the actual airframe command vector consisted only of the commanded blended responses, Q_{Vc} and V_{Vc}, and the commanded flight path angle, γ_c. The other responses are regulated, or their commands are zero. Define here the 1x3 matrix $D_A(j\omega)$ as the "subset" of $D_A(j\omega)$ consisting of those elements corresponding to Q_{Vc}, V_{Vc} and γ_c. Fig. 16 shows the magnitudes of the elements of $D_A(j\omega)$. These terms are seen to be approximately -10 dB in magnitude below 1.0 rad/sec.

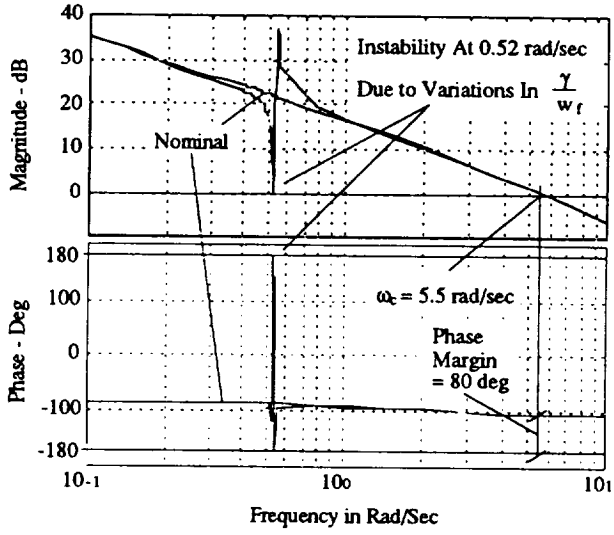

Figure 15 - Engine Fan Speed Loop Bode Plot With All Other Loops Closed

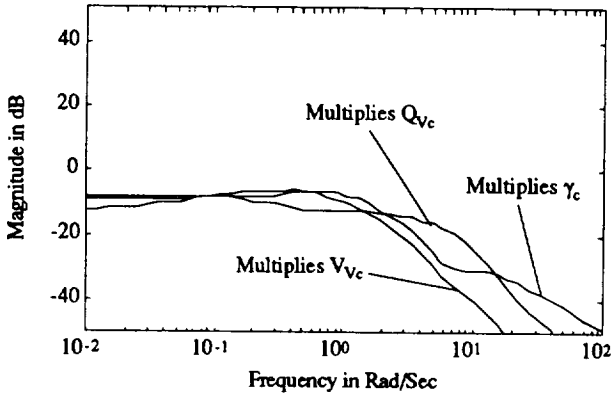

Figure 16 - Frequency Response Magnitudes Of $D_A(j\omega)$

The closed-loop engine response (Eq. (19)) is the sum of two quantities: the complementary sensitivity function operating on the engine commands, and the product of the sensitivity function and $D_A(j\omega)$ operating on the airframe commands. Fig. 17 presents the magnitude of the fan speed response from commanded fan speed, N_{2c} (the complementary sensitivity function), and the maximum singular value of the fan speed response from the nonzero airframe commands (the product of the sensitivity function and $D_A'(j\omega)$). It can be seen from Fig. 17 that at all frequencies the magnitude of the fan speed response from the commanded fan speed is at least approximately 17 dB greater than the maximum singular value of the fan speed response from the airframe commands. In other words, the maximum singular value of the fan speed response from the airframe commands is at most only approximately 14% of the magnitude of the fan speed response from commanded fan speed. Unless more disturbance rejection performance is required, it would seem that the fan speed loop should be able to adequately reject disturbances from airframe commands.

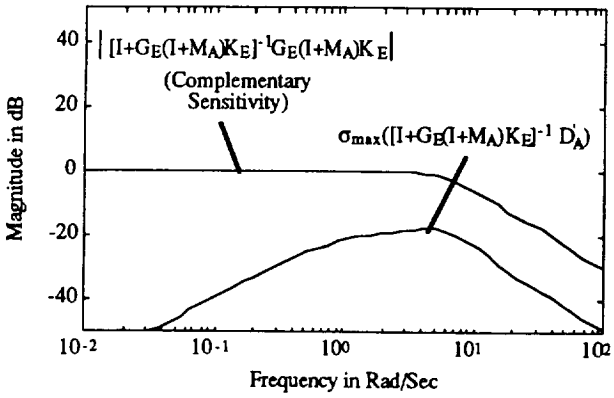

Figure 17 - Fan Speed Complementary Sensitivity Function And Disturbance Response From Airframe Interactions

Fig. 18 presents the fan speed time response from a step flight path angle command, γ_c. The flight path angle was commanded to 4 degrees, which is its maximum allowable value, as given in Table 2(a). This constitutes a "worst case" fan speed disturbance response from commanded flight path angle. It can be seen from this figure that the fan speed response has a peak magnitude of approximately 5% of the maximum allowable fan speed response of 120 rpms, also given in Table 2(a). Although not presented, the peak magnitudes of the fan speed response from the other airframe commands were even less than that shown in Fig. 18. Therefore, the fan speed loop seems to adequately reject disturbances from airframe commands, consistent with the results in Fig. 17.

Finally, recall that the system stability was sensitive to magnitude and phase variations in the flight path angle-to-fuel flow rate coupling transfer function, γ/w_f, and that a magnitude variation, δ_m, of 10 dB, and a phase variation, δ_ϕ, of -37 degrees in this coupling transfer function caused instability. Therefore, performance robustness to uncertainties in the interactions should also be addressed. Although the focus of the analysis so far has been the airframe's effects on the engine, the engine will also affect the airframe. Fig. 19 shows the magnitude of the airframe's closed-loop frequency response of flight path angle-to-commanded flight path angle, γ/γ_c. This response is presented because it was found to be the most sensitive to variations in the flight path angle-to-fuel flow rate coupling transfer function, γ/w_f. It can be seen that for the nominal response, good command following performance is obtained out to a bandwidth of approximately 0.5 rad/sec. However, responses are also shown that correspond to perturbations in the flight path angle-to-fuel flow rate coupling transfer function. With a perturbation of 6 dB and -22 degree (60% of 10 dB and 60% of -37 degrees), a peak magnitude of over 6 dB is seen in the flight path angle's closed loop response occurring at approximately 0.4 rad/sec. This will clearly lead to unacceptable handling. Hence, although the perturbations in this interaction are not "large" enough to cause instability, their effect on the closed-loop response is quite significant.

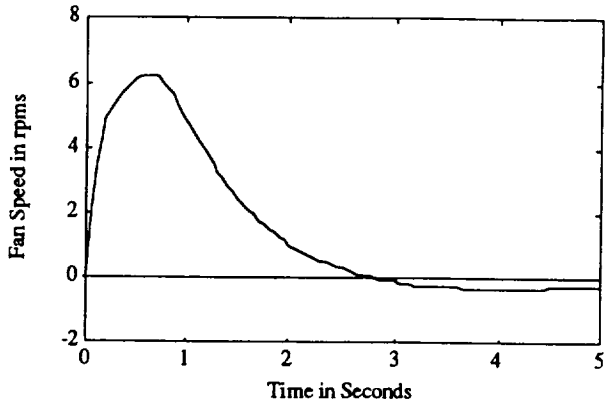

Figure 18 - Fan Speed Response From A Maximum Allowable 4 Degree Step Flight Path Angle Command

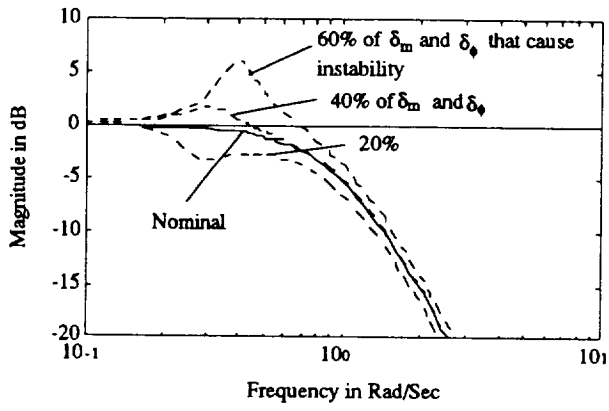

Figure 19 - Closed Loop Flight Path Angle Response From Flight Path Angle Command

Conclusions

For a particular airframe/engine system and integrated control law, a critical frequency range was identified along with potentially poor stability robustness due to the interactions between the airframe and engine. It was found that, within this critical frequency range, stability and performance were sensitive to variations in the coupling between the airframe's flight path angle and the engine's fuel flow rate. A stability sensitivity study indicated that the interactions between flight path angle and fuel flow rate

were, in fact, potentially the most critical. Instability occurred in the critical frequency range indicated by a stability robustness criterion, while the gain cross-over frequency for a classical single-loop analysis did not correspond to this critical frequency. Although the engine's fan speed loop seemed to adequately reject disturbances from airframe commands, it was shown that uncertainties in the coupling between flight path angle and fuel flow rate may lead to unacceptable flight path angle command following performance.

Appendix A. State Space Description Of System Dynamics And Control Law

Airframe/Engine System:

$\dot{x} = Ax + Bu$

$y = Cx + Du$

Control Law:

$\dot{x}_c = A_c x_c + B_c(y_c - y)$

$u = C_c x_c + D_c(y_c - y)$

State Vector:

$x = [u, w, q, \theta, N_2, N_{25}, T_{41}, T_3, P_6]^T$

Definition Of States:

u = axial velocity (ft/sec)
w = vertical velocity (ft/sec)
q = pitch rate (rad/sec)
θ = pitch attitude (rad)
N_2 = fan speed (rpms)
N_{25} = compressor speed (rpms)
T_{41} = compressor turbine inlet temp. (degrees, R)
T_3 = combustor inlet temp. (degrees, R)
P_6 = tailpipe entrance total pressure (psi)

Response And Control Vectors: (see Table 2)

$y = [Q_V, q, \theta, \gamma, V_V, \dot{V}, V, N_2]^T$

$u = [\delta_E, A_q, \angle_8, \eta, \angle_{79}, A_{78}, A_8, w_f]^T$

A Matrix: Columns 1 To 4

```
-5.905e-2  7.184e-2 -2.283e+1 -3.193e+1
-1.369e-1 -4.031e-1  1.297e+2 -3.922e+0
-1.240e-2  1.890e-2 -5.480e-1 -1.402e-7
 0.000e+0  0.000e+0  1.000e+0  0.000e+0
-7.286e-1 -1.282e-1  0.000e+0 -1.258e-3
 3.557e-1  6.258e-2  0.000e+0  6.142e-4
 1.523e-1  2.679e-2  0.000e+0  2.630e-4
 4.853e+0  8.537e-1  0.000e+0  8.379e-3
-4.623e-1 -8.133e-2  0.000e+0 -7.983e-4
```

A Matrix: Columns 5 To 9

```
 1.120e-3  3.348e-4  1.564e-5  6.916e-4  1.448e-1
-7.208e-3 -2.109e-3 -9.950e-5 -4.360e-3  1.546e-1
 2.572e-4  7.677e-5  3.693e-6  1.596e-4 -3.305e-3
 0.000e+0  0.000e+0  0.000e+0  0.000e+0  0.000e+0
-5.300e+0  5.580e+0 -1.659e-2  2.906e+0  5.050e+1
 7.035e-1 -4.365e+0  7.495e-1  5.763e+0 -1.442e+0
 3.419e-1  5.981e+0 -3.495e+1  1.720e+0 -2.982e+0
-1.948e+0 -1.529e+1  2.882e+1 -3.477e+1  2.701e+1
 1.528e+0  4.518e-1  2.064e-2  9.388e-1 -1.992e+2
```

B Matrix: Columns 1 To 4

```
-3.178e-2 -1.030e-1 -1.974e-1 -7.991e-2
-2.129e-1 -8.065e-2 -7.841e-2 -1.100e-1
-2.340e-2  2.629e-1 -1.710e-2  2.988e-2
 0.000e+0  0.000e+0  0.000e+0  0.000e+0
 0.000e+0 -3.786e+2 -6.630e-5  4.304e+1
 0.000e+0 -5.645e+2 -2.978e-3 -1.348e+0
 0.000e+0 -3.604e+2 -5.016e-3 -2.494e+0
 0.000e+0  1.664e+3  1.217e-2  2.289e+1
 0.000e+0 -1.401e+2 -5.077e-3 -2.838e+1
```

B Matrix: Columns 5 To 8

```
-1.418e-5  8.810e-3  4.259e-2  5.857e-6
-8.863e-2  3.009e-2  7.319e-2 -6.828e-5
-2.204e-2 -4.393e-3 -1.890e-3  3.523e-6
 0.000e+0  0.000e+0  0.000e+0  0.000e+0
 1.733e-2  2.239e+1  2.383e+1  3.131e-2
 4.208e-2 -6.814e-1 -7.588e-1  4.036e-2
-1.570e-3 -1.296e+0 -1.474e+0  2.943e-2
-1.059e-2  1.193e+1  1.256e+1  4.780e+0
-7.510e-3 -1.477e+1 -1.573e+1  1.733e-2
```

C Matrix: Columns 1 To 4

```
 0.000e+0  0.000e+0  5.730e+1  1.719e+1
 0.000e+0  0.000e+0  5.730e+1  0.000e+0
 0.000e+0  0.000e+0  0.000e+0  5.730e+1
 7.348e-2 -4.176e-1  0.000e+0  5.730e+1
 1.661e-2  1.821e-2  7.367e-5 -3.213e+1
-8.188e-2  8.843e-4  7.367e-5 -3.213e+1
 9.849e-1  1.733e-1  0.000e+0  1.526e-3
 0.000e+0  0.000e+0  0.000e+0  0.000e+0
```

C Matrix: Columns 5 To 9

```
 0.000e+0  0.000e+0  0.000e+0  0.000e+0  0.000e+0
 0.000e+0  0.000e+0  0.000e+0  0.000e+0  0.000e+0
 0.000e+0  0.000e+0  0.000e+0  0.000e+0  0.000e+0
-8.637e-8 -2.494e-8 -1.160e-9 -5.135e-8  1.851e-6
-1.465e-4 -3.587e-5 -1.849e-6 -7.480e-5  1.693e-1
-1.460e-4 -3.573e-5 -1.842e-6 -7.449e-5  1.693e-1
-5.080e-6 -1.477e-6 -6.915e-8 -3.047e-6  1.094e-4
 1.000e+0  0.000e+0  0.000e+0  0.000e+0  0.000e+0
```

D Matrix: Columns 1 To 4

```
 0.000e+0  0.000e+0  0.000e+0  0.000e+0
 0.000e+0  0.000e+0  0.000e+0  0.000e+0
 0.000e+0  0.000e+0  0.000e+0  0.000e+0
-2.861e-6  0.000e+0  1.885e-6  4.061e-6
-6.820e-2  0.000e+0 -2.080e-1 -9.775e-2
-6.820e-2  0.000e+0 -2.080e-1 -9.776e-2
 0.000e+0  0.000e+0  8.042e-5  9.331e-5
 0.000e+0  0.000e+0  0.000e+0  0.000e+0
```

D Matrix: Columns 5 To 8

```
 0.000e+0  0.000e+0  0.000e+0  0.000e+0
 0.000e+0  0.000e+0  0.000e+0  0.000e+0
 0.000e+0  0.000e+0  0.000e+0  0.000e+0
 0.000e+0 -3.569e-7  8.772e-7  0.000e+0
-1.538e-2  1.389e-2  5.462e-2 -6.069e-6
-1.538e-2  1.389e-2  5.462e-2 -6.064e-6
 3.446e-8 -1.763e-6  5.181e-5 -4.058e-8
 0.000e+0  0.000e+0  0.000e+0  0.000e+0
```

Ac Matrix: 14x14 Block Diagonal - Elements Not Listed = 0

```
Diagonal: (1,1) Through (5,5):
-3.186e-3 -3.543e-3 -4.476e-3 -4.481e-3 -7.440e-3
Diagonal: (6,6) Through (10,10):
-8.954e-3 -1.817e-1 -8.370e-1 -1.348e+0 -1.348e+0
Diagonal: (11,11) Through (14,14)
-2.360e+0 -3.023e+0 -7.749e+0 -7.749e+0
Other Nonzero Elements:
Ac(9,10)=7.494e-2, Ac(10,9)=-7.494e-2
Ac(13,14)=5.629e+0, Ac(14,13)=-5.629e+0
```

Bc Matrix: Columns 1 To 4

```
-3.522e-2 -8.032e-6 -3.826e-6 -1.142e+1
 1.673e-1  1.700e-4  1.399e-4  3.077e-1
-8.150e-3 -1.847e-5 -1.588e-5 -4.455e-3
-1.919e-3 -1.497e-5 -1.074e-5 -1.810e-3
 7.453e-2 -4.129e-6  4.612e-6  9.322e-4
-1.458e+1 -3.065e-5 -1.950e-5  9.773e-5
 2.107e+1 -9.964e-1 -7.692e-1 -3.191e+0
-8.423e-1  3.781e+0  2.923e+0 -6.516e-1
 1.198e+1 -6.278e+0 -4.850e+0 -1.174e+1
-4.336e+0  1.726e+0  1.337e+0  3.342e+0
 1.506e+0 -1.180e+0 -9.109e-1 -2.414e+0
 2.166e+0 -2.430e+0 -1.878e+0 -3.891e+0
 2.259e+0  1.453e+0  1.123e+0  1.515e-1
-7.202e+0 -6.871e+0 -5.308e+0 -1.043e+0
```

Bc Matrix: Columns 5 To 8

```
-3.908e-1  1.040e-5 -3.613e-5  2.995e-3
 1.777e+1 -9.835e-5  1.144e-4 -2.044e-2
 2.467e-2  3.965e-6  2.092e-7 -1.451e-6
 1.833e-3  6.492e-6  3.166e-6  3.359e-5
-2.056e-2 -2.179e-6  1.678e-5 -1.200e+0
 1.880e-3  1.469e-5  4.748e-6 -6.802e-4
 1.728e+1  3.871e-1  2.986e-1 -1.380e-1
 4.657e-1 -1.466e+0 -1.134e+0 -6.050e-3
 1.303e+0  2.436e+0  1.881e+0 -7.524e-2
-1.097e+0 -6.671e-1 -5.184e-1 -3.618e-2
-3.617e-1  4.585e-1  3.532e-1  8.077e-3
 3.378e-1  9.406e-1  7.284e-1  4.108e-2
-1.650e-4 -5.650e-1 -4.357e-1 -1.211e-1
 5.437e-1  2.666e+0  2.059e+0 -1.079e-1
```

Cc Matrix: Columns 1 To 5

```
-1.033e-1 -1.322e-1  1.611e-1 -5.057e-3 -4.509e-3
-1.118e-3 -1.720e-3 -9.294e-4 -5.827e-4 -5.309e-4
 3.429e-2 -8.450e-2 -1.243e-1 -3.421e-2 -1.122e-2
-1.315e-1 -2.194e-1  1.221e-1 -2.706e-2 -4.730e-2
-1.343e-1 -2.199e-1  2.956e-1  1.504e-5 -3.630e-3
 7.977e-1  9.973e-1 -1.172e+0  4.544e-2 -3.251e-1
 4.042e-1  5.964e-1 -4.976e-1  4.357e-2 -6.710e-2
-1.892e+1 -2.098e+1  2.626e+1 -7.981e-1 -1.412e+1
```

Cc Matrix: Columns 6 To 10

```
 1.866e-1  1.504e-1  9.785e-2 -1.857e-1  4.699e-3
-7.758e-4 -6.743e-5  7.813e-3  3.705e-3  1.039e-3
-4.394e-2 -9.341e-2  1.598e-1  1.773e-1  1.110e-2
 1.316e-1  1.477e-1  3.251e-1 -9.063e-2  3.817e-2
 2.588e-1  2.826e-1  9.965e-2 -4.655e-1  3.603e-2
-9.835e-1 -1.162e+0 -1.185e+0  1.266e+0 -1.071e-1
-5.213e-1 -5.207e-1 -5.652e-1  5.410e-1 -2.526e-2
 2.246e+1  2.480e+1  1.703e+1 -2.308e+1  7.521e-1
```

Cc Matrix: Columns 11 To 14

```
 3.658e-1 -5.758e-2  5.675e-2  1.330e-1
-1.670e-2  1.529e-2  8.853e-3 -2.657e-2
-9.900e-1  2.647e-1 -6.822e-2  2.457e-1
-1.322e-1  4.603e-1 -1.151e-1 -4.293e-1
 1.471e+0  4.467e-1 -2.130e-2  1.164e-1
-9.120e-1 -2.423e+0  1.531e+0  1.402e+0
-7.606e-1 -1.544e-1  1.184e-1  3.201e-1
 1.004e+1  1.295e+1  2.233e+1 -1.169e+1
```

Dc Matrix: Columns 1 To 4

```
-6.800e-3 -6.484e-2 -4.982e-2 -7.060e-2
 4.612e-4  4.161e-3  3.206e-3  4.498e-3
 1.239e-3  1.225e-2  9.787e-3  1.300e-2
 7.468e-3  6.278e-2  4.860e-2  6.805e-2
 1.123e-3  1.555e-2  1.199e-2  1.754e-2
 3.713e-2  3.194e-1  2.456e-1  3.468e-1
 1.911e-2  1.161e-1  8.783e-2  1.212e-1
 7.759e+0  2.472e+1  1.911e+1  2.549e+1
```

Dc Matrix: Columns 5 To 8

```
 7.570e-4  2.518e-2  1.931e-2 -1.088e-2
-1.019e-4 -1.607e-3 -1.243e-3  8.586e-4
-1.842e-3 -4.433e-3 -3.797e-3  4.780e-3
-1.377e-3 -2.395e-2 -1.884e-2  2.000e-2
 2.039e-4 -6.021e-3 -4.647e-3  2.161e-3
-2.155e-3 -1.229e-1 -9.522e-2  9.407e-2
 1.093e-3 -4.552e-2 -3.403e-2  3.272e-2
 1.276e+0 -9.525e+0 -7.411e+0  4.660e+0
```


Acknowledgements

This work was sponsored by the NASA Lewis Research Center under Grant # NAG3-998. Dr. Sanjay Garg is the technical program manager.

References

[1] Schmidt, D., Schierman, J., Garg, S., "Analysis of Airframe/Engine Interactions - An Integrated Control Perspective," AIAA Paper No. 90-1918, presented at the 26th Joint Propulsion Conference, Orlando, Florida., July, 1990.

[2] Schierman, J., Schmidt, D., "Analysis Of Airframe/Engine Interactions In Integrated Flight And Propulsion Control," AIAA No. 91-2794, presented at the AIAA Guidance, Navigation and Control Conference, New Orleans, Louisiana, August, 1991.

[3] Schierman, J., Schmidt, D., "Analysis Of Airframe And Engine Control Interactions And Integrated Flight/Propulsion Control," September, 1991, to be published in the *Journal Of Guidance, Control, And Dynamics.*

[4] Garg, S., Mattern, D.L., and Bullard, R.E., "Integrated Flight/Propulsion Control System Design Based on a Centralized Approach," *Journal of Guidance*, Vol. 14, No. 1, pp. 107-116, Jan.-Feb., 1991. Originally presented as AIAA Paper No. 89-3520, AIAA Guidance, Navigation and Control Conference, Boston, Massachusetts, August, 1989.

[5] Garg, S., Ouzts, P., "Integrated Flight/Propulsion Control Design for a STOVL Aircraft Using H-Infinity Control Design Techniques," presented at American Control Conference, Boston, Massachusetts, June, 1991.

[6] Garg, S., Mattern, D.L., "Application of an Integrated Flight/Propulsion Control Design Methodology to a STOVL Aircraft," AIAA Paper No. 91-2792, presented at the AIAA Guidance, Navigation and Control Conference, New Orleans, Louisiana, August, 1991.

[7] Shaw, P., et al., "Development and Evaluation of an Integrated Flight and Propulsion Control System," AIAA Paper No. 85-1423, presented at the AIAA Joint Propulsion Conference, Monterey, California, July, 1985.

[8] Rock, S.M., Emami-Naeini, A., Anex, R.P., "Propulsion Control Specifications in Integrated Flight/Propulsion Control Systems," AIAA Paper No. 88-3236, presented at the AIAA Joint Propulsion Conference, Boston, Massachusetts, 1988.

[9] Doyle, J. "Analysis of Feedback Systems With Structured Uncertainties" *Proceedings of the Institute of Electrical Engineers*, Part D., 129, pp. 242-250, 1982.

[10] Maciejowski, J.M., *Multivariable Feedback Design*, Addison-Wesley Publishing Company, New York, 1989.

[11] Kwakernaak, H., Sivan, R., *Linear Optimal Control Systems*, Wiley-Interscience, New York, 1972.

[12] Doyle, J., Stein, G., "Multivariable Feedback Design: Concepts for a Classical/Modern Synthesis," *IEEE Transactions on Automatic Controls*, Vol. AC-26, No. 1, pp. 4-16, Feb., 1981.

A Comparative Study of Multivariable Robustness Analysis Methods as Applied to Integrated Flight and Propulsion Control†

John D. Schierman‡, T. Alan Lovell* and David K. Schmidt**
Aerospace Research Center
College of Engineering and Applied Sciences
Arizona State University

Abstract

Three multivariable robustness analysis methods will be compared and contrasted. The focus of the analysis will be on system stability and performance robustness to uncertainty in the coupling dynamics between two interacting subsystems. Of particular interest is interacting airframe and engine subsystems and an example airframe/engine vehicle configuration is utilized in the demonstration of these approaches. The Singular Value (SV) and Structured Singular Value (SSV) Analysis methods will be compared to a method especially well suited for analysis of robustness to uncertainties in subsystem interactions. This approach is referred to here as the Interacting Subsystem (IS) Analysis method. This method has been used previously to analyze airframe/engine systems, emphasizing the study of stability robustness. However, performance robustness is also investigated here, and a new measure of allowable uncertainty for acceptable performance robustness is introduced. The IS methodology does not require plant uncertainty models to measure the robustness of the system, and will be shown to yield valuable information regarding the effects of subsystem interactions. In contrast, the SV and SSV methods allow for the evaluation of the robustness of the system to particular models of uncertainty, and do not directly indicate how the airframe (engine) subsystem interacts with the engine (airframe) subsystem.

Introduction

The objective of this paper will be to compare and contrast aspects of three multivariable robustness analysis methods when applied to interacting airframe/engine subsystems. These three approaches are denoted here as:

(1) Singular Value (SV) Analysis[1,2,3]
(2) Structured Singular Value (SSV) Analysis[3,4] and
(3) Interacting Subsystem (IS) Analysis.[5-7]

This paper will focus on the analysis of both stability and performance robustness with all three methods.

The SV and SSV methods have been used for analysis of multivariable systems in general. The development of the IS analysis method was motivated by the integrated flight/propulsion control problem.[5-7] A measure of the allowable magnitude of airframe-to-engine interactions to assure acceptable performance was recently developed and is presented as part of the IS methodology. The focus of the IS methodology is analysis of system stability and performance robustness to uncertainties in the dynamic cross-coupling between airframe and engine subsystems. However, although this approach was developed for analysis of interactions between the airframe and engine, its application is not limited to these types of systems alone.

The STOVL configuration analyzed in Ref. [7] is considered representative of an advanced highly maneuverable aircraft with integrated flight/propulsion control. This vehicle has the capabilities of re-directing engine thrust to generate forces and moments on the airframe, enhancing the lifting and maneuvering capabilities. For this and similar configurations, the potential two-directional interactions between the airframe and engine subsystems are of major concern.[8] Engine thrust can now directly influence the lift and attitude motion of the airframe, and in turn, the dynamic motion of the airframe can affect the engine dynamics. Hypersonic single-stage-to-orbit vehicles, such as the X-30 aircraft design concept, are also considered to possess significant airframe/propulsion subsystem interactions, and will require integrated airframe/engine control.[9,10] The dynamic interactions between airframe and engine subsystems are frequently difficult to model, and the uncertainties in these interactions can be potentially significant. Analysis methods are sought which can characterize effects of the interactions, such as critical frequencies where robustness problems are most likely to occur.

The airframe/engine plant and control law used to demonstrate the three analysis techniques is presented in the next section. The three sections following this will present the SV, SSV and IS analyses of this vehicle configuration, respectively. Each section presents first the stability robustness analysis, then the performance robustness analysis. A brief review of the analysis theory is given in each section before presenting numerical results. Finally, findings from this study are summarized and conclusions are drawn.

System Description and Nomenclature

The vehicular system's input-output characteristics will be defined at one operating point by the matrix of transfer functions

$$\begin{bmatrix} y_A \\ y_E \end{bmatrix} = \begin{bmatrix} G_A & G_{AE} \\ G_{EA} & G_E \end{bmatrix} \begin{bmatrix} u_A \\ u_E \end{bmatrix} \qquad (1)$$

$$\text{or} \quad y(s) = G(s)u(s)$$

---

† Pres. at the AIAA GN&C Conf., Monterey, 1993.
‡ Doctoral Candidate, Student Member, AIAA.
* Graduate Fellow.
** Prof. of Aero. Eng., Now with the Dept. of Aero Eng., Univ. of Maryland, Assoc. Fellow, AIAA.

The airframe and engine response (y) and control (u) vectors are denoted respectively by the subscripts "A" and "E." Likewise, $G_A(s)$ and $G_E(s)$ represent the airframe and engine dynamics, respectively. Dynamic interactions between the airframe and engine are reflected in the off-diagonal transfer function matrices, $G_{AE}(s)$ and $G_{EA}(s)$, referred to as the engine-to-airframe and the airframe-to-engine coupling or interaction matrices, respectively.

The control law is defined here as

$$\begin{bmatrix} u_A \\ u_E \end{bmatrix} = \begin{bmatrix} K_A & K_{AE} \\ K_{EA} & K_E \end{bmatrix} \begin{bmatrix} y_{Ac} - y_A \\ y_{Ec} - y_E \end{bmatrix} \qquad (2)$$

$$\text{or } u(s) = K(s)\{y_c(s) - y(s)\})$$

$y_{Ac}(s)$ and $y_{Ec}(s)$ are the vectors of commanded airframe and engine responses. $K_A(s)$ and $K_E(s)$ are the feedback control compensation matrices associated with the airframe and the engine control subsystems, respectively. The control cross-feeds are indicated by $K_{AE}(s)$ and $K_{EA}(s)$.

The airframe/engine vehicle model analyzed in Ref. [7] will also be considered here. It is a delta wing supersonic aircraft with STOVL capabilities. The reference point about which the nonlinear system is linearized is the steady-state wings-level decelerating transition, approaching hover. Note that the airframe's short period mode is unstable for this configuration and flight condition. At this reference point, the forces and moments controlling the aircraft are transitioning from those generated by the aerodynamic control surfaces to those generated by the propulsion system.

In this paper four responses and four controls (yielding a 4x4 compensation matrix) will be considered, and they are listed in Table 1. The first three responses listed in this table are airframe responses, while the fan speed, N_2, is a critical engine response. Therefore, the airframe and engine response vectors are (see Eq. (1)):

$$y_A(s) = [\theta, \gamma, V]^T \quad \text{and} \quad y_E(s) = N_2 \qquad (3)$$

The airframe and engine control vectors were selected as (see Eq. (1)):

$$u_A(s) = [A_q, \eta, A_8]^T \quad \text{and} \quad u_E(s) = w_f \qquad (4)$$

The Reaction Control System (RCS) draws bleed air from the engine's compressor, and the Pitch RCS area controls the magnitude of RCS thrust. The ejector butterfly valve angle controls the amount of engine flow to the ejectors, thus the amount of ejector thrust. The magnitude of aft thrust is largely determined by the aft nozzle throat area. With this selection, referring to Eq. (1), the airframe transfer matrix, $G_A(s)$, is 3x3, and the engine transfer function, $G_E(s)$, is a scalar. Thus, the engine-to-airframe coupling transfer matrix, $G_{AE}(s)$, is 3x1, and the airframe-to-engine coupling transfer matrix, $G_{EA}(s)$, is 1x3.

Note that the responses and controls were normalized by estimates of their respective maximum allowable perturbations from reference values, presented in Table 1. With this normalization, magnitudes of transfer functions can be more meaningfully compared. The normalized frequency response magnitudes of the airframe's pitch attitude (θ) to all control inputs listed in Table 1 are shown in Fig. 1. Likewise, the engine's fan speed (N_2) responses are shown in Fig. 2. Although not shown here, the flight path angle (γ) and forward velocity (V) frequency responses are presented in Ref. [7]. It is evident from these figures that the airframe/engine system is quite multivariable in nature in that each response is significantly influenced by several controls. The engine-to-airframe and airframe-to-engine coupling transfer functions in $G_{AE}(j\omega)$ and $G_{EA}(j\omega)$ are comparatively large in magnitude. Fig. 1 shows that the fuel flow rate may significantly affect the airframe's pitch attitude response. Although not shown here, the fuel flow rate has an even more significant effect on the flight path angle response. In turn, Fig. 2 shows that the magnitudes of the engine's fan speed responses from the airframe controls are not insignificant.

Table 1 - System Responses and Controls and Their Maximum Values

System Responses	Maximum Value
θ - pitch attitude (deg)	21 deg
γ - long. flight path angle (deg)	4.0 deg
V - true airspeed (ft/sec)	76 ft/sec
N_2 - fan speed (rpm's)	120 rpm's
System Control Inputs	**Maximum Value**
A_q - pitch RCS area (in^2)	0.7 in^2
η - ejector butterfly valve angle (deg)	8.0 deg
A_8 - aft nozzle throat area (in^2)	20 in^2
w_f - fuel flow rate (lbm/hr)	1000 lbm/hr

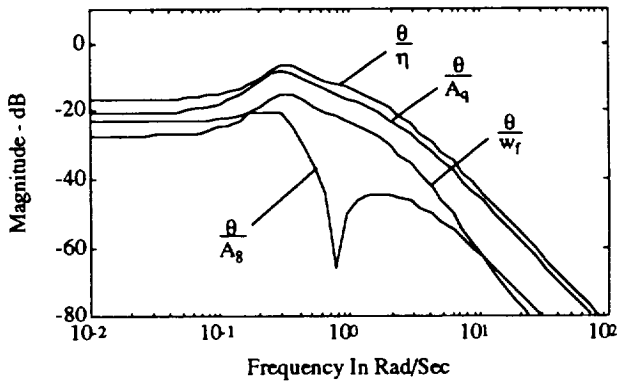

Figure 1 - Pitch Attitude Frequency Response Magnitudes

The feedback compensation for this system was designed using a standard H_∞ control law synthesis formulation.[3,11] In this particular formulation, Fig. 3 shows the sensitivity transfer function matrix weighted by $S_d^{-1}(s)$ (where $S_d(s)$ is the "desired" sensitivity matrix), along with the control effort weighted by $W_c(s)$. $S_d(s)$ was chosen to equal the sensitivity matrix obtained by the system presented in Ref. [7] (in which eight responses and

controls were utilized). $W_c(s)$ was chosen to weight the control effort greatest beyond specified actuation bandwidths. Note that the purpose of this paper is neither to promote nor refute the H_∞ control law synthesis methodology. The elementary formulation shown in Fig. 3 was used simply to obtain a compensator in order to demonstrate the analysis methodologies presented in the next sections.

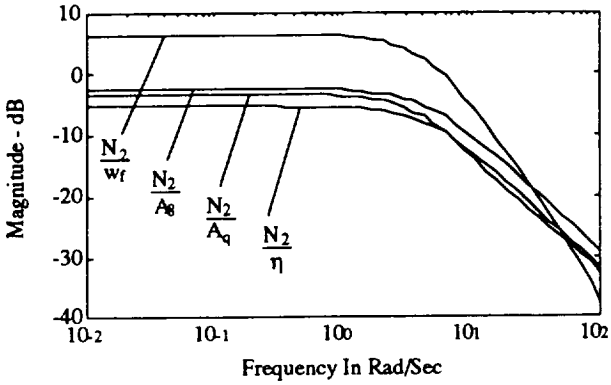

Figure 2 - Fan Speed Frequency Response Magnitudes

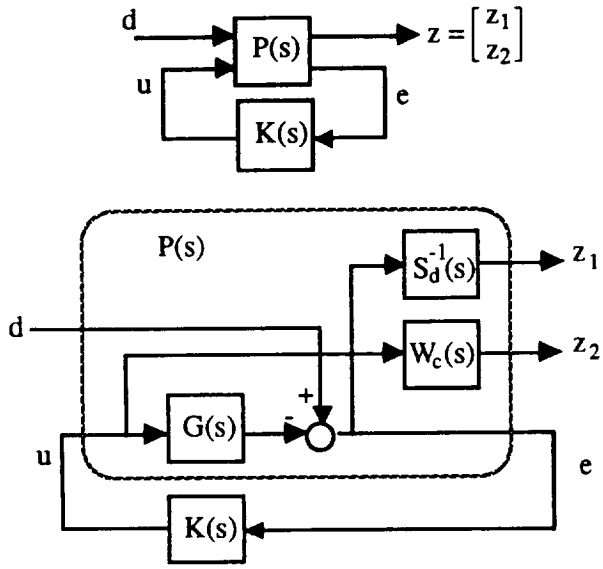

Figure 3 - An Elementary H_∞ Formulation

The compensator synthesized by this procedure delivered tracking and disturbance rejection performance that approximately matched the performance obtained by the system presented in Ref. [7], and the closed-loop frequency response magnitudes did not exceed specified maximum allowable upper bounds. Further, the individual loop transfers (with all other loops closed) exhibited acceptable loop shapes and typically good classical gain and phase margins. The pitch attitude, flight path, forward speed and engine fan speed loops have cross-over frequencies of 1.8, 1.5, 0.19 and 3.5 rad/sec, respectively. The pitch attitude and flight path angle loops both have approximately 60 degrees of phase margin, and 16 and -10 dB of gain margin, respectively. The forward speed loop has gain and phase margins of 55 dB and 75 degrees, while the fan speed loop has infinite gain margin and a phase margin of 90 degrees. Finally, the frequency response magnitudes of the elements within K(s) were approximately the same order of magnitude as the corresponding elements of the compensator matrix presented in Ref. [7] (in which the control actuation was not considered excessive).

The compensator obtained by this synthesis procedure was of 28th order, and was subsequently reduced to 14th order by a frequency-weighted internally-balanced order reduction method presented in Ref. [12]. The partitioning of the control law matrix follows from the response vector (Eq. (3)) and the selection of airframe and engine controls (Eq. (4)). $K_A(s)$ is therefore 3x3, and $K_E(s)$ is a scalar. The control cross-feed matrices, $K_{AE}(s)$ and $K_{EA}(s)$ are 3x1 and 1x3, respectively. The eigenvalues of the open-loop airframe/engine plant, compensator and closed-loop system are presented in Table 2.

Table 2 - Open/Closed-Loop Eigenvalues

Eigenvalues of the Open Loop Plant	Closed-Loop Eigenvalues
-1.9970e+02	-1.9959e-02
-3.8212e+01	-2.1121e-01 ±2.6096e+01i
-2.9395e+01	-3.7869e-01
-7.1087e+00	-3.1371e-01 ±6.6357e-01i
-4.1220e+00	-2.2255e-01
1.2939e+00	-1.5838e+01 ±5.4784e+00i
-1.0629e-01 ±2.7932e-01i	-9.2770e-00
-2.0918e+00	-3.9046e+00 ±4.2411e+00i
Eigenvalues of the Compensator	-3.1070e+00 ±1.1347e+00i
-2.2543e+01 ±2.4624e+01i	-2.4429e+00 ±1.0952e+00i
-3.2040e+01	-2.1509e+00
-2.3301e+01	-8.9366e-02 ±2.9916e-01i
-1.6773e+01 ±6.2915e+00i	-5.4206e-01
-4.9100e+00 ±4.5882e+00i	-2.6680e-01 ±1.9755e-01i
-4.2717e+00	-2.3179e-01
-5.4666e-01	
-9.9883e-03	
-8.3853e-03	
-8.4735e-03	
-1.0029e-02	

The closed-loop responses from commands ($y_c(s)$) and disturbances (d(s)) for the systems are

$$y(s) = T(s)\, y_c(s) + S(s)\, d(s) \qquad (5)$$

where T(s) and S(s) are the complementary sensitivity and sensitivity transfer function matrices, respectively. Fig. 4 presents the closed-loop pitch attitude (θ) frequency response magnitude from a pitch attitude command, θ_c. This figure also presents the "desired" performance (that which was obtained by the feedback system presented in Ref. [7]) and the specified maximum allowable upper bound. From the definition of the response vector given in Eq. (3), the frequency response of θ/θ_c corresponds to the (1,1) element in T(s). Fig. 5 presents the closed-loop engine fan speed (N_2) frequency response magnitude from a fan speed command, N_{2c}, along with its respective "desired" performance and upper bound. This response corresponds to the (4,4) element of T(s). Although not shown, similar disturbance rejection performances were seen for these loops. Further, both the tracking and disturbance rejection performances for the flight path angle (γ) and forward velocity (V) responses were likewise acceptable.

Note, however, that the closed-loop system is not decoupled, and each command can elicit responses in the other channels. Fig. 6 presents the pitch attitude response from flight path, velocity, and engine fan speed commands. These responses correspond to the (1,2), (1,3) and (1,4) elements in $T(j\omega)$ (as well as in $S(j\omega)$). It can be seen that a flight path angle command can produce a pitch attitude response greater than -20 dB between approximately 0.05 and 10 rad/sec. Although not shown, a pitch attitude command can, in turn, produce a significant flight path angle response within this frequency range. Both pitch RCS jets and ejector thrust produce airframe pitching moments, and it would be difficult to decouple pitch attitude and flight path angle responses. (Note that even larger magnitudes were seen in the corresponding off-diagonal elements of $T(j\omega)$ and $S(j\omega)$ for the system presented in Ref. [7].) In general, it was found that $T(j\omega)$ was not decoupled above approximately 0.05 rad/sec, and $S(j\omega)$ was not decoupled below approximately 10 rad/sec. However, the responses did not exceed their respective allowable upper bounds, and therefore the over-all closed-loop performance for this system was deemed acceptable.

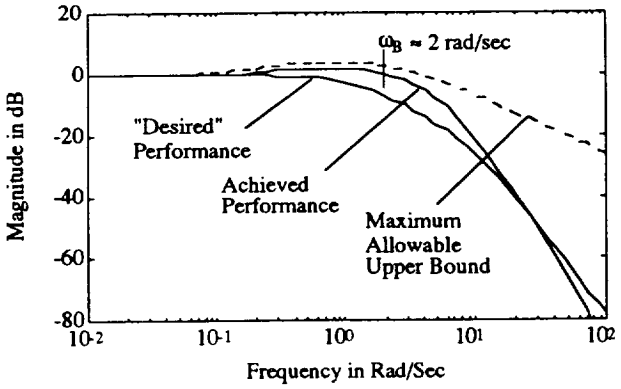

Figure 4 - Pitch Attitude-From-Pitch Attitude Command

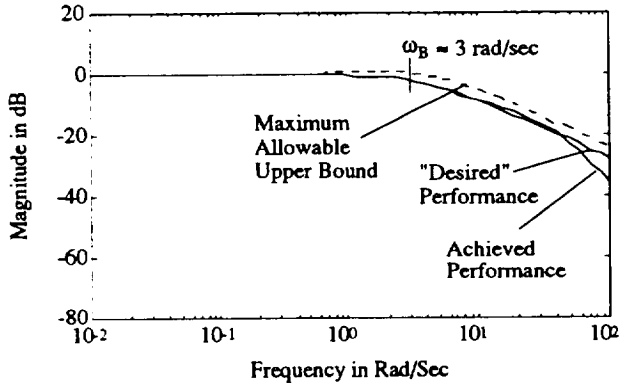

Figure 5 - Fan Speed From Fan Speed Command

Note that the upper bounds shown in Figs. 4-6 will be utilized in the analyses discussed next. The matrix of maximum allowable upper bounds on the complementary sensitivity matrix is denoted $T_u(j\omega)$, and likewise the matrix of maximum allowable upper bounds on the sensitivity matrix is denoted $S_u(j\omega)$.

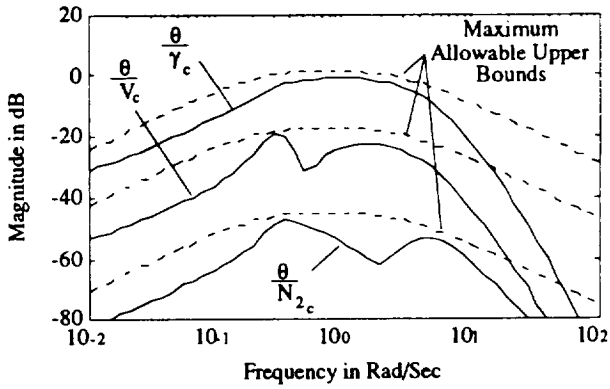

Figure 6 - Pitch Attitude From Other Commands

Singular Value (SV) Analysis

The integrated airframe/engine system with unstructured output multiplicative uncertainty is shown in Fig. 7. In this figure, the response, control and command vectors, $y(s)$, $u(s)$ and $y_c(s)$, and the plant and control law transfer function matrices, $G^*(s)$ and $K(s)$, are defined as in Eqs. (1) and (2). Note that $G^*(s)$ denotes the "nominal" plant with no uncertainty ($M(s)=0$). Again, $d(s)$ in Fig. 7 is a vector of exogenous disturbances corrupting the responses of the system.

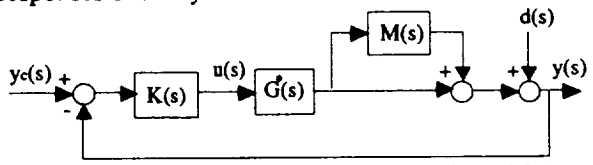

Figure 7 - Feedback System With Uncertainty, M(s)

Stability Robustness Analysis

It is shown in Refs. [1] and [2] that for a system with unstructured output multiplicative plant uncertainty, $M(s)$, system stability is assured if $K(s)$ stabilizes the nominal system ($M(s)=0$), if $M(j\omega)$ does not alter the encirclement requirement (for stability) of the Nyquist plot (plot of $\det[I+(I+M)GK]$), and if

$$\sigma_{max}(M(j\omega)) < \sigma_{min}(I+[G(j\omega)K(j\omega)]^{-1}) \text{ for all } \omega>0 \quad (6)$$

where $\sigma_{max}(\,)$ and $\sigma_{min}(\,)$ are the maximum and minimum singular values, respectively. This inequality may be used as a stability robustness criterion. If this criterion is not met, stability can no longer be assured. Although the analysis presented in this paper will focus on uncertainty at the plant output, a complete analysis should also address robustness to multiplicative uncertainty at the plant input, which may be analyzed by a similar criterion.

The uncertainty matrix, $M(j\omega)$, in Eq. (6) can be of any general structure. However, since the focus of this study is robustness to uncertainties in the airframe/engine interactions ($G_{AE}(s)$ and $G_{EA}(s)$), consider that the airframe and engine plants, $G_A(s)$ and $G_E(s)$, are reasonably well modeled, but the interactions contribute the most significant sources of uncertainty in the model of the system's dynamics. The airframe/engine plant description with additive uncertainty in the coupling dynamics is

$$G(s) = G^*(s) + \Delta(s), \text{ where}$$

$$G^*(s) = \begin{bmatrix} G_A & G^*_{AE} \\ G^*_{EA} & G_E \end{bmatrix} \text{ and } \Delta(s) = \begin{bmatrix} 0 & \Delta_{AE} \\ \Delta_{EA} & 0 \end{bmatrix} \quad (7)$$

Consider, as an example, the following constant uncertainty matrix for the airframe/engine system under study (recall, Δ_{AE} is 3x1 and Δ_{EA} is 1x3),

$$\Delta = \delta_o \Delta_1, \ \Delta_1 = \begin{bmatrix} 0 & 0 & 0 & 1 \\ 0 & 0 & 0 & 1 \\ 0 & 0 & 0 & 1 \\ 1 & 1 & 1 & 0 \end{bmatrix} \quad (8)$$

where δ_o is a scalar. Using the following relationship between additive and output multiplicative uncertainty,

$$G(s) = G^*(s) + \Delta(s) = (I + M(s))G^*(s) \quad (9)$$

the equivalent multiplicative uncertainty for this example is

$$M(s) = \Delta(G^*(s))^{-1} = \delta_o M_1(s) \quad (10)$$

where

$$M_1(s) = \Delta_1(G^*(s))^{-1} \quad (11)$$

Fig. 8 presents the plot of Eq. (6) for the feedback system discussed in the previous section along with the example uncertainty above. It can be seen that the minimum value of $\sigma_{min}(I+[G(j\omega)K(j\omega)]^{-1})$ is approximately -7 dB and occurs in the frequency range between 0.4 rad/sec and 0.8 rad/sec. However, it is also shown in this figure that when δ_o = 8.5e-4, Eq. (6) is no longer satisfied for frequencies greater than 30 rad/sec. Yet, the system is stable for this uncertainty. Note that the criterion of Eq. (6) is known to be a conservative measure of stability robustness. From the Nyquist plot, it was found that when δ_o = -0.0665 the system becomes unstable at a frequency of 0.36 rad/sec. This is an increase from 8.5e-4 by approximately 38 dB (a factor of 78). Further note that the frequency at which the criterion fails in Fig. 8 does not correspond to the frequency of instability.

Again, the multiplicative uncertainty defined in Eq. (10) is just an example. Different uncertainty matrices with smaller maximum singular values may exist which cause the system to become unstable. Finding the particular critical multiplicative uncertainty matrix with smallest maximum singular value (thus minimizing the conservatism of the criterion of Eq. (6)) can be a difficult task, and it may represent variations in the plant that are physically unrealistic.

Performance Robustness Analysis

The closed-loop responses of the system shown in Fig. 7 are

$$y(s) = (I + (I+M)GK)^{-1}(I+M)GK\, y_c(s) + (I + (I+M)GK)^{-1} d(s) \quad (12)$$

or,

$$y(s) = T(s)\, y_c(s) + S(s)\, d(s) \quad (13)$$

where again T(s) and S(s) are defined as the complementary sensitivity and sensitivity transfer function matrices, respectively. The nominal (M=0) complementary sensitivity and sensitivity transfer function matrices shall be denoted as $T^*(s)$ and $S^*(s)$, respectively.

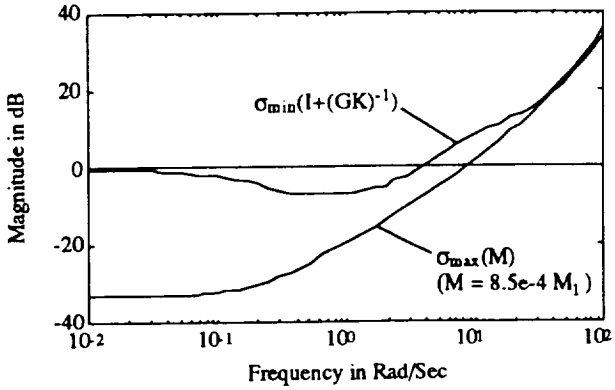

Figure 8 - Singular Value Stability Robustness Criterion

Often, aspects of aircraft flying or handling qualities are considered acceptable if frequency response magnitudes (such as pitch rate-to -pilot stick input) lie within defined upper and/or lower allowable bounds. Allowable bounds may also be utilized to determine acceptable tracking and disturbance rejection performance of the engine loops. Recall that upper bounds on the elements of $T(j\omega)$ and $S(j\omega)$ were presented in the last section, and the matrices of these allowable upper bounds were denoted $T_u(j\omega)$ and $S_u(j\omega)$. It is stated in Ref. [3] that multivariable tracking and disturbance rejection performance may be defined acceptable if

$$\sigma_{max}(T_u^{-1}(j\omega)\, T(j\omega)) \le 1 \text{ for all } \omega$$
$$\sigma_{max}(S_u^{-1}(j\omega)\, S(j\omega)) \le 1 \text{ for all } \omega \quad (14)$$

These inequalities constitute multivariable performance robustness criteria. Acceptable performance is assured if these criteria are met for all frequencies.

Fig. 9 presents the complementary sensitivity performance robustness criterion of Eq. (14) for the feedback system under study. It can be seen that this criterion is not met for the nominal system (M=0), even though the magnitudes of all closed-loop frequency responses lie below their upper bounds (see Figs. 4-6). Thus, the criterion of Eq. (14) is conservative in this case. Recall that $T(j\omega)$ is not decoupled (not diagonally dominant) beyond approximately 0.05 rad/sec, and $\sigma_{max}(T_u^{-1}(j\omega)\, T^*(j\omega))$ begins to grow larger than 0 dB around this frequency. Recall as well that $S(j\omega)$ is not decoupled below approximately 10 rad/sec, and, although not shown, $\sigma_{max}(S_u^{-1}(j\omega)\, S^*(j\omega))$ is greater than 0 dB until approximately this frequency. The maximum singular value of a matrix is only an accurate measure of the magnitude of the element with largest magnitude when the matrix is diagonally dominant. Holding the diagonal elements constant, as the off-diagonal elements increase in magnitude, the maximum singular value will also increase in size. This property adds to the conservatism of the criterion of Eq. (14).

Fig. 9 also shows the criterion for the system with an example $M(j\omega) = -0.016\, M_1(j\omega)$ (=25% of the uncertainty which causes instability), and Fig. 10 presents the pitch

attitude (θ) response from fan speed command (N_{2c}) for the system with this value of uncertainty. It can be seen that this response increased beyond its maximum allowable upper bound for frequencies above 0.1 rad/sec. Although not shown, the increases in magnitudes of the flight path angle and velocity responses from fan speed command were just as large. Although an increase in $\sigma_{max}(T_u^{-1}(j\omega)\, T(j\omega))$ from the nominal value $\sigma_{max}(T_u^{-1}(j\omega)\, T^*(j\omega))$ is noted in Fig. 9, the performance degradations in the airframe responses from engine commands were discovered only after investigating all closed-loop responses from all commands.

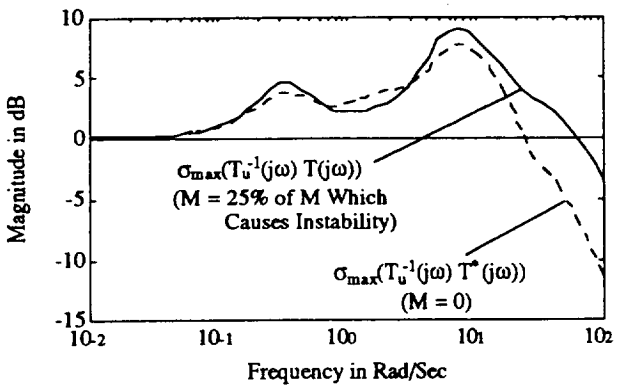

Figure 9 - SV Performance Robustness Criterion

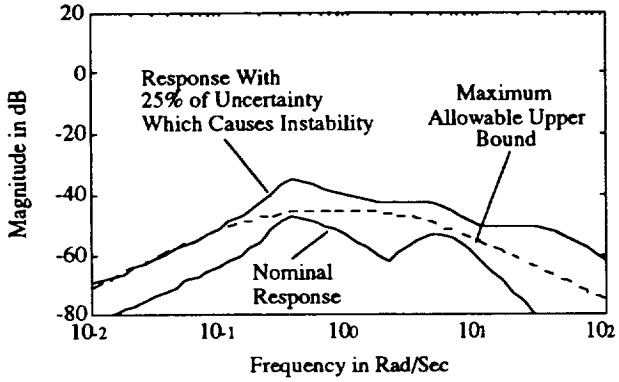

Figure 10 - Pitch Attitude From Fan Speed Command

Structured Singular Value (SSV) Analysis

When more structure can be given to the uncertainty in the system, the SSV analysis method takes advantage of this knowledge to give a less conservative measure of stability robustness. For this method, the feedback loop for the overall interacting system is represented as shown in Fig. 11. Utilizing the specific structure of uncertainty as defined in Eq. (7), $\Delta_D(s)$ in Fig. 11 reflects the uncertainties in the coupling dynamics into the following block-diagonal form:

$$\Delta_D(s) = \begin{bmatrix} \Delta_{AE} & 0 \\ 0 & \Delta_{EA} \end{bmatrix} \qquad (15)$$

Q(s) in Fig. 11 represents the nominal *closed-loop* system, and it can be shown that

$$\begin{bmatrix} y \\ u' \end{bmatrix} = \begin{bmatrix} Q_{11} & Q_{12} \\ Q_{21} & Q_{22} \end{bmatrix} \begin{bmatrix} y_c \\ y' \end{bmatrix}$$

where, (16)

$$Q_{11} = G^*K(I+G^*K)^{-1}, \quad Q_{12} = (I+G^*K)^{-1}$$
$$Q_{21} = P\,(I+KG^*)^{-1}K, \quad Q_{22} = -P\,(I+KG^*)^{-1}K$$

Note that P relates the off-diagonal uncertainty matrix, $\Delta(s)$, to the block-diagonal uncertainty matrix, $\Delta_D(s)$. That is,

$$\Delta(s) = \Delta_D(s)\, P, \quad P = \begin{bmatrix} 0 & I \\ I & 0 \end{bmatrix} \qquad (17)$$

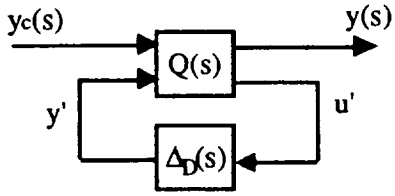

Figure 11 - System With Block-Diagonal Uncertainty

Stability Robustness Analysis

From Refs. [3] and [4], the system shown in Fig. 11 remains stable if and only if

$$\|\Delta_D\|_\infty < \frac{1}{\|Q_{22}\|_\mu}, \text{ where} \qquad (18)$$

$\|Q_{22}\|_\mu = \sup_\omega [\mu(Q_{22}(j\omega))]$, & $\|\Delta_D\|_\infty = \sup_\omega [\sigma_{max}(\Delta_D(j\omega))]$. Here $\mu(Q_{22}(j\omega))$ is the structured singular value of $Q_{22}(j\omega)$.

Fig. 12 presents the inverse of $\mu(Q_{22}(j\omega))$ for the feedback system under consideration. It can be seen that the minimum value of $1/\mu(Q_{22}(j\omega))$ is -31 dB at a frequency of approximately 0.36 rad/sec. The structured singular value theory states that at each frequency an uncertainty matrix $\Delta_{Dcrit}(j\omega)$ exists that causes the system to become unstable and $\sigma_{max}(\Delta_{Dcrit}(j\omega)) = 1/\mu(Q_{22}(j\omega))$. Therefore, at 0.36 rad/sec an uncertainty matrix $\Delta_{crit}(j\omega)$ exists that causes instability and has a corresponding block-diagonal matrix, $\Delta_{Dcrit}(j\omega)$, with a maximum singular value equal to -31 dB. Recall that for the uncertainty matrix $\Delta = -0.0665\, \Delta_1$, where Δ_1 is defined in Eq. (8), instability occurred at 0.36 rad/sec. Unlike the SV analysis method, here the frequency of instability is consistent with the critical frequency indicated in Fig. 12.

However, as also shown in Fig. 12, for the specific structure of uncertainty defined in Eq. (8), $\sigma_{max}(\Delta_D) = -31$ dB when $\delta_o = 0.016$, hence, the criterion of Eq.(18) is no longer satisfied. Yet, recall that this is only approximately 25% of the value of uncertainty that causes instability. Again, the additive uncertainty defined in Eq. (8) is just an example, and is certainly not the critical uncertainty matrix, $\Delta_{crit}(j\omega)$. $\Delta_{crit}(j\omega)$, may have different magnitudes and phases for each element.

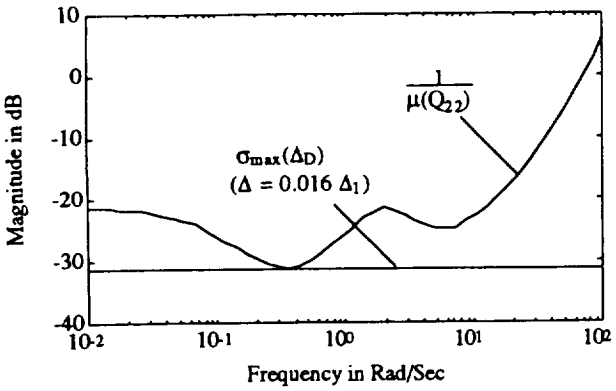

Figure 12 - SSV Stability Robustness Criterion

Finally, although the structured singular value stability criterion in Fig. 12 has only just failed for $\Delta = -0.016\ \Delta_1$, recall from Fig. 10 that for this value of uncertainty the pitch attitude response from engine fan speed command violates its maximum allowable upper bound. As expected, uncertainty in the system will cause performance requirements to fail before stability robustness requirements.

Performance Robustness Analysis

The structured singular value performance robustness criterion, introduced in Ref. [13], is also presented in Ref. [3]. Note that in Fig. 11,

$$y'(s) = \Delta_D(s)\, u'(s) \tag{19}$$

Substituting Eq. (19) into Eq. (16) , the closed-loop responses of the system shown in Fig. 11, with the uncertainty matrix $\Delta_D(s)$, are

$$y(s) = \{Q_{11} + Q_{12}(I-\Delta_D Q_{22})^{-1}\Delta_D Q_{21}\}\, y_c(s) \tag{20}$$

In Ref. [3], the system outputs are then redefined to be

$$y(s) = \begin{bmatrix} S_u^{-1}(s)\{y_c(s)-y(s)\} \\ T_u^{-1}(s)\, y(s) \end{bmatrix} \tag{21}$$

Again, $T_u(s)$ and $S_u(s)$ are the matrices of maximum allowable upper bounds on the closed-loop frequency response magnitudes. With this selection of outputs,

$$Q_{11} = \begin{bmatrix} S_u^{-1}(s)\, S^*(s) \\ T_u^{-1}(s)\, T^*(s) \end{bmatrix}, \quad Q_{12} = \begin{bmatrix} -S_u^{-1}(s)\, S^*(s) \\ T_u^{-1}(s)\, S^*(s) \end{bmatrix} \tag{22}$$

Note that Q_{21} and Q_{22} remain the same as in Eq. (16). Using Eq. (20) with these new definitions for Q_{11} and Q_{12}, performance robustness of the system may be considered acceptable if

$$\sigma_{max}(Q_{11} + Q_{12}(I-\Delta_D Q_{22})^{-1}\Delta_D Q_{21}) \le 1 \text{ for all } \omega \tag{23}$$

Note that the nominal ($\Delta_D(j\omega)=0$) performance robustness criterion is $\sigma_{max}(Q_{11}) \le 1$ for all ω. From Eq. (22), it can be seen that the performance robustness criterion of Eq. (23) simply "combines" the singular value tracking and disturbance rejection performance criteria of the last section (see Eq. (14)).

Fig. 13 presents the criterion of Eq. (23) for the feedback system under study. Just as with the SV analysis, it can be seen that the criterion is not met even for the nominal system since $\sigma_{max}(Q_{11}) > 1$ throughout the frequency range shown. Again, this is due to the fact that the closed-loop system is not diagonally dominant.

Fig. 13 also shows the criterion of Eq. (23) for the system with $\Delta = -0.016\Delta_1$ (25% of uncertainty that causes instability). Although an increase from the nominal value ($\sigma_{max}(Q_{11})$) is noted in Fig. 13, as with the SV analysis, this criterion does not directly indicate which elements of $T(j\omega)$ are increasing in magnitude.

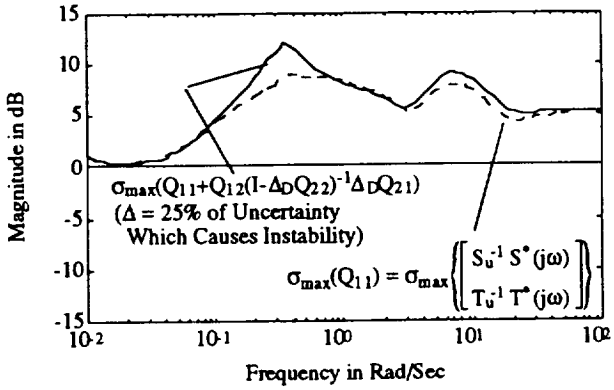

Figure 13 - Performance Robustness Criterion of Eq. (23)

Finally, as discussed in Ref. [3], note that both robust stability and performance can be assured by one structured singular value criterion. That is, the stability criterion of Eq. (18) and the performance criterion of Eq. (23) are assured to be met if and only if

$$1 < \frac{1}{\| Q \|_\mu} \tag{24}$$

Although further manipulations on the system and block-diagonal uncertainty matrix are required in the development of this criterion, the matrix Q in this inequality is essentially that defined by Eqs. (16) and (22). The criterion of Eq. (24) can also be used as an objective in the control law synthesis. If it is met, robust stability and performance are assured for uncertainty in the interactions between the airframe and engine. Although not shown, this criterion is not met for the feedback system analyzed here, since the criterion of Eq. (23) is not met even for the nominal system (see Fig. 13).

Interacting Subsystem (IS) Analysis

The main objective of this analysis methodology is to reveal how the interactions between the airframe and engine are manifested, and to assess their significance. This method is presented in Refs. [5]-[7]. It is shown in these references that through block-diagram manipulation, the airframe/engine plant (Eq. (1)) and the control law of Eq. (2) may be described as shown in Fig. 14. The effects of the airframe on the engine loop due to the dynamic coupling between these subsystems is represented by the

multiplicative and disturbance interaction matrices, $M_A(s)$ and $D_A(s)$. It can be shown that

$$M_A(s)=\{G_{EA}\mathcal{K}_{AE} - (G_{EA} + G_E\mathcal{K}_{EA})\mathcal{R}\}G_E^{-1}$$

where,

$$\mathcal{R}= K_A[I+(G_A+G_{AE}\mathcal{K}_{EA})K_A]^{-1}(G_{AE}+G_A\mathcal{K}_{AE}) \quad (25)$$

$$D_A(s) = (G_{EA}+G_E\mathcal{K}_{EA})K_A[I+(G_A+G_{AE}\mathcal{K}_{EA})K_A]^{-1}$$

where, with reference to Eq. (2), note that

$$K_{AE}(s) = \mathcal{K}_{AE}(s)K_E(s),\ K_{EA}(s) = \mathcal{K}_{EA}(s)K_A(s) \quad (26)$$

Also, note that the engine affects the airframe in a dual manner, and the dual expressions for these interaction terms can be found by interchanging all subscripts A and E in the above expressions.

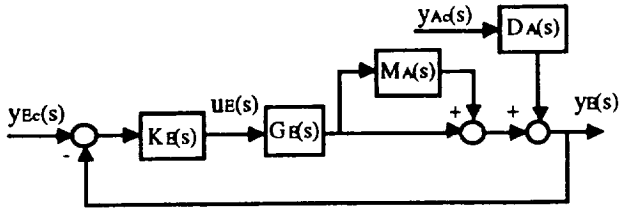

Figure 14 - Engine Loop With Effects From Airframe

Stability Robustness Analysis

The determinant of the return difference matrix for the airframe/engine system (Eqs. (1),(2)) may be expressed as

$$\det[I+GK] = \det[I+(G_A+G_{AE}\mathcal{K}_{EA})K_A]\det[I+(I+M_A)G_EK_E] \quad (27)$$

Therefore a *necessary* condition guaranteeing $\det[I+G(j\omega)K(j\omega)]\neq 0$ is that the $\det[I+(I+M_A)G_EK_E]$ is nonzero for all frequency, and this is assured if the engine control law $K_E(s)$ stabilizes the (non-interacting) engine loop (in which case the $\det[I+G_EK_E]\neq 0$), and if[1]

$$\sigma_{max}(M_A(j\omega))< \sigma_{min}(I+[G_E(j\omega)K_E(j\omega)]^{-1}) \text{ for all } \omega > 0 \quad (28)$$

This inequality may be considered a stability robustness criterion. In order to assure that the $\det[I+(I+M_A)G_EK_E]$ is nonzero at each frequency, $\sigma_{min}(I+(G_E(j\omega)K_E(j\omega))^{-1})$ is the maximum *allowable* size of $\sigma_{max}(M_A(j\omega))$. The *smallest* difference between $\sigma_{max}(M_A(j\omega))$ and $\sigma_{min}(I+[G_E(j\omega)K_E(j\omega)]^{-1})$ may therefore be considered a "robustness margin," which indicates the "size" of allowable uncertainty in $M_A(j\omega)$. Note that Eq. (25) shows that $M_A(s)$ is an explicit function of the coupling matrices $G_{AE}(s)$ and $G_{EA}(s)$, and uncertainty associated with the coupling dynamics is therefore reflected in the uncertainty in $M_A(j\omega)$.

Fig. 15 shows the plot of the stability robustness criterion of Eq. (28) for the airframe/engine system under study. This figure indicates that the smallest difference between $|M_A(j\omega)|$ and $|1+[G_E(j\omega)K_E(j\omega)]^{-1}|$ occurs between the frequencies of 0.2 and 0.5 rad/sec, and that the "robustness margin" is seen to be approximately 6 dB.

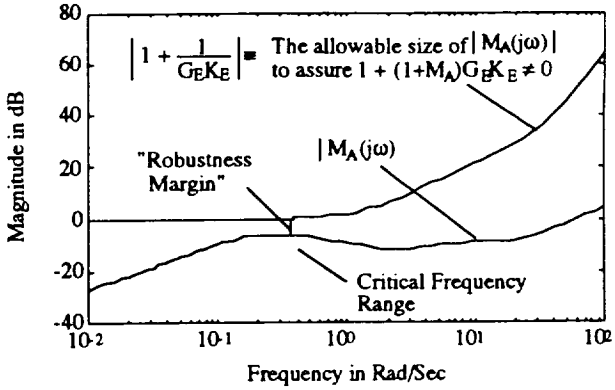

Figure 15 - IS Stability Robustness Criterion

Fig. 16 presents the criterion of Eq. (28) with the uncertainty matrix $\Delta=-0.058\Delta_1$, where Δ_1 is defined in Eq. (8). Recall from the previous section that instability occurs when $\Delta = -0.0665\ \Delta_1$. Also recall that the structured singular value stability robustness criterion failed for $\Delta=-0.016\Delta_1$. Hence, for this particular structure of uncertainty, this analysis method gives the least conservative measure of stability robustness. Note too, as indicated in Fig. 16, the criterion first fails at 0.36 rad/sec, which is precisely the frequency at which instability occurs for this structure of uncertainty. Finally, the dual of the criterion of Eq. (28) (for analysis of the engine's effects on the airframe loops) was also seen to indicate the frequency of 0.36 rad/sec as most critical.

Fig. 17 presents the Bode plot of the airframe's pitch attitude loop (with all other loops closed). It can be seen that this loop nominally has a minimum gain margin of 16 dB at a phase cross-over frequency of 6.5 rad/sec, and a phase margin of 60 degrees at a gain cross-over frequency of 1.8 rad/sec. However, the instability that occurs at 0.36 rad/sec due to the uncertainty ($\Delta=-0.0665\Delta_1$) in the interactions between the airframe and engine is also shown. The gain and phase cross-over frequencies in the classical single-loop analysis do not correspond to this critical frequency. However, the SV, SSV and IS stability robustness criteria all correctly indicated frequency ranges around 0.36 rad/sec as being critical.

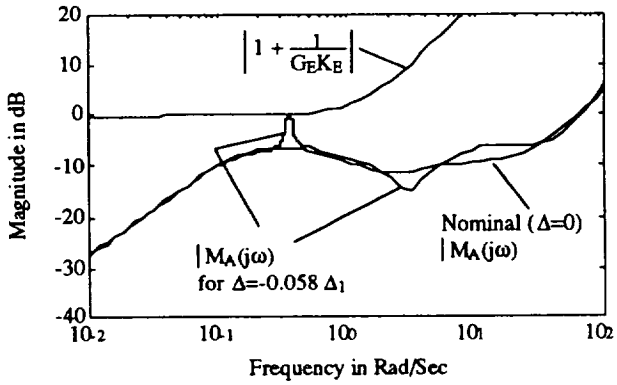

Figure 16 - IS Robustness Criterion With Uncertainty

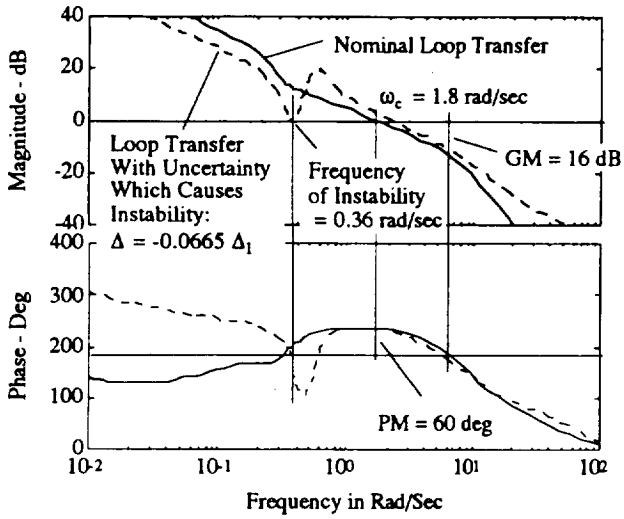

Figure 17 - Pitch Attitude Loop Transfer Function

Engine Performance Robustness Analysis

From Fig. 14, the engine response from engine command for the integrated system is

$$y_E(s) = [1 + (1+M_A)G_EK_E]^{-1}(1+M_A)G_EK_E\, y_{Ec}(s), \text{ or} \quad (29)$$

$$y_E(s) = T_E(s)\, y_{Ec}(s)$$

When $M_A(s)=0$, the "non-interacting" closed-loop engine response is defined as

$$y_E(s) = [1 + G_EK_E]^{-1}\, G_EK_E\, y_{Ec}(s)$$

or, (30)

$$y_E(s) = T_E'(s)\, y_{Ec}(s)$$

The tracking performance may be considered acceptable if the magnitude of the engine response for the *interacting* system ($M_A(j\omega)\neq 0$) lies below the magnitude of the upper bound defined as $|T_u(j\omega)|$. Fig. 18 shows the magnitude of $T_E'(j\omega)$ along with the magnitude of the specified upper bound, $|T_u(j\omega)|$, as already shown in Fig. 5.

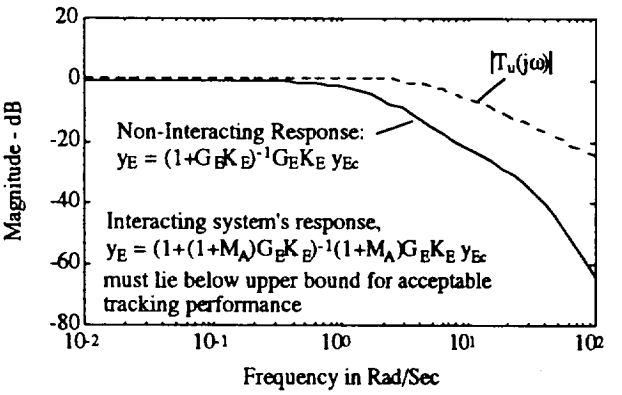

Figure 18 - Non-Interacting Fan Speed Response

$\mathcal{M}_A(j\omega)$ is defined here as the maximum *allowable* magnitude of $M_A(j\omega)$ that assures the *interacting* engine's closed-loop frequency response magnitude is less than its maximum allowable upper bound. That is, if the actual magnitude of $M_A(j\omega)$ is smaller than $\mathcal{M}_A(j\omega)$, then acceptable tracking performance is assured.

For scalar engine systems, $\mathcal{M}_A(j\omega)$ can be directly calculated. $\mathcal{M}_A(j\omega)$ is determined by solving a static minimization problem at each frequency. The loss function to be minimized is

$$J = |M_A(j\omega)| \quad (31)$$

with the constraint

$$|T_u(j\omega)| = |(1+(1+M_A)G_EK_E)^{-1}\,(1+M_A)G_EK_E|$$

or, (32)

$$|T_u(j\omega)| = |T_E(j\omega)|$$

The augmented loss function was therefore defined as

$$\mathcal{J} = |M_A(j\omega)|$$
$$+ \lambda\{|T_u(j\omega)|^2 - |(1+(1+M_A)G_EK_E)^{-1}\,(1+M_A)G_EK_E|^2\} \quad (33)$$

where λ is the Lagrange multiplier. (Note that the square of the magnitudes was utilized in order to simplify the problem.) The following are the necessary conditions for finding the minimum magnitude of $M_A(j\omega)$:

$$\frac{\partial \mathcal{J}}{\partial |M_A|} = 0, \quad \frac{\partial \mathcal{J}}{\partial \angle(M_A)} = 0, \quad \frac{\partial \mathcal{J}}{\partial \lambda} = 0 \quad (34)$$

Expanding these necessary conditions and solving for $\angle(M_A)$ gives the phase angle for $\mathcal{M}_A(j\omega)$ as

$$\angle(\mathcal{M}_A) = \tan^{-1}\left\{\frac{-|T_u|^2 \sin(\phi)}{|T_u|^2(m+\cos(\phi))-m}\right\} \quad (35)$$

where m and ϕ are defined as the magnitude and phase of the "non-interacting" engine loop transfer function. That is,

$$G_EK_E = m\, e^{j\phi} \quad (36)$$

Once the phase of $\mathcal{M}_A(j\omega)$ is determined, the magnitude of $\mathcal{M}_A(j\omega)$ the root of the following quadratic with minimum magnitude:

$$C_1|M_A|^2+[C_2\cos(\angle(\mathcal{M}_A))+C_3\sin(\angle(\mathcal{M}_A))]\,|M_A|+C_4 = 0 \quad (37)$$

$$C_1 = m^2(|T_u|^2 - 1),\quad C_2 = 2(C_1 + m\,|T_u|^2\cos(\phi))$$
$$C_3 = -2m\,|T_u|^2\sin(\phi),\quad C_4 = C_1 + 2m\,|T_u|^2\cos(\phi) + |T_u|^2$$

For the airframe/engine system considered here, Fig. 19 shows $|\mathcal{M}_A(j\omega)|$, the actual $|M_A(j\omega)|$, and the allowable $|M_A(j\omega)|$ that assures that the $1+(1+M_A)G_EK_E\neq 0$ (the stability robustness metric - see Fig. 15). It can be seen that the magnitude of $\mathcal{M}_A(j\omega)$ is lower than that which indicates stability robustness (as expected). A "performance robustness margin" may be defined in a manner analogous to the "stability robustness margin," as the minimum difference between $|\mathcal{M}_A(j\omega)|$ and $|M_A(j\omega)|$. In Fig. 19, it can be seen that this "robustness margin" is approximately only 1 dB less than the "stability robustness margin." In fact, as shown in the figure, the engine's closed-loop fan speed response will not exceed its upper bounds until $\Delta=-0.055\Delta_1$. This is a comparatively large

uncertainty and indicates that the engine system's tracking performance is robust to uncertainties in the airframe/engine interactions. Although not shown, this result is consistent with closed-loop fan speed frequency responses with uncertainty in the system.

Finally, note that the maximum allowable magnitude of $M_A(j\omega)$ such that the engine's *sensitivity* function lies below its upper bound can be solved in the manner just described.

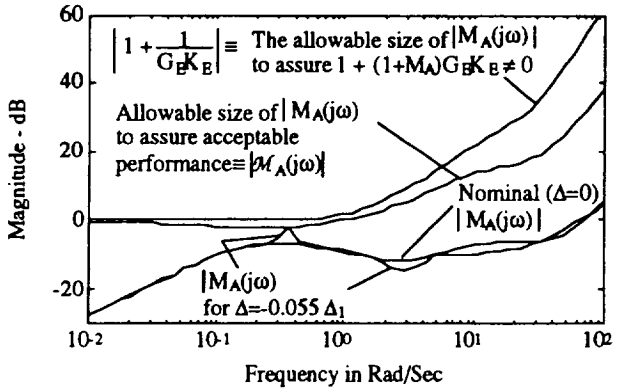

Figure 19 - $\mathcal{M}_A(j\omega)$ = Allowable $|M_A|$

Airframe Performance Robustness Analysis

It can be shown that the integrated system's airframe responses are

$$y_A(s) = [I + (I+M_E)G_A K_A]^{-1} (I+M_E)G_A K_A\, y_{Ac}(s) + [I + (I+M_E)G_A K_A]^{-1} D_E\, y_{Ec}(s) \quad (38)$$

or,

$$y_A(s) = T_A(s)\, y_{Ac}(s) + S_A(s)\, D_E(s)\, y_{Ec}(s) \quad (39)$$

where $M_E(s)$ is the dual of $M_A(s)$. When $M_E(s)=0$, the "non-interacting" closed-loop airframe responses from airframe commands is defined as

$$y_A(s) = [I + G_A K_A]^{-1} G_A K_A\, y_{Ac}(s)$$

or, (40)

$$y_A(s) = T_A'(s)\, y_{Ac}(s)$$

Now define the maximum singular value of the "ratio" of $T_A'(j\omega)$ and $T_A(j\omega)$ as

$$\mathcal{T}(j\omega) = \sigma_{max}((T_A'(j\omega))^{-1} T_A(j\omega)) \quad (41)$$

If no interactions are present ($M_E(j\omega)=0$) then $\mathcal{T}(j\omega)=1$ for all frequency. Therefore, with interactions ($M_E(j\omega)\neq 0$), $\mathcal{T}(j\omega)$ can indicate those frequencies where the effects of the uncertainties in the interactions will be most prominent for the closed-loop airframe responses *only* from airframe commands. Unlike the performance robustness criteria of the SV and SSV analyses (see Figs. 9 and 13), this measure will not be "clouded" by the effects of the engine commands on the airframe responses. Fig. 20 presents the plot of $\mathcal{T}(j\omega)$ for the airframe/engine system under study, and indicates frequencies centering around 0.3 and 30 rad/sec as critical. Fig. 21 presents the pitch attitude response from pitch attitude command for an uncertainty $\Delta = -0.058\ \Delta_1$ (that just causes the stability robustness criterion of Eq. (28) to fail - see Fig. 16), and shows that the frequencies at which this response deviates greatest from the nominal are consistent with the critical frequency ranges indicated by the plot in Fig. 20.

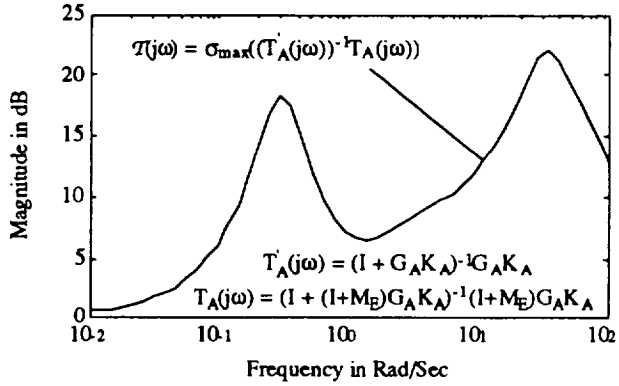

Figure 20 - Performance Robustness Measure - $\mathcal{T}(j\omega)$

From Eq. (39) it can be seen that the effect of the engine commands on the airframe responses may be indicated by comparing the "sizes" of the airframe's complementary sensitivity matrix, $T_A(j\omega)$, with the product of the airframe's sensitivity matrix, $S_A(j\omega)$, and the disturbance interaction matrix, $D_E(j\omega)$. Fig. 22 shows the minimum singular value of $T_A(j\omega)$ along with the maximum singular value of $(S_A(j\omega)D_E(j\omega))$ (a "worst case" study). It is seen that beyond 1 rad/sec the "size" of the responses due to engine commands becomes greater than 10 percent of the "size" of the responses due to airframe commands. Uncertainty in the system can increase the "sizes" of both the airframe's sensitivity matrix and the disturbance interaction matrix (both are functions of the interactions $G_{AE}(j\omega)$ and $G_{EA}(j\omega)$), further increasing the magnitudes of the responses from engine commands, and this is consistent with the result shown in Fig. 10.

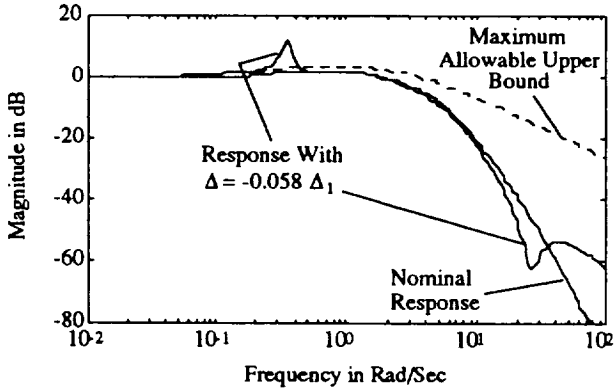

Figure 21 - Pitch Attitude From Pitch Attitude Command

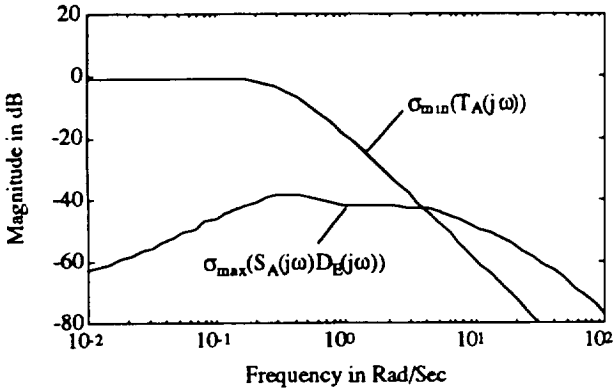

Figure 22 - A "Worst Case" Measure of the Effects of Engine Commands On Airframe Responses

Conclusions

The Interacting Subsystem (IS) analysis method specifically addresses effects of the interactions between the airframe and engine. The Singular Value (SV) and Structured Singular Value (SSV) methods provide criteria that, if met, assure robust stability and performance. However, if these criteria are not met, the causes of the problems are not apparent.

It was seen that the stability robustness criterion of the SV analysis method can be a conservative measure. Further, for the case study, the critical frequency range indicated by the stability robustness criterion of the SV analysis method did not correspond to the frequency of instability. Uncertainty was considered to be significant only in the interactions between the airframe and engine. Utilizing this structured uncertainty, the stability robustness criterion of the SSV analysis method indicated a critical frequency range that was consistent with the frequency of instability. This critical frequency of instability was also accurately indicated by the IS analysis method. Further, for this case study, the IS method gave the least conservative measure of stability robustness.

Although the performance of the nominal airframe/engine system was considered acceptable, the performance robustness criteria of both the SV and SSV analysis methods were not met for the nominal system. These criteria were conservative because the closed-loop system was not diagonally dominant. Further, little insight into the effects of uncertainty on the closed-loop performance was gained by these criteria. However, the IS analysis method was able to indicate an accurate "performance robustness margin" that measured the allowable magnitude of the interactions from the airframe such that acceptable tracking performance in the engine was still assured. The IS analysis method also indicated critical frequency ranges where the airframe tracking performance would be most affected by uncertainty in the interactions. Finally, this analysis method also correctly indicated that disturbances from the engine's fan speed command could be significant on the closed-loop airframe responses.

Acknowledgments

This work is sponsored by the NASA Lewis Research Center under Grant # NAG3-998. Dr. Sanjay Garg is the technical program manager.

References

[1] Doyle, J., Stein, G., "Multivariable Feedback Design: Concepts for a Classical/Modern Synthesis," *IEEE Transactions on Automatic Controls*, Vol. AC-26, No. 1, pp. 4-16, Feb., 1981.

[2] Ridgely, D., Banda, S., "Introduction to Robust Multivariable Control," AFWAL-TR-85-3102, Flight Dynamics Lab, Air Force Wright Aeronautical Labs, Dayton, February, 1986.

[3] Maciejowski, J.M., *Multivariable Feedback Design*, Addison-Wesley Publishing Company, New York, 1989.

[4] Doyle, J. "Analysis of Feedback Systems With Structured Uncertainties" *Proceedings of the Institute of Electrical Engineers*, Part D., 129, pp. 242-250, 1982.

[5] Schierman, J., Schmidt, D., "Analysis Of Airframe And Engine Control Interactions and Integrated Flight/Propulsion Control," *Journal Of Guidance, Control, And Dynamics*, Vol. 15, No. 6, Nov.-Dec., 1992, pp. 1388-1396.

[6] Schierman, J., Schmidt, D., "Analysis Of Airframe/Engine Interactions In Integrated Flight And Propulsion Control," AIAA No. 91-2794, proceedings of the AIAA Guidance, Navigation and Control Conference, New Orleans, August, 1991.

[7] Schierman, J., Schmidt, D., Lovell, T., "Analysis Of Airframe/Engine Interactions For A STOVL Aircraft With Integrated Flight/Propulsion Control," AIAA No. 92-4623, proceedings of the AIAA Guidance, Navigation and Control Conference, Hilton Head, August, 1992.

[8] Garg, S., Mattern, D.L., "Application of an Integrated Flight/Propulsion Control Design Methodology to a STOVL Aircraft," AIAA Paper No. 91-2792, proceedings of the AIAA Guidance, Navigation and Control Conference, New Orleans, Louisiana, August, 1991.

[9] Schmidt, D., "Dynamics and Control of Hypersonic Aeropropulsive/Aeroelastic Hypersonic Vehicles," AIAA Paper No. 92-4326, proceedings of the AIAA Guidance, Navigation and Control Conference, pp. 161-171, Hilton Head, South Carolina, August, 1992.

[10] Schmidt, D., "Integrated Control of Hypersonic Vehicles - A Necessity Not Just a Possibility," AIAA Paper No. 93-3761, to be presented at the Guidance, Navigation and Control Conference, Monterey, August, 1993.

[11] Doyle, J., Glover, K., et. al, "State-Space Solutions to Standard H_2 and H_∞ Control Problems," proceedings of the American Control Conference, Atlanta, June, 1988, pp. 1691-1696.

[12] Bacon, B., Schmidt, D., "Multivariable Frequency-Weighted Order Reduction," *Journal of Guidance*, Vol. 12, No. 1, Jan.-Feb., 1989, pp. 97-107.

[13] Doyle, J., Wall, J., Stein, G., "Performance and Robustness Analysis for Structured Uncertainty," proceedings of the IEEE Conference on Decision and Control, Orlando, 1982, pp. 629-636.